



# **Oxyde de tungstène et de molybdène fonctionnalisés par des composés organiques comme catalyseur hétérogène performant pour la coupure oxydante de l'acide oléique en acides carboxyliques**

**Thèse**

**Amir Enferadi-Kerenkan**

**Doctorat en génie chimique  
Philosophiae Doctor (Ph.D.)**

Québec, Canada

© Amir Enferadi-Kerenkan, 2018



## Résumé

Les huiles et corps gras d'origines végétales ou animales ont récemment attiré un grand intérêt comme matériel de base dans les industries oléochimiques. Cette attention ne provient pas uniquement des raisons environnementales mais aussi de l'avantage économique de ces nouveaux produits. Les acides gras insaturés, composants principaux des lipides, peuvent être oxydés pour la production de mono- ou de di-acides carboxyliques ; ces derniers sont à la base d'une grande variété de matériaux dans de nombreuses industries. Ce procédé d'oxydation est nommé « clivage oxydatif », en effet, durant la réaction, une double liaison carbone-carbone est brisée. L'exemple le plus représentatif est l'acide azélaïque, C<sub>9</sub> contenant une double fonction acide carboxylique - un produit à haute valeur ajoutée qui est obtenu à partir de l'acide oléique. Actuellement, cette réaction, en industrie, est effectuée par ozonolyse, or, ces réactions ont récemment été classées comme risqué dû aux problèmes associés à l'utilisation d'ozone. Cependant, l'utilisation d'un oxydant plus doux requiert l'utilisation d'un catalyseur. Dans les travaux présentés, nous avons développé un catalyseur hétérogène innovant à partir d'oxydes de tungstène et de molybdène pour la coupure oxydante de l'acide oléique utilisant le peroxyde d'hydrogène comme oxydant. Afin de trouver un catalyseur performant, différents catalyseurs ont été préparés et testés, tels que des oxydes de tungstène mésoporeux, possédant une très grande surface spécifique supportés par de l'alumine gamma, des nanoparticules (NPs) de trioxyde de tungstène de structures différentes (hydraté ou anhydre), de peroxyde de tungstène, d'oxyde de molybdène, mais aussi d'amas de polyoxotungstates (POTs) sous forme de structure de Keggin.

Alors que l'utilisation de catalyseur homogène a été largement reportée pour cette réaction, les travaux effectués sur des catalyseurs hétérogènes sont moins rapportés. En effet, l'efficacité des catalyseurs solides est moindre compte tenu du plus faible nombre de sites actifs en contact avec la phase liquide et donc le substrat ; or pour les catalyseurs homogènes cette surface de contact est optimum. Pour s'affranchir de cet obstacle dans ces travaux, nous avons choisi d'utiliser des catalyseurs présentant des tensioactifs à partir de molécules organiques. Ces catalyseurs permettent d'augmenter les propriétés hydrophobes/hydrophiles de la surface de la nanoparticule, et aussi d'améliorer la compatibilité entre la surface du catalyseur solide, le substrat de la réaction - l'acide oléique - et l'oxydant en phase aqueuse. Pour remplir cet objectif, plusieurs cations d'amines quaternaire ont été utilisés dans la synthèse, tel que le l'hexadécyltriméthylammonium (CTA<sup>+</sup>), le

tétraméthylammonium ( $\text{TMA}^+$ ), le tétrapropylammonium ( $\text{TPA}^+$ ) et le tétrabutylammonium ( $\text{TBA}^+$ ).

Nous avons développé une approche simple et écoresponsable pour la synthèse et le greffage de tensioactifs de nanoparticules d'oxyde de tungstène et de molybdène à partir de la dissolution oxydante de poudre micrométrique de tungstène et de molybdène métallique. Par la suite, avec quelques modifications dans l'approche ainsi que l'utilisation de sels d'amine quaternaire possédant une chaîne alcane plus importante lors de la synthèse, nous avons réussi à mettre au point une nouvelle méthode de synthèse pour la préparation de POTs hybride, organique-inorganique. En termes de réaction catalytique, c'est la première fois que l'utilisation de POT comme catalyseurs hétérogènes pour des réactions d'oxydation d'acides gras insaturés est rapportée. Le catalyseur synthétisé présente généralement une excellente activité, comparé aux autres catalyseurs hétérogènes rapportés. Une conversion complète de l'acide oléique initial avec un rendement maximum pour le diacide espéré (acide azélaïque) de 80% a pu être atteint en optimisant la quantité d'amine quaternaire cationique à la surface du catalyseur. Grâce à la présence de molécules organiques comme tensioactifs, ce catalyseur efficace en solution aqueuse ne présente pas de lixiviation significative. De plus, il est facilement récupérable et peut être réutilisé sans perte d'activité significative jusqu'à quatre cycles.

## Abstract

Oils and fats of vegetable and animal origin have recently attracted a growing interest as renewable raw materials in oleochemical industries. This attention arises from not only the environmental reasons, but also economic ones. Unsaturated fatty acids (UFAs), as the constituent of lipids, can be oxidized to produce mono- and dicarboxylic acids which are applicably valuable materials in different industries. This oxidation process is so-called oxidative cleavage, since during the reaction carbon-carbon double bond(s) get cleaved. The most striking instance is production of azelaic acid, a valuable C9 diacid, from oleic acid (C18:1). Currently, this reaction is carried out in industry via ozonolysis, which, nowadays, has been converted to a controversial challenge due to the hazardous problems associated with use of ozone. Employing an eco-friendlier oxidant requires an active catalyst to be employed, as well. In this research, we have developed advanced heterogeneous catalysts based on tungsten and molybdenum oxides for oxidative cleavage of oleic acid with hydrogen peroxide as oxidant. To find a highly efficient catalyst, different catalysts were prepared and tried including high surface area mesoporous tungsten oxide supported on  $\gamma$ -alumina, nanoparticles (NPs) of different structures of tungsten trioxide (hydrated and anhydrous), tungsten peroxide, and molybdenum oxide, as well as Keggin clusters of polyoxotungstates (POTs).

While employing homogeneous catalysts in this reaction has been widely reported, the works on the heterogeneous catalysts are very rare, most probably due to the poor reactant/solid catalyst contact in liquid-phase reactions of lipids resulting in much lower catalytic efficiency of solid catalysts compared to the homogeneous ones. To tackle this obstacle in this research, we leveraged the strategy of organo-functionalization of the solid catalyst's surface, to not only tune the hydrophobicity/hydrophilicity properties of the surface, but also improve the compatibility of the solid catalysts with the organic substrate, oleic acid, and the aqueous oxidant. For this purpose, different quaternary ammonium cations were employed in the synthesis including cetyltrimethylammonium (CTA<sup>+</sup>), tetramethylammonium (TMA<sup>+</sup>), tetrapropylammonium (TPA<sup>+</sup>), and tetrabutylammonium (TBA<sup>+</sup>).

We have developed a green and straightforward approach for the synthesis and organo-functionalization of tungsten and molybdenum oxide NPs based on oxidative dissolution of micrometer-scale bare W and Mo powders. Interestingly, with some slight modifications in this

approach and using larger quaternary ammonium salts in the synthesis we have succeeded to present a novel synthesis method for preparation of hybrid organic-inorganic POTs. In terms of catalytic reaction, application of heterogeneous POT catalysts in oxidation of UFAs has been reported for the first time in this work. The synthesized catalysts, generally, exhibited excellent activity compared to the reported heterogeneous ones. Full conversion of the initial oleic acid, with the highest yield of production of the desired diacid (azelaic acid) ~80 %, was achieved by optimization of the amount of the quaternary ammonium cation on the catalyst's surface. Thanks to the organo-functionalization, these water-tolerant catalysts exhibited no significant leaching, as well as convenient recovery and steady reuse without noticeable decrease in activity, at least up to four cycles.

# Table of contents

<b>RÉSUMÉ</b> .....	<b>III</b>
<b>ABSTRACT</b> .....	<b>V</b>
<b>TABLE OF CONTENTS</b> .....	<b>VII</b>
<b>LIST OF TABLES</b> .....	<b>XII</b>
<b>LIST OF FIGURES</b> .....	<b>XIV</b>
<b>LIST OF SCHEMES</b> .....	<b>XVIII</b>
<b>LIST OF ABBREVIATIONS</b> .....	<b>XIX</b>
<b>ACKNOWLEDGMENT</b> .....	<b>XXI</b>
<b>DEDICATION</b> .....	<b>XXIII</b>
<b>PREFACE</b> .....	<b>XXV</b>
<b>CHAPTER 1. INTRODUCTION</b> .....	<b>1</b>
1.1 PROBLEM STATEMENT .....	2
1.2 SCOPE OF THE RESEARCH.....	3
1.3 ORGANIZATION OF THE THESIS .....	4
<b>CHAPTER 2. CHEMICALLY CATALYZED OXIDATIVE CLEAVAGE OF UNSATURATED FATTY ACIDS AND THEIR DERIVATIVES</b> .....	<b>7</b>
2.1 OILS AND FATS AS RENEWABLE RAW MATERIALS.....	8
2.1.1 Globalization of oils and fats.....	9
2.1.2 Oleochemical industries .....	11
2.1.2.1 Polymer industry .....	13
2.1.2.1.1 Long-chain dicarboxylic acids .....	13
2.2 FATTY ACIDS AND THEIR REACTIONS.....	15
2.2.1 Fatty acids: a primer .....	15
2.2.1.1 Oleic acid .....	17
2.2.2 Reactions of unsaturated fatty acids .....	18
2.2.2.1 Oxidation.....	19
2.2.2.1.1 Epoxidation .....	19
2.2.2.1.2 Oxidative cleavage .....	20

2.3	DIFFERENT CATALYST-OXIDANT SYSTEMS FOR OXIDATIVE CLEAVAGE OF UNSATURATED FATTY ACIDS .....	22
2.3.1	Mechanisms of the reaction .....	23
2.3.2	Homogeneous catalysts .....	25
2.3.2.1	Osmium .....	26
2.3.2.2	Cobalt .....	26
2.3.2.3	Molybdenum .....	26
2.3.2.4	Iron .....	29
2.3.2.5	Ruthenium .....	29
2.3.2.6	Tungsten .....	31
2.3.3	Heterogeneous catalysts .....	33
2.3.4	Nanoparticle-based catalysts .....	36
2.3.4.1	Performance enhancement of NP-based catalysts in oxidative cleavage of UFAs	
	39	
2.4	HETEROGENEOUS TUNGSTEN-BASED POLYOXOMETALATE CATALYSTS .....	42
2.4.1	Tungsten: a fascinating metal for catalysis .....	42
2.4.2	Fundamentals of polyoxometalate catalysis .....	44
2.4.3	Polyoxotungstates .....	46
2.4.3.1	Inorganic cation substituted solid POTs .....	48
2.4.3.2	Organo-solidified POTs .....	54
2.4.3.3	POTs solidified via immobilization onto supports or into matrixes .....	64
2.4.3.4	POTs heterogenized via combined strategies .....	65
2.5	CONCLUSION AND PERSPECTIVE .....	77
<b>CHAPTER 3.</b>	<b>CHARACTERIZATION TECHNIQUES AND REACTION ANALYSIS .....</b>	<b>79</b>
3.1	CHARACTERIZATION TECHNIQUES .....	80
3.1.1	X-ray Diffractometry .....	80
3.1.2	Infrared Spectroscopy .....	81
3.1.3	Thermogravimetric analysis .....	82
3.1.4	Nitrogen physisorption .....	83
3.1.5	Electron microscopy .....	85
3.1.6	Elemental analysis .....	85
3.1.7	Zeta potential analysis .....	87
3.2	QUANTITATIVE ANALYSIS OF THE CATALYTIC TESTS .....	89



3.2.1	Derivatization process prior to GC-MS analysis .....	89
3.2.2	Chromatograms analysis and calculation procedure .....	91
3.2.3	Apparatus and design.....	93

**CHAPTER 4. SYNTHESIS OF MESOPOROUS TUNGSTEN OXIDE/Γ-ALUMINA AND SURFACTANT-CAPPED TUNGSTEN OXIDE NANOPARTICLES AND THEIR CATALYTIC ACTIVITIES IN OXIDATIVE CLEAVAGE OF OLEIC ACID..... 95**

RÉSUMÉ		96
ABSTRACT.....		97
4.1	INTRODUCTION .....	98
4.2	EXPERIMENTAL .....	99
4.2.1	Materials and reagents .....	99
4.2.2	Synthesis.....	100
4.2.3	Characterization.....	101
4.2.4	Oxidative cleavage reaction of oleic acid.....	101
4.3	RESULTS AND DISCUSSIONS.....	102
4.3.1	Synthesized samples characterization.....	102
4.3.2	Catalytic study .....	107
4.4	CONCLUSION.....	110

**CHAPTER 5. SYNTHESIS, ORGANO-FUNCTIONALIZATION, AND CATALYTIC PROPERTIES OF TUNGSTEN OXIDE NANOPARTICLES AS HETEROGENEOUS CATALYST FOR OXIDATIVE CLEAVAGE OF OLEIC ACID AS A MODEL FATTY ACID INTO DIACIDS 111**

RÉSUMÉ		112
ABSTRACT.....		113
5.1	INTRODUCTION .....	114
5.2	EXPERIMENTAL .....	115
5.2.1	Synthetic details and characterization .....	115
5.2.2	Catalytic test .....	116
5.3	RESULTS AND DISCUSSIONS.....	116
5.3.1	Catalysts synthesis and characterization.....	116
5.3.1.1	Crystalline structural features.....	117
5.3.1.2	Spectral analysis.....	119
5.3.1.3	Thermal analysis .....	121

5.3.1.4 Other aspects of the synthesized samples .....	123
5.3.2 Catalytic test results.....	126
5.3.2.1 Influence of different catalysts on the reaction .....	127
5.3.2.2 Effects of temperature and time on the reaction.....	128
5.3.2.3 Recyclability of the catalysts.....	129
5.4 CONCLUSIONS.....	131
5.5 SUPPORTING INFORMATION.....	132
5.5.1 Characterization techniques.....	132
5.5.2 Analysis of the reaction products .....	132
5.5.2.1 Sample preparation for GC-MS analysis.....	132
5.5.2.2 Quantitative analysis .....	134
5.5.2.3 GC-MS specifications .....	135

**CHAPTER 6. NOVEL TETRA PROPYL/BUTYL AMMONIUM ENCAPSULATED  
KEGGIN-TYPE POLYOXOTUNGSTATES: SYNTHESIS, STRUCTURAL  
CHARACTERIZATION, AND CATALYTIC CAPABILITY IN OXIDATIVE CLEAVAGE OF  
UNSATURATED FATTY ACIDS..... 146**

RÉSUMÉ	147
ABSTRACT.....	148
6.1 INTRODUCTION .....	149
6.2 EXPERIMENTAL .....	150
6.2.1 Materials and synthesis.....	150
6.2.2 Characterization techniques.....	151
6.2.3 Catalytic test .....	151
6.2.4 Analysis of the reaction products .....	152
6.3 RESULTS AND DISCUSSION.....	152
6.3.1 Catalysts characterization .....	152
6.3.2 Catalytic tests results .....	160
6.3.3 Recyclability of the catalysts .....	163
6.4 CONCLUSION.....	165
6.5 SUPPORTING INFORMATION.....	167

**CHAPTER 7. SUSTAINABLE OXIDATIVE CLEAVAGE OF VEGETABLE OILS INTO  
DIACIDS BY ORGANO-MODIFIED MOLYBDENUM OXIDE HETEROGENEOUS  
CATALYSTS 175**

RÉSUMÉ	176
ABSTRACT	177
7.1 INTRODUCTION	178
7.2 EXPERIMENTAL	179
7.2.1 Synthetic details	179
7.2.2 Characterization equipment	180
7.2.3 Catalytic test	180
7.2.4 Quantitative analysis of the product	180
7.3 RESULTS AND DISCUSSION	181
7.3.1 Characterization of the catalysts	181
7.3.2 Catalytic tests results	189
7.3.3 Recyclability of the catalysts	192
7.4 CONCLUSIONS	193
7.5 SUPPORTING INFORMATION	195
<b>CHAPTER 8. CONCLUSION AND FUTURE SCOPE</b>	<b>196</b>
8.1 GENERAL CONCLUSIONS	197
8.2 FUTURE SCOPE	199
<b>REFERENCES</b>	<b>202</b>
<b>LIST OF PUBLICATIONS</b>	<b>234</b>

# List of tables

TABLE 2.1. FOOD AND NON-FOOD CONSUMPTIONS (MILLION TONS AND %) OF NINE MAJOR VEGETABLE OILS BETWEEN 1999/00 AND 2011/12 {, #179}.....	11
TABLE 2.2. SUMMARY OF THE APPLICATIONS OF BASIC OLEOCHEMICALS. ....	13
TABLE 2.3. EXAMPLES OF APPLICATIONS OF OILS AND FATS IN POLYMER INDUSTRY [9]. ....	14
TABLE 2.4. COMMON FATTY ACIDS OF ANIMAL AND PLANT ORIGINS; STRUCTURES AND NOMENCLATURE SYSTEMS [28,4].....	16
TABLE 2.5. DIFFERENT HOMOGENEOUS CATALYTIC SYSTEMS REPORTED FOR THE OXIDATIVE CLEAVAGE OF UFAS AND THEIR DERIVATIVES. 27	
TABLE 2.6. DIFFERENT HETEROGENEOUS CATALYTIC SYSTEMS REPORTED FOR THE OXIDATIVE CLEAVAGE OF UFAS AND THEIR DERIVATIVES. ....	38
TABLE 2.7. DIFFERENT SEMIHETEROGENEOUS (NANOPARTICLE-BASED) CATALYTIC SYSTEMS REPORTED FOR THE OXIDATIVE CLEAVAGE OF UFAS AND THEIR DERIVATIVES. ....	38
TABLE 2.8. DIFFERENT STRUCTURES OF POLYOXOMETALATES. ....	45
TABLE 2.9. INORGANIC CATIONS SUBSTITUTED POTs FOR GENERAL CATALYTIC PURPOSES. ....	51
TABLE 2.10. INORGANIC CATIONS SUBSTITUTED POTs FOR ACID CATALYSIS REACTIONS. ....	52
TABLE 2.11. INORGANIC CATIONS SUBSTITUTED POTs FOR OXIDATION REACTIONS.....	53
TABLE 2.12. ORGANO-SOLIDIFIED POTs FOR ACID CATALYSIS REACTIONS. ....	59
TABLE 2.13. ORGANO-SOLIDIFIED POTs FOR OXIDATION REACTIONS.....	61
TABLE 2.14. POTs SOLIDIFIED WITH IMMOBILIZATION ON SUPPORTS FOR ACID CATALYSIS REACTIONS. ....	66
TABLE 2.15. POTs SOLIDIFIED WITH IMMOBILIZATION ON SUPPORTS FOR OXIDATION REACTIONS.....	70
TABLE 2.16. POTs HETEROGENIZED VIA COMBINED STRATEGIES. ....	75
TABLE 3.1. CONCORDANCE CRITERIA OF CHNS ANALYSIS <sup>1</sup> .....	87
TABLE 4.1. SYNTHESIS CONDITIONS AND PREPARED SAMPLES. ....	100
TABLE 4.2. N <sub>2</sub> -ADSORPTION/DESORPTION ISOTHERMS RESULTS.....	104
TABLE 4.3. CATALYTIC TEST RESULTS. ....	107
TABLE 5.1. SYNTHESIS CONDITIONS AND PREPARED SAMPLES. ....	117
TABLE 5.2. CATALYTIC TESTS RESULTS (CONVERSION OF OLEIC ACID AND YIELDS OF PRODUCTION OF DESIRED PRODUCTS) AND WEIGHT FRACTIONS OF WO <sub>3</sub> IN THE CATALYSTS AS THE ASSUMED ACTIVE SITES. ....	126
TABLE 5.3. ASSIGNMENTS OF THE FTIR ABSORPTION BANDS OF THE PREPARED SAMPLES [369]. ....	144
TABLE 5.4. BET SURFACE AREAS OF THE SYNTHESIZED SAMPLES.....	145
TABLE 5.5. WEIGHT LOSSES OF THE SYNTHESIZED CATALYSTS DURING THE DIFFERENT CYCLES OF THE REACTION.....	145
TABLE 6.1. CATALYTIC TESTS RESULTS (CONVERSION OF OLEIC ACID AND YIELDS OF PRODUCTION OF DESIRED PRODUCTS).....	163
TABLE 6.2. ASSIGNMENTS OF THE FTIR ABSORPTION BANDS OF THE PREPARED SAMPLES [383]. ....	173
TABLE 6.3. ELEMENTAL ANALYSIS (C/H/N/S ANALYSIS) RESULTS FOR THE PREPARED HYBRID MATERIALS <sup>1</sup> .....	173
TABLE 6.4. BET SURFACE AREAS OF THE PREPARED SAMPLES. ....	174
TABLE 6.5. WEIGHT LOSSES OF THE SYNTHESIZED CATALYSTS DURING THE DIFFERENT CYCLES OF THE REACTION.....	174

<b>TABLE 7.1.</b> CATALYTIC TESTS RESULTS (CONVERSION OF OLEIC ACID AND YIELDS OF PRODUCTION OF DESIRED PRODUCTS).....	190
<b>TABLE 7.2.</b> COMPARISON OF CATALYTIC EFFICIENCY OF MO-CTAB1:3 WITH RECENT REPORTED WORKS IN THE LITERATURE. ....	191
<b>TABLE 7.3.</b> CATALYTIC EFFICIENCIES OBTAINED BY CATALYST MO-CTAB1:3 IN DIFFERENT REACTION CYCLES.....	193

# List of figures

<b>FIGURE 2.1.</b> PRODUCTION PROFILES OF OIL AND GAS 2010 BASE CASE (GBOE: GIGABARRELS OF OIL EQUIVALENT) [11]	8
<b>FIGURE 2.2.</b> WORLD AREA AND PRODUCTION OF THE MAJOR 10 OILSEEDS (SOYBEANS, COTTON SEED, RAPESEED, SUNFLOWER SEED, GROUNDNUTS (SHELLED), SESAME SEED, PALM KERNELS, COPRA, LINSEED AND CASTOR SEED) [15].	9
<b>FIGURE 2.3.</b> WORLD PRODUCTION OF OILSEEDS BY MAIN REGIONS (YEAR 2011) [15].	10
<b>FIGURE 2.4.</b> CONSUMPTION OF VEGETABLE OILS BY MAJOR COUNTRIES (MNT) (YEAR 2011/12 vs. 1996/97) [15].	10
<b>FIGURE 2.5.</b> TYPICAL EXAMPLE OF A LIPID STRUCTURE WITH GLYCEROL AND THREE FATTY ACIDS (PALMITIC ACID, OLEIC ACID, AND ALPHA-LINOLENIC ACID, FROM TOP TO BOTTOM) [7].	12
<b>FIGURE 2.6.</b> OLEOCHEMICAL BASE MATERIALS AS STARTING MATERIALS FOR CHEMICAL INDUSTRIES: OLEIC ACID (1A), LINOLEIC ACID (2A), LINOLENIC ACID (3A), ERUCIC ACID (4A), RICINOLEIC ACID (5A), PETROSELINIC ACID (6A), 5-EICOSENOIC ACID (7A), CALENDIC ACID (8A), A-ELEOSTEAR ACID (9A), PUNIC ACID (10A), SANTALBIC ACID (11A), VERNOLIC ACID (12A), 10-UNDECENOIC ACID (13A), AND THE RESPECTIVE METHYL ESTERS (1B-13B) AND ALCOHOLS (1C-13C) [20].	12
<b>FIGURE 2.7.</b> A DICARBOXYLIC ACID WITH TWO CARBOXYL GROUPS AS A VALUABLE CHEMICAL IN THE POLYMER INDUSTRY.	14
<b>FIGURE 2.8.</b> FATTY ACIDS STRUCTURE.	15
<b>FIGURE 2.9.</b> DIFFERENT C18 MONO AND POLY-UFAS.	17
<b>FIGURE 2.10.</b> 3-D MODELS OF DIFFERENT FATTY ACID TYPES. ARACHIDIC, STEARIC, AND PALMITIC ACIDS ARE SATURATED. ERUCIC AND OLEIC ACIDS ARE MONOUNSATURATED, AND LINOLENIC, LINOLEIC AND ARACHIDONIC ARE POLYUNSATURATED FATTY ACIDS [30].	17
<b>FIGURE 2.11.</b> EFFECT OF C=C IN THE PACKING OF SATURATED AND UNSATURATED FATTY ACIDS.	18
<b>FIGURE 2.12.</b> A GENERIC EPOXIDE.	19
<b>FIGURE 2.13.</b> APPLICATIONS OF EPOXIDIZED FATTY ACIDS AND THEIR DERIVATIVES [42].	21
<b>FIGURE 2.14.</b> (A) OLEIC ACID-CAPPED NPs OF SOME METALS/METAL OXIDES DISPERSED IN TOLUENE (CLEAR/TRANSPARENT SOLUTIONS) AND (B) THOSE NPs PRECIPITATED WITH EXCESS ETHANOL [89].	41
<b>FIGURE 2.15.</b> AMAZINGLY COLORFUL WORLD OF THE TUNGSTEN OXIDES: YELLOW WO <sub>3</sub> , BLUE WO <sub>2.9</sub> , VIOLET WO <sub>2.72</sub> , BROWN WO <sub>2</sub> , AND GRAY W METAL [105].	44
<b>FIGURE 2.16.</b> SURFACE AREA AND ACIDITY OF CSXH <sub>3</sub> -XPW12O40 AS A FUNCTION OF CS <sup>+</sup> CONTENT [131,148].	49
<b>FIGURE 2.17.</b> DIFFERENT STRATEGIES FOR PREPARATION OF COVALENT POT- ORGANIC HYBRIDS. PATH (I): DIRECT FUNCTIONALIZATION, PATHS (II, III): POST-FUNCTIONALIZATION. THE LACUNARY POM IS REPRESENTED IN BLUE, WHILE THE ANCHORING TETHER IS LILAC AND THE ADDED FUNCTIONAL MOIETY (F) IS BEIGE [175].	57
<b>FIGURE 2.18.</b> A) MACROSCOPIC VIEWS OF THE WATER/TOLUENE/[C12]3[PW12O40] SYSTEM BEFORE EMULSIFICATION, DURING THE REACTION, AND AFTER CENTRIFUGATION (FROM LEFT TO RIGHT). B) SCHEMATIC REPRESENTATION OF THE CATALYTIC EPOXIDATION OF OLEFINS INSIDE THIS EMULSION [195].	58
<b>FIGURE 2.19.</b> SIZE-SELECTIVE OXIDATION OF OLEFINS OVER [(N-C4H9)4N]4[Γ-SiW10O34(H2O)2].H2O SYNTHESIZED VIA BOTTOM-UP APPROACH [196].	64

<b>FIGURE 2.20.</b> CONTROLLING MORPHOLOGY AND DISPERSION OF SUPPORTED POT HETEROGENEOUS CATALYSTS VIA ORGANO-MODIFICATION OF THE POT [317].	74
<b>FIGURE 3.1.</b> SCHEMATIC ILLUSTRATION OF THE BRAGG'S LAW.	80
<b>FIGURE 3.2.</b> MEASUREMENT PRINCIPLES OF DTA.	83
<b>FIGURE 3.3.</b> IUPAC CLASSIFICATION OF THE PHYSISORPTION ISOTHERMS.	84
<b>FIGURE 3.4.</b> ZETA POTENTIAL AND IONIC DISTRIBUTION OF A NEGATIVELY CHARGED PARTICLE.	88
<b>FIGURE 3.5.</b> DIFFERENT PARTS OF A GC-MS SYSTEM.	90
<b>FIGURE 3.6.</b> TYPICAL CALIBRATION CURVES OF (A) METHYL OLEATE, (B) DIMETHYL AZELATE, AND (C) METHYL PELARGONATE.	92
<b>FIGURE 3.7.</b> A TYPICAL GAS CHROMATOGRAM OF THE PRODUCTS (AFTER DERIVATIZATION) OF OXIDATIVE CLEAVAGE OF OLEIC ACID.	93
<b>FIGURE 4.1.</b> N <sub>2</sub> -ADSORPTION/DESORPTION ISOTHERMS AND PORE SIZE DISTRIBUTIONS OF (A) SAMPLE I, (B) SAMPLE II, (C) SAMPLE III, (D) SAMPLE IV, AND (E) SAMPLE V.	103
<b>FIGURE 4.2.</b> SEM IMAGES OF (A) SAMPLE I, (B) SAMPLE II, (C) SAMPLE III, (D) SAMPLE IV, (E) SAMPLE V, AND (F) SAMPLE VI.	105
<b>FIGURE 4.3.</b> XRD PATTERNS OF (A) SAMPLE I, (B) SAMPLE II, (C) SAMPLE III, (D) SAMPLE IV, AND (E) SAMPLE V.	105
<b>FIGURE 4.4.</b> EDS SPECTRUMS OF (A) SAMPLE I, (B) SAMPLE II, (C) SAMPLE III, AND (D) SAMPLE IV.	106
<b>FIGURE 4.5.</b> THERMOGRAVIMETRIC BEHAVIOR OF SAMPLE VI.	106
<b>FIGURE 5.1.</b> XRD PATTERNS OF (A) SAMPLE I, (B) SAMPLE II, (C) SAMPLE III, (D) SAMPLE IV, (E) SAMPLE V, AND (F) SAMPLE VI. (o) (WO <sub>2</sub> )O <sub>2</sub> .H <sub>2</sub> O (PDF NO. 50-0233), (+) WO <sub>3</sub> (PDF NO. 83-0950), (●) WO <sub>3</sub> .0.33H <sub>2</sub> O (PDF NO. 35-0270), AND (◇) WO <sub>3</sub> .H <sub>2</sub> O (PDF NO. 43-0679).	118
<b>FIGURE 5.2.</b> FTIR SPECTRA OF (A) SAMPLE I, (B) SAMPLE II, (C) SAMPLE III, (D) SAMPLE IV, (E) SAMPLE V, AND (F) SAMPLE VI.	120
<b>FIGURE 5.3.</b> (A-E): TGA AND DTA CURVES OF (A) SAMPLE I, (B) SAMPLE III, (C) SAMPLE IV, (D) SAMPLE V, AND (E) SAMPLE VI. (F): ALL THE TGA CURVES.	122
<b>FIGURE 5.4.</b> TEM IMAGES OF (A) AND (B) SAMPLE I (WITH DIFFERENT MAGNIFICATIONS), (C) SAMPLE II, AND (D) SAMPLE III.	124
<b>FIGURE 5.5.</b> TEM IMAGES OF (A) SAMPLE IV, (B) SAMPLE V, AND (C) SAMPLE VI.	124
<b>FIGURE 5.6.</b> SURFACE ZETA POTENTIAL DISTRIBUTION OF TUNGSTEN OXIDE NPS DISPERSED IN THE SYNTHESIS SOLUTION WITHOUT ADDING CTAB AT PH 1.6-1.8.	126
<b>FIGURE 5.7.</b> RECYCLABILITY OF THE SYNTHESIZED CATALYSTS; YIELDS OF PRODUCTION OF AZELAIC ACID OVER THE SYNTHESIZED CATALYSTS IN FOURTH CYCLES (REACTION CONDITIONS: TIME: 5 H, TEMPERATURE: 120 °C, SOLVENT: TERT-BUTANOL, INITIAL AMOUNTS OF OLEIC ACID: 1 G, T-BUTANOL: 7.5 ML, H <sub>2</sub> O <sub>2</sub> : 4 ML, CATALYST: 0.45 G, AGITATION RATE: ~ 400 RPM).	130
<b>FIGURE 5.8.</b> GAS CHROMATOGRAM OF PRODUCTS OF THE CATALYTIC TEST IN ABSENCE OF CATALYST (ENTRY 1, TABLE 5.2).	136
<b>FIGURE 5.9.</b> GAS CHROMATOGRAM OF PRODUCTS OF THE CATALYTIC TEST OVER COMMERCIAL TUNGSTEN OXIDE (ENTRY 2, TABLE 5.2).	136
<b>FIGURE 5.10.</b> GAS CHROMATOGRAM OF PRODUCTS OF THE CATALYTIC TEST OVER SAMPLE I (ENTRY 3, TABLE 5.2).	137
<b>FIGURE 5.11.</b> GAS CHROMATOGRAM OF PRODUCTS OF THE CATALYTIC TEST OVER SAMPLE II (ENTRY 4, TABLE 5.2).	137
<b>FIGURE 5.12.</b> GAS CHROMATOGRAM OF PRODUCTS OF THE CATALYTIC TEST OVER SAMPLE III (ENTRY 5, TABLE 5.2).	138
<b>FIGURE 5.13.</b> GAS CHROMATOGRAM OF PRODUCTS OF THE CATALYTIC TEST OVER SAMPLE IV (ENTRY 6, TABLE 5.2).	138
<b>FIGURE 5.14.</b> GAS CHROMATOGRAM OF PRODUCTS OF THE CATALYTIC TEST OVER SAMPLE V (ENTRY 7, TABLE 5.2).	139

<b>FIGURE 5.15.</b> GAS CHROMATOGRAM OF PRODUCTS OF THE CATALYTIC TEST OVER SAMPLE VI (ENTRY 8, TABLE 5.2). .....	139
<b>FIGURE 5.16.</b> FTIR SPECTRA OF SAMPLE I: (A) BEFORE REACTION, (B) AFTER 1 <sup>ST</sup> CYCLE, (C) AFTER 2 <sup>ND</sup> CYCLE, (D) AFTER 3 <sup>RD</sup> CYCLE, AND (E) AFTER 4 <sup>TH</sup> CYCLE. ....	140
<b>FIGURE 5.17.</b> FTIR SPECTRA OF SAMPLE II: (A) BEFORE REACTION, (B) AFTER 1 <sup>ST</sup> CYCLE, (C) AFTER 2 <sup>ND</sup> CYCLE, (D) AFTER 3 <sup>RD</sup> CYCLE, AND (E) AFTER 4 <sup>TH</sup> CYCLE. ....	140
<b>FIGURE 5.18.</b> FTIR SPECTRA OF SAMPLE III: (A) BEFORE REACTION, (B) AFTER 1 <sup>ST</sup> CYCLE, (C) AFTER 2 <sup>ND</sup> CYCLE, (D) AFTER 3 <sup>RD</sup> CYCLE, AND (E) AFTER 4 <sup>TH</sup> CYCLE. ....	141
<b>FIGURE 5.19.</b> FTIR SPECTRA OF SAMPLE IV: (A) BEFORE REACTION, (B) AFTER 1 <sup>ST</sup> CYCLE, (C) AFTER 2 <sup>ND</sup> CYCLE, (D) AFTER 3 <sup>RD</sup> CYCLE, AND (E) AFTER 4 <sup>TH</sup> CYCLE. ....	141
<b>FIGURE 5.20.</b> FTIR SPECTRA OF SAMPLE V: (A) BEFORE REACTION, (B) AFTER 1 <sup>ST</sup> CYCLE, (C) AFTER 2 <sup>ND</sup> CYCLE, (D) AFTER 3 <sup>RD</sup> CYCLE, AND (E) AFTER 4 <sup>TH</sup> CYCLE. ....	142
<b>FIGURE 5.21.</b> FTIR SPECTRA OF SAMPLE VI: (A) BEFORE REACTION, (B) AFTER 1 <sup>ST</sup> CYCLE, (C) AFTER 2 <sup>ND</sup> CYCLE, (D) AFTER 3 <sup>RD</sup> CYCLE, AND (E) AFTER 4 <sup>TH</sup> CYCLE. ....	142
<b>FIGURE 5.22.</b> XRD PATTERN OF SAMPLE I AFTER REACTION; WO <sub>3</sub> .0.33H <sub>2</sub> O (PDF NO. 87-1203). ....	143
<b>FIGURE 6.1.</b> XRD PATTERNS OF (A) TO (INTENSITIES ARE MAGNIFIED BY 2.5), (B) TO-TMA, (C) TO-TPA, AND (D) TO-TBA .....	153
<b>FIGURE 6.2.</b> XRD PATTERNS OF (A) TO-TMA1/2, (B) TO-TMA, AND (C) TO-TMA2. ....	154
<b>FIGURE 6.3.</b> FTIR SPECTRA OF (A) TO, (B) TO-TMA, (C) TO-TPA, AND (D) TO-TBA. ....	156
<b>FIGURE 6.4.</b> TGA CURVES OF (A) TO, (B) TO-TMA, (C) TO-TPA, AND (D) TO-TBA. ....	156
<b>FIGURE 6.5.</b> XRD PATTERN OF TO-TBA AFTER TGA (PURE ORTHORHOMBIC WO <sub>3</sub> , PDF NO. 20-1324). ....	157
<b>FIGURE 6.6.</b> (A) TGA AND DTG (DW/DT, WHERE W IS WEIGHT %) CURVES AND (B) DTA ( $\Delta T = T_s - T_r$ WHERE $T_s$ IS SAMPLE'S TEMPERATURE AND $T_r$ IS THE REFERENCE'S TEMPERATURE) CURVE OF TO-TBA VERSUS TEMPERATURE .....	158
<b>FIGURE 6.7.</b> COMPARISON OF THE SECOND AND THE THIRD WEIGHT LOSSES OF TO-TBA WITH THOSE OF TO-TBA2. ....	159
<b>FIGURE 6.8.</b> TEM IMAGES OF (A) TO, (B) TO-TMA, (C) TO-TPA, AND (D) TO-TBA. ....	160
<b>FIGURE 6.9.</b> YIELDS OF PRODUCTION OF AZELAIC ACID OVER THE PREPARED CATALYSTS IN FOUR CYCLES (REACTION CONDITIONS: TIME: 5 H, TEMPERATURE: 120 °C, SOLVENT: TERT-BUTANOL, INITIAL AMOUNTS OF OLEIC ACID: 1 G, T-BUTANOL: 7.5 ML, H <sub>2</sub> O <sub>2</sub> : 4 ML, CATALYST: 0.45 G, AGITATION RATE $\approx$ 400 RPM). ....	164
<b>FIGURE 6.10.</b> ADDITIONAL TEM IMAGES OF (A) TO, (B) TO-TMA1/2, (C) TO-TMA, AND (D) TO-TMA2. ....	167
<b>FIGURE 6.11.</b> EDS SPECTRA OF (A) TO-TMA, (B) TO-TPA, AND (C) TO-TBA (AU AND Pd ARE FROM THE INSTRUMENT). ....	168
<b>FIGURE 6.12.</b> SURFACE ZETA POTENTIAL OF TO PARTICLES (pH 1.7–1.9). ....	168
<b>FIGURE 6.13.</b> SURFACE ZETA POTENTIAL OF TO-TMA PARTICLES (pH 1.7–1.9). ....	169
<b>FIGURE 6.14.</b> SURFACE ZETA POTENTIAL OF TO-TPA PARTICLES (pH 1.7–1.9). ....	169
<b>FIGURE 6.15.</b> SURFACE ZETA POTENTIAL OF TO-TBA PARTICLES (pH 1.7–1.9). ....	170
<b>FIGURE 6.16.</b> GAS CHROMATOGRAM OF PRODUCTS OF THE CATALYTIC TEST OVER TO CATALYST. ....	170
<b>FIGURE 6.17.</b> GAS CHROMATOGRAM OF PRODUCTS OF THE CATALYTIC TEST OVER TO-TMA CATALYST. ....	171



<b>FIGURE 6.18.</b> GAS CHROMATOGRAM OF PRODUCTS OF THE CATALYTIC TEST OVER TO-TPA CATALYST. ....	171
<b>FIGURE 6.19.</b> GAS CHROMATOGRAM OF PRODUCTS OF THE CATALYTIC TEST OVER TO-TBA CATALYST. ....	172
<b>FIGURE 6.20.</b> FTIR SPECTRA OF THE CATALYSTS: (A) BEFORE REACTION, (B) AFTER 1 <sup>ST</sup> CYCLE, (C) AFTER 2 <sup>ND</sup> CYCLE, (D) AFTER 3 <sup>RD</sup> CYCLE, AND (E) AFTER 4 <sup>TH</sup> CYCLE. ....	172
<b>FIGURE 7.1.</b> XRD PATTERNS OF THE SYNTHESIZED MOLYBDENUM OXIDES (A) MO (WITHOUT SURFACTANT) (B) MO-TMA1:2, AND (C) MO-CTAB1:2. ....	182
<b>FIGURE 7.2.</b> SEM IMAGES OF THE SYNTHESIZED MOLYBDENUM OXIDES: (A) MO (B) MO-CTAB1:4, (C) MO-CTAB1:3, (D) MO-CTAB1:2, (E) MO-TMA1:4, (F) MO-TMA1:3, AND (G) MO-TMA1:2. ....	184
<b>FIGURE 7.3.</b> FTIR SPECTRA OF THE MOLYBDENUM OXIDES PREPARED WITH CTAB AT VARIOUS CONCENTRATIONS: (A) MO-CTAB1:2, (B) MO-CTAB1:3, (C) MO-CTAB1:4, (D) MO, AND (E) CTAB. ....	186
<b>FIGURE 7.4.</b> FT-IR SPECTRA OF THE MOLYBDENUM OXIDES PREPARED WITH TMA AT VARIOUS CONCENTRATIONS: (A) MO-TMA1:2, (B) MO-TMA1:3, (C) MO-TMA1:4, (D) MO, AND (E) TMA. ....	186
<b>FIGURE 7.5.</b> TGA CURVES OF THE MOLYBDENUM OXIDES PREPARED WITH DIFFERENT AMOUNTS OF CTAB: (A) MO-CTAB1:2, (B) MO-CTAB1:3, (C) MO-CTAB1:4, AND (D). MO.....	188
<b>FIGURE 7.6.</b> TGA CURVES OF THE MOLYBDENUM OXIDES PREPARED WITH DIFFERENT AMOUNTS OF TMA: (A) MO-TMA1:2, (B) MO-TMA1:3, AND (C) MO. ....	188
<b>FIGURE 7.7.</b> FT-IR SPECTRA OF MO-CTAB1:3 CATALYST AFTER DIFFERENT REACTION CYCLES: (A) AFTER CYCLE 1, (B) AFTER CYCLE 2, (C) AFTER CYCLE 3, AND (D) AFTER CYCLE 4. ....	193

# List of schemes

<b>SCHEME 2.1.</b> EPOXIDATION OF A LIPID [7].	20
<b>SCHEME 2.2.</b> A GENERAL OXIDATIVE CLEAVAGE PROCESS.	21
<b>SCHEME 2.3.</b> OXIDATION OF OLEIC ACID INTO ALDEHYDES (I) AND OVER-OXIDATION INTO CARBOXYLIC ACIDS (II).	22
<b>SCHEME 2.4.</b> OXIDATIVE DOUBLE BOND CLEAVAGE OF UFAs TO ALDEHYDES, KETONES, AND CARBOXYLIC ACIDS [45].	24
<b>SCHEME 2.5.</b> FIRST MECHANISM OF OXIDATIVE CLEAVAGE OF UFAs [45,49].	25
<b>SCHEME 2.6.</b> SECOND MECHANISM OF OXIDATIVE CLEAVAGE OF UFAs [45].	25
<b>SCHEME 2.7.</b> OXIDATIVE CLEAVAGE OF C-C DOUBLE BONDS BY RuO <sub>4</sub> (FORMATION OF CYCLIC PERRUTHENATE ESTER) [67].	30
<b>SCHEME 2.8.</b> SCHEMATIC ILLUSTRATION FOR SCNPs AS EFFICIENT NANOCATALYST. (A) SURFACTANT MOLECULE, (B) HYDROPHOBIC SCNPs SURFACE AND (C) PERFORMANCE IN THE BIPHASIC OXIDATIVE CLEAVAGE OF OLEIC ACID USING H <sub>2</sub> O <sub>2</sub> AS OXIDANT. PRESENCE OF SURFACTANT (I) CONTRIBUTE TO THE STABILITY OF EMULSION, (II) PREVENTS AGGREGATION OF THE NPs, AND (III) MAKE THE RECOVERY OF CATALYSTS EASIER [91].	40
<b>SCHEME 2.9.</b> SCHEMATIC VIEW OF PREPARATION OF COVALENT POT-ORGANIC HYBRIDS [186].	56
<b>SCHEME 2.10.</b> SCHEMATIC DIAGRAM OF A TYPICAL ORGANIC LIQUID-PHASE REACTION OVER ORGANIC-POT HYBRIDS WITH SELF-SEPARATION PERFORMANCE.	58
<b>SCHEME 3.1.</b> THREE STEPS MECHANISMS OF ESTERIFICATION OF MONO AND DICARBOXYLIC ACIDS OVER ACID CATALYSTS.	91
<b>SCHEME 4.1.</b> SCHEMATIC ILLUSTRATION FOR SURFACTANT-CAPPED TUNGSTEN OXIDE NANOPARTICLES AS EFFICIENT NANOCATALYST. (A) SURFACTANT (OLEIC ACID) MOLECULE, (B) HYDROPHOBIC SURFACE OF SURFACTANT-CAPPED NANOPARTICLES AND (C) PERFORMANCE IN THE BIPHASIC OXIDATIVE CLEAVAGE OF OLEIC ACID. PRESENCE OF SURFACTANT (I) CONTRIBUTE TO THE STABILITY OF EMULSION AND (II) PREVENTS AGGREGATION OF THE CATALYST PARTICLES [91].	109
<b>SCHEME 5.1.</b> ESTERIFICATION OF OLEIC, AZELAIC, AND PELARGONIC ACIDS WITH METHANOL TO METHYL OLEATE, DIMETHYL AZELATE, AND METHYL PELARGONATE, RESPECTIVELY, OVER AN ACID CATALYST, BF <sub>3</sub> .	133
<b>SCHEME 6.1.</b> THERMOLYSIS OF TO-TBA (THE BULK PROTON SITES IN THE KEGGIN STRUCTURE ARE REPRESENTED AS DI-AQUAHYDROGEN IONS, H <sub>5</sub> O <sub>2</sub> <sup>+</sup> , EACH OF WHICH LINKS FOUR NEIGHBORING HETEROPOLYANIONS BY FORMING HYDROGEN BONDS WITH THE TERMINAL W=O).	158
<b>SCHEME 6.2.</b> SCHEMATIC VIEW OF THE REACTOR SETUP (LEFT) AND THE PSEUDO-HOMOGENEOUS BEHAVIOR OF TO-TMA, TO-TPA, AND TO-TBA CATALYSTS DURING THE REACTION.	162
<b>SCHEME 6.3.</b> DIFFERENT STEPS OF OXIDATIVE CLEAVAGE OF OLEIC ACID WITH H <sub>2</sub> O <sub>2</sub> OVER THE W-BASED CATALYSTS.	163

## List of abbreviations

AA	Azelaic acid
BET	Brunauer–Emmett–Teller
CHNS analysis	Carbon-hydrogen-nitrogen-sulphur analysis
CTAB	Cetyl trimethylammonium bromide
DHA	Docosahexaenoic acid
DTA	Differential thermal analysis
DTG	Differential thermogravimetric
EDS	Energy-dispersive X-ray spectroscopy
EIA	Elaidic acid
EPA	Eicosapentaenoic acid
ErA	Erucic acid
FTIR	Fourier transform infrared spectroscopy
Gboe	Giga barrels of oil equivalent
GC	Gas chromatography
GLC	Gas liquid chromatography
HPA	Heteropoly acid
HPTA	Heteropoly tungstic acid
M9-ON	Methyl 9-oxononanoate
MA	Methyl azelate
MB	Methyl brassylate
ME	Methyl erucate
MO	Methyl oleate
MS	Mass spectrometry
NL	Nonanal
NP	Nanoparticle
OA	Oleic acid
PA	Pelargonic acid
PCWP	peroxo-tris (cetylpyridinium)12-tungstophosphate
POM	Polyoxometalate

POT	Polyoxotungstate
PTA	Phase transfer agent
SCNP	Surfactant-capped nanoparticle
SEM	Scanning electron microscopy
TBA	Tetrabutylammonium
TEM	Transmission electron microscopy
TGA	Thermogravimetric analysis
TMA	Tetramethylammonium
TPA	Tetrapropylammonium / Tungstophosphoric acid
TO	Tungsten oxide
UFA	Unsaturated fatty acid
XRD	X-ray diffraction
XPS	X-ray photoelectron spectroscopy

# Acknowledgment

After an intensive period of almost 4 years, today is the day: writing this note of thanks is the finishing touch on my thesis. It has been a period of intense learning for me, not only in the scientific arena, but also on a personal level. Studying in PhD has had a big impact on me. I would like to reflect on the people who have supported and helped me so much throughout this period.

I would first like to thank my supervisor, Prof. Trong-On Do, for giving me the opportunity to study at Université Laval, for his continuous support throughout my PhD study, and for his motivation, enthusiasm, and immense knowledge. Prof. Do gave me incredible freedom to pursue my own interest, but the door of his office was always open whenever I ran into a trouble spot or had a question about my research. Exceptionally, I am truly grateful towards my supervisor for his confidence in my ability, which has allowed me to relish the opportunity of PhD at Laval to freely and innovatively foster my expertise.

I would also like to thank Prof. Serge Kaliaguine, whose insightful and in-depth knowledge and expertise, added considerably to my graduate experience. I greatly appreciate his vast knowledge and skill in many areas, and his assistance in writing my second review paper, which has on occasion made me "GREEN" with envy.

A very special thanks goes out to Dr. Hooshang Pakdel, without whose assistance my experimental works would have not been accomplished. Throughout my PhD study, although he did not have responsibility in the project, he provided us with technical support of our GC-MS instrument in a sympathetic and sincere manner, from which, I have learnt a lot. I doubt that I will ever be able to convey my appreciation fully, but I owe him my eternal gratitude.

I must also acknowledge Oleotek Inc. and its staff, particularly Mr. David Berthiaume, Mr. Alain Tremblay, and Dr. Dominic Thibeault, for stimulating discussions and comments presented in the regular meetings, and, of course, for the thermogravimetric analysis of our prepared materials.

My sincere thanks also goes to my colleagues at the Do Research Group, all the past and current members: Dr. Bousselham Echchahed who, first, trained me to work with various experimental setups and instruments, Dr. Aimé Serge Ello, with whom I enjoyed working, Dr. Gia-Thanh Vuong, Dr. Cao-Thang Dinh, Dr. Minh-Hao Pham, Mohammad Reza Gholipour, Chinh-Chien Nguyen, Arnaud Gandon, Kouakou Vianet Bossombra, Dr. Sibi Malayil, Mathieu St-Jean, Nhu-Nang Vu, Manh-Hiep Vu, and Duc-Trung Nguyen. Our scientific debates, exchanges of knowledge, skills, cooperation, feedback, and

venting of frustration during my graduate program definitely helped me to enrich my experiences. I wish them all the best of luck in their future careers.

I am also grateful to the Université Laval and the department of Chemical Engineering and their all staff for all the technical and administrative assistance that I received during the entire period of my study, particularly Andre Ferland and Richard Janvier for electron microscopy analysis, Jean Frenette for XRD analysis, Yann Giroux, Jean-Nicolas Ouellet, Marc Lavoie, Jérôme Noël, Ann Bourassa, France Cayouette, Nadia Dumontier, and the previous and current directors of the department, Prof. Alain Garnier and Prof. Bruno Gaillet, respectively, and all other professors of the department.

I sincerely thank Parag Bhargava and Lee Durham, the service engineers of ATS Scientific Inc., for their time, and helpful and meticulous technical consultations regarding the maintenance of our BET instrument.

I gratefully acknowledge the Natural Science and Engineering Research Council of Canada (NSERC) for funding our research. I would also like to thank SiliCycle and Oleotek Inc. as well as the Centre in Green Chemistry and Catalysis (CGCC) and the Department of Chemical Engineering at Université Laval for additional financial support.

On a personal level, there are my friends. We were not only able to support each other by deliberating over our problems and findings, but also happily by talking about things other than just our papers. Many thanks.

And finally, last but by no means least, I would like to thank my families who have all contributed to my thesis work in their own special ways. My most profound gratitude goes out to my parents for their wise counsel and sympathetic ear. You are always there for me. Special thanks to my brothers and sister and my parents-in-law for their spiritual support and encouragement during my study. The most special thanks to my beloved wife, Narges, for her endless love and amazing companionship during this long journey, words cannot express how grateful I am to her. This accomplishment would not have been possible without them.

Thank you all from the bottom of my heart.

Amir Enferadi-Kerenkan

Québec, December 14, 2017

*To my dear parents and my loving wife, Narges*

*“The noblest pleasure is the joy of understanding.”*

*Leonardo da Vinci*

*Go beyond your boundaries...*

*Explore the new...*

*Learn about yourself...*

*Expand your horizon...*

*Be international.*



## Preface

This thesis consists of eight chapters. Four of them (Chapters 4-7) were written in the form of scientific papers that have been published. The candidate is the primary author of three of these papers, and the second author, having equally contributed with the first author, of another one.

Also, the literature review section, Chapter 2, has been chiefly compiled from the two review papers, in which the candidate is the primary author. The first review paper has been published as A. Enferadi Kerenkan, F. Béland, T. O. Do, “*Chemically catalyzed oxidative cleavage of unsaturated fatty acids and their derivatives into valuable products for industrial applications: a review and perspective*”, *Catalysis Science & Technology*, 2016, 6, 971-987. The second review paper, entitled “*Heterogeneous catalysis by tungsten-based heteropoly compounds*”, has been recently accepted by the journal of *Catalysis Science & Technology* (DOI: 10.1039/C8CY00281A). To meet the thesis contents requirement and to provide seminal studies for the next chapters, these review papers have been modified and updated in Chapter 2.

Chapter 4 has been published as A. Enferadi Kerenkan, A. S. Ello, B. Echchahed, T. O. Do, “*Synthesis of mesoporous tungsten oxide/ $\gamma$ -alumina and surfactant-capped tungsten oxide nanoparticles and their catalytic activities in oxidative cleavage of oleic acid*”, *International Journal of Chemical Reactor Engineering*, 2016, 14(4), 899-907.

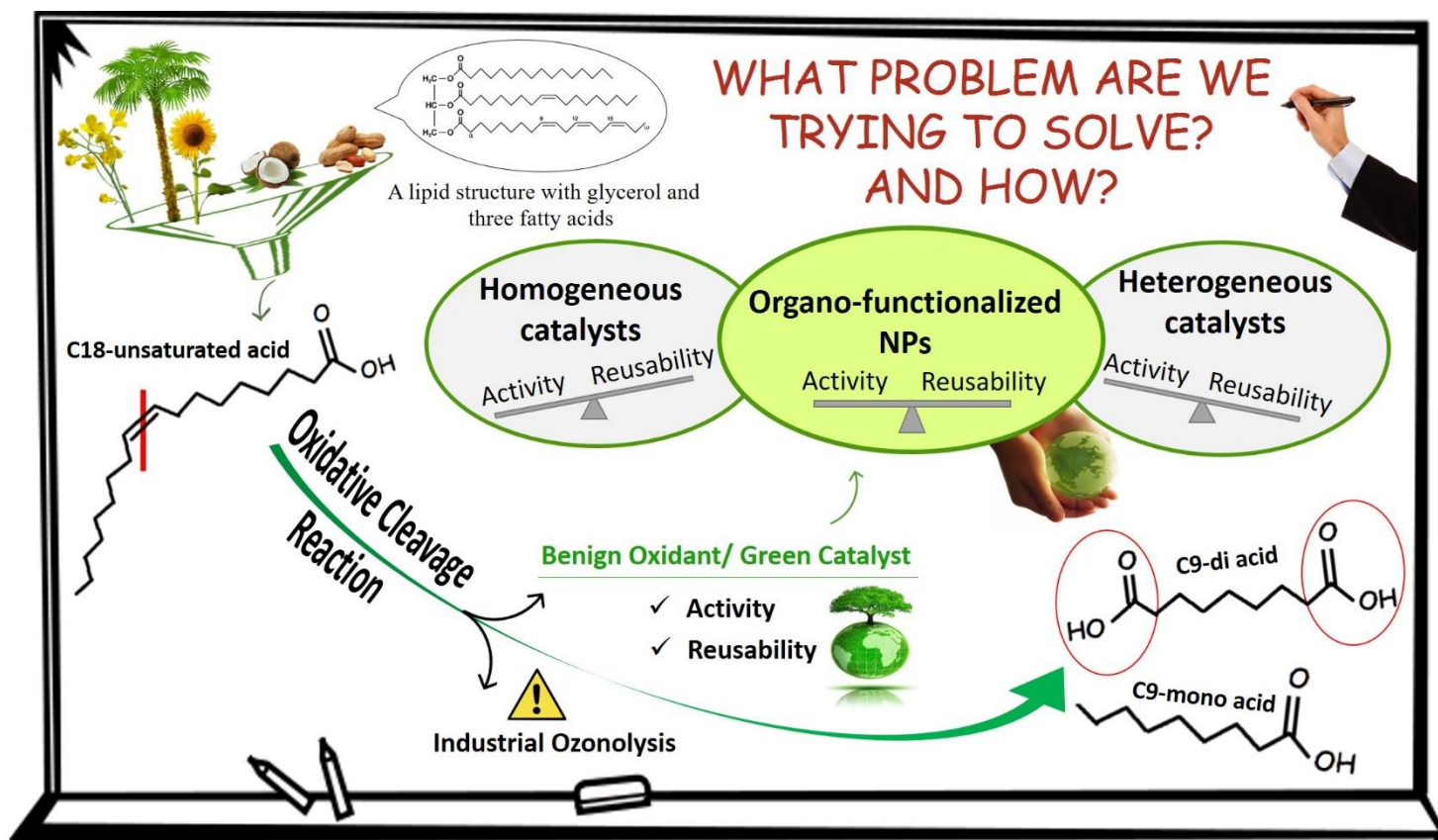
Chapter 5 has been published as A. Enferadi Kerenkan, A. S. Ello, T. O. Do, “*Synthesis, organo-functionalization, and catalytic properties of tungsten oxide nanoparticles as heterogeneous catalyst for oxidative cleavage of oleic acid as a model fatty acid into diacids*”, *Industrial & Engineering Chemistry Research*, 2017, 56 (38), 10639-10647.

Chapter 6 has been published as A. Enferadi Kerenkan, A. Gandon, T. O. Do, “*Novel tetra propyl/butyl ammonium encapsulated Keggin-type polyoxotungstates: synthesis, structural characterization, and catalytic capability in oxidative cleavage of unsaturated fatty acids*”, *Dalton Transactions*, 2017, DOI: 10.1039/C7DT04469K.

Chapter 7 has been published as A. S. Ello, A. Enferadi Kerenkan, A. Trokourey, T. O. Do, (equal contribution of the first two authors) “*Sustainable oxidative cleavage of vegetable oils into diacids by organo-modified molybdenum oxide heterogeneous catalysts*”, *Journal of the American Oil Chemists' Society*, 2017, 94, 1451-1461.

In the latter paper (Chapter 7), the candidate contributed equally with Dr. Aimé Serge Ello to the work. In all other papers, the candidate designed and performed all the experiments under the supervision of Prof. Trong On Do, and the help from other coauthors. The candidate collected the data and wrote the first drafts of all manuscripts. All the authors revised the manuscripts prior to publication.

# Chapter 1. Introduction



In this chapter, seminal concepts of the oleochemical science and oxidative cleavage of oleic acid are quite succinctly presented to bring up the problem statement, and then, the scope and organization of the thesis are elucidated.

## 1.1 Problem statement

Nowadays, sustainable development in the field of chemistry has propelled the industry to utilize renewable raw materials, which exploit the synthetic capabilities of nature, instead of petroleum materials. Among all feedstock materials, oils and fats of vegetable and animal origins have attracted considerable attention over the past decades. This attention arises from not only the environmental reasons, but also economic ones. Unsaturated fatty acids (UFAs) with long hydrocarbon chain, which are the constituent of lipids molecules, have several functional sites for chemical modifications in their structures. Accordingly, a variety of products with different properties can be obtained from the reactions of oils and fats.

In polymer industry, dicarboxylic acids are precious materials to make building blocks for polymers. These acids can be produced from UFAs via oxidation process. At present, azelaic acid (C<sub>9</sub>, dicarboxylic acid) as a very industrially important chemical is produced in large scale via ozonolysis of oleic acid (C<sub>18</sub>:1, the most widely distributed and abundant UFA). Pelargonic acid (C<sub>9</sub>, monocarboxylic acid) is obtained as a co-product but also a valuable chemical [1]. These types of saturated acids that have short and odd hydrocarbon chains are rare in natural resources [2]. On the other hand, they are very attractive initial materials for the development of numerous bio-based products [3,4]. For instance, azelaic acid converts into different esters for the preparation of polymers (Nylon 6:9), plasticizers, adhesives, solvents, biodegradable lubricants, corrosion inhibitors, and anti-acneic agent for cosmetics [2,3]. Pelargonic acid is an intermediate in the production of lubricants, plasticizers, perfumes, herbicides, fungicides, resins [3,5].

A variety of non-eco-friendly problems associated with use of ozone, however, is not in line with the principles of sustainable chemistry, and therefore, developing an industrial alternative to the hazardous ozonolysis of oleic acid would be a great breakthrough in industry. This alternative process requires a highly efficient catalyst/oxidant system. Combination of hydrogen peroxide with transition metal compounds would be a promising candidate, since such systems have shown high oxidizing ability, particularly in homogeneous form in lab scale. Large scale applications of the homogeneous catalysts, however, have been always a controversial challenge to the industry, due to the lack of recyclability. On the other hand, catalytic activity of the heterogeneous catalysts, with high recyclability, in liquid phase reactions of lipids, roughly speaking, is not comparable to that of homogeneous ones, which

has been often ascribed to the poor reactant/catalyst contact. To address this matter, this research project was planned about five years ago.

## 1.2 Scope of the research

The primary goal of this research project is to propose a new alternative process for the hazardous ozonolysis of UFAs via developing a highly efficient catalyst for the liquid phase oxidative cleavage of oleic acid with hydrogen peroxide. Use of the green and safe H<sub>2</sub>O<sub>2</sub> as oxidant produces only water as a waste product. Given the outlook of this research toward the large-scale applications and based on what the industrial partner of the project, Oleotek Inc., desired, the economic aspects of the process were highly considered. In doing so, our interest was focused on development of a catalysts that possesses efficient and facile recyclability as well as low-cost preparation, in addition to the excellent activity. Therefore, we have tried a variety of synthetic approaches with different precursors, but we ignored those approaches and materials that not only were costly, but also, held often the lab-scale fascination. In this thesis, we have tried to present our most important findings with the utmost conciseness consistent with clarity. Since the subject and field of this research were completely new in our group, we have pioneered a number of methodologies, particularly regarding the analysis of fatty acids with GC-MS. Such seminal works, along with designing the equipment and experimental setup, although were laborious, have not been reported in this thesis. Otherwise, the thesis would be too lengthy and tedious for the readership.

In order to follow a systematic research path for this PhD project, first, all the reported works in literature on different catalyst/oxidant systems for oxidation of UFAs and their derivatives were reviewed. This comprehensive study not only elucidated the plan of our further works, but also resulted in publishing a review paper. We found that among all the used transition metals as catalytic core in such reactions (Os, Co, Ru, Cr, Au, Mn, Fe, Mo, and W), tungsten has attracted a great deal of attention. Homogeneous tungsten-based catalysts have exhibited high potentials in oxidation of UFAs, however with generally low recovery efficiency. Then, our focus was placed, chiefly, on tungsten-based heterogeneous catalysts. Additionally, molybdenum as a metal inherently close to tungsten, which has occasionally shown even better catalytic activity, was our secondary interest.

In order to overcome the reported drawbacks of conventional solid catalysts in the reactions of oils and fats (e.g. low catalyst/reactant contact and pore diffusion limitations), we examine different strategies in the following chapters including:

- Increasing the catalyst's surface area via incorporation of the active sites in a mesostructured support to reach a higher dimensionality of the interaction between the organic reactant and the catalyst's surface (Chapter 4).
- Preparation of nanocatalysts to increase the dispersion of the solid catalysts in the reaction medium (Chapters 4, 5, and 7)
- Exploiting organo-functionalization of the solid catalyst's surface with different organic moieties, to enhance the compatibility of the hybrid organic-inorganic catalyst in the reaction (Chapters 5, 6, and 7).
- Employing the fascinating solid acid catalyst, polyoxotungstates, which their lack in the reported works on oxidation of UFAs is curious (Chapter 6).
- Evaluation of molybdenum oxide catalysts in the reaction (Chapter 7)

### **1.3 Organization of the thesis**

This short introduction chapter is followed by Chapter 2, which contains our theoretical studies on the subject. In this chapter, first the fundamentals of oils and fats as renewable raw materials and their applications in oleochemical industries, with an emphasis on the target application, are presented (section 2.1). Then, the basic concepts and seminal studies of UFAs and their reactions, which have been widely reviewed [6-9], with an emphasis on oxidation will be shortly summarized (section 2.2) in order to approach to the main topic. The recent works regarding use of different catalyst/oxidant systems in the oxidative cleavage of UFAs and their derivatives will be then discussed (section 2.3). Herein, we divided the reported catalytic systems into three classes: homogenous, heterogeneous, and semi-heterogeneous (NP-based) catalysts. Important features such as catalytic activity and recoverability with specific respect to commercializing viewpoint are discussed in a critical fashion for each class to be able to reasonably plan future works. The unique and interesting properties of NPs propose them as the frontier of homogeneous and heterogeneous catalysts that can

simultaneously exploit the best features of both. These properties along with the recent breakthroughs which would interestingly increase the performance of NP-based catalysts in the biphasic oxidative cleavage reaction of UFAs, are also reviewed. Finally, in section 2.4, we thoroughly discuss heterogeneous catalysis by tungsten-based polyoxometalates, after brief introductions on (i) the interesting inherent properties of tungsten (section 2.4.1), and (ii) the fundamentals of POMs (section 2.4.2). We have tried to review all the recent works on solid polyoxotungstate catalysts and their applications in liquid phase organic reactions. We have divided the reported works into four groups, based on the heterogenization strategy that they used to solidify the inherently homogeneous POTs (sections 2.4.3.1-4). Also, the target organic reaction, although it includes a variety of reactions, has been classified into two major classes, oxidation reaction and acid catalysis reactions, to gain a better outcome.

In Chapter 3, the characterization techniques employed throughout our works are explained (section 3.1), however with the utmost conciseness, since details of these methods are not only beyond the scope of this thesis, but also available in many books. We have succinctly reviewed the fundamentals of each method along with bolding the information that we acquired from them. Then, we will explain, in details, the quantitative analysis of the reaction products with GC-MS, along with the sample preparation prior to injection and calculation procedure of the reaction efficiency (section 3.2).

In Chapter 4, we report a solvothermal synthesis method for preparation of high surface area mesoporous  $\text{WO}_3$  supported on  $\gamma$ -alumina with narrow particle size distribution using glucose as template. This chapter chiefly concentrates on increasing the catalyst surface area via incorporation of the active sites in the mesostructured support, followed by examination of this increase in the catalytic activity of the prepared catalysts by changing the ratio of  $\text{WO}_3/\text{Al}_2\text{O}_3$ .

In Chapter 5, we present syntheses of different structures of tungsten oxide like  $[(\text{WO}_2)\text{O}_2\cdot\text{H}_2\text{O}]$ ,  $\text{WO}_3$ ,  $\text{WO}_3\cdot 0.33\text{H}_2\text{O}$ , and  $\text{WO}_3\cdot\text{H}_2\text{O}$  via a straightforward and green method based on oxidative dissolution of bare W powder in  $\text{H}_2\text{O}_2$ . Moreover, organo-functionalization of the nanocatalysts surfaces by CTAB is reported. The key features of this approach are using cheap W powder as precursor, avoiding use of time- and energy-consuming operations in the synthetic procedure such as thermal treatment in autoclave and purification, as well as avoiding use of organic solvents, metal salts, and/or coordination compounds. Optimization of the organic moiety amount on the surface of catalyst is, also, discussed.

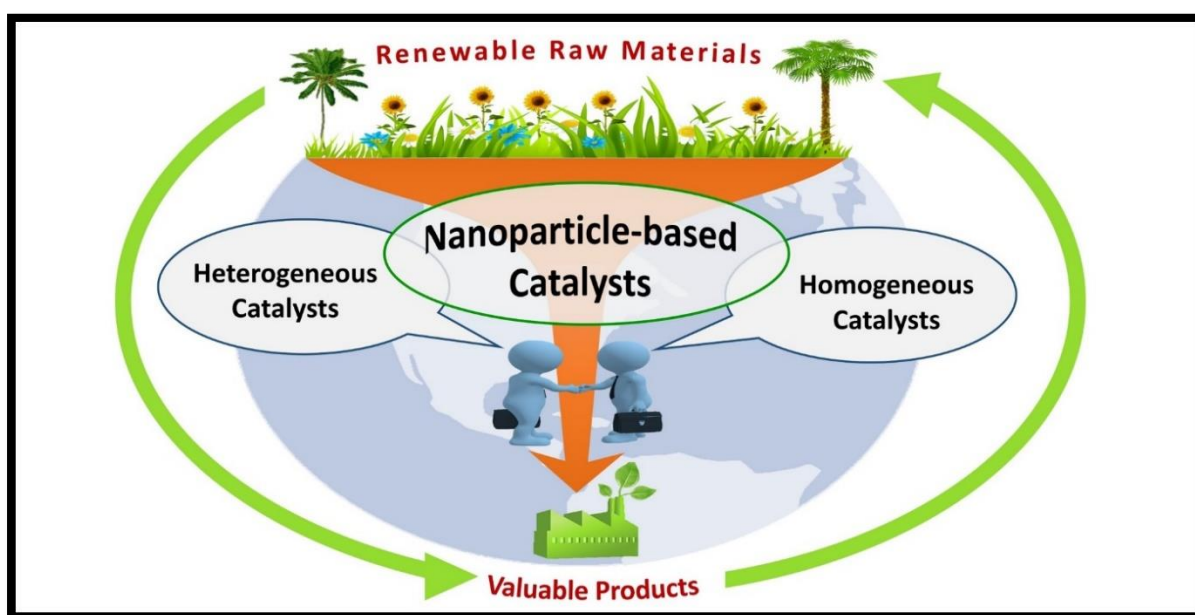
In chapter 6, we introduce a novel, one-pot, and green synthesis method, complying with the principles of “Chimie Douce”, for preparation of hybrid organic-inorganic POTs, starting with tungsten powder as precursor, by contrast to the prior methods that often use phosphotungstic or tungstic acid. Two novel hybrid organic-inorganic Keggin compounds are introduced in this chapter:  $\text{TPA}_x[\text{H}_{8-x}\text{W}_{12}\text{O}_{40}] \cdot n\text{H}_2\text{O}$  and  $\text{TBA}_x[\text{H}_{8-x}\text{W}_{12}\text{O}_{40}] \cdot n\text{H}_2\text{O}$  (TPA: tetrapropylammonium and TBA: tetrabutylammonium). Furthermore, a pioneer application for solid POT catalysts in the oxidative cleavage of oleic acid is reported in this chapter.

Chapter 7, includes the results of our works on molybdenum oxide catalysts, synthesized via almost the same synthesis approach as Chapter 5. Organo-functionalization by two quaternary ammonium cations with different lengths, CTAB and TMA (tetramethylammonium), and effects of concentration of these organic surfactants on physicochemical properties and catalytic activities of the products are also reported.

In Chapter 8, we highlight the major conclusions derived from the works in this research. Suggestions to foster the future works are also succinctly presented.



## Chapter 2. Chemically catalyzed oxidative cleavage of unsaturated fatty acids and their derivatives



This chapter provides an introduction to the field of oleochemical science. The recent works regarding use of different catalysts in oxidative cleavage of unsaturated fatty acids and their derivatives are reviewed. Furthermore, tungsten-based heteropoly compounds and their applications in organic liquid reactions are discussed.

## 2.1 Oils and fats as renewable raw materials

Facing with the warning “sorry, out of gas” in near future is one of the most concerning challenges in all around the world nowadays. During the last decades, fossil feedstock derived from oil and gas has always been the most important raw materials for the chemical industry, accounting for more than 90%. Even with this enormous amount, chemical industries have occupied the third position as the user of oil and gas feedstock, after energy generation and transportation [10]. Understandably, the shortage in the petroleum reservoirs in the near future is a worldwide crisis which can be confirmed by Figure 2.1 [11]. It shows the oil and gas production profiles in the past and future for the whole earth which was published in an ASPO<sup>1</sup> Newsletter in 2009. As can be seen, starting from 2010, a downward trend is obvious in the oil and gas production.

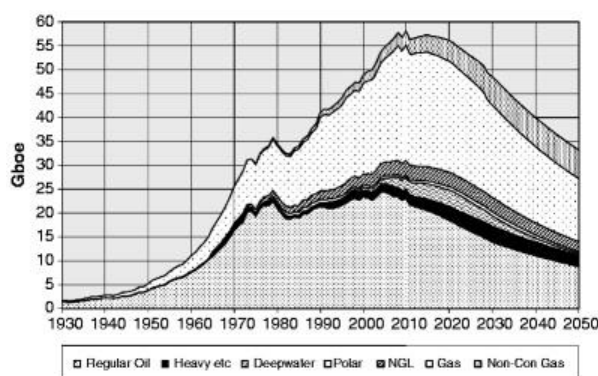


**Figure 2.1.** Production profiles of oil and gas 2010 base case (Gboe: gigabarrels of oil equivalent) [11]

In addition, global concerns for environmental pollutions associated with petroleum materials have propelled the attention of researchers to the renewable raw materials. Among feedstock from renewable resources, oils and fats of vegetable and animal origin could become one of the major players in the chemical industry in near future, due to not only the economic reasons, but also environmental ones [8,12]. Oils and fats have chemical structures giving them a potential for the industrial development in the field of feedstock materials [13]. On one hand, their structures are similar to petroleum materials with long hydrocarbon chains. On the other hand, they include several functional sites for chemical modifications. Moreover, they are abundant in nature, biodegradable, and have nontoxic properties that make them promising candidates for replacing petrochemical materials.

<sup>1</sup> The association for the study of peak oil and gas

## 2.1.1 Globalization of oils and fats

Oils and fats differ in the state of material; oils are often liquid at ambient temperature, but fats are solid. They are derived from vegetable origins such as palm, soybean, rapeseed (canola), sunflower seed (so-called four major vegetable oils), palm kernel, coconut and olive, or animal origins such as butter, lard, tallow, and fish oil. There is no widely-accepted definition for lipid, but the one which is presented by AOCS<sup>2</sup> would be the best [14]: “Lipids are fatty acids and their derivatives, and substances related biosynthetically or functionally to these compounds.”

Nowadays, extraction of oils and fats from bio-based materials is being rapidly globalized. Oilseeds are obtained in all over the world, under all sorts of climates, in both northern and southern hemispheres and from a variety of plants. In the recent 30 years, production of oilseeds has dramatically increased (see Figure 2.2). Rising from about 190 million tons in 1985 to more than 453 million tons in 2011 shows a 136% increase in the production of the major 10 oilseeds (soybeans, cotton seed, rapeseed, sunflower seed, groundnuts (shelled), sesame seed, palm kernels, copra, linseed and castor seed) in a period of 26 years. It makes more sense when compared with the “grains” (wheat, coarse grains and rice) with only 34% increase in production in the same period. In addition, the area of harvest of oilseeds rose from 160 million hectares to 260 million hectares during the same period, which in turn confirms the increase in productivity from 1.19 tons/hectare in 1985 to 1.74 tons/hectare in 2011 [15].

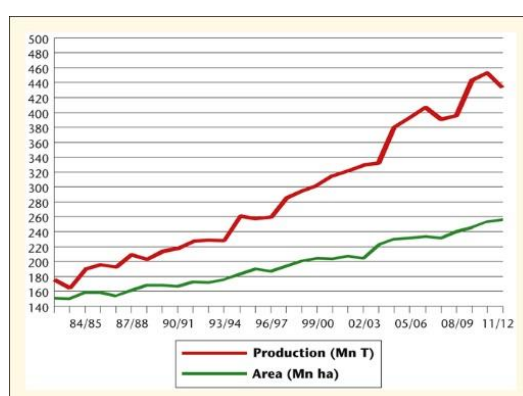


**Figure 2.2.** World area and production of the major 10 oilseeds (soybeans, cotton seed, rapeseed, sunflower seed, groundnuts (shelled), sesame seed, palm kernels, copra, linseed and castor seed) [15].

<sup>2</sup> The American oil chemists' society

From the total production of about 450 million tons in 2011, more than 57% of all oilseeds were produced in the Americas continent, as Figure 2.3 shows [15]. However, Figure 2.4 indicates that in terms of consumption, Asia continent had a higher rank than Americas [15]. In addition, despite the fact that overall world consumption had about 99% growth in the period of 1996 to 2012, the portion of the Americas continent decreased from 22.8% to 19.5%. One reason would refer to the use of oils and fats as human foods and higher populations increase rate in Asia, because the majority of yearly produced oils and fats are, these days, used in food industries [6].

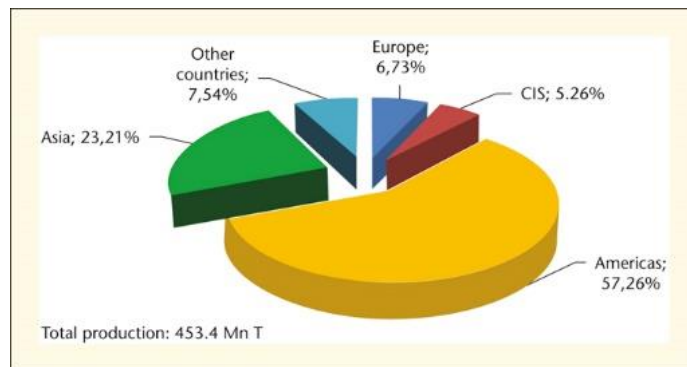


**Figure 2.3.** World production of oilseeds by main regions (Year 2011) [15].

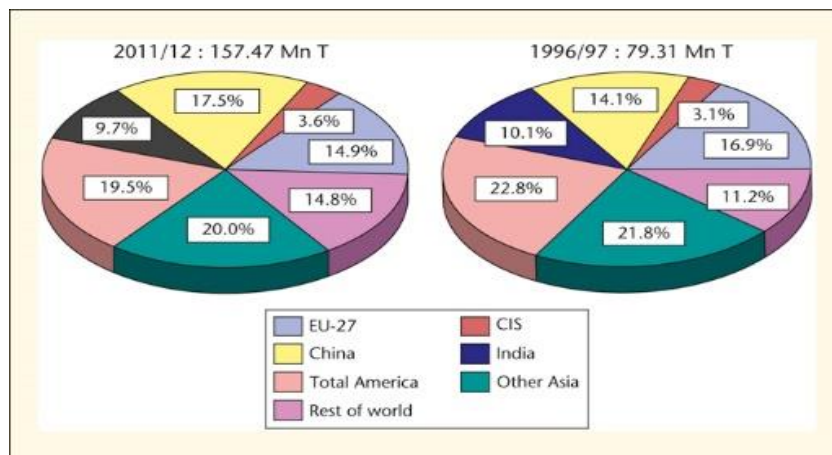


**Figure 2.4.** Consumption of vegetable oils by major countries (MnT) (year 2011/12 vs. 1996/97) [15].

Presenting some statistical data about the different industrial users of oils and fats in the world, would give a better outlook. In addition to the food industry, oils and fats are used as the basis of the oleochemical industry, as well as a very small portion for animal feeds. Interestingly, a significant growth in the portion of non-food uses is obvious in the data presented in Table 2.1 [16]. It shows the distribution of nine major vegetable oils (coconut, cottonseed, olive, palm, palm kernel, peanut, rapeseed, soybean, and sunflower) between non-

food and food use over the last recent years. Since the year 1999 to 2012, the non-food portion has increased from 10.5 to 23.9%. This increase is particularly remarkable from 2003/04 onwards.

Table 2.1. Food and non-food consumptions (million tons and %) of nine major vegetable oils between 1999/00 and 2011/12 [16].

	TOTAL	FOOD	NON-FOOD	NON-FOOD %
1999/00	82.9	74.2	8.7	10.5
2000/01	88.8	78.6	10.2	11.5
2001/02	91.1	80.2	10.9	12.0
2002/03	95.1	82.9	12.2	12.8
2003/04	100.7	86.9	13.8	13.7
2004/05	108.2	91.5	16.7	15.4
2005/06	114.7	94.2	20.5	17.9
2006/07	119.4	95.9	23.5	19.7
2007/08	125.1	98.8	26.3	21.0
2008/09	129.7	101.4	28.3	21.8
2009/10	137.8	106.4	31.4	22.8
2010/11	144.6	110.9	33.7	23.3
2011/12	150.0	114.2	35.8	23.9

According to what was mentioned above, it can be concluded that a significant growth in the production of oils and fats in the recent years is clear in all around the world. One reason would be the human food use of oils and fats and growing populations of the world. Data in Table 2.1, however, confirms the increasing rate of non-food use of oils and fats in the world, in particular during the last decade. This makes it highly desirable to conduct extensive researches in this field in the region of the Americas continent.

### 2.1.2 Oleochemical industries

Oleochemical industries are those which exploit oils and fats to produce valuable materials. They are being rapidly developed as a result of the rapid globalization of such feedstock. In order to use oils and fats in the advanced chemical industries, it is necessary to split them into the so-called oleochemical base materials [17]. The lipids are made from triglyceride, which, in turn, consists of glycerine and three fatty acids (Figure 2.5) [7]. The triglycerides which form animal fats, typically have more saturated fatty acids while those triglycerides constitute vegetable oils, have more unsaturated fatty acids [18] (for more information about saturated and unsaturated fatty acids see section 2.2.1).

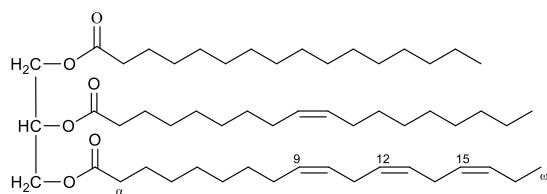


**Figure 2.5.** Typical example of a lipid structure with glycerol and three fatty acids (palmitic acid, oleic acid, and alpha-linolenic acid, from top to bottom) [7].

Decomposition of the triglycerides results in the release of oleochemical base materials which are shown in Figure 2.6. They mainly include fatty acids (ca. 52%), fatty acid methyl esters (ca. 11%), fatty amines (ca. 9%), and fatty alcohols (ca. 25%) [6] [19].

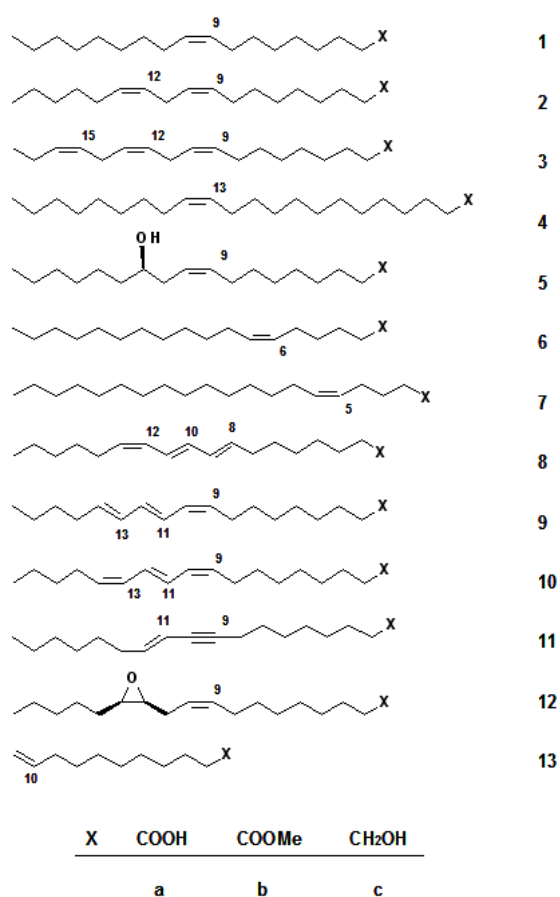


**Figure 2.6.** Oleochemical base materials as starting materials for chemical industries: oleic acid (1a), linoleic acid (2a), linolenic acid (3a), erucic acid (4a), ricinoleic acid (5a), petroselinic acid (6a), 5-eicosenoic acid (7a), calendic acid (8a),  $\alpha$ -eleostearic acid (9a), punicic acid (10a), santalbic acid (11a), vernolic acid (12a), 10-undecenoic acid (13a), and the respective methyl esters (1b-13b) and alcohols (1c-13c) [20].

The oleochemical base materials have a variety of chemical applications that is scarcely less than that of petrochemicals [6,17]. Table 2.2 summarizes these applications. Polymer is one of the most important industries which can exploit lipids and convert them into valuable products. Next section will be detailed on this.

**Table 2.2.** Summary of the applications of basic oleochemicals.

Oleochemical base materials	Applications
Fatty acids and derivatives (52 %)	Plastics; metal soaps; washing and cleaning agents; soaps; alkyd resins; dyestuffs; textile, leather and paper industries; rubbers; lubricants
Fatty acid methyl esters (11 %)	Cosmetics; toothpastes; pharmaceuticals; foodstuffs; lacquers; plastics; synthetic resins; tobacco; explosives; cellulose processing
Fatty alcohols and derivatives (25 %)	Washing and cleaning agents; cosmetics; textile, leather and paper industries; mineral oil additives
Fatty amines and derivatives (9 %)	Fabric conditioners; mining; road-making; biocides; textile and fiber industries; mineral oil additives
Neutral oils and derivatives	Lacquers; dyestuffs; varnishes; linoleum, soaps

### 2.1.2.1 Polymer industry

Oils and fats have been employed in polymer industry for many years, either in the form of triglycerides or oleochemical base materials. The main applications are categorized in three groups in Table 2.3 including polymer materials (linseed oil and soybean oil as drying oils), polymer additives (epoxidized soybean oil as plasticizer), and building blocks for polymer (dicarboxylic acids for polyesters or polyamides) [9]. Such applications are currently undergoing rapid development to extend scope of the specialty and commodity products. One of the most important applications is preparing building blocks for polymers. Long-chain dicarboxylic acids required for this purpose, are the major product of complete oxidation of unsaturated fatty acids. There are numerous reactions in which unsaturated fatty acids could be involved and form a variety of products (more information in section 2.2.2). In these reactions, carboxylic groups or the carbon-carbon double bonds of unsaturated fatty acids can take part. The oxidation of unsaturated fatty acids includes partial or complete cleavage of the carbon-carbon double bond(s). The latter results in obtaining mono- and dicarboxylic acids.

#### 2.1.2.1.1 Long-chain dicarboxylic acids

Dicarboxylic acids,  $\text{HOOC}(\text{CH}_2)_n\text{COOH}$  ( $n$  represents the number of methylene groups and their derivatives, see Figure 2.7), are industrially important chemicals due to their potential in the production of various intermediates [21]. As mentioned in Table 2.3, long-chain dicarboxylic acids are used as polymer intermediates in polyamides, polyesters, and alkyd

resins. One of the most striking polymers obtained from dicarboxylic acids is nylon 1313 (produced from brassylic acid) which interestingly shows enhanced properties in comparison with common nylons (a lower melting point, lower density, and more hydrophobicity than nylon-11 and nylon-12) [22]. Furthermore, the esters of dicarboxylic acids are used as lubricants and hydraulic fluids over a wide temperature range [21], as well as plasticizers for polyvinyl chloride [21,20].

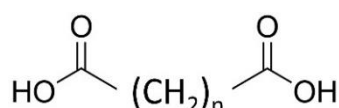


**Figure 2.7.** A dicarboxylic acid with two carboxyl groups as a valuable chemical in the polymer industry.

Dicarboxylic acids are produced from petrochemical feedstock (e.g., production of adipic acid from the multistage butadiene oxidation [23]). Also, ring-opening oxidation of cyclic compounds is another route to produce these chemicals [1]. Biotechnology techniques have been also developed for this purpose [24]. Until recently, the production of only two of these dicarboxylic acids from oleochemical base materials has been commercialized, including sebacic acid which is obtained by alkaline cleavage of castor oil [1] and azelaic acid which is produced from oxidation of oleic acid through ozonolysis [25]. Surprisingly, these oleochemically derived dicarboxylic acids can simplify condensation of the polymers, as a result of their special properties such as high impact strength, hydrolytic stability, hydrophobicity, lower glass transition temperatures, and flexibility [26,9].

**Table 2.3.** Examples of applications of oils and fats in polymer industry [9].

Raw materials (oleochemical base or triglycerides)	Product	Application	Category
Castor and soybean oils Linseed oil	Polymerized castor and soybean oils Polymerized linseed oil	Drying oils Linoleum	Polymer materials
Soybean oil Rapeseed oil Stearic acid	Epoxides Fatty acid esters and amides Soaps	Stabilizers and plasticizers Lubricants, Stabilizers	Polymer additives
Castor, soybean, sunflower, linseed, and tall oils and oleic acid	Dicarboxylic acids and ether/ester polyols	Polyamides, polyesters, alkyd resins, and polyurethanes	Building blocks for polymers



## 2.2 Fatty acids and their reactions

### 2.2.1 Fatty acids: a primer

As mentioned earlier, the constituents of lipids are fatty acids. A general definition of fatty acids is a carboxylic acid with a long hydrocarbon chain, which consists of two parts: hydrophilic carboxyl group and hydrophobic alkane chain (Figure 2.8).

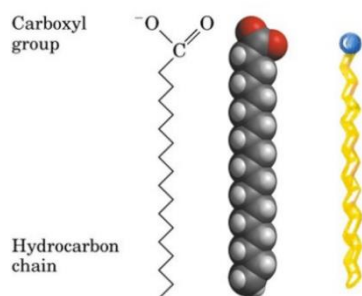


**Figure 2.8.** Fatty acids structure.

In the most generic classification, fatty acids are divided into saturated (without carbon-carbon double bond) and unsaturated (with carbon-carbon double bond(s)) types. UFAs can, in turn, be categorized in mono-unsaturated (with one double bond) and poly-unsaturated (with more than one double bonds). The two carbon atoms just near the double bond can occur in *cis* or *trans* configurations. However, most of naturally UFAs have *cis* configuration [27].

The common UFAs derived from vegetable oils, have 16 to 18 carbons in their hydrocarbon chain with up to three double bonds. Animal fats, in addition to these UFAs, contain other even carbon numbered fatty acids, such as  $C_{20}$  and  $C_{22}$ , and up to six double bonds (in fish oils) [14]. Table 2.4 shows the common fatty acids extracted from animal and plant origins with their structures and different nomenclature systems [14,28]. In nature, the most abundant saturated fatty acid is palmitic acid ( $C_{16}$ ) and the most abundant monounsaturated fatty acid is oleic acid ( $C_{18}$ ) [29]. The  $C_{18}$  polyunsaturated fatty acids like linoleic or *cis*-9, *cis*-12-octadecadienoic acid ( $18:2(n-6)$ ) and  $\alpha$ -linolenic or *cis*-9, *cis*-12, *cis*-15-octadecatrienoic acid ( $18:3(n-3)$ ), are also of the main components of most plant lipids, including many of the commercially important vegetable oils. The structures of these  $C_{18}$  unsaturated fatty acids are shown in Figure 2.9.

**Table 2.4.** Common fatty acids of animal and plant origins; structures and nomenclature systems [28,4].

Systematic name	Common name	Chemical structure	Shorthand
<b>Saturated fatty acids</b>			
Ethanoic	Acetic	CH <sub>3</sub> COOH	2:0
Butanoic	Butyric	CH <sub>3</sub> (CH <sub>2</sub> ) <sub>2</sub> COOH	4:0
Hexanoic	Caproic	CH <sub>3</sub> (CH <sub>2</sub> ) <sub>4</sub> COOH	6:0
Octanoic	Caprylic	CH <sub>3</sub> (CH <sub>2</sub> ) <sub>6</sub> COOH	8:0
Decanoic	Capric	CH <sub>3</sub> (CH <sub>2</sub> ) <sub>8</sub> COOH	10:0
Dodecanoic	Lauric	CH <sub>3</sub> (CH <sub>2</sub> ) <sub>10</sub> COOH	12:0
Tetradecanoic	Myristic	CH <sub>3</sub> (CH <sub>2</sub> ) <sub>12</sub> COOH	14:0
Hexadecanoic	Palmitic	CH <sub>3</sub> (CH <sub>2</sub> ) <sub>14</sub> COOH	16:0
Octadecanoic	Stearic	CH <sub>3</sub> (CH <sub>2</sub> ) <sub>16</sub> COOH	18:0
Eicosanoic	Arachidic	CH <sub>3</sub> (CH <sub>2</sub> ) <sub>18</sub> COOH	20:0
Docosanoic	behenic	CH <sub>3</sub> (CH <sub>2</sub> ) <sub>20</sub> COOH	22:0
<b>Monounsaturated fatty acids</b>			
<i>cis</i> -9-hexadecenoic	Palmitoleic	CH <sub>3</sub> (CH <sub>2</sub> ) <sub>5</sub> CH=CH(CH <sub>2</sub> ) <sub>7</sub> COOH	16:1(n-7)
<i>cis</i> -6-octadecenoic	Petroselinic	CH <sub>3</sub> (CH <sub>2</sub> ) <sub>10</sub> CH=CH(CH <sub>2</sub> ) <sub>4</sub> COOH	18:1(n-12)
<i>cis</i> -9-octadecenoic	Oleic	CH <sub>3</sub> (CH <sub>2</sub> ) <sub>7</sub> CH=CH(CH <sub>2</sub> ) <sub>7</sub> COOH	18:1(n-9)
<i>cis</i> -11-octadecenoic	<i>cis</i> -vaccenic	CH <sub>3</sub> (CH <sub>2</sub> ) <sub>5</sub> CH=CH(CH <sub>2</sub> ) <sub>9</sub> COOH	18:1(n-7)
<i>cis</i> -13-docosenoic	Erucic	CH <sub>3</sub> (CH <sub>2</sub> ) <sub>7</sub> CH=CH(CH <sub>2</sub> ) <sub>11</sub> COOH	22:1(n-9)
<i>cis</i> -15-tetracosenoic	Nervonic	CH <sub>3</sub> (CH <sub>2</sub> ) <sub>7</sub> CH=CH(CH <sub>2</sub> ) <sub>13</sub> COOH	24:1(n-9)
<b>Polyunsaturated fatty acids</b>			
9,12-octadecadienoic	linoleic	CH <sub>3</sub> (CH <sub>2</sub> ) <sub>4</sub> CH=CHCH <sub>2</sub> CH=CH(CH <sub>2</sub> ) <sub>7</sub> COOH	18:2(n-6)
9,12,15-octadecatrienoic	$\alpha$ -linolenic	CH <sub>3</sub> CH <sub>2</sub> CH=CHCH <sub>2</sub> CH=CHCH <sub>2</sub> CH=CH(CH <sub>2</sub> ) <sub>7</sub> COOH	18:3(n-3)
6,9,12-octadecatrienoic	$\gamma$ -linolenic	CH <sub>3</sub> (CH <sub>2</sub> ) <sub>4</sub> CH=CHCH <sub>2</sub> CH=CHCH <sub>2</sub> CH=CH(CH <sub>2</sub> ) <sub>4</sub> COOH	18:3(n-6)
5,8,11,14-eicosatetraenoic	arachidonic	CH <sub>3</sub> (CH <sub>2</sub> ) <sub>4</sub> CH=CHCH <sub>2</sub> CH=CHCH <sub>2</sub> CH=CHCH <sub>2</sub> CH=CH(CH <sub>2</sub> ) <sub>3</sub> COOH	20:4(n-6)
5,8,11,14,17-eicosapentaenoic	EPA	CH <sub>3</sub> CH <sub>2</sub> CH=CHCH <sub>2</sub> CH=CHCH <sub>2</sub> CH=CHCH <sub>2</sub> CH=CHCH <sub>2</sub> CH=CH(CH <sub>2</sub> ) <sub>3</sub> COOH	20:5(n-3)
4,7,10,13,16,19-docosahexaenoic	DHA	CH <sub>3</sub> CH <sub>2</sub> CH=CHCH <sub>2</sub> CH=CHCH <sub>2</sub> CH=CHCH <sub>2</sub> CH=CHCH <sub>2</sub> CH=CHCH <sub>2</sub> CH=CH(CH <sub>2</sub> ) <sub>2</sub> COOH	22:6(n-3)

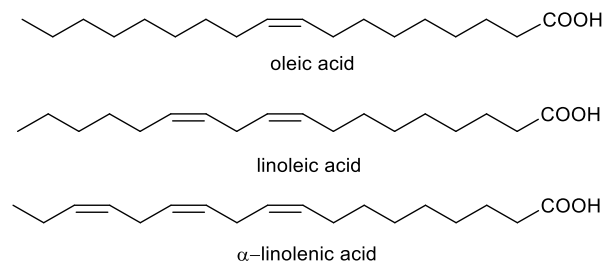


**Figure 2.9.** Different C18 mono and poly-UFAs.

Presence of the rigid double bond(s) in *cis*-unsaturated fatty acids causes the chain to bend. The increase in such double bonds decreases the flexibility of the chain and results in more curved shape of the chain. As can be seen in Figure 2.10, oleic acid with one double bond, has a “kink” in it, whereas the curvatures in linoleic acid, with two double bonds, and  $\alpha$ -linolenic acid, with three double bonds, are more intense [30]. The direct result is that the presence of *cis* bonds prevents tight packing of fatty acids in the molecules of triglycerides, and therefore the lipids formed by such acids, usually have liquid state at ambient temperature (so-called oils). By contrast, saturated fatty acids can tightly attach to form a solid-state lipid (so-called fats) (see Figure 2.11).

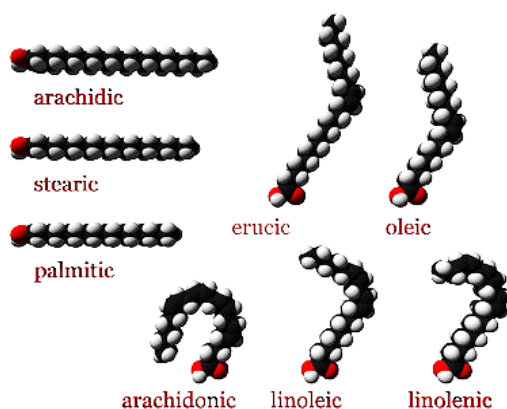


**Figure 2.10.** 3-D models of different fatty acid types. Arachidic, stearic, and palmitic acids are saturated. Erucic and oleic acids are monounsaturated, and linolenic, linoleic and arachidonic are polyunsaturated fatty acids [30].

### 2.2.1.1 Oleic acid

The most abundant mono-UFA in nature is oleic acid (C<sub>18</sub>) [29], which exists in various vegetable and animal oils and fats. Its systematic name is *cis*-9-octadecenoic acid with shorthand form 18:1 (n-9) that shows it has 18 carbon atoms with one carbon-carbon double bond on the ninth carbon atom (chemical formula CH<sub>3</sub>(CH<sub>2</sub>)<sub>7</sub>CH=CH(CH<sub>2</sub>)<sub>7</sub>COOH) [31]. Oleic acid,

like other fatty acids, mainly emerges in the form of triglycerides, and these oleic acid containing triglycerides constitute the majority of olive oils [32]. That is why it has been called "oleic" which means come from oil or olive. It is worth pointing out that these triglycerides are also available in relatively large amounts in pecan, peanut, macadamia, sunflower, grape seed, sea buckthorn, sesame, wild apricot seed, rapeseed, and poppyseed oils [33-35]. In addition, they are abundantly present in many animal fats such as chicken and turkey fat and lard [36].

Currently, although oleic acid has a variety of industrial applications like, as a component of human diet (in triglyceride form), major component of soaps (in sodium salt form), and in pharmaceuticals [31], the most important one is production of dicarboxylic acids via ozonolysis [25], which will be discussed further in section 2.2.2.1.2.

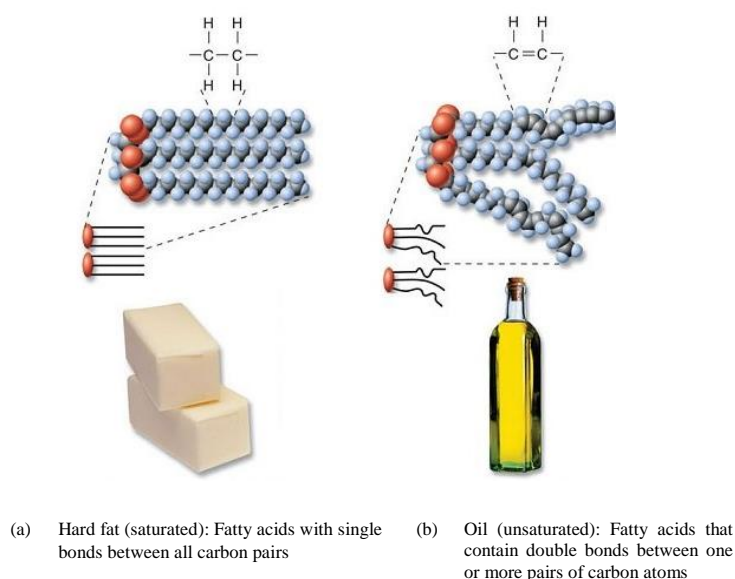


**Figure 2.11.** Effect of C=C in the packing of saturated and unsaturated fatty acids.

## 2.2.2 Reactions of unsaturated fatty acids

According to what was explained in the previous section, there are various functional sites in the structure of fatty acids. The differences between the length of aliphatic chain, geometry of the molecule (*cis* or *trans* configurations) and the number and position of C-C double bond(s), play a crucial role in biological processes, and consequently, lead to the possibility for variety of products even more than petrochemistry products [7].

The reactive sites in the structure of a fatty acid can be categorized in two parts; the double bond(s) in the chain and the acidic group. The majority of industrial reactions is carried out at the carboxylic group (>90%, in 2000), while remarkably very few industrial reactions (less than 10% in 2000) are involved in the hydrocarbon chain in oleochemical industries [9,7]. However, because of wider range of obtainable products from the latter, progress in such reactions is highly-demanded [7]. At present, converting natural oils into nonedible products is limited, mainly because of economic reasons; the production costs of oleochemical processes cannot compete effectively with mature petrochemical industries [37]. To address this problem and improve the economic aspects, optimization of reaction conditions and, also, employing efficient catalysts are called for. Oxidation of UFAs is one of the reactions that targets C-C double bond(s) which will be explained in the following section. Other reactions of fatty acids such as hydrogenation or hardening, metathesis, C-H bond activation, hydroxylation, pericyclic, radical additions, and Lewis acid induced cationic addition have been nicely and widely reviewed in the literature [7,29,6].

### 2.2.2.1 Oxidation

From the industrial point of view, oxidation of UFAs possesses a great importance, since it has shown considerable potentials in the production of invaluable materials. Dicarboxylic acids, as mentioned earlier, are a striking example of such products, on which, this research focuses. Herein, two main oxidation pathways of UFAs are discussed.

#### 2.2.2.1.1 Epoxidation

The carbon-carbon double bonds in oils and fats of vegetable and animals can be functionalized via epoxidation and, consequently, produce epoxidized oils and fats which contain epoxide groups or oxirane rings [38]. The term epoxide can be defined as a cyclic ether which has three ring atoms (Figure 2.12) and the general process for the synthesis of the epoxide groups is known as epoxidation reaction. Epoxides can be prepared from hydroperoxides, hydrogen peroxide, or molecular oxygen in the presence of different catalysts [39].

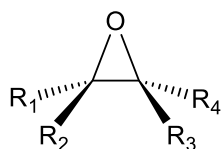
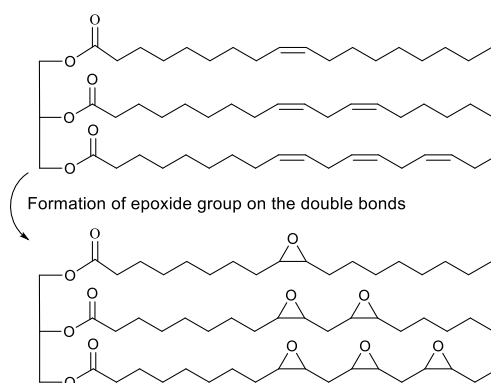


**Figure 2.12.** A generic epoxide.

Several methods have been reported for epoxidation of unsaturated fatty compounds such as *in situ* performic acid procedure, epoxidation with aldehydes and molecular oxygen, dioxiranes, H<sub>2</sub>O<sub>2</sub>/tungsten heteropolyacids, H<sub>2</sub>O<sub>2</sub>/methyl trioxorhenium, and enzymatic epoxidation [6,7,17]. Scheme 2.1 shows a typical epoxidation of a lipid including oleic acid, linoleic acid and  $\alpha$  linolenic acid and formation of epoxide groups on the C-C double bonds.

Although, the epoxidized oils and fats have their own valuable applications such as plastic additives [40,41], plasticizers [40], flame retardants [7], heat stabilizers [7], antioxidants and light stabilizers [7], lubricants, cosmetics and biochemical applications [42,43] (which are summarized in Figure 2.13) , obtaining dicarboxylic acids via epoxidation requires a further reaction of ring opening of epoxides which, in turn, often needs different catalysts. Therefore, epoxidation does not seem to be reasonable method to produce dicarboxylic acids.



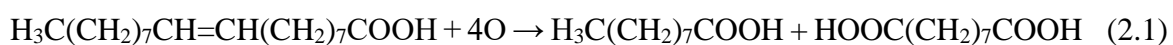
**Scheme 2.1.** Epoxidation of a lipid [7].

#### 2.2.2.1.2 Oxidative cleavage

The term “oxidative cleavage” in olefins generally means breaking carbon-carbon bonds and forming carbon-oxygen double bonds (see Scheme 2.2). Sometimes, carbon-hydrogen bonds get cleaved in addition to carbon-carbon bonds. Therefore, a variety of products such as alcohols, aldehydes or ketones, and carboxylic acids can be obtained depending on the type of bond being oxidized and the reaction conditions [44].

Oxidative cleavage of olefins in large-scale typically occurs by ozonolysis with high yield. Ozone, O<sub>3</sub>, is an allotrope of oxygen that can be added rapidly to the carbon-carbon double bonds,

and transform alkenes into aldehydes or carboxylic acids without the use of a metal as catalyst [44]. Currently, azelaic acid (C9, dicarboxylic acid) as a very industrially important chemical is produced in large-scale via ozonolysis of oleic acid (Equation 2.1). Pelargonic acid (C9, monocarboxylic acid) is obtained as a co-product but also a valuable chemical [1]. These types of saturated acids that have short and odd hydrocarbon chains are rare in natural resources [2]. On the other hand, they are very attractive initial materials for the development of numerous bio-based products [3,4]. For instance, azelaic acid converts into different esters for the preparation of polymers (Nylon 6:9), plasticizers, adhesives, solvents, biodegradable lubricants, corrosion inhibitors, and anti-acneic agent for cosmetics [2,3]. Pelargonic acid is an intermediate in the production of lubricants, plasticizers, perfumes, herbicides, fungicides, resins [3,5].



These two valuable products are obtained only in the case of over-oxidation, whereas partial oxidative cleavage of oleic acid produces aldehyde nonanal and 9-oxononanoic acid [45] (Scheme 2.3). Presence of strong oxidants such as ozone favors over-oxidation.

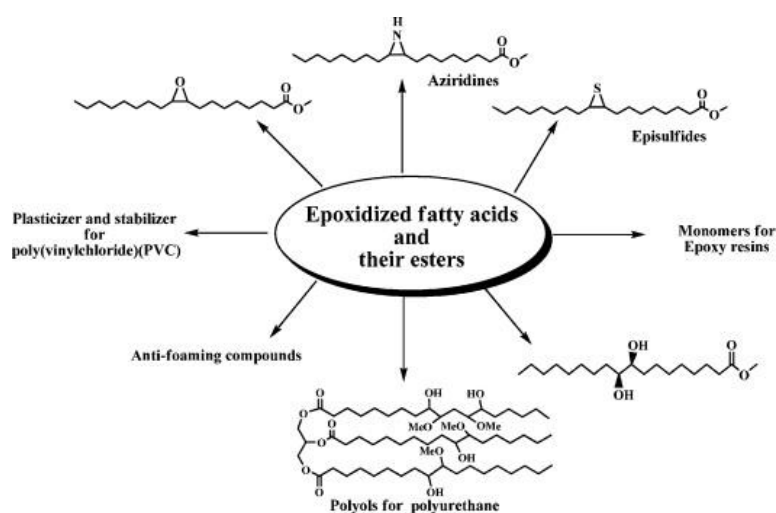
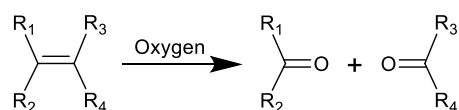
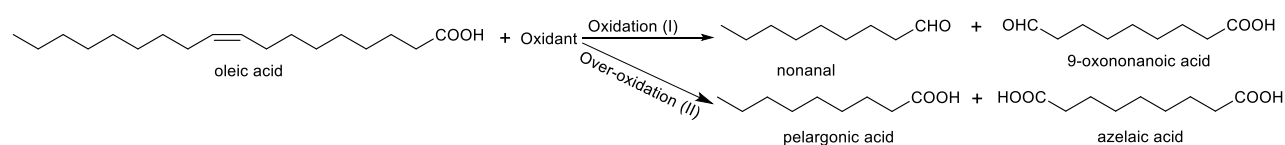


**Figure 2.13.** Applications of epoxidized fatty acids and their derivatives [42].



**Scheme 2.2.** A general oxidative cleavage process.

Although the ozonolysis of oleic acid has shown high conversion and selectivity [1-3,46,25], hazardous problems associated with the use of ozone have always been a challenge [8]. That is why the commercial applications of ozonolysis processes are still restricted. Handling of ozone has always various safety risks such as explosion and toxicity of ozone. Moreover, enormous energy demand of ozonolysis process and high-technology equipment required make the capital cost of process high [47,46]. Therefore, a new alternative method with safer and economically more viable process to produce dicarboxylic acids from oxidation of UFAs is of great interest to the industry. The dangerous ozone should be replaced by a safe and green oxidant. This makes it necessary to employ a highly efficient catalyst in the oxidative cleavage process. Therefore, in the following sections different types of oxidants and catalysts reported in the literature for oxidative cleavage of UFAs are reviewed.



**Scheme 2.3.** Oxidation of oleic acid into aldehydes (I) and over-oxidation into carboxylic acids (II).

## 2.3 Different catalyst-oxidant systems for oxidative cleavage of unsaturated fatty acids

Transition metal-based catalytic systems are considered to be most suitable for the oxidative cleavage of olefins. Their high catalytic activities make it possible to use more benign oxidants. Osmium, ruthenium, and tungsten are three metals that have attracted the most attentions for oxidation of unsaturated hydrocarbons. In the case of UFAs, on which tiny portion of oxidative cleavage-based research works have focused, the emphasis has been placed on the latter two, particularly tungsten. Additionally, iron, molybdenum, cobalt, chromium, manganese and gold are other metals that have been less investigated. Pure metals, simple metal salts, metal oxides and different metal complexes are different forms of metals that have been employed as catalysts. One



noticeable point is that the common side reactions such as epoxidations, dihydroxylation or allylic oxidations should be prevented or minimized, which strongly depends on the nature of the transition metal used as catalyst.

Oxidants are the source of oxygen during the oxidation reaction. Several oxidants have been reported in the literature to oxidize unsaturated fatty acids. Depending on the oxidizing power some oxidants need the aid of catalyst to act as co-oxidant, and some do not need. The strong oxidants such as sodium periodate, sodium hypochlorite, potassium permanganate, potassium peroxomonosulfate (oxone), peracetic acid, nitric acid and tert-butyl hydroperoxide (TBHP) can usually oxidize substrates without the need for an active catalyst [2,46,48,39]. But, the problem is that most of these oxidants are not eco-friendly, and the desired products are obtained in low yields due to the waste generation. Using the relatively moderate oxidants such as molecular oxygen and hydrogen peroxide could overcome this problem, because they produce no waste. However, in order to have acceptable reaction conversion and selectivity in such systems it is necessary to employ a highly efficient catalytic system [2,3].

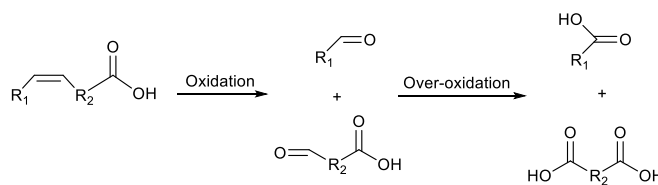
In this section, we have tried to review all of the recent works which exploited different catalyst/oxidant systems in the oxidative cleavage of, only, UFAs and their derivatives. With specific respect to commercializing viewpoint arising from the global demand for developing a greener alternative for the conventional oxidative cleavage methods, we will compare the results of previous works in three groups: homogeneous, heterogeneous and semiheterogeneous (NP-based) catalysts. This classification associated with the critical discussions presented on the important features such as catalytic activity and recoverability would be helpful for future works planning. In addition, investigation of recent breakthroughs of NP-based catalysts that can increase their performance specially in the oxidative cleavage of UFAs, would present an outlook in the development of advanced catalysts for such reactions.

### **2.3.1 Mechanisms of the reaction**

To reach a comprehensive interpretation, firstly it is important to investigate different proposed mechanisms for the oxidative cleavage reactions. In general, oxidative cleavage of C-C double bonds in the fatty molecules involves scission of the double bonds followed by incorporation of oxygen atoms into the two produced sections (see Scheme 2.4). Aldehydes and

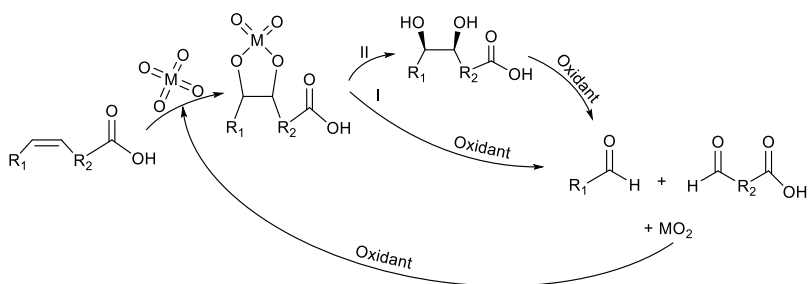
ketones are often the initial products whereas over-oxidation yields in the production of carboxylic acids [46].

Several mechanisms have been proposed for the oxidative cleavage of alkenes and cyclic olefins. For UFAs, however, the mechanism seems to be more complicated. The main reason would be the presence of carboxylic group which may results in side reactions. In addition, oxidative cleavage of cyclic olefins and alkenes is typically easier than fatty acids due to the role of the ring strain instability. This intermediate state can promote the oxidation reaction, while it is not highly effective in the case of fatty acids. Moreover, formation of radical intermediates in the oxidative cleavage of UFAs is very difficult, unlike the cyclic olefins. Herein, we presented the modified versions of two of proposed mechanisms for general olefins that are applicable to UFAs. Further works to propose a mechanism that carefully considers the mentioned difficulties, however, should be encouraged.



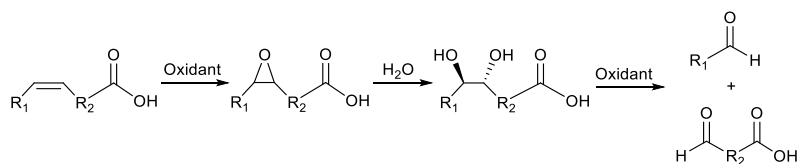
**Scheme 2.4.** Oxidative double bond cleavage of UFAs to aldehydes, ketones, and carboxylic acids [45].

The first mechanism, which is shown in Scheme 2.5, describes a catalytic system based on transition metals tetroxide such as  $RuO_4$  and  $OsO_4$  [45,49]. These oxides can be formed during the reaction also, and in the presence of oxidants, when their corresponding metal salts are used as catalysts [50,51]. In terms of selectivity,  $RuO_4$  indicates better performance compared to  $OsO_4$ , because the reaction mechanism for  $RuO_4$  does not involve dihydroxylated intermediates (Scheme 2.5 mechanism I) and immediately after the formation of metal diester as the main intermediate, the aldehydes will be formed, while  $OsO_4$  tends to form diols after formation of the metal diester (Scheme 5 mechanism II) rather than aldehydes. The main advantage of osmium in comparison with ruthenium is the lower required metal loadings at the same conditions [45]. However, the toxic properties of osmium are stronger than ruthenium.



**Scheme 2.5.** First mechanism of oxidative cleavage of UFAs [45,49].

The second mechanism is based on the formation of epoxide groups following by the hydrolysis to diols and final oxidation to obtain aldehydes or carboxylic acids. This mechanism, which is schematically shown in Scheme 2.6, is mainly ascribed to the presence of tungsten compounds as catalyst [45].



**Scheme 2.6.** Second mechanism of oxidative cleavage of UFAs [45].

### 2.3.2 Homogeneous catalysts

Homogeneous catalytic systems are believed to effectively increase the conversion in oils and fats reactions which are conducted mainly in liquid phase. The high performance of such catalysts owes to the formation of uniform mixture with the reactants resulting in minimum mass transfer limitations and high reaction rates.

In oxidative cleavage reactions of fatty acids, different coordination of metals such as simple metal salts, metal-oxo or peroxy complexes, and other metal complexes have been used as homogeneous catalyst. It is worth pointing out studies in this field, in order to find an alternative for ozonolysis process, are currently passing through lab-scale requirements such as better understanding of the reaction mechanism and, thus, have been less focused on industrialization aspects. In fact, that is why the use of homogeneous catalysts has been generally preferred in the literature. While heterogeneous catalysts are of interest to industry for their ease of recovery, homogeneous catalysts show more advantages for research-scale works such as lower mass transfer limitations which results in higher conversion. Therefore, the number of researches focused on

homogenous system is much higher than heterogeneous one. Table 2.5 summarized the details of reported homogeneous catalytic systems for the oxidative cleavage of UFAs and their derivatives.

### **2.3.2.1 Osmium**

Osmium is one of the first metals which have been investigated in catalytic oxidative cleavage of olefins [52]. The catalytic application of Os is usually accompanied with using NaIO<sub>4</sub> or KHSO<sub>5</sub> as secondary oxidants (Table 2.5, entry 1) [53]. Sodium periodate and oxone can form Os tetroxide from its precursor, in addition to their role in oxidizing the diol intermediates to aldehydes. Although catalytic systems based on Os require less loading of catalyst, its applications have been restricted due to the significant toxic properties of Os.

### **2.3.2.2 Cobalt**

Diol oxidation can also be done with the cobalt polyoxometallate (POM) as shown by Santacesaria (Table 2.5, entry 2) [54]. Using cobalt acetate, they reported a POM based on the mixture of cobalt and tungsten. As soon as hydrogen peroxide is added to the system, the POM catalyst can be formed in situ which is introduced to be H<sub>6</sub>CoW<sub>12</sub>O<sub>40</sub>. However, the production yield of azelaic acid from oleic acid using this catalytic system is not high enough (52.5%).

### **2.3.2.3 Molybdenum**

Turnwald reported the complex formed on the basis of molybdenum to convert oleic acid into pelargonic and azelaic acid with excess hydrogen peroxide (Table 4, entry 3) [3]. Using 2,6-dipicolinate as ligand, the active oxo-peroxo complex [MoO(O<sub>2</sub>)(2,6-dipicolinate)](H<sub>2</sub>O) could be formed as the catalyst which resulted in 82% yield of azelaic acid after 5 h at 90 °C, albeit the large amount of H<sub>2</sub>O<sub>2</sub>, which should be employed, make such systems unreasonable for large-scale applications.

**Table 2.5.** Different homogeneous catalytic systems reported for the oxidative cleavage of UFAs and their derivatives.

Metal	Entry	Reactants	Main products	Catalyst/oxidant system	Reaction conditions <sup>1</sup>	System's efficiency (Yield) <sup>2,3</sup>	Reference
Os	1	Methyl oleate	Pelargonic acid Monomethyl azelate	OsO <sub>4</sub> /oxone in DMF	3 h, RT	PA: 93%	[53]
Co	2	Oleic acid	Pelargonic acid Azelaic acid	A cobalt-based POM: H <sub>6</sub> CoW <sub>12</sub> O <sub>40</sub> / H <sub>2</sub> O <sub>2</sub> -O <sub>2</sub>	4.5 h, 70 °C	AA: 52.5%	[54]
Mo	3	Oleic acid	Pelargonic acid Azelaic acid	A molybdenum-based POM: [MoO(O <sub>2</sub> )(2,6-dipicolinate)](H <sub>2</sub> O)/H <sub>2</sub> O <sub>2</sub>	5 h, 90 °C	AA: 82%	[3]
Fe	4	Oleic acid Methyl oleate Elaidic acid Erucic acid Methyl erucate	Nonanal	An Iron-based complex/H <sub>2</sub> O <sub>2</sub> and NaIO <sub>4</sub>	24 h, RT	NL from OA: 90% NL from MO: 96% NL from ELA: 69% NL from ErA: 73% NL from ME 70%	[55]
	5	Oleic acid Methyl oleate	Nonanal Pelargonic acid Azelaic acid	An Iron-based complex/H <sub>2</sub> O <sub>2</sub> and NaIO <sub>4</sub>	48 h, RT	PA from OA: 85% NL from OA: 5% PA from MO: 82% NL from MO: 9%	[56]
Ru	6	Oleic acid	Pelargonic acid Azelaic acid	RuCl <sub>3</sub> /NaIO <sub>4</sub>	0.75 h, RT Ultrasonic radiation	AA: 81% PA: 96%	[57]
	7	Oleic acid	Pelargonic acid Azelaic acid	RuCl <sub>3</sub> /NaIO <sub>4</sub>	8 h, RT Using ultrasonic radiation Organic solvent-free	AA: 62% PA: 98%	[58]
	8	Oleic acid Methyl oleate	Pelargonic acid Azelaic acid	A ruthenium-based POM: [Ru(2,6-dipicolinate) <sub>2</sub> ]/H <sub>2</sub> O <sub>2</sub>	24 h, 80 °C	PA from OA: 59% PA from MO: 81%	[59,60]

**Table 2.5.** Different homogeneous catalytic systems reported for the oxidative cleavage of UFAs and their derivatives, continued.

Metal	Entry	Reactants	Main products	Catalyst/oxidant system	Reaction conditions <sup>1</sup>	System's efficiency (Yield) <sup>2,3</sup>	Reference
W	9	Oleic acid	Pelargonic acid Azelaic acid	H <sub>2</sub> WO <sub>4</sub> and Co(acac) <sub>3</sub> /H <sub>2</sub> O <sub>2</sub> and NHPI in O <sub>2</sub>	5 h, 70-75 °C	AA: 15% PA: 15%	[61]
	10	Methyl oleate	Pelargonic acid Methyl azelate	H <sub>2</sub> WO <sub>4</sub> and Co(acac) <sub>3</sub> /H <sub>2</sub> O <sub>2</sub> and NHPI in O <sub>2</sub>	5 h, 70-75 °C	MA: 19% PA: 20%	[61]
	11	Methyl erucate	Pelargonic acid Methyl brassylate	H <sub>2</sub> WO <sub>4</sub> and Co(acac) <sub>3</sub> /H <sub>2</sub> O <sub>2</sub> and NHPI in O <sub>2</sub>	5 h, 70-75 °C	MB: 41% PA: 54%	[61]
	12	Oleic acid	Pelargonic acid Azelaic acid	PCWP/H <sub>2</sub> O <sub>2</sub>	5 h, 90 °C Organic solvent-free	AA: 57%	[3]
	13	Oleic acid	Pelargonic acid Azelaic acid	A peroxy-tungsten complex with Cs <sup>+</sup> as PTA/H <sub>2</sub> O <sub>2</sub>	10 h, 90 °C Organic solvent-free	AA: 28%	[3]
	14	Oleic acid	Pelargonic acid Azelaic acid	PCWP/H <sub>2</sub> O <sub>2</sub>	4 h, 80 °C	AA: 86% PA: 82%	[62]
	15	Methyl oleate	Pelargonic acid Methyl azelate	A peroxy-tungsten complex with Aliquat® 336 as PTA/H <sub>2</sub> O <sub>2</sub>	4 h, 85 °C Organic solvent-free	MA: 83% PA: 84%	[63]
	16	Methyl ricinoleate	Methyl azelate Hydroxynonanoic acid	A peroxy-tungsten complex with Aliquat® 336 as PTA/H <sub>2</sub> O <sub>2</sub>	4 h, 85 °C Organic solvent-free	MA: 85% PA: 84%	[63]
	17	Oleic acid	Pelargonic acid Azelaic acid	A peroxy-tungsten complex with Aliquat® 336 as PTA/H <sub>2</sub> O <sub>2</sub>	5 h, 80 °C	AA: 79% PA: 82%	[64]
	18	Oleic acid	Pelargonic acid Azelaic acid	PCWP/H <sub>2</sub> O <sub>2</sub>	5 h, 85 °C Organic solvent-free	AA: 81% PA: 86%	[2]
19	Methyl oleate	Nonanal	A peroxy-tungsten complex with Alk-PEI as PTA/H <sub>2</sub> O <sub>2</sub>	24 h, 70 °C Organic solvent-free	NL: 97%	[65]	

1. RT: room temperature

2. The best result of each work is presented in the table.

3. PA: pelargonic acid, AA: azelaic acid, NL: nonanal, OA: oleic acid, MO: methyl oleate, EIA: Elaidic acid, ErA: Erucic acid, ME: methyl erucate, MA: methyl azelate, and MB: methyl brassylate.

#### 2.3.2.4 Iron

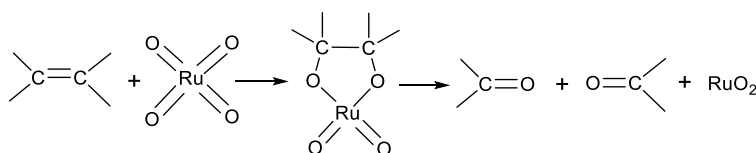
Although the first-row transition metals have the advantages of being cheaper and more environmentally friendly, their use in catalytic oxidative cleavage of UFAs has been limited due to their generally lower oxidizing potential compared to second- and third-row transition metals. It seems that the catalytic systems based on only first-row transition metals like iron have less ability to over-oxidize UFAs and produce dicarboxylic acids.

Spanning *et al.* have introduced a catalytic system based on the first-row transition metal for the oxidation of UFAs (Table 2.5, entries 4 and 5) [55,56]. They used Fe-based coordination metal complexes to produce aldehydes (entry 4) and carboxylic acids (entry 5). For the first case (aldehyde), the iron complex  $[\text{Fe}(\text{OTf})_2(\text{mix-BPBP})]$  has been used as catalyst and hydrogen peroxide and sodium periodate as oxidant in acetonitrile, where OTf is trifluoromethane sulfonate anion and mix-BPBP is the mixture of R,S-, R,R- and S,S isomers of N,N'-bis(2-picolyloxy)-2,2'-bipyrrrolidine). After epoxidation, water was added followed by acidification with  $\text{H}_2\text{SO}_4$  and subsequent pH neutralization using  $\text{NaHCO}_3$  to perform the epoxide hydrolysis and diol cleavage (second mechanism, Scheme 2.6). Adding acetic acid to increase the conversion, they succeeded to produce nonanal with the yields of 96 and 90% from methyl oleate and oleic acid, respectively. The total time of reaction was 24 hours at ambient temperature. However, longer reaction time (48 h) is needed to produce carboxylic acids using Fe-based complexes (see Table 2.5, entry 5). The complex used for this purpose was  $[\text{Fe}(\text{OTf})_2(6\text{-Me-PyTACN})]$  where 6-Me-PyTACN is 1-[(6-methyl-2-pyridyl)methyl]-4,7-dimethyl-1,4,7-triazacyclononane. Here, the mechanism includes the direct *cis*-dihydroxylation of the double bond, oxidative cleavage and subsequent over-oxidation to the carboxylic acids. Applying several one-pot procedures with different combinations of oxidants and additives resulted in different substrate conversions and product distributions. The best obtained yields, which are presented in Table 2.5, are 82 and 85% for pelargonic acid from methyl oleate and oleic acid, respectively. Nevertheless, the low oxidizing power of iron, which leads to the longer reaction time, is still the main disadvantage of such catalytic systems.

#### 2.3.2.5 Ruthenium

Ruthenium is one of the oldest transition metals which have been employed in the oxidative cleavage of C-C double bonds [66,50,51]. Its tetroxide is an interesting metal oxide, because the

stoichiometric oxidation of double bonds by RuO<sub>4</sub> is fast and very selective. This arises from the fact that the reaction mechanism does not involve epoxide or hydroxylated intermediates. This mechanism is shown in Scheme 2.7, (mechanism I in Scheme 2.5) and involves the formation of a cyclic perruthenate ester [67]. RuO<sub>4</sub> can also be used as catalyst when RuCl<sub>3</sub> is employed with a secondary oxidant like NaIO<sub>4</sub>, NaClO, *t*-BuOOH or RCOOOH. These oxidants can perform the re-oxidation of RuO<sub>2</sub> to RuO<sub>4</sub>. By contrast to the common metal oxides like MnO<sub>2</sub>, ruthenium oxide is soluble in solvents such as CCl<sub>4</sub> or MeCN and this property, is crucial in its catalytic applications [68].



**Scheme 2.7.** Oxidative cleavage of C-C double bonds by RuO<sub>4</sub> (formation of cyclic perruthenate ester) [67].

Optimization of the methods presented by Zimmermann *et al.* [69] for the oxidative cleavage of oleic acid using RuCl<sub>3</sub> as catalyst and NaIO<sub>4</sub> as oxidant, resulted in the production of azelaic and pelargonic acid with 81 and 96% yield, respectively, in the mixture of acetonitrile and water (Table 2.5, entry 6) [57]. Using the surfactant Aliquat® 336 (methyltrioctylammonium chloride) and ultrasonication in the system significantly increased the reaction rate and made these yields possible in only 45 minutes at ambient temperature. Further improvement including the elimination of organic solvent by means of 20 kHz ultrasonic irradiation and increasing the reaction time was obtained by Rup *et al.* (Table 2.5, entry 7) [58].

Recently, Behr and his co-workers tried to eliminate the secondary oxidant NaIO<sub>4</sub> using Ru-based metal complexes (Table 2.5, entry 8) [59,60]. They demonstrated that the presence of excess amount of a ligand and *in situ* formation of the complex, make the oxidative cleavage possible only with hydrogen peroxide. The procedure includes the use of Ru(acac)<sub>3</sub> as a precursor and 2,6-dipicolinic acid as a ligand in the mixture of tert-butyl alcohol and water and reaction at 80 °C for 24 h. However, the yield of production of pelargonic acid with this system (59 and 81% from oleic acid and methyl oleate, respectively) are lower than those systems based on Ru salt and NaIO<sub>4</sub>. This is mainly because of the higher number of side reactions in this case.



Ruthenium is one of the rare transition metals, and its precursors are very expensive. Its toxic property, although less than Os, is another problem. Considering scale up aspects, therefore, an alternative transition metal is desirable for catalytic oxidation of olefins.

#### 2.3.2.6 Tungsten

Since the mechanism of W-based catalytic oxidative cleavage of olefins (Scheme 2.6) includes formation of epoxides and hydroxylated intermediates, performing the reaction in one step and minimization of by-products are very important. Oakley *et al.* reported using tungsten oxide (in hydrated form is tungstic acid,  $\text{H}_2\text{WO}_4$ ) as catalyst for the oxidative cleavage of oleic acid, methyl oleate and methyl erucate (Table 2.5, entries 9, 10 and 11) [61]. The catalytic system includes using  $\text{Co}(\text{acac})_3$ , and N-hydroxyphthalimide (NHPI) in  $\text{O}_2$  and  $\text{H}_2\text{O}_2$  as oxidant in order to over-oxidize the intermediates diols into carboxylic acids. This system provides one-pot reaction and use of a limited amount of  $\text{H}_2\text{O}_2$ , but the production yields are very low (see Table 2.5).

Many efforts have been done to eliminate the secondary oxidants in the oxidative cleavage of olefins during the last decades. For this purpose, tungsten-containing catalysts are ideal, because they have a unique ability in combination with hydrogen peroxide that makes elimination of the secondary oxidants possible. That is the main reason for the much more frequent applications of tungsten as catalyst in the oxidation of UFAs in recent years. Moreover, W is cheaper and less toxic compared to Ru and Os.

Recently, catalytic systems that involve W-based POM have been significantly investigated. Such systems mainly include a phase transfer agent (PTA) (usually a quaternary ammonium salt) to increase the solubility of substrates in the biphasic reaction, often tungstophosphoric acid (TPA,  $\text{H}_3\text{PW}_{12}\text{O}_{40}$ ) as the W precursor and hydrogen peroxide solution. The *in situ* protocol upon the addition of  $\text{H}_2\text{O}_2$  leads to the formation of peroxo-tungsten complex  $\text{Q}_3\{\text{PO}_4[\text{WO}(\text{O}_2)_2]_4\}$ , where Q is the cationic part of the quaternary ammonium salt. Several salts have been used for this purpose such as cetylpyridinium chloride (CPC), methyltrioctylammonium chloride (Aliquat® 336), tetrabutylammonium chloride and tetraoctylammonium chloride. The most common one is CPC which causes the complex peroxo-tris (cetylpyridinium)12-tungstophosphate (PCWP) to be formed with the chemical formula  $\{\text{C}_5\text{H}_5\text{N}-\text{C}_{16}\text{H}_{33}\}_3\{\text{PO}_4[\text{WO}(\text{O}_2)_2]_4\}$ .

Turnwald *et al.* reported one step solvent-free oxidative cleavage of oleic acid to produce azelaic and pelargonic acids using PCWP (Table 2.5, entry 12) [3]. After 5 h reaction at 90 °C, the yield of azelaic acid was 57%. Increasing the reaction time to 10 h led to higher yield (64%), but the catalyst was decomposed. The substitution of counter-ion cetylpyridinium with Cs<sup>+</sup> (the complex tris (caesium) tungstophosphate), increased the thermal stability of the complex, but the obtained yield was lower even in longer time (28%) (Table 2.5, entry 13).

With the same catalytic system and only altering the amounts of initial reactants, Pai *et al.* reported a higher yield (86% for azelaic acid) in even shorter time (4 h) and lower temperature (80 °C) (Table 2.5, entry 14) [62]. Changing the phase transfer agent, Khlebnikova *et al.* employed another catalytic peroxy-tungsten complex system to perform the oxidative cleavage on methyl esters of fatty acids (Table 2.5, entries 15 and 16) [63]. Using Aliquat® 336 instead of CPC, they succeeded to synthesize the complex methyltrioctylammonium tetra (diperoxotungsto) phosphate. In comparison with entry 14, it is interesting to say that at the same reaction time and, almost, temperature, the obtained yields were also the same, however the catalyst loadings used for the oxidation of fatty acids (entry 14) are higher than those used for the oxidation of their corresponding methyl esters (entry 15).

Antonelli *et al.* tried to apply the same complex system as entry 15 and 16 for the oxidative cleavage of oleic acid into pelargonic acid and azelaic acid (Table 2.5, entry 17) [64]. Performing the reaction at 80 °C for 5 h resulted in the production of azelaic acid with the 79% yield which is slightly lower than what was obtained using CPC (entry 14).

In order to obtain a more precise comparison between the performances of different phase transfer agents in the oxidation of UFAs, Godard *et al.* employed four PTA including CPC, Aliquat® 336, tetra butyl and tetra octyl ammonium chloride in a same oxidative cleavage of oleic acid (Table 2.5, entry 18) [2]. CPC and subsequent catalytic complex system PCWP were found to give the best results and further optimizations of the reaction conditions led to the production of azelaic and pelargonic acid with 81 and 86% yields, respectively, in organic solvent-free system and in 5 h at 85 °C.

A new type of phase transfer agent is introduced in the work that was done by Haimov *et al.* (Table 2.5, entry 19) [65]. The alkylated form of polyethyleneimine (Alk-PEI) was used in the production of aldehydes from methyl oleate. The system showed high selectivity for nonanal (97% yield) with the reaction temperature of 70 °C and relatively long reaction time (24 h) in the absence of organic solvent.

The majority of homogeneous catalytic systems reported here have conversions of more than 90%. Nevertheless, their applications in industry are restricted as a result of problems such as lack of recycling ability, metal contamination, poor control of selectivity, and disposal of potentially toxic wastes. Since employing insoluble heterogeneous catalytic systems is an efficient strategy in order to achieve the isolation and separation of catalysts, developing solid catalysts would be favorable to solve these problems.

### 2.3.3 Heterogeneous catalysts

Employing solid catalysts in liquid phase reactions has been always proposed as a promising way in large-scale production of chemicals. The most important feature of heterogeneous catalysts is their recycling ability, owing to the ease of recovery, which makes them able to be commercialized. In spite of many positive aspects, application of heterogeneous catalysts in oils and fats reactions has been restricted, mainly because of poor reactant/catalyst contact which, in turn, arises from pore diffusion limitations or low active site availability. This would be a main reason that heterogeneous catalytic systems for the oxidative cleavage of UFAs have been remarkably less documented. The results of these systems are summarized in Table 2.6.

Noureddini *et al.* investigated the liquid-phase catalytic oxidation of oleic acid with hydrogen peroxide in the presence of different metals or metal oxides, supported and unsupported (Table 2.6, entries 1 and 2) [48]. They reported the production of azelaic and pelargonic acids as the major products and some by-products mainly including C<sub>5</sub>-C<sub>8</sub> carboxylic acids. Using metals including tungsten, tantalum, molybdenum, zirconium and niobium in the form of a wire, and tungsten oxide and tantalum oxide as catalyst showed that transition metals in their pure form could not be efficient catalysts, in particular for large-scale applications. It is believed that the metal oxide is responsible for catalyzing the oxidation of UFAs. Therefore, in the case of using pure metals, firstly they have to be oxidized to metal oxides and then, catalyze the reaction. This multi-step process reaction requires larger amounts of oxidant. Supported tungsten oxide showed the highest

conversion at reaction temperature of 130 °C. About 79% of the initial oleic acid was converted after 1 h, 96% in 2 h and 98% after 3 h and longer. One interesting point mentioned in this work is that during the reaction, the concentrations of the main products, azelaic and pelargonic acid, showed an increasing trend until reaching a maximum and then started to decrease. This arises from the degradation of azelaic and pelargonic acids in the prolonged heating process. The time at which maximal concentration of desired product was obtained depended on the type of catalyst used. For supported tungsten oxide, maximal azelaic acid concentration was reached in 1 h or less. Therefore, optimization of the reaction residence time to obtain the highest yield (and acceptable conversion) seems critical, in particular for scale up of the reaction. Another interesting point in this work is the effect of the support. Initially higher pore diffusion resistance of the porous support led to a lower catalytic activity of supported tungsten oxide in comparison with the unsupported form, only in the early stages of the reaction. After about 20 min, however, a significant increase in catalytic activity of the supported catalyst was obtained while the activity of the unsupported catalyst stayed constant throughout the whole 1 h of the reaction. The selectivity of azelaic and pelargonic acids in the case of the supported catalyst (32 and 36%, respectively) were slightly higher compared to unsupported catalyst (30 and 29%, respectively). Finally, it is clear that the conversions, in both cases of supported and unsupported catalysts, are not as high as what was obtained in homogeneous catalytic oxidation of oleic acid.

Porous solids have been widely employed in a variety of reactions to improve the performance of heterogeneous catalytic systems. In a classification presented by IUPAC<sup>‡</sup>, there are three types of porous solids: (i) microporous materials (e.g., zeolites) with pore diameter less than 2 nm, (ii) mesoporous materials with pore diameter between 2 and 50 nm and (iii) macroporous materials with the pore diameter larger than 50 nm [70]. Microporous zeolites, which generally have very high surface area and crystalline structure with uniform micropore size, are widely used as heterogeneous catalysts in the refining and petrochemical industry. However, these materials are not useful for the oils and fats reactions because of the relatively large molecular size of oleochemicals. For example, employing zeolites (pore size less than 1.5 nm [71]) as catalysts in oxidative cleavage of oleic acid (molecular size about 2 nm [72]) does not seem favorable due to the lower dimensionality of the interaction between the components and the catalyst surface. On

the other hand, catalytic activity of macroporous materials is poor as the result of their relatively low surface area. Efforts to increase the pore size of catalytic materials while maintaining high surface area led to the discovery of mesoporous materials in 1992 by Mobil Research and Development Corporation [73]. This type of porous materials has shown potential applications as either catalyst or support for liquid-phase reactions of oils and fats [37]. A comprehensive review on the catalytic applications of mesostructured materials has been presented in our previous work [74].

Using mesoporous molecular sieves (Cr-MCM-41, Mn-MCM-41, Co-MCM-41) and microporous zeolites (Cr-APO-5, Co-MFI, Mn-MFI) as supports, Dapurkar *et al.* employed chromium, manganese and cobalt as active sites to oxidize oleic acid into azelaic and pelargonic acids in supercritical carbon dioxide (scCO<sub>2</sub>) media with molecular oxygen (Table 2.6, entry 3) [75]. The reaction was performed at 80 °C for 8 h. Mesoporous MCM-41 containing chromium converted more than 95% of initial oleic acid with almost the same products yields (32.4% for azelaic acid, and 32.2% for pelargonic acid) as the previous work. Their results confirm the advantages of mesoporous catalysts in comparison with microporous catalysts in the reactions of fats and oils. However, the disadvantage of this catalytic system is an insufficient selectivity for azelaic and pelargonic acids, due to the production of C<sub>6</sub>–C<sub>10</sub> di- and monocarboxylic acids as by-product.

While reusability of heterogeneous catalysts would make them cost effective for large-scale applications, their lower conversion, yield or selectivity in the oxidative cleavage of UFAs compared to homogeneous ones is a big obstacle to commercialization. Tackling this obstacle requires some improvements in the structure of solid catalysts. An advanced heterogeneous catalytic system should be developed that includes the advantages of homogeneous catalysts on one hand, and the recycling ability on the other hand. NP-based catalysts seem to be most suitable for this purpose, since it has been shown that they can act like a homogeneous catalyst in the reaction medium insofar as sometimes discriminating NPs and homogenous catalysts requires different techniques such as NMR, DFT, electron microscopy imaging, dynamic light scattering (DLS), X-ray photoelectron microscopy (XPS), magnetometry, and multiphasic analysis [76]. Hopefully, it can be said that homogenization of heterogeneous catalyst in order to combine the

best properties of both homogeneous and heterogeneous catalysts would be possible by employing NP-based catalysts.

### 2.3.4 Nanoparticle-based catalysts

Owing to the natural high surface-to-volume ratio and quantum size effects, NPs demonstrate unique properties which make them prominent compared to larger particles or bulk materials for catalytic applications [77-85]. This can be confirmed by the fact that NP-based catalysts have, generally, exhibited higher catalytic activity compared to conventional catalysts in different types of reactions. For example, Carrettin *et al.* showed that nanocrystalline CeO<sub>2</sub>-supported Au catalysts are 2 orders of magnitude more active than conventional Au/CeO<sub>2</sub> catalysts for the CO oxidation [86]. In spite of this, curiously only few research works have employed NPs as catalyst in the oxidative cleavage of UFAs (Table 2.7). Ho *et al.* reported using ruthenium NPs supported on hydroxyapatite in the oxidative cleavage of alkenes and unsaturated fatty compounds with sodium periodate as oxidant (Table 2.7, entry 1) [87]. Their results showed that applying this catalytic system for UFAs, however, is not favorable. While full conversion was obtained for alkenes oxidation in the reaction time of 2-7 h, only 16% of methyl oleate was converted to aldehyde with this system even after 12 h, albeit at good yields (84% for nonanal and 79% for methyl 9-oxononanoate).

Recently, vicinal dihydroxy derivatives of oleic acid, methyl oleate, and erucic acid were converted by oxidative cleavage to the respective di- and monocarboxylic acids in the presence of supported gold catalyst and molecular oxygen as oxidant by Kulik *et al.* (Table 2.7, entry 2) [1]. Deposition of Au NPs on different supports (Al<sub>2</sub>O<sub>3</sub>, CeO<sub>2</sub>, TiO<sub>2</sub>, and ZrO<sub>2</sub>) was investigated. The obtained results showed that the highest catalytic activity belonged to Au/Al<sub>2</sub>O<sub>3</sub> catalyst with highly dispersed gold particles which could convert more than 80% of 9,10-dihydroxystearic acid in 260 min at 80 °C yielding 86% azelaic acid and 99% pelargonic. The main drawback of this system is the significant decrease in the catalytic activity after the catalyst recovery. After two recycling experiments using the Au/Al<sub>2</sub>O<sub>3</sub> catalyst, considerable decrements were observed in the catalyst activity; conversion decreased from 94% to 77%, and production yields of azelaic and

pelargonic acids decreased by 30%, approximately. Since Au is an expensive metal, this weak recovery potential prevents commercializing of the gold-based heterogeneous catalytic systems.

**Table 2.6.** Different heterogeneous catalytic systems reported for the oxidative cleavage of UFAs and their derivatives.

Metal	Entry	Reactants	Main products	Catalyst/oxidant system	Reaction conditions <sup>1</sup>	System's efficiency <sup>2,3</sup>	Reference
W	1	Oleic acid	Azelaic acid Pelargonic acid	Tungsten oxide supported on silica/ H <sub>2</sub> O <sub>2</sub>	1 h, 130 °C	Conversion: 79% Selectivity (AA): 32% Selectivity (PA): 36%	[48]
	2	Oleic acid	Azelaic acid Pelargonic acid	Tungsten oxide (unsupported)/ H <sub>2</sub> O <sub>2</sub>	1 h, 130 °C	Conversion: 56% Selectivity (AA): 30% Selectivity (PA): 29%	[48]
Cr	3	Oleic acid	Azelaic acid Pelargonic acid	Chromium supported on MCM-41/ O <sub>2</sub>	8 h, 80 °C	Conversion > 95% Yield (AA): 32.4% Yield (PA): 32.2%	[75]

1. RT: room temperature
2. The best result of each work is presented in the table.
3. AA: azelaic acid and PA: pelargonic acid.

**Table 2.7.** Different semiheterogeneous (nanoparticle-based) catalytic systems reported for the oxidative cleavage of UFAs and their derivatives.

1. RT: room temperature

Metal	Entry	Reactants	Main products	Catalyst/oxidant system	Reaction conditions <sup>1</sup>	System's efficiency <sup>2,3</sup>	Reference
Ru	1	Methyl oleate	Nonanal methyl 9-oxononanoate	Ruthenium nanoparticles supported on hydroxyapatite/ NaIO <sub>4</sub>	12 h, RT	Conversion: 16% Yield (NL): 84% Yield (M9-ON): 79%	[87]
Au	2	9,10-dihydroxystearic acid	Azelaic acid Pelargonic acid	Gold nanoparticles supported on alumina/ O <sub>2</sub>	4.33 h, 80 °C	Conversion > 80% Yield (AA): 86% Yield (PA): 99%	[1]

2. The best result of each work is presented in the table.
3. NL: nonanal, M9-ON: methyl 9-oxononanoate, AA: azelaic acid, and PA: pelargonic acid.



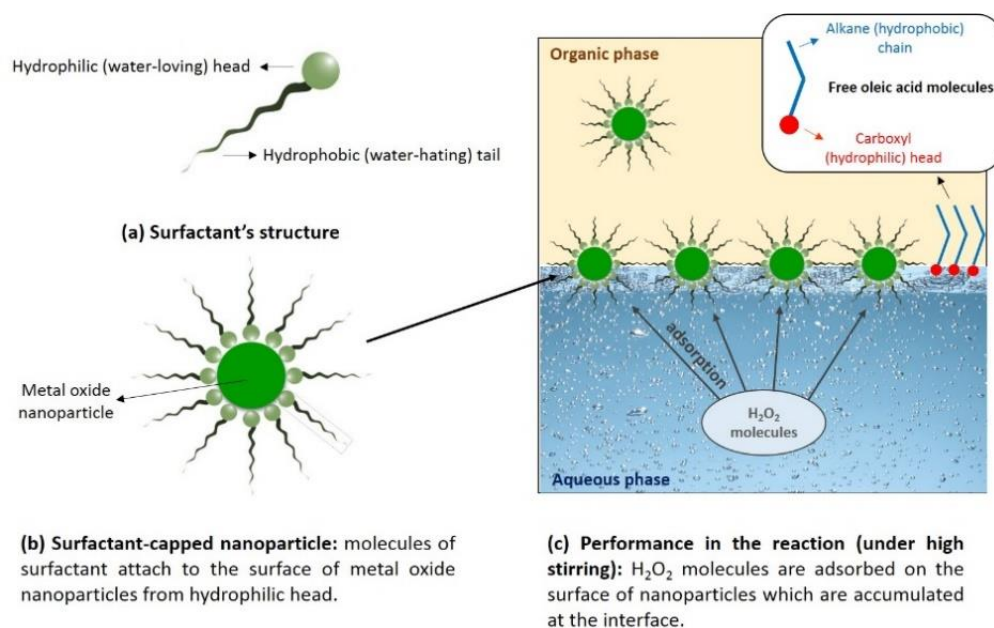
Exploiting the interesting and unique properties of NP-based catalysts in the oxidative cleavage of UFAs has sparsely investigated in the literature. The two mentioned papers above, which are the only works done in this field to our knowledge, seem curiously insufficient. On the other hand, thanks to the explosive development of nanomaterials science, new breakthroughs in nanocatalysis are appearing at a fast rate, which have been reviewed in our recent feature article [88]. Further works, therefore, seem to be required to push the use of NP-based catalysts to the oxidative cleavage of UFAs. For this purpose, the interesting features of NPs which would enhance their efficiency in the oxidative cleavage of UFAs will be discussed in the following section.

#### **2.3.4.1 Performance enhancement of NP-based catalysts in oxidative cleavage of UFAs**

One strategy to increase the catalytic performance of NPs in some reaction media is capping their surfaces with a surfactant. This increase, however, depends on several parameters such as surface properties of NPs, the type and amount of surfactant, and the involving phases in the reaction and their miscibility. Using surfactant, not only size and shape of NPs can be controlled during the synthesis [89] but this could also result in a better dispersion of NPs in the liquid medium of oils and fats reactions due to the fact that surfactants can oppose van der Waals forces. In this way, the aggregation of particles will be prevented and, consequently, catalytic activity of the catalyst will not decrease during the reaction [90]. The role of surfactant becomes more crucial, if we consider a typical oxidative cleavage reaction of UFAs which uses hydrogen peroxide as the most common benign oxidant. Presence of aqueous  $H_2O_2$ , on one hand and organic reactants, on the other hand provides a biphasic reaction with immiscible phases. In this circumstance, the presence of a well-chosen surfactant on the surface of NPs can increase their dispersion.

To illustrate the role of surfactant better, Scheme 2.8 shows the performance of surfactant-capped nanoparticles (SCNPs) as catalyst in the oxidative cleavage of oleic acid, as an example for UFAs, with hydrogen peroxide. The surfactant capped on the surface of metal oxide NPs can be oleylamine, oleic acid or other similar chemicals. Having both hydrophilic head and hydrophobic chain, surfactants reinforce the stability of emulsion in the biphasic reaction which consists of aqueous phase and organic phase. It should be noted that free molecules of the reactant, oleic acid, also would contribute to the emulsion stability, because they can be laid at the interface due to their

hydrophilic and hydrophobic parts. Since the reaction takes place mostly at the interface, high concentration of the catalyst particles at the interface is preferred which would be possible by using SCNPs. This arises from two counter effects; while hydrophilic surface of transition metals oxides immerses them into the aqueous phase, hydrophobic chain of surfactant drags SCNPs toward the organic phase. The presence of SCNPs at the interface will make adsorption of  $H_2O_2$  molecules from aqueous phase easier. Consequently, a kind of peroxy-metal complex will be formed at the surface of NPs. On the other hand, the hydrophobic chain of the surfactant attracts the oleic acid molecules, as the main reactant, from organic phase, and then the reaction will occur on the surface of SCNPs. The peroxy-metal complex, as discussed in homogeneous catalysts, is believed to be able to efficiently oxidize the olefins. Due to the presence of SCNPs at the interface, as soon as consumption of molecules of  $H_2O_2$  and formation of a peroxy species on the NPs surface, another molecule of hydrogen peroxide will be adsorbed on the surface and this process will be continuously repeated. In fact, the role of phase transfer agent (PTA) in the homogenous systems, to which the high reaction efficiency was attributed, can be played by the surfactant in heterogeneous systems.



**Scheme 2.8.** Schematic illustration for SCNPs as efficient nanocatalyst. (a) Surfactant molecule, (b) hydrophobic SCNPs surface and (c) Performance in the biphasic oxidative cleavage of oleic acid using  $H_2O_2$  as oxidant. Presence of surfactant (i) contribute to the stability of emulsion, (ii) prevents aggregation of the NPs, and (iii) make the recovery of catalysts easier [91].

Capping the NPs of an active metal oxide with an appropriate surfactant, a catalytic system may be developed that has the best properties of both homogeneous and heterogeneous systems. Moreover, considering the significant effects of SCNPs, it is highly likely that the reaction solvent can be eliminated, like what happened in the case of using homogeneous catalysts. Even, a decrease in the amount of solvent would be a great milestone in the oxidative cleavage reactions of UFAs, which will result in fewer by-products, easier separation of the products and lower operating cost.

The presence of a surfactant on the surface of metal oxide NPs provides another substantial advantage in terms of economic aspects. SCNPs can be easily separated from the mixture after the reaction and reused via the method which was developed in our previous work [89]. Based on the hydrophobic or hydrophilic properties of the surface of NPs, changing the solvent from nonpolar, e.g. toluene, to polar, e.g. ethanol or vice versa will result in the precipitation of the SCNPs. This method is shown in Figure 2.14.  $\text{ZrO}_2$ ,  $\text{TiO}_2$ , Au and Cu particles capped by oleic acid are highly dispersed in toluene and make a clear solution (Figure 5a), while they will be precipitated in ethanol (Figure 2.14 b).

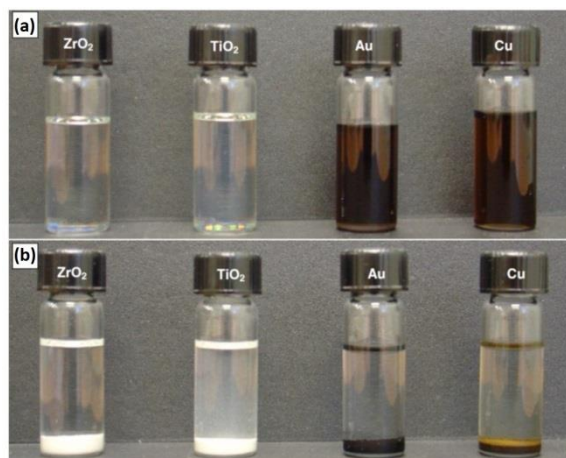


**Figure 2.14.** (a) Oleic acid-capped NPs of some metals/metal oxides dispersed in toluene (clear/transparent solutions) and (b) those NPs precipitated with excess ethanol [89].

Other approaches to address the recyclability of NP-based catalysts, as the main bottleneck for their industrial application, are currently undergoing rapid development. The efforts done in this field have been well documented in several review papers [92-98]. A facile, highly efficient, economical and environmentally benign method that attracted lots of attention is magnetic separation. The main issue, however, is that magnetic separation is only applicable to the materials

which have intrinsically magnetic parts. Nevertheless, the high efficiency of magnetic separation compared to filtration and centrifugation [99-101] has led to developing different strategies for the preparation of either magnetic nanocatalysts or non-magnetic catalysts immobilized onto magnetic nanomaterials, which have been separately investigated in the recent review papers of Hudson et al. [102] and Rossi *et al.* [103], respectively. A thorough review of the applications of magnetically recyclable nanocatalysts has been presented in the recent and precious review paper of Wang and Astruc [104]. Given the wide range of reactions such as oxidation of alcohols, epoxidation of alkenes, hydrogenation of unsaturated compounds, C-C coupling, reduction of nitroaromatics, arylation and alkylation, extension of the scope of magnetically recyclable nanocatalysts for oxidative cleavage of UFAs seems to be of great interest.

## **2.4 Heterogeneous tungsten-based polyoxometalate catalysts**

### **2.4.1 Tungsten: a fascinating metal for catalysis**

At the end of 18<sup>th</sup> century and dawn of tungsten chemistry, when the charming yellow color of tungsten oxide fascinated the chemists to propose its use as artist's color and Rudolf Erich Raspe, a German Geologist and the famous author of "The Adventures of Baron Munchausen", said that "In beauty it exceeds Turner's well-known yellow by far" [105], probably they did not think that this pretty color material would find wide applications in industry. Over the years, however, different combinations of tungsten oxide have been developed in a variety of industries, insofar as, nowadays tungsten oxide is counted indispensable to our lives. Besides its application in hydrogen reduction to manufacture elemental tungsten for industries such as electronic and electrical, alloy and steel, jewellery, biology, sport and leisure equipment, etc., tungsten oxide is used for many purposes in everyday life such as production of smart windows, fireproofing fabrics, gas sensors, semiconductors and efficient catalysts and photocatalysts [106].

The major modern days use of tungsten oxides is nevertheless in the area of catalysis. Oil industry is the most striking consumer of tungsten catalysts for treating of crude oils since the 1930's [107]. Basic reactions such as hydrotreating (hydrodesulphurization, hydrodenitrogenation,

and hydrodearomatisation), de-NO<sub>x</sub>, and reforming are of the most important reactions catalyzed by tungsten compounds in chemical industry [108,109]. Since then, tungsten oxide-based catalysts have received continuous attention because of their increasing advantages in catalysis. First, although tungsten was previously classified as a rare metal, nowadays it is found in most countries, with less price and toxic properties compared to its alternatives from second and third rows of transition metals for organic reactions (chiefly osmium and ruthenium) [45]. Second, tungsten oxides and sulfides exhibit very strong Brønsted acid sites, to which catalytic activities of transition metals in many reactions are attributed [110-112], either as a bulk oxide or when supported [113-118]. Compared to other metal oxides, tungsten oxide has shown relatively low point of zero charges (PZCs) in the literature [119], which complies with its high surface acidity. Third, tungsten oxide includes many chemical structures arising from the distinct inherent properties of tungsten, which enable a variety of properties and morphologies for catalytic applications in many chemical reactions. Numerous oxidation states of tungsten from -2 to +6 [120,121] have led to several tungsten oxides WO<sub>x</sub> (x mainly between 2-3) including WO<sub>3</sub> (yellowish), WO<sub>2.9</sub> or W<sub>20</sub>O<sub>58</sub> (bluish), WO<sub>2.72</sub> or W<sub>18</sub>O<sub>49</sub> (violet), and WO<sub>2</sub> (brownish), as can be seen in Figure 2.15 [105]. The most common state is tungsten trioxide, which in turn, includes hydrated (WO<sub>3</sub>.nH<sub>2</sub>O) and anhydrous (WO<sub>3</sub>) form. It has even been shown that the number of water molecules in the structure affects the catalytic activity, particularly in oxidation reactions [122]. Furthermore, WO<sub>3</sub> can crystallize in many polymorphs with various crystal structures such as monoclinic, orthorhombic, and tetragonal. Moreover, peroxotungstic acid or hydrated tungsten peroxide is another interesting tungsten oxide-based structure that has shown great potential for catalytic applications.

Applications of the tungsten containing materials in heterogenous catalytic oxidation reactions have been nicely and recently reviewed [123]. However, this review does not cover polyoxotungstates, which are another type of tungsten oxide-based catalysts increasingly attracting interest nowadays. In what follows, we will discuss about this type.

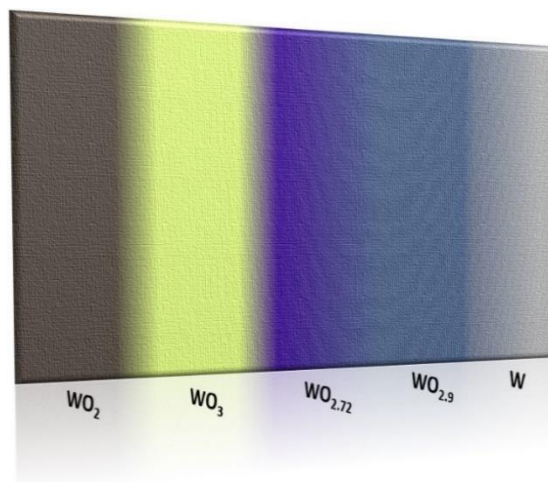


**Figure 2.15.** Amazingly colorful world of the tungsten oxides: yellow  $WO_3$ , blue  $WO_{2.9}$ , violet  $WO_{2.72}$ , brown  $WO_2$ , and gray W metal [105].

## 2.4.2 Fundamentals of polyoxometalate catalysis

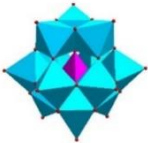
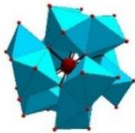
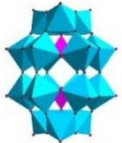
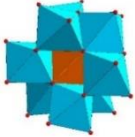
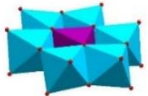
Polyoxometalates or their more descriptive synonym heteropoly oxoanions are polymeric oxoanions formed by condensation of more than two different oxoanions, which can give heteropoly acids. In contrast, isopolyanions are composed of one kind of oxoanions, which their acid forms are called isopoly acids. In fact, although the words POM and HPA (heteropoly acid) are inadvertently being used instead of each other, it should be noticed that a HPA is the acid form of its corresponding POM, and vice versa, a POM is the conjugate anion of HPA.

Despite some disagreement over the history of POMs, majority of the literature cites Berzelius, who reported the preparation of ammonium 12-molybdophosphate in 1826, as the pioneer of heteropoly compounds science. About 40 years later, however, the first tungsten-based heteropoly compound, 12-tungstosilicic acid, was discovered in 1862 by Marignac. The full history of POMs and their progress are available in several reviews and books (e.g. [124,125]), and hence would be redundant here. Over the years, with the better understanding of POMs chemistry, various structures were discovered, which are summarized in Table 2.8. Further information on details of POMs structures are available in numerous papers and books (e.g. [126,127,124,128]).

Although some POMs with Dawson, Anderson, Allman-Waugh, and, less known, Preyssler structures have been also examined as catalyst, most of the heteropoly oxometallate catalysts are

of Keggin structure, which has been reported for the first time in 1934 by Keggin [129], most likely because of higher thermal stability and ease of synthesis of this structure compared to others [130]. The Keggin cluster of POMs has the general formula  $H_nXM_{12}O_{40}$ , in which X is the heteroatom (X has been known to be from the p-block of the periodic table (e.g., P, Si, Ge, As), but nowadays is not restricted to them), and M is the addenda atom (mainly W, Mo, and V).

**Table 2.8.** Different structures of polyoxometalates.

Name	General formula <sup>1</sup>	X (typical examples)	Structure
Keggin	$XM_{12}O_{40}^{n-}$	$P^{5+}$ , $As^{5+}$ , $Si^{4+}$ , $Ge^{4+}$	
Dexter-Silverton	$XM_{12}O_{42}^{n-}$	$Ce^{4+}$ , $Th^{4+}$	
Dawson	$X_2M_{18}O_{62}^{n-}$	$P^{5+}$ , $As^{5+}$	
Allman-Waugh	$XM_9O_{32}^{n-}$	$Mn^{4+}$ , $Ni^{4+}$	
Anderson (type A)	$XM_6O_{24}^{n-}$	$Te^{6+}$ , $I^{7+}$	

1. M =  $Mo^{VI}$ ,  $W^{VI}$ ,  $V^{V, VI}$  etc.

Heteropoly compounds are progressively attracting interest in catalysis science particularly in the last decade. Widely tunable physical and chemical properties of POMs at molecular level have been the subject of extensive research in recent years giving them promise for applications in various fields such as medicine, material science, photochromism, electrochemistry, magnetism as well as catalysis. Their strong acidity has tempted the researchers to examine their efficiency in the reactions currently catalyzed by conventional acids (e.g.  $H_2SO_4$  and  $AlCl_3$ ) such as Friedel-Crafts,

esterification, hydration, hydrolysis, and acetalization, where the problems associated with use of conventional acids like high toxicity, catalyst waste, corrosion, difficulty of separation and recovery have provided a controversial challenge, nowadays. On the other hand, POMs are more thermally and oxidatively stable to oxygen donors in comparison with other organometallic complexes [131].

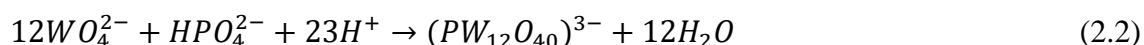
Interestingly and uniquely, the key properties of POMs like acidity, redox capability, and solubility in water or polar solvents can be readily and stably tuned to enhance their efficiency for specific purposes. Such structure modifications are generally carried out at molecular or atomic level by removing one or more constituent transition metal atoms giving the parent POM a defected structure, so-called lacunary structure, and then, incorporation of another transition metal(s) into the structure. According to this, different metal-oxygen clusters of POMs containing several early transition metals such as tungsten, molybdenum, vanadium, niobium, tantalum, iron, cobalt, nickel, copper, titanium, zinc, manganese and even lanthanoid metals (Gd, Eu, Yb, and Lu [132]) have been reported up to now in two forms of heterogeneous solid catalysts and homogeneous solution catalysts, which have been widely reviewed for general [133,125,134-136] or specific [137-140] catalytic applications. In 1983, when the number of known structures of POMs was not even as much as now, Pope noted in his inspiringly famous book “Heteropoly and Isopoly Oxometalates” that POMs have been prepared with more than 65 elements as the central atom (in Pope’s terminology the heteroatom) [127,128].

### **2.4.3 Polyoxotungstates**

Among all the mentioned transition metals, a great deal of attention has been paid to tungsten, since its heteropoly compounds have shown considerable superiorities, especially in heterogeneous form in terms of acidity, thermal stability, and hydrophobicity, in comparison with the other metals [126,131] [130]. Hereafter, W-based HPA and POM are designated as heteropoly tungstic acid (HPTA) and polyoxotungstate (POT), respectively (which can be used roughly instead of each other). POTs can be easily prepared and polymerized by dehydration from tungstate and a heteroatom oxoanion in acidified aqueous solution. Equation 2.2 indicates the formation of



phosphotungstate, the most common POM, from tungstate and phosphate under controlled temperature and pH:



Generally, HPTAs are soluble in water and polar solvents, and thus, form homogeneous catalytic systems in many reactions involving such solvents. Although the overwhelming majority of such homogeneous catalytic systems have demonstrated better efficiency than their heterogeneous counterparts, especially in organic transformations where heterogeneous systems possess poor reactant/catalyst contact arising from pore diffusion limitations and mass transfer resistance, the use of homogeneous systems in large-scale may not be in line with sustainable chemistry due to lack of catalyst reusability. This gave rise to the rapid development of heterogenization of originally homogenous W-based heteropoly compounds. Interestingly, solid POT catalysts have exhibited unique pseudo-liquid phase properties in liquid organic reactions, particularly in the presence of highly polar and small size substrates, which enables them with good catalytic efficiency despite their generally non-porous structures [141-143]. Moreover, compared to the other solid acids, heterogeneous HPTAs have shown excellent water-tolerant properties [131], which hold a promise for their application in the reactions involving water such as hydrolysis, hydration, esterification, and acetalization where a major problem in the use of solid acids is the poisoning of acid sites by water resulting in loss of their catalytic activities. Additionally, relatively low thermal stability of HTPAs leading to difficult catalyst regeneration process, which had influenced their application to some extent, has been overcome by offering some approaches such as developing novel HTPAs enjoying high thermal stability, modification of HTPAs to enhance coke combustion, preventing coke formation on HTPAs during the reaction, employing supercritical fluids as the reaction medium and cascade reactions using multifunctional HTPA catalysis [144].

So far, solidification of HPTAs have been done mainly via substitution of some protons of their structure by inorganic cations, grafting functional organic species to POTs, and immobilization of HPTAs on supports. Occasionally, these strategies have been exploited simultaneously to fabricate a heterogeneous POT, in which, it is difficult to clearly determine which part shoulders the responsibility for heterogenization (inorganic cation or organic species or support). In what follows, we have tried to review all of the recent works on heterogeneous POM-

based catalysts made of W as central atom. Herein, different solid POT catalysts are classified based on the heterogenization strategy, which will be investigated in sections 2.4.3.1-6, along with their applications in liquid phase organic reactions. The target reactions, although include a variety of liquid organic reactions, can be conveniently categorized into two general groups, acid catalysis and oxidation reactions. In order to enable a better comparison and outlook, the reported works in the literature have been tabulated in the following sections (Tables 2.9-2.16).

### 2.4.3.1 Inorganic cation substituted solid POTs

Substitution of protons by a cation with appropriate size, amount, charge, and hydrophobicity could result in insoluble solids, provided that the substituted cation can make strong ionic interactions with POT. About three decades ago, Moffat et al. reported synthesis of microporous POT catalysts using salts of heteropoly compounds with different monovalent cations [145]. To date, cations such as  $\text{Cs}^+$ ,  $\text{Na}^+$ ,  $\text{K}^+$ ,  $\text{NH}_4^+$ ,  $\text{Ag}^+$ ,  $\text{Sn}^{2+}$ ,  $\text{Zn}^{2+}$ ,  $\text{Bi}^{3+}$ ,  $\text{Mn}^{2+}$ ,  $\text{Co}^{2+}$ , and  $\text{Cu}^{2+}$  have successfully substituted protons of the homogeneous POTs to heterogenize them. They are listed in Tables 2.9, 2.10, and 2.11. Although the synthesis of solid POT catalysts would attract more scientific and industrial attention when associated with a practical application in a typical reaction, tuning the properties of solidified POTs with inorganic cations has been the sole subject of several articles for many years (Table 2.9). Tables 2.10 and 2.11 list the works in this field, including applications in acid catalysis and oxidation reactions, respectively.

Extensive researches have focused particularly on caesium cation, most likely because of its unique effects not only on the solubility but also on surface area, pore structure and surface acidity of the resultant POT [131]. Professors Okuhara, Mizuno and Misono and their colleagues have thoroughly investigated the changes in catalytically important aspects of  $\text{Cs}^+$  substituted phosphotungstic acid (PTA) in their inspiring works [131,146-148]; water soluble PTA was converted to a water-tolerant acid catalyst ( $\text{Cs}_x\text{H}_{3-x}\text{PW}_{12}\text{O}_{40}$ ), the hydrophobicity of which is even higher than silica-alumina and some zeolites [131] and, interestingly, its catalytic features could be well tuned via varying the amount of  $\text{Cs}^+$  cations. Changing the pore structure from ultramicropores (pore width 0.43 to 0.50 nm) in  $\text{Cs}_{2.1}\text{H}_{0.9}\text{PW}_{12}\text{O}_{40}$  to mesopores in  $\text{Cs}_{2.5}\text{H}_{0.5}\text{PW}_{12}\text{O}_{40}$  enables

shape-selective catalysis properties. More importantly, upon incorporation of Cs<sup>+</sup> in PTA, the surface area slightly decreased from 6 m<sup>2</sup>/g at x=0 to 1 m<sup>2</sup>/g at x=2, but further increasing the Cs<sup>+</sup> content to x=3 surprisingly increased the surface area to 156 m<sup>2</sup>/g [147]. Figure 2.16 shows the surface area as well as surface concentration of acid sites of Cs<sub>x</sub>H<sub>3-x</sub>PW<sub>12</sub>O<sub>40</sub> as a function of Cs<sup>+</sup> content [131,148].

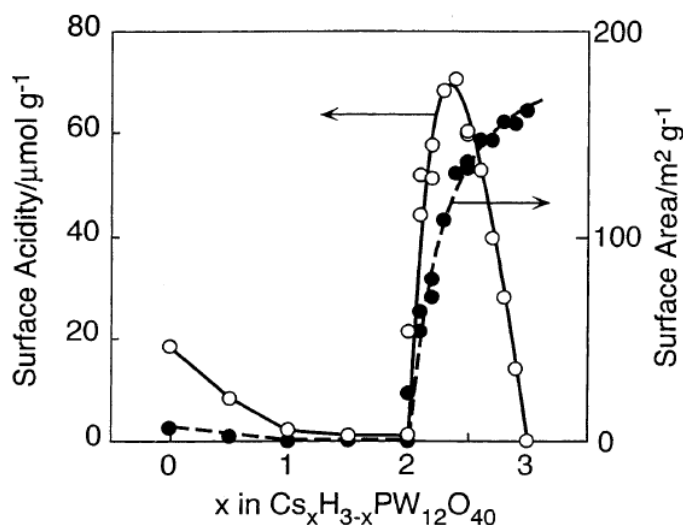


**Figure 2.16.** Surface area and acidity of Cs<sub>x</sub>H<sub>3-x</sub>PW<sub>12</sub>O<sub>40</sub> as a function of Cs<sup>+</sup> content [131,148].

As Figure 2.16 shows, the surface acidity (number of protons on the surface), which was determined by IR spectroscopic studies of CO adsorption at 110 K, reached a maximum at x=2.5. This remarkably high surface acidity along with the reported higher acid strength of Cs<sub>2.5</sub>H<sub>0.5</sub>PW<sub>12</sub>O<sub>40</sub> (abbreviated as Cs2.5), measured by microcalorimetry of NH<sub>3</sub> adsorption and TPD of NH<sub>3</sub>, compared to the common solid acid catalysts (e.g. H-ZSM-5 and SiO<sub>2</sub>-Al<sub>2</sub>O<sub>3</sub>) [149,147] have proposed Cs2.5 as a superior solid acid catalyst. Recently, a great deal of attention has been paid to catalytic applications of Cs2.5, particularly in acid catalysis reactions (Table 2.10). Cs3, in spite of its weaker acidity compared to the more known Cs2.5, has been also investigated as support for Ru nanoparticles in conversion of cellobiose and cellulose into sorbitol in aqueous medium [150].

Silicotungstic acid is another POT that has been heterogenized by substitution of Cs<sup>+</sup> cations [151-153]. For example, Pesaresi et al. have reported the synthesis of Cs<sub>x</sub>H<sub>4-x</sub>SiW<sub>12</sub>O<sub>40</sub> and its application for C<sub>4</sub> and C<sub>8</sub> triglyceride transesterification and palmitic acid esterification with

methanol [153]. The degree of heterogenization strongly depends on the amount of caesium cations: at lower Cs content ( $x \leq 0.8$ ) these catalysts showed partially homogeneous properties, while at higher Cs loading they exhibited entirely heterogeneous properties.

**Table 2.9.** Inorganic cations substituted POTs for general catalytic purposes.

Entry	Counter-cation	IC-substituted POT <sup>1</sup>	Remarks	Ref.
1		Cs <sub>2.5</sub> H <sub>0.5</sub> PW <sub>12</sub> O <sub>40</sub>	- Meso- and microporous structure of the POT have been examined. - Presence of very strong acidic sites on the POT has been indicated.	[147]
2	Cs <sup>+</sup>	Cs <sub>3</sub> PW <sub>12</sub> O <sub>40</sub>	- Self-organization of the POT nanocrystallites has been successfully controlled by the changes in the synthetic temperatures and counteranions (Cs <sup>+</sup> , Ag <sup>+</sup> , and NH <sub>4</sub> <sup>+</sup> ). - Formation and growth mechanism of the POT particles have been investigated.	[154]
3		(NH <sub>4</sub> ) <sub>3</sub> PW <sub>12</sub> O <sub>40</sub>	- “Sponge crystals” of the POT have been defined as molecular single crystals including continuous voids originating from series of neighboring vacancies of the constituent large molecules, which has afforded nanospaces in the crystals. - Changing the synthesis temperature, the POTs with high surface areas, ranging from 65 to 116 m <sup>2</sup> /g, have been prepared.	[155,156]
4		(NH <sub>4</sub> ) <sub>3</sub> PW <sub>12</sub> O <sub>40</sub>	- Self-organization of the POT nanocrystallites has been successfully controlled by the changes in the synthetic temperature and counteranion (Cs <sup>+</sup> , Ag <sup>+</sup> , and NH <sub>4</sub> <sup>+</sup> ). - Formation and growth mechanism of the POT particles have been investigated.	[154]
5	Ag <sup>+</sup>	Ag <sub>3</sub> PW <sub>12</sub> O <sub>40</sub>	- Self-organization of the POT nanocrystallites has been successfully controlled by the changes in the synthetic temperature and counteranion (Cs <sup>+</sup> , Ag <sup>+</sup> , and NH <sub>4</sub> <sup>+</sup> ). - Formation and growth mechanism of the POT particles have been investigated.	[154]

1. IC: inorganic cation

**Table 2.10.** Inorganic cations substituted POTs for acid catalysis reactions.

Entry	Counter-cation	IC-substituted POT	Reaction	Remarks	Ref.
1		$\text{Cs}_{2.2}\text{H}_{0.8}\text{PW}_{12}\text{O}_{40}$	decomposition of ester, dehydration of alcohol, and alkylation of aromatics	- Pore size of the POT was precisely controlled by $\text{Cs}^+$ content. - This POT was reported as the first example of shape-selective catalysis by solid superacid in liquid organic reaction.	[148]
2		$\text{Cs}_x\text{H}_{4-x}\text{SiW}_{12}\text{O}_{40}$	Transesterification of $\text{C}_4$ and $\text{C}_8$ triglycerides and esterification of palmitic acid	- Changing the homogeneous properties of the POT to heterogeneous properties by increasing $\text{Cs}^+$ content has been investigated.	[153]
3		$\text{Cs}_{2.5}\text{H}_{0.5}\text{PW}_{12}\text{O}_{40}$	Microwave-assisted transesterification of yellow horn oil	- Optimizing the reaction conditions, the POT has been shown to be an efficient catalyst for production of biodiesel-fuel by means of microwave irradiation.	[157]
4		$\text{Cs}_x\text{H}_{3-x}\text{PW}_{12}\text{O}_{40}$ ( $x=1, 1.5, 2, 2.5, 3$ )	Ultrasound-assisted transesterification of crude <i>Jatropha</i> oil	- Changes in the POT properties and catalytic activity have been investigated.	[158]
5	$\text{Cs}^+$	$\text{Cs}_{2.5}\text{H}_{0.5}\text{PW}_{12}\text{O}_{40}$	cycloaddition of crotonaldehyde to monoterpene alkenes	- Catalytic activity of the POT has been compared with silica-supported HTPA ( $\text{H}_3\text{PW}_{12}\text{O}_{40}$ ).	[159]
6		$\text{Cs}_3\text{PW}_{12}\text{O}_{40}$	Conversions of cellobiose and cellulose into sorbitol in water	- Ru nanoparticles have been supported on the POT, which despite of not having strong acidity, was efficient catalyst.	[150]
7		$\text{Cs}_{2.5}\text{H}_{0.5}\text{PW}_{12}\text{O}_{40}$	Glycerol acetalization with formaldehyde	- Catalytic activity of the POT has been compared with that of periodic mesoporous organosilicas, zeolite ZSM-5, and commercial catalyst Amberlyst-15, which showed superiority.	[160]
8		$\text{Cs}_2\text{HPW}_{12}\text{O}_{40}$ $\text{Cs}_3\text{HSiW}_{12}\text{O}_{40}$	Carbonylation of dimethyl ether to methyl acetate	- The POT was modified by adding Rh to its structure, which greatly increased the conversion because a multiplier effect occurred between Rh and the POT.	[151]
9		$\text{Cs}_{2.5}\text{H}_{0.5}\text{PW}_{12}\text{O}_{40}$	Synthesis of xanthenedione derivatives from aldehydes	- $\text{CS}_{2.5}$ has been employed for the first time for synthesis of 1,8-dioxo-octahydroxanthenes by the reaction of aldehydes with 1,3-cyclohexanedione/dimedone, and exhibited high yields of products and short reaction time.	[161]
10		$\text{Cs}_{2.5}\text{H}_{0.5}\text{PW}_{12}\text{O}_{40}$	Thioacetalization and transtioacetalization reactions	- The POT was an effective catalyst with high selectivity.	[162]
11		$\text{Cs}_{2.5}\text{H}_{0.5}\text{PW}_{12}\text{O}_{40}$ $\text{Cs}_{3.5}\text{H}_{0.5}\text{SiW}_{12}\text{O}_{40}$	Production of methyl <i>tert</i> -butyl ether (MTBE) from methanol and <i>tert</i> -butyl alcohol	- The Cs substituted POTs exhibited higher activity compared to the parent POTs and activated carbon supported POTs, which was discussed from kinetic viewpoints.	[152]
12	$\text{Ag}^+$	$\text{Ag}_x\text{H}_{4-x}\text{SiW}_{12}\text{O}_{40}$ $x=0, 1, 2, 3, \text{ and } 4$	Transformation of alkynylloxiranes to furan	- Ag content to reach good catalytic efficiency was optimized.	[163]

13		Ag <sub>3</sub> PW <sub>12</sub> O <sub>40</sub>	Conversion of fructose and glucose into 5-hydroxymethylfurfural	-	The POT was tolerant to high concentration feedstock, and showed environmentally benign properties with double acidity.	[164]
14		Ag <sub>3</sub> PW <sub>12</sub> O <sub>40</sub>	Intermolecular hydroamination of olefins	-	Compared to the parent HPTA, the synthesized POT exhibited lower catalytic efficiency.	[165]
15	Na <sup>+</sup>	H <sub>14</sub> [NaP <sub>5</sub> W <sub>29</sub> MoO <sub>110</sub> ]	Different functional groups protective reactions such as tetrahydropyranlation of phenol and alcohols, acetylation of alcohols, phenols, amines and thiols with Ac <sub>2</sub> O, trimethylsilylation of phenols and alcohols	-	The Mo-substituted Preyssler structure POT has shown higher activity than Keggin or Wells Dawson heteropolyacids due to its higher number of acidic protons.	[166]
16		Na <sub>8</sub> H[PW <sub>9</sub> O <sub>34</sub> ]	Knoevenagel condensation and cyanosilylation of various aldehydes and ketones and the synthesis of benzoxazole derivatives	-	The POT could catalyze the reactions at 25 °C under mild conditions in chloride-free solvents.	[167]
17	K <sup>+</sup>	K <sub>2.2</sub> H <sub>0.8</sub> PW <sub>12</sub> O <sub>40</sub>	Esterification of 2-keto-L-gulonic acid	-	The POT showed good catalytic activity (slightly lower than that of homogeneous HPTA).	[168]
18		K <sub>x</sub> H <sub>3-x</sub> PW <sub>12</sub> O <sub>40</sub> (x= 2 and 2.5)	Dehydration of ethanol	-	The POTs have exhibited higher reactivity than HPTA. Thermal stability of the POTs in x=2.5 is higher than x=2.	[169]
19	NH <sub>4</sub> <sup>+</sup>	(NH <sub>4</sub> ) <sub>3</sub> PW <sub>12</sub> O <sub>40</sub>	Intermolecular hydroamination of olefins	-	Compared to PTA, the POT exhibited lower catalytic efficiency.	[165]
20		(NH <sub>4</sub> ) <sub>2</sub> HPW <sub>12</sub> O <sub>40</sub>	Thioacetalization and transthoacetalization reactions	-	The POT was an effective catalyst with high selectivity.	[162]
21	Sn <sup>2+</sup>	Sn <sub>x</sub> [H <sub>3</sub> PW <sub>12</sub> O <sub>40</sub> ] (x= 0.5, 1, and 1.5)	Benzylation of arenes with benzyl alcohol	-	Dependency of the catalytic activity on Sn <sup>2+</sup> content has been investigated	[170]
22	Zn <sup>2+</sup>	Zn <sub>1.2</sub> H <sub>0.6</sub> PW <sub>12</sub> O <sub>40</sub>	Esterification of palmitic acid and transesterification of waste cooking oil	-	The POT has shown superior catalytic activity compared to HTPA due to introduction of Lewis acid sites by partial exchange of H <sup>+</sup> by Zn <sup>2+</sup> , high acid strength by Lewis site-assisted Brønsted sites, a high surface area, and nanostructure.	[171]
23	Bi <sup>3+</sup>	BiPW <sub>12</sub> O <sub>40</sub>	Esterification of oleic acid with <i>n</i> -butanol	-	In addition to BiPW, other metal salts of PTA were synthesized including LaPW, CuPW, AlPW, FePW, and SnPW, however, the most efficient catalyst was bismuth salt of PTA.	[172]

**Table 2.11.** Inorganic cations substituted POTs for oxidation reactions.

Entry	Counter-cation	IC-substituted POT	Reaction	Remarks	Ref.	
1	K <sup>+</sup>	K <sub>6</sub> [PW <sub>9</sub> V <sub>3</sub> O <sub>40</sub> ]	Amoximation of different ketones and aldehydes	-	The V-substituted POT has been proved to be heterogeneous in isopropanol and recyclable.	[173]
2	Mn <sup>2+</sup> Co <sup>2+</sup> Cu <sup>2+</sup>	{[M <sub>2</sub> (H <sub>2</sub> O) <sub>6</sub> ][Mn <sub>4</sub> (H <sub>2</sub> O) <sub>16</sub> ][WZn(Mn(H <sub>2</sub> O)) <sub>2</sub> (ZnW <sub>9</sub> O <sub>34</sub> ) <sub>2</sub> ]} · 10H <sub>2</sub> O (M = Co <sup>II</sup> and Cu <sup>II</sup> )	Oxidative aromatization of Hantzsch 1,4-dihydropyridines	-	The POT-based solid was prepared by using {Mn <sub>2</sub> Zn <sub>3</sub> W <sub>19</sub> } as a building block and Mn <sup>II</sup> cation as a connecting node. Induced by Co <sup>2+</sup> and Cu <sup>2+</sup> and solvent molecules, this solid was transformed into the final interesting 3D solid framework.	[174]

Substitution of some other inorganic cations including  $\text{Na}^+$ ,  $\text{K}^+$ ,  $\text{NH}_4^+$ ,  $\text{Ag}^+$ ,  $\text{Sn}^{2+}$ ,  $\text{Zn}^{2+}$ ,  $\text{Bi}^{3+}$ ,  $\text{Mn}^{2+}$ ,  $\text{Co}^{2+}$ , and  $\text{Cu}^{2+}$  into the POTs structures in order to heterogenize them have been also documented, but not as much as cesium (please see Tables 2.10 and 2.11). As these Tables show, this class of solidified POT catalysts are more interesting for acid catalysis reactions compared to oxidation reactions, most probably because of their high and tunable acidity.

#### 2.4.3.2 Organo-solidified POTs

Parallel to the intrinsically interesting properties of POMs, succinctly summarized in section 2.4.2, their potential for functionalization via organic compounds is a tremendous impetus that has pushed working and research on POMs in the last ten years. Such functionalization has been found compulsory for implementation of POMs to some, mainly new, applications, since organo-modified POMs render several opportunities for facile integration of POMs into functional architectures and devices that original POMs cannot [175]. This gives an additional firm rise to push the essentially attractive area of organic-inorganic hybrid materials to be applied in POMs preparation.

In the field of catalysis, employing hybrid organic-inorganic polyoxometallate-based catalysts is currently a hot topic being enthusiastically and rapidly explored, not only for heterogenization purposes, but also for their versatilities in liquid organic reactions arising from the wide variety of organic groups and proper adjustment of the surface state. Indisputable merits of exploiting organic species in POTs structures are increasing catalyst hydrophobicity, and thus, preventing (i) aggregation of catalyst particles, and (ii) poisoning of acid sites by  $\text{H}_2\text{O}$  in water-involving reactions. On the other hand, functionalization and even post-functionalization of POTs with organic moieties are currently performed under either hydrothermal condition benefiting from a simple, often one-pot, procedure or mild synthetic conditions complying with the principles of “Chimie Douce” [176-178]. Given the aforementioned positive features and comparatively huge number of recent publications in this domain, incorporation of organic groups into the structure of POMs has been the sole subject of several recent review papers [177,179-183,175,184-186].

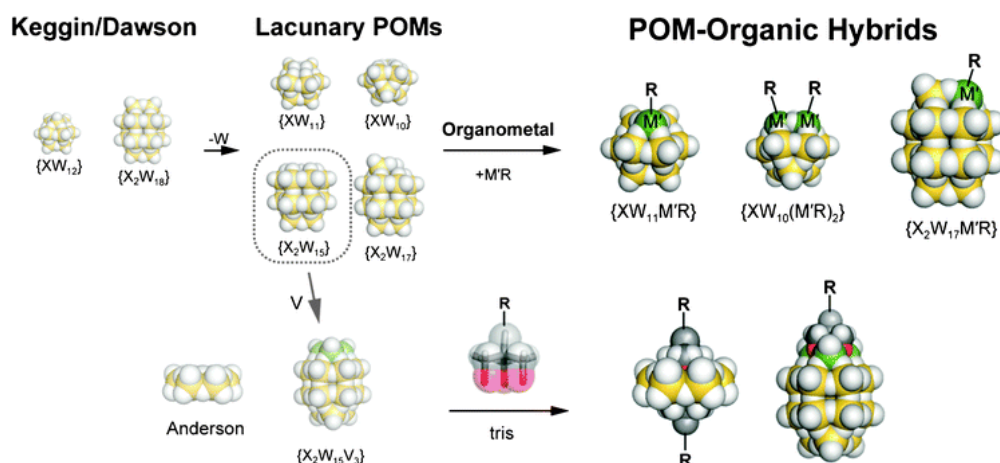


Different techniques developed for design and synthesis of organic-inorganic hybrid POM compounds have been widely investigated. Abridgedly, they have been categorized into two classes based on the nature of interactions between organic and inorganic parts: non-covalent and covalent POT-organic hybrids. In these two classes, many organic compounds have been encapsulated into POTs structures to modify its heterogeneous catalytic properties such as surfactants, especially nitrogen containing ones, amines, ionic liquids, etc. With the aid of crystal engineering and supramolecular cooperation, although the first group has been more deeply investigated [187-189], most probably due to its comparatively convenient fabrication, the second group is currently undergoing a rapid development not only because of some unavoidable drawbacks of the first group (e.g. catalyst leaching despite appreciable stability in the reaction media), but also because of the undisputed advantages of covalently linked hybrids such as fine control of the interaction between the components resulting in enhancement of synergistic effects, better dispersion of POMs in matrices, and, most importantly, higher and more lasting stability of the assembly.

The first class, non-covalent hybrids, encompasses those hybrids with electrostatic interactions, hydrogen bonds or van der Waals forces. The most distinguished example of this group is organic cation substituted POMs; the anionic character of POMs renders the exchange of their counter cations feasible. As mentioned before, POTs are originally soluble in water and polar solvents, while generally metal oxides are not. Since complete dissolution and solvolysis of the components to give charged species are required for formation of ionic bonding, POTs, unlike the metal oxides, are capable to electrostatically interact with positively charged solutes, resulting in facile incorporation of inorganic and organic cations into the structures of POTs. Organic cations in ionic liquids have attracted a large attention to act as counter-cation pairing with POT anions since 2004 [190,191]. This attention arises not only from the ease of synthesis procedure, but also from increasing interest in ionic liquids due to their unique properties such as low melting point, non-volatility and flammability, and ionic conductivity. These interesting features, firstly, rendered the resultant POT-organic hybrid efficiently applicable in electrochemical processes and practically applicable in surface and interface science through fabrication of self-assembled films (e.g. layer-by-layer (LbL) or Langmuir-Blodgett (LB) films) [192,186]. Many works have then been done on the preparation of catalytically active solid POT-organic hybrids out of ionic liquids. Hydrogen bonding in fabrication of POM-organic hybrids based on non-covalent interactions has

been also reported, like what was obtained in linking proteins to POMs [193,194], however, the overwhelming majority of the non-covalent interactions involve ionic bonding.

The second class contains those hybrids in which organic and inorganic parts are connected via strong covalent or ionic-covalent bonds. These hybrids are usually formed either by substitution of an oxo group of the POMs by an organic ligand or approaching electrophilic organic components to the nucleophilic surface oxygen atoms of POMs. Undoubtedly, this class of organo-modified POTs is more stable due to the stronger interactions between the organic and inorganic parts. However, fabrication of their assemblies often involves sophisticated functionalization. The first step is removing one or more addenda atoms and their attendant oxide ions from the structure, giving lacunary structure. Then, organic moieties can be grafted to the organometallic compounds of lacunary POT clusters (Scheme 2.9). Different strategies for the second step have been employed based on functionalization and/or post-functionalization of POTs (Figure 2.17), which have been nicely investigated and compared in a critical review paper presented by Proust et al. [175].



**Scheme 2.9.** Schematic view of preparation of covalent POT-organic hybrids [186].

Some of the previously mentioned review papers on organo-modification techniques of POMs have covered their catalytic aspects also as a subsection, however, particular focus that thoroughly covers the catalytic applications of POM-based organic-inorganic hybrids has been less documented [179,183,184]; Nlate and Jahire presented a microreview on dendritic POM-based hybrid catalysts for oxidation reactions, which although efficient and recoverable, are categorized

under homogeneous catalysis [183], while the other two references addressed heterogeneous catalysis by organic-inorganic hybrids POMs [179,184]. Herein, we have listed the catalytic applications of organo-solidified W-based POMs (POTs), to encourage exploiting the inherently interesting properties of tungsten, succinctly mentioned in section 2.4.1, and heterogeneous organo-modified POMs, simultaneously, which could be advantageous to be employed in several organic liquid reactions. Tables 2.12 and 2.13 summarize the organo-modified POT catalysts with their applications in acid catalysis and oxidation reactions, respectively.

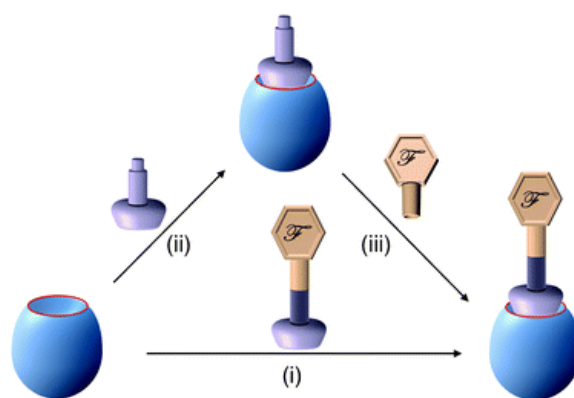
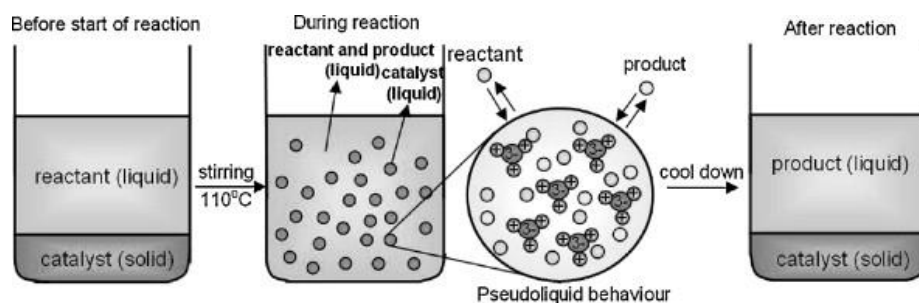


**Figure 2.17.** Different strategies for preparation of covalent POT- organic hybrids. Path (i): direct functionalization, paths (ii, iii): post-functionalization. The lacunary POM is represented in blue, while the anchoring tether is lilac and the added functional moiety (F) is beige [175].

One of the most common and unique advantages of organo-solidified POTs is their improved compatibilities with the liquid medium of organic reactions, resulting in not only comparable and even sometimes superior, catalytic efficiencies to the corresponding homogeneous POTs, but also self-separation performance at the end of reaction. Intriguingly, the organic-POT hybrid catalyst is capable to change its heterogeneous behavior during liquid-phase organic reactions; in the beginning of reaction, it is obviously a solid catalyst in the reaction mixture, which would then turn into pseudo-homogeneous system during the reaction, often upon heating. Afterwards, the reaction mixture keeps a pseudo-liquid phase until the end of reaction, when the catalyst starts to precipitate, often upon cooling down to room temperature (Scheme 2.10). This enables self-separation and easy recovery of the organo-solidified POT catalyst.

Leclercq et al. have stabilized pickering emulsion medium for oxidation reactions by using  $[C_{12}]_3PW_{12}O_{40}$  in the presence of water and an aromatic solvent (Figure 2.18). Combining the advantages of biphasic catalysis and heterogeneous catalysis in such catalytic emulsions made

separation of the products easy and prevented catalyst leaching [195]. Mizuno et al. have reported preparation of a size-selective catalyst via organo-modification of the POT silicododecatungstate by tetrabutylammonium, which was synthesized through a bottom-up approach. The resultant hybrid gave excellent catalytic activity because of the high mobility of the catalyst in the solid bulk and easy cosorption of the substrate and oxidant,  $\text{H}_2\text{O}_2$  (Figure 2.19) [196].



**Scheme 2.10.** Schematic diagram of a typical organic liquid-phase reaction over organic-POT hybrids with self-separation performance.

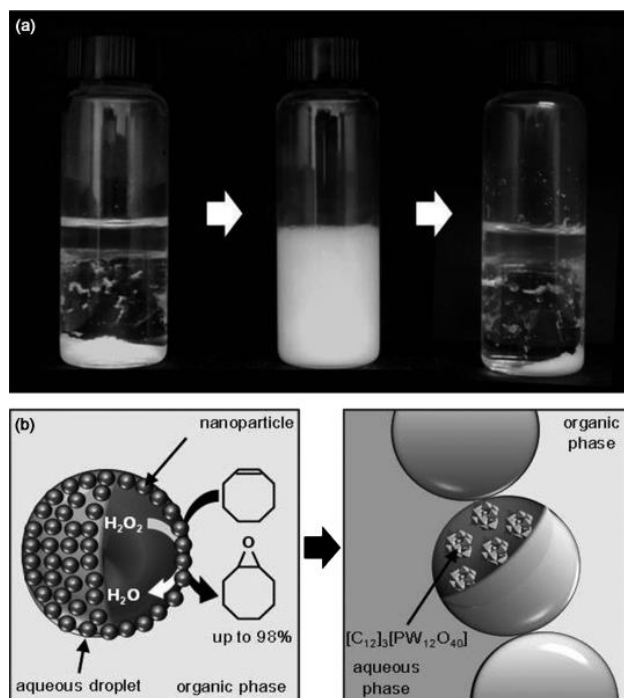


**Figure 2.18.** a) Macroscopic views of the water/toluene/[C12]3[PW12O40] system before emulsification, during the reaction, and after centrifugation (from left to right). b) Schematic representation of the catalytic epoxidation of olefins inside this emulsion [195].

**Table 2.12.** Organo-solidified POTs for acid catalysis reactions.

Entry	Organic source	POT-organic hybrid	Reaction	Remarks	Ref.
1	Amino acid: lysine	$(ly)_xH_{3-x}PW_{12}O_{40}$ x= 1, 2	Transesterification of triglycerides and esterification of free fatty acids	- The POT is an acid-base bifunctional nanocatalyst, which allowed acid-base tandem conversions in one-pot. - The acidic or basic strength could be modulated by changing the ratio of HTPA anion to amino acid	[197]
2	Organosulfate surfactant: dodecyl sulfate	$Cr[(DS)H_2PW_{12}O_{40}]_3$ (DS: $OSO_3C_{12}H_{25}$ dodecyl sulfate)	Conversion of cellulose into HMF	- Good catalytic activity of the POT was mainly attributed to double Brønsted and Lewis acidities, and the micellar structured catalytic system with hydrophobic groups.	[198]
3	Quaternary ammonium surfactant: CTAB	$[C_{16}H_{33}N(CH_3)_3]H_2PW_{12}O_{40}$	Hydrolysis of polysaccharides into glucose	- The POT was designed to form a micellar catalytic system, which gave good efficiency toward production of glucose.	[199]
4	Ionic liquid	$[MIMPS]_3PW_{12}O_{40}$ $[PyPS]_3PW_{12}O_{40}$ $[TEAPS]_3PW_{12}O_{40}$	Esterification of free fatty acids	- The POT showed high catalytic activity, self-separation, and easy reuse. - Good solubility in reactants, nonmiscibility with ester product, and high melting point of the POT enable the reaction-induced switching from homogeneous to heterogeneous with subsequent precipitation of the catalyst.	[200, 201]
5	Ionic liquid	$[TPSPP]_3PW_{12}O_{40}$	Esterification of free fatty acids	- High efficiency of the POT came from its pseudo-liquid phase behavior, phase transfer phenomena, and stabilization effect of the heteropolyanion on carbonium ionic intermediates.	[202]
6	Ionic liquid	$[MIM-PSH]_xH_{3-x}PW_{12}O_{40}$ x: 1 to 3	Esterification of palmitic acid	- Superior catalytic efficiency of the POT arose from better super-acidity and lower molecular transport resistance of catalyst.	[203]
7	Ionic liquid	$[NMP]_3PW_{12}O_{40}$	Prins cyclization of styrene with formalin	- Excellent catalytic performance of the POT was because of its pseudo-liquid behavior and stabilization effect of carbonyl in amide on protonated formaldehyde of the reaction intermediate, together with its solid nature and insolubility.	[204]
8	Ionic liquid	$[MIMPS]_3PW_{12}O_{40}$	Beckmann rearrangements of ketoximes	- Using $ZnCl_2$ as cocatalyst, the POT was highly efficient and recoverable.	[205]
9	Ionic liquid	$[DPySO_3H]_{1.5}PW_{12}O_{40}$	Beckmann rearrangement of cyclohexanone oxime	- In the absence of environmentally harmful cocatalyst $ZnCl_2$ , the POT was highly efficient and recoverable.	[206]

10	Ionic liquid	[PyBS] <sub>3</sub> PW <sub>12</sub> O <sub>40</sub> [TEABS] <sub>3</sub> PW <sub>12</sub> O <sub>40</sub> [MIMBS] <sub>3</sub> PW <sub>12</sub> O <sub>40</sub> [PyBS] <sub>4</sub> SiW <sub>12</sub> O <sub>40</sub> [TEABS] <sub>4</sub> SiW <sub>12</sub> O <sub>40</sub> [MIMBS] <sub>4</sub> SiW <sub>12</sub> O <sub>40</sub>	Transesterifications of trimethylolpropane	- The [PyBS] <sub>3</sub> PW <sub>12</sub> O <sub>40</sub> POT acted as homogeneous catalyst during the reaction which upon cooling down at the end of reaction, became solid enabling self-separation performance.	[207]
11	Ionic liquid	[MIMBS] <sub>3</sub> PW <sub>12</sub> O <sub>40</sub>	Conversion of furfuryl alcohol into alkyl levulinates	- The POT was highly efficient and recoverable.	[208]
12	Ionic liquid	[TMEDASO <sub>3</sub> H] <sub>1.5</sub> PW <sub>12</sub> O <sub>40</sub>	Conversion of fructose into 5-hydroxymethylfurfural (HMF) and alkyl levulinate	- The POT could perform one-pot conversion of fructose into HMF and alkyl levulinate. - Catalytic activities of the POTs followed the order of their acid strength.	[209]
13	Ionic liquid	[PySalm] <sub>3</sub> PW <sub>12</sub> O <sub>40</sub>	Knoevenagel condensation	- The acid–base bifunctional POT provided a controlled nearby position for the acid–base dual sites.	[210]
14	Ionic liquid	PEG-2000 chain-functionalized alkylimidazolium H <sub>3</sub> PW <sub>12</sub> O <sub>40</sub>	Esterification of alcohols and aldehydes	- Emulsion was formed between the POT and substrates during the reaction promoting catalytic process, which, after reaction, was broken by addition of a weakly polar organic solvent to facilitate separation of the POT.	[211]
15	Organozirconium complexes	[( <i>n</i> -C <sub>4</sub> H <sub>9</sub> ) <sub>4</sub> N] <sub>6</sub> [α-PW <sub>11</sub> Al(OH)O <sub>38</sub> ZrCp <sub>2</sub> ] <sub>2</sub> [( <i>n</i> -C <sub>4</sub> H <sub>9</sub> ) <sub>4</sub> N] <sub>6</sub> [α-SiW <sub>11</sub> Al(OH) <sub>2</sub> O <sub>38</sub> ZrCp <sub>2</sub> ] <sub>2</sub> ·2H <sub>2</sub> O (Cp = η <sup>5</sup> -C <sub>5</sub> H <sub>5</sub> <sup>-</sup> )	Esterification of fatty acids with methanol	- The P containing POT exhibited higher activity than the Si containing one, due to its Lewis acidity; fatty acids interacted with the Lewis acid sites in the catalysts.	[212]
16	Cationic Al(III)-Schiff base complex (Al(III)-salphen)	[Al(salphen)(H <sub>2</sub> O) <sub>2</sub> ] <sub>3</sub> [α-PW <sub>12</sub> O <sub>40</sub> ]· <i>m</i> C <sub>8</sub> H <sub>10</sub> · <i>n</i> CH <sub>3</sub> COCH <sub>3</sub>	Pinacol rearrangement	- The organo-modified POT exhibited higher activity than its parent components, arising from synergetic effect of Al(III)-salphen and POT in a porous framework.	[213]

TPSP: triphenyl(3-sulfopropyl)phosphonium

MIM-PS: zwitterion 3-(1-methylimidazolium-3-yl) propane-1-sulfonate

NMP: *N*-methyl-2-pyrrolidonium

DPySO<sub>3</sub>: *N,N'*-di(3-sulfopropyl) 4,4'-dipyridinium

MIMBS: methylimidazolebutylsulfate

PySalm: 1-(2-salicylaldimine)pyridinium

Salphen = *N,N'*-phenylenebis(salicylideneimine)

**Table 2.13.** Organo-solidified POTs for oxidation reactions.

Entry	Organic source	POT-organic hybrid	Reaction	Remarks	Ref.
1	Quaternary ammonium surfactant: tetra- <i>n</i> -butylammonium	$[(n-C_4H_9)_4N]_4[\gamma-SiW_{10}O_{34}(H_2O)_2]$ . H <sub>2</sub> O	Size-selective oxidation of various organic substrates, including olefins, sulfides, and silanes with H <sub>2</sub> O <sub>2</sub>	- The nonporous POT has been synthesized via a bottom-up approach, which gave good catalytic activity because of high mobility of the catalyst in the solid bulk and easy cosorption of the substrate and oxidant.	[196]
2	Quaternary ammonium surfactant: tetra methylammonium Tetra- <i>n</i> -propylammonium tetra- <i>n</i> -butylammonium tetra- <i>n</i> -pentylammonium	$[(CH_3)_4N]_4[\gamma-SiW_{10}O_{34}(H_2O)_2]$ $[(n-C_3H_7)_4N]_4[\gamma-SiW_{10}O_{34}(H_2O)_2]$ $[(n-C_4H_9)_4N]_4[\gamma-SiW_{10}O_{34}(H_2O)_2]$ $[(n-C_5H_{11})_4N]_4[\gamma-SiW_{10}O_{34}(H_2O)_2]$	Epoxidation of alkenes (propene and 1-hexene)	- High catalytic activity of the POT arises from flexibility of crystal structures of the POT, and high mobility of alkylammonium cations resulting in uniform distribution of reactant and oxidant molecules throughout the solid bulk of the catalyst. - Not only atomic structures of the active sites but also the structures and dynamics of the surroundings is important for the design and synthesis of highly active POT.	[214]
3	Quaternary ammonium surfactants with varying alkyl chain length: DDA, TDA, HAD, and ODA	(DDA) <sub>3</sub> PW <sub>12</sub> O <sub>40</sub> (TDA) <sub>3</sub> PW <sub>12</sub> O <sub>40</sub> (HDA) <sub>3</sub> PW <sub>12</sub> O <sub>40</sub> (ODA) <sub>3</sub> PW <sub>12</sub> O <sub>40</sub>	Oxidative desulphurization of dibenzothiophene with H <sub>2</sub> O <sub>2</sub>	- The mesostructured POT was highly efficient due to presence of long alkyl chains on its surface that provided suitable hydrophobic-hydrophobic properties and polarity resulting in better adsorption of the substrate sulfide molecules and desorption of the products sulfones.	[215]
4	Quaternary ammonium surfactant: CTAB	$[C_{16}H_{33}(CH_3)_3N]_4H_2SiV_2W_{10}O_{40}$	catalytic wet peroxide oxidation (CWPO) of phenol	- High performance of the POT catalyst was attributed to: (i) micellar structure formed by surfactant and (ii) catalytic center H <sub>2</sub> SiV <sub>2</sub> W <sub>10</sub> O <sub>40</sub> <sup>4+</sup> .	[216]
5	Quaternary ammonium surfactants with varying alkyl chain length: DA, DDA, and TDA	$[C_n]_3PW_{12}O_{40}$ n= 10, 12, 14	Epoxidation of olefins with H <sub>2</sub> O <sub>2</sub>	- The (DDA) <sub>3</sub> PW <sub>12</sub> O <sub>40</sub> POT formed a Pickering emulsion in the presence of water and an aromatic solvent, which is particularly efficient for the epoxidation of olefins.	[195]
6	Quaternary ammonium surfactants with varying alkyl chain length: DDA, TSA, and DODA	(DDA) <sub>9</sub> LaW <sub>10</sub> O <sub>36</sub> (TSA) <sub>9</sub> LaW <sub>10</sub> O <sub>36</sub> (DODA) <sub>9</sub> LaW <sub>10</sub> O <sub>36</sub>	Oxidative desulphurization of dibenzothiophene with H <sub>2</sub> O <sub>2</sub>	- Alkyl chains on surface of the amphiphilic POT adsorbed weakly polar sulfide by hydrophobic-hydrophobic interactions, where they were oxidized to sulfones by active POT species.	[217]
7	Ionic liquid	[PSPy] <sub>3</sub> PW <sub>12</sub> O <sub>40</sub>	Oxidative desulphurization of dibenzothiophene (DBT), 4,6-dimethyldibenzothiophene (4,6-DMDBT), and benzothiophene (BT) with H <sub>2</sub> O <sub>2</sub>	- Catalytic oxidation activity of the sulfur-containing compounds occurred in the following order: DBT > 4,6-DMDBT > BT	[218]
8	Ionic liquid	[BuPyPS] <sub>3</sub> PW <sub>12</sub> O <sub>40</sub> [PhPyPS] <sub>3</sub> PW <sub>12</sub> O <sub>40</sub> [BzPyPS] <sub>3</sub> PW <sub>12</sub> O <sub>40</sub>	Oxidation of thioethers and thiophenes and desulfurization of model fuels	- The POTs showed thermoregulated phase-separable behavior in the reaction. - Temperature-dependent solubility of the POTs as a function of the organic cation in water was studied.	[219]
9	Ionic liquid	[HDIm] <sub>2</sub> {[W=O(O <sub>2</sub> ) <sub>2</sub> ] <sub>2</sub> (μ-O)} [HHIm] <sub>2</sub> {[W=O(O <sub>2</sub> ) <sub>2</sub> ] <sub>2</sub> (μ-O)}	Epoxidation of olefins	- Efficient reaction-induced phase-separation POT has been developed in this work. The reaction system	[220]

10	Ionic liquid	PEG chain-functionalized <i>N</i> -dodecylimidazolium POT	Epoxidation of olefins with H <sub>2</sub> O <sub>2</sub>	- The highly efficient POT was also self-separation catalyst.	[221]
11	Ionic liquid	[PEG-300-C <sub>12</sub> MIM] [W=O(O <sub>2</sub> ) <sub>2</sub> ] <sub>2</sub> (μ-O) [PEG-800-C <sub>12</sub> MIM] [W=O(O <sub>2</sub> ) <sub>2</sub> ] <sub>2</sub> (μ-O)	Epoxidation of olefins with H <sub>2</sub> O <sub>2</sub>	- Although the POT was dissolved considerably by increasing the temperature during the reaction, it was recovered well by a thermoregulated-phased separation after the reaction.	[222]
12	Ionic liquid	MimAM(H)-PW	Epoxidation of alkenes with H <sub>2</sub> O <sub>2</sub>	- The POT exhibited advantages of convenient recovery, steady reuse, simple preparation, and flexible composition.	[223]
13	Ionic liquid	DPyAM(H)-PW	Oxidation of benzyl alcohol with H <sub>2</sub> O <sub>2</sub>	- The POT gave high conversion and selectivity in the heterogeneous solvent-free catalytic system.	[224]
14	Ionic liquid	[Dmim] <sub>1,5</sub> PW	Oxidation of alcohols with H <sub>2</sub> O <sub>2</sub>	- The POT was an efficient solid catalyst with easy recovery, and good reusability.	[225]
15	Ionic liquid	[C <sub>4</sub> mim] <sub>3</sub> PW <sub>12</sub> O <sub>40</sub> [C <sub>4</sub> mim] <sub>4</sub> SiW <sub>12</sub> O <sub>40</sub>	Oxidation of sulfides with H <sub>2</sub> O <sub>2</sub>	- Excellent performance of the POT was attributed to its promoted redox property arising from neighboring functionalized ionic liquid-cations.	[226]
16	Ionic liquid	[TMGDH] <sub>2,3</sub> H <sub>0,7</sub> PW [TMGDH] <sub>3</sub> PW [TMGOH] <sub>2,2</sub> H <sub>0,8</sub> PW [TMG] <sub>3</sub> PW	Epoxidation of <i>cis</i> -cyclooctene with H <sub>2</sub> O <sub>2</sub>	- The mesostructured POT exhibited superior activity because of controllable introduction of hydroxyl groups into its structure resulting in promotion of unusual morphology and pore structure, together with a hydrogen-bonding-enriched microenvironment surrounding the POT anion.	[227]
17	Ionic liquid	[TMGHA] <sub>2,4</sub> H <sub>0,6</sub> PW	Oxidation of benzyl alcohol with H <sub>2</sub> O <sub>2</sub>	- High activity of the POT was ascribed to its mesoporosity and dual wettability for water and alcohols.	[228]
18	Amine: hexamethylenetetramine	[C <sub>6</sub> H <sub>13</sub> N <sub>4</sub> ] <sub>2</sub> [HPW <sub>12</sub> O <sub>40</sub> ] <sub>2</sub> ·2H <sub>2</sub> O	Oxidative desulfurization of sulfur-containing model fuel with H <sub>2</sub> O <sub>2</sub>	- The Hybrid POT was highly active and recoverable.	[229]
19	Tripodal organic triammonium cation: BTE	BTE-PW <sub>11</sub> O <sub>39</sub>	Epoxidation of olefins with H <sub>2</sub> O <sub>2</sub>	- The hybrid POT catalyzed olefins epoxidation efficiently.	[230]
20	Quaternary ammonium surfactant: DA	DA <sub>11</sub> [La(PW <sub>11</sub> O <sub>39</sub> ) <sub>2</sub> ]	Oxidation of alkenes, alkenols, sulfides, silane and alcohol with H <sub>2</sub> O <sub>2</sub>	- The catalyst played a dual trapping role for both substrate and oxidant.	[231]
21	C <sub>12</sub> mim CTA TBA	[C <sub>12</sub> mim] <sub>5</sub> PTiW <sub>11</sub> O <sub>40</sub> [CTA] <sub>5</sub> PTiW <sub>11</sub> O <sub>40</sub> [TBA] <sub>5</sub> PTiW <sub>11</sub> O <sub>40</sub>	Epoxidation of olefins with H <sub>2</sub> O <sub>2</sub>	- Organic counteranions greatly affected catalytic activity.	[232]



22	Tripodal cations	polyammonium	$[\text{WZnZn}_2(\text{H}_2\text{O})_2][(\text{ZnW}_9\text{O}_{34})_2]^{12-}$	Epoxidation of allylic alcohols and oxidation of secondary alcohols with $\text{H}_2\text{O}_2$	- Mesoporosity of the synthesized catalyst enabled oxidation of many organic substrates irrespective of molecular shape, with efficiency similar to corresponding homogeneous catalyst. - The catalyst showed three-dimensional perforated coral-shaped amorphous materials with the organic cations surrounding the POT anions.	[233]
23	Coordination polymers		$[\text{Cu}^{\text{II}}_2(\text{C}_5\text{H}_5\text{NCOO})_2(4\text{-bpo})_2(\text{H}_2\text{O})_2]\text{SiW}_{12}\text{O}_{40}\cdot\text{H}_2\text{O}$ (1) $[\text{Cu}^{\text{I}}_4(4\text{-bpo})_6]\text{SiW}_{12}\text{O}_{40}\cdot 3\text{H}_2\text{O}$ (2) $[\text{Cu}^{\text{I}}_4(3\text{-bpo})_4]\text{SiW}_{12}\text{O}_{40}\cdot 3\text{H}_2\text{O}$ (3)	Epoxidation of styrene with <i>tert</i> -butyl hydroperoxide	- Geometry and coordination mode of bpo ligands played important roles in the formation of the hybrid solidified POT.	[234]
24	Coordination polymers		$[\{\text{Cu}(\text{en})_2\}_3\{\text{TeW}_6\text{O}_{24}\}]\cdot 6\text{H}_2\text{O}$	Epoxidation of cyclohexene and styrene by <i>tert</i> -butyl hydroperoxide	- One of the rare examples on Anderson structure of the POTs, which gave high catalytic efficiency and suggested that Anderson POTs can be further explored as a template for generation of ladder architecture.	[235]
25	Metalloporphyrins		$\{[\text{Cd}(\text{DMF})_2\text{Mn}^{\text{III}}(\text{DMF})_2\text{TPyP}](\text{PW}_{12}\text{O}_{40})\}\cdot 2\text{DMF}\cdot 5\text{H}_2\text{O}$	Selective oxidation of alkylbenzenes	- The POT-porphyrin hybrid combined multiple functional groups in a single structure, which resulted in excellent activity and size selectivity of the catalyst in accordance with its pore dimensions.	[236]

(DA.Br) decyltrimethylammonium bromide, dodecyltrimethylammonium bromide (DDA.Br), tetradecyltrimethylammonium bromide (TDA.Br), hexadecyltrimethylammonium bromide (HDA.Br), and octadecyltrimethylammonium bromide (ODA.Br).

dodecyltrimethylammonium bromide (DDA.Br), trimethylstearylammmonium bromide (TSA.Br), and dimethyldioctadecylammonium bromide (DODA.Br)

(DDA=dimethyldioctadecylammonium, omim=1-octyl-3-methyl-imidazolium)

DIm: protic N-dodecylimidazolium

HIm: N-hexylimidazolium

MimAM: 1-aminoethyl-3-methylimidazolium

DPyAM: amino-attached 4,4-bipyridine

Dmim: 1,1'-(butane-1,4-diyl)-bis(3-methylimidazolium)

C<sub>4</sub>mim: 1-n-butyl-3-methylimidazolium

TMGDH: dihydroxy-tethered tetramethylguanidinium

TMGOH: monohydroxy-tethered tetramethylguanidinium

TMG: tetramethylguanidinium

BTE: benzene-1,3,5-[tris(phenyl-4-carboxylic acid)] tris(2-trimethyl-ammonium ethyl) ester

C<sub>12</sub>mim: 1-dodecyl-3-methylimidazolium

CTA: cetyltrimethylammonium

TBA: tetrabutylammonium

n-bpo: (2,5-bis(n-pyridyl)-1,3,4-oxadiazole)

en: ethylene-diamine

DMF: *N,N*-dimethylformamide; TPyP: tetrapyridylporphyrin

DA: dodecyltrimethylammonium bromide

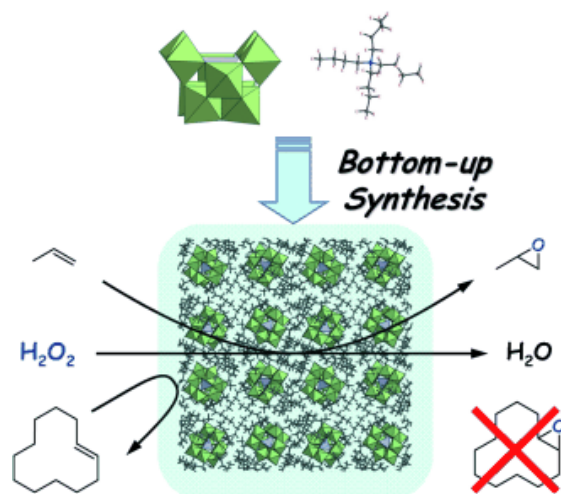


**Figure 2.19.** Size-selective oxidation of olefins over  $[(n-C_4H_9)_4N]_4[\gamma-SiW_{10}O_{34}(H_2O)_2] \cdot H_2O$  synthesized via bottom-up approach [196].

### 2.4.3.3 POTs solidified via immobilization onto supports or into matrixes

The most conventional method to prepare heterogenous POT-based catalysts is deposition of POTs onto supports or into matrixes [237]. Depending on the nature of POTs and type of support, different strategies have been developed for immobilization of POTs on supports. Examples, mainly, include impregnation, ion exchange, adsorption, encapsulation, covalent linkage, etc. Different supports have been introduced as immobilizer: graphite (HOPG) [238-240], carbon nanotubes (CNTs) [241-248], and metals surfaces such as Au [249,250] and Ag [251] have been employed as support for several applications like microscopy imaging, electrodes and electro-assisted catalysis and sensing.

Focusedly on catalysis applications, employing porous (often meso) supports such as silica, alumina, transition metal oxides, metal-organic frameworks (MOFs), magnetic nanoparticles (MNPs), zeolites, carbons, etc., as well as polymeric matrixes to host POTs has been reported. Roughly speaking, most of the reported immobilized POTs on the support encompass non-covalent interactions between POTs and support, which has provoked a criticism that such solid catalysts leach into the liquid medium of the reaction due to the weak interactions between active species and support causing eventually deactivation of the catalysts. To address this matter, efforts on covalently linking POTs to supports, which requires, often, advanced functionalization prior or

during the immobilization, are rapidly underway today. These efforts have chiefly focused on using polymeric and MOFs-made supports due to their capabilities to covalently encapsulate POTs arising from their organic frameworks. This is, most probably, the reason for much more reported works on these two supports to carry catalytically active POMs compared to the other types of supports, and consequently, for presenting exclusive review papers on POM-MOF [252] and POM-polymer [253,189] hybrids.

In general, thanks to intrinsic properties of the supports, the immobilized POTs have exhibited enhanced catalytically important features compared to their bulk forms. The most striking feature is porosity; larger surface area and pore volume, as well as narrower pore size distribution have been obtained by employing mesoporous silica, alumina, transition metal oxides, polymers, zeolites, MOFs, and carbon materials. Hydrophilic-hydrophobic properties have been adjusted by employing MOFs and polymers. Intriguingly for liquid organic reactions, the catalyst can be compatibilized toward organic substrates with the aid of organic framework of the polymers. Employing transition metal oxides as support, strong host-guest interactions, as well as tunable chemical composition and active sites can be obtained. MNPs-supported POTs have been endowed with a feasible magnetic separation and recovery, which is industrially applicable and fascinating. Further details about these different types of supports as well as immobilization strategies and catalytic applications have been elegantly reviewed by Kholdeeva et al. in 2010 [137] and Zhou et al. in 2014 [191]. Herein we try to cover all of the recent works dealing, exclusively, with tungsten-based POMs immobilized on supports and their catalytic applications. Tables 2.14 and 2.15 show the reported POT/support catalytic systems along with their applications in acid catalysis and oxidation reactions.

#### **2.4.3.4 POTs heterogenized via combined strategies**

Combining the three heterogenization strategies, discussed in sections 2.4.3.1-3, offers some additional advantages in the design of heterogeneous catalysts making the resultant solid POT catalysts more fascinating. In the case of supported POTs, organo-modification of the surfaces (of the POTs or the supports or both) can be employed prior to immobilization in order to either enhance the stability of the supported POTs or improve dispersion of the POT active sites into the support's structure.

**Table 2.14.** POTs solidified with immobilization on supports for acid catalysis reactions.

Entry	Support	POT	Reaction	Remarks	Ref.
1	C <sub>8</sub> -AP grafted SBA-15	H <sub>3</sub> PW <sub>12</sub> O <sub>40</sub>	Hydrolysis of ester	- The supported POT was surrounded by hydrophobic alkyl groups in channels of mesoporous silica nanostructured, which afforded paths for the efficient approach of reactant molecules and water to the active sites.	[254]
2	AP grafted SBA-15	H <sub>3</sub> PW <sub>12</sub> O <sub>40</sub>	Acid-base tandem reaction	- The supported POT could be easily tuned: predominantly basic, or predominantly acidic, or equally acidic and basic by changing the ratio of polyacid and amine groups.	[255]
3	SiO <sub>2</sub>	H <sub>3</sub> PW <sub>12</sub> O <sub>40</sub>	Polymerization of $\beta$ -pinene	- The supported POT had no poison to hydrogenation catalysts, as well as low corrosion to polymerization and hydrogenation equipment.	[256]
4	SiO <sub>2</sub>	H <sub>3</sub> PW <sub>12</sub> O <sub>40</sub>	Esterification of camphene with carboxylic acids	- The supported POT exhibited very good activity, high turnover number, and steady reuse without loss of activity and selectivity.	[257]
5	SiO <sub>2</sub>	H <sub>3</sub> PW <sub>12</sub> O <sub>40</sub>	Isomerization of $\alpha$ -pinene and longifolene	- The catalyst was very active in small amounts, exhibiting high turnover numbers, good stability and steady reuse without loss of activity.	[258]
6	SiO <sub>2</sub>	H <sub>3</sub> PW <sub>12</sub> O <sub>40</sub>	Conversion of citronellal to menthol	- Adding Pd to the supported POT's structure, a bifunctional catalyst was developed that direct the reaction via acid-catalyzed cyclization followed by Pd-catalyzed hydrogenation.	[259]
7	SiO <sub>2</sub>	H <sub>4</sub> SiW <sub>12</sub> O <sub>40</sub>	Esterification of oleic acid with methanol	- The supported POT showed high catalytic activity close to that of unsupported one; however, leaching of active sites resulted in gradual deactivation of the catalyst.	[260]
8	- Mesoporous ZrO <sub>2</sub> - Mesoporous ZrO <sub>2</sub> - ethane-bridged organosilica	H <sub>3</sub> PW <sub>12</sub> O <sub>40</sub>	Transesterification of Eruca Sativa Gars oil	- The ethane-containing supported POT exhibited higher catalytic activity due to combination of strong Brønsted acidity, 3D interconnected mesostructure, and enhanced hydrophobicity.	[261]

9	- Mesoporous ZrO <sub>2</sub> - Mesoporous benzene/ethane-bridged organosilica	ZrO <sub>2</sub> -	H <sub>3</sub> PW <sub>12</sub> O <sub>40</sub>	Esterification of levulinic acid	- The alkyl-containing supported POT exhibited higher catalytic activity due to the combination of strong Brønsted acidity, well-defined ordered mesostructure, homogeneous dispersion of active sites, and enhanced surface hydrophobicity of the hybrid catalysts	[262,263]
10	Ta <sub>2</sub> O <sub>5</sub>		H <sub>3</sub> PW <sub>12</sub> O <sub>40</sub>	Esterification of acetic acid with ethanol	- The POT kept its Keggin structure after immobilization and micro- or micro/meso porosities and nanometer sizes. It showed higher activity than the parent PTA.	[264]
11	Hydrous ZrO <sub>2</sub>		H <sub>3</sub> PW <sub>12</sub> O <sub>40</sub>	Condensation of dimedones, urea, aryl aldehydes, enolizable ketones, and acetyl chlorides	- Structural integrity and good dispersion of the POT in the support were responsible for high catalytic efficiency.	[265]
12	ZrO <sub>2</sub>		H <sub>3</sub> PW <sub>12</sub> O <sub>40</sub>	Regioselective monobromination of aromatic substrates	- The supported POT exhibited excellent yields and efficient recovery.	[266]
13	MIL-101 (Cr)		H <sub>3</sub> PW <sub>12</sub> O <sub>40</sub>	Knoevenagel condensation of benzaldehyde, esterification of acetic acid, dehydration of methanol	- The supported POT was bi-functional porous solid with outstanding catalytic performance in base- and acid-catalyzed reactions, which was obtained by direct and one-pot encapsulation of POT into support.	[267]
14	MIL-101 (Cr)		H <sub>3</sub> PW <sub>12</sub> O <sub>40</sub>	Dehydration of fructose and glucose to HMF	- Different loadings of POT were investigated resulting in highly active and recyclable solid acid catalyst.	[268]
15	MIL-101 (Cr)		Ru- H <sub>3</sub> PW <sub>12</sub> O <sub>40</sub>	Conversion of cellulose and cellobiose into sorbitol	- The ratio of acid site density (comes from the POT) to the number of Ru surface atoms in the Ru-POT/MIL-100(Cr) was optimized to reach highest reaction efficiency.	[269]
16	MIL-101 (Cr)		H <sub>3</sub> PW <sub>12</sub> O <sub>40</sub>	Baeyer condensation of benzaldehyde and 2-naphthol and epoxidation of caryophyllene by H <sub>2</sub> O <sub>2</sub>	- Under microwave-assisted heating reaction, the supported POT was highly active and exceptionally stable.	[270]
17	MIL-101 (Cr)		H <sub>3</sub> PW <sub>12</sub> O <sub>40</sub>	Alcoholysis of styrene oxide	- Probing the acid sites using in situ FTIR showed generation of additional hydroxyl groups and Lewis acid sites, which were responsible for high efficiency of the supported POT in a short reaction time.	[271]
18	Polymeric ionic liquid: Poly(VMPS)		H <sub>3</sub> PW <sub>12</sub> O <sub>40</sub>	Esterification of alcohols	- Both polymeric framework and large heteropolyanion were responsible for solid nature of the catalyst. - Excellent catalytic activity came from acidic SO <sub>3</sub> H functional groups in the hybrid catalyst.	[272]

19		Povidone (PVP)	H <sub>3</sub> PW <sub>12</sub> O <sub>40</sub>	Azidation of alcohols	- Higher surface area of the PVP-POT (10.5 m <sup>2</sup> g <sup>-1</sup> ) compared to PTA was responsible for enhancing catalytic activity.	[273]
20		PDVC (Poly ( <i>P</i> -divinylbenzene, 4-vinylbenzyl chloride))	H <sub>3</sub> PW <sub>12</sub> O <sub>40</sub>	Acetylation of glycerol	- Ethylenediamine was used as soft linker between polymer and PTA. The POT showed hybrid characteristic of heterogeneous and homogeneous catalysts, resulting in superior activity compared to the literature.	[274]
21	Magnetic NPs	organo- functionalized SiO <sub>2</sub> (shell)-iron oxide (core)	H <sub>3</sub> PW <sub>12</sub> O <sub>40</sub>	Friedel–Crafts reactions of indoles	- The first report on non-covalent immobilization of POT on MNPs.	[275]
22		organo- functionalized SiO <sub>2</sub> (shell)-iron oxide (core)	H <sub>3</sub> PW <sub>12</sub> O <sub>40</sub>	Esterification of free fatty acid	- The first-time application of MNPs-supported POTs in esterification reactions.	[276]
23		poly(glycidyl methacrylate) (PGMA) (shell)-iron oxide (core)	H <sub>3</sub> PW <sub>12</sub> O <sub>40</sub>	Esterification of free fatty acids and transesterification of triglycerides	- Good catalytic performance was ascribed to high acidity and nano-size of the catalyst. - Firm attachment of POT on MNPs via covalent binding, stable PGMA shell, and superparamagnetic properties of MNPs led to high stability and recyclability of the catalyst.	[277]
24		Diamine-functionalized magnetite (Fe <sub>3</sub> O <sub>4</sub> ) silica-coated	H <sub>3</sub> PW <sub>12</sub> O <sub>40</sub>	Synthesis of tetrahydrobenzo[b]pyrans and Knoevenagel condensation	- The catalyst had relatively uniform spherical nanoparticles with a 60 nm average size, and offered high reaction efficiency, recyclability, and avoidance of organic solvent.	[278]
25	Zeolites	Zeolite imidazolate framework (ZIF-67)	H <sub>3</sub> PW <sub>12</sub> O <sub>40</sub>	Friedel–Crafts acylation of anisole with benzoyl chloride	- Excellent dispersion of the POT over ZIF-67 was achieved, with different amounts of PTA encapsulated in the support structure resulting in high activity, stability and reusability.	[279]
26	Carbon materials	Activated carbon	H <sub>3</sub> PW <sub>12</sub> O <sub>40</sub>	Polymerization of β-pinene	- The POT could interact strongly with surface oxygen-containing groups on the activated carbon, resulting in stable immobilization of POT, which led to a decrease in the specific surface area of the activated carbon.	[280]
27	Other supports	Mineral clay: Bentonite (BNT)	H <sub>3</sub> PW <sub>12</sub> O <sub>40</sub>	Hydroxyalkylation of phenol	- Optimized amount of the POT supported on BNT showed higher product yield and selectivity than those of parent POT and BNT, mainly due to excellent dispersion of the POT on BNT resulting in redistribution of Brønsted and Lewis acid sites on BNT.	[281]

28	Clay: K10 and KSF montmorillonite	$H_3PW_{12}O_{40}$	Condensation of 1,2-phenylenediamines and ketones	The supported POT was highly active, non-hygroscopic, non-corrosive, and efficiently recyclable. [282]
----	-----------------------------------	--------------------	---	--

AP: 3-aminopropyl  
 VMPS: 1-vinyl-3-propane sulfonate imidazolium

**Table 2.15.** POTs solidified with immobilization on supports for oxidation reactions.

Entry	Support	POT	Reaction	Remarks	Ref.
1	Ionic liquid-modified SiO <sub>2</sub>	$[\{W(=O)(O_2)_2(H_2O)\}_2(\mu-O)]^{2-}$	Epoxidation of olefins with H <sub>2</sub> O <sub>2</sub>	- Activity of the supported POT was comparable to homogeneous analogue, confirming successful heterogenization. - No leaching of active sites was obtained.	[283]
2	Ionic liquid-modified SBA-15	H <sub>3</sub> PW <sub>12</sub> O <sub>40</sub>	Oxidation of alcohols with H <sub>2</sub> O <sub>2</sub>	- The supported POT exhibited high catalytic activity and selectivity and reusability without leaching in solvent-free catalytic reaction.	[284]
3	Ionic liquid-modified SBA-15	H <sub>3</sub> PW <sub>12</sub> O <sub>40</sub>	Oxidation of alcohols with H <sub>2</sub> O <sub>2</sub>	- The supported POT prepared via one-pot procedure. - Occasion of adding POT as well as location of the organic cations in the mesostructure played a crucial role in catalytic performance.	[285]
4	Ionic liquid-modified SBA-15	H <sub>3</sub> PW <sub>12</sub> O <sub>40</sub>	Oxidative desulfurization of fuels	- The hybrid POT possessed ordered mesopore structure and high specific surface area. Due to the introduction of imidazole-based ionic liquid, the catalyst exhibited good wettability for model oil, which had significant contribution to desulfurization activity.	[286]
5	Mesoporous SBA-16	H <sub>6</sub> P <sub>2</sub> W <sub>18</sub> O <sub>62</sub>	Epoxidation of olefins and oxidation of alcohols with H <sub>2</sub> O <sub>2</sub>	- Pore entrance size of the SBA-16 was modified by silylation reaction to enable trapping the POT.	[287]
6	Ordered mesoporous ZrO <sub>2</sub>	H <sub>3</sub> PW <sub>12</sub> O <sub>40</sub> H <sub>4</sub> SiW <sub>12</sub> O <sub>40</sub>	Oxidation of alkenes with H <sub>2</sub> O <sub>2</sub>	- The supported POT exhibited higher catalytic activity compared to its parents: ZrO <sub>2</sub> and heteropoly acids.	[288]
7	MIL-101	[PW <sub>4</sub> O <sub>24</sub> ] <sup>3-</sup> [PW <sub>12</sub> O <sub>40</sub> ] <sup>3-</sup>	Oxidation of alkenes with H <sub>2</sub> O <sub>2</sub>	- The supported POTs demonstrated good activity comparable to that of homogeneous heteropoly acids. - In contrast to homogeneous systems, use of a higher H <sub>2</sub> O <sub>2</sub> /alkene molar ratio allowed increasing both alkene conversion and epoxide selectivity, arising from specific sorption properties of support.	[289]
8	MIL-101 (Cr)	[PW <sub>11</sub> O <sub>39</sub> ] <sup>7-</sup> [SiW <sub>11</sub> O <sub>39</sub> ] <sup>8-</sup>	Oxidation of alkenes with H <sub>2</sub> O <sub>2</sub>	- The supported POTs were highly active, selective (comparable to homogeneous ones) and recyclable catalysts.	[290]



9	rht-MOF-1	$H_3PW_{12}O_{40}$	Oxidation of alkylbenzene	- The Keggin POT could be immobilized into the $\beta$ -cage of rht-MOF-1 by a solvothermal method with highly ordered and porous structure, resulting in good dispersion of POT in the reaction and enhancement of catalytic activity.	[291]	
10	$Cu_3(BTC)_2$ MOF (HKUST-1)	$H_3PW_{12}O_{40}$ $H_4SiW_{12}O_{40}$	Oxidative desulfurization of model fuels	- The POT encapsulated in MOF showed selective oxidation of sulfides to corresponding sulfones or sulfoxides with efficient reusability.	[292]	
11	Copper organic frameworks with pyrazine derivatives	$H_3PW_{12}O_{40}$ $H_4SiW_{12}O_{40}$	Epoxidation of alkenes with $H_2O_2$	- The heterogenized POT showed higher catalytic activity compared to the corresponding homogeneous POT.	[293]	
12	Metal-organic coordination network (MOCN): (1) $Co(BBTZ)_{1.5}(HBBTZ)(H_2O)_2$ (2) $Co_{2.5}(BBTZ)_4(H_2O)_2$ (3) $Cu(BBTZ)_2$	$PW_{12}O_{40}$ $BW_{12}O_{40}$	Oxidative desulfurization of dibenzothiophene	- A new non-porous POT-based MOCN was synthesized, which showed good catalytic activity in contrast to the parent POT, due to monodispersion of POT units in the MOCN at molecular level exposing more active POT sites.	[294]	
13	$[Cu(4,4'-bipy)_2(H_2O)_2]_n^{2n+}$ (bipy = bipyridine)	$H_3PW_{12}O_{40}$ $H_4SiW_{12}O_{40}$	Oxidation of ethylbenzene	- Oxidation of the substrate occurred in the pore of the framework, and valence of the metal ion in the POTs significantly influenced catalytic activity of the 3D framework.	[295]	
14	MIL-101 (Cr)	$[PW_{11}CoO_{39}]^{5-}$ $[PW_{11}TiO_{40}]^{5-}$	Oxidation of alkenes with molecular oxygen and $H_2O_2$	- The POTs were electrostatically attached to surfaces of the support, which showed good stability and no leaching under mild conditions ( $T < 50\text{ }^\circ\text{C}$ ).	[296]	
15	MIL-101 (Cr)	$[Ln(PW_{11}O_{39})_2]^{11-}$ $Ln = Eu^{3+}$ and $Sm^{3+}$	Oxidation of styrene with $H_2O_2$	- The supported POTs exhibited higher activity than that of homogeneous parent POTs, which was further increased by microwave-assisted oxidative reactions.	[297]	
16	MIL-101 (Cr)	$[Tb(PW_{11}O_{39})_2]^{11-}$	Oxidative desulfurization of fuels	- Higher desulfurization efficiency was obtained by the supported POT compared to the homogeneous parent POT.	[298]	
17	Polymers	Ionic copolymer: AM-BM	$H_3PW_{12}O_{40}$	Epoxidation of alkenes with $H_2O_2$	- Peroxo-W active sites in the POT promoted by the amino groups in polymer matrix was responsible for catalyst's excellent performances. Stable structure of the catalyst came from cross-linked structure of the copolymer cations.	[299]
18		Ionic copolymer: DIM-CIM	$H_3PW_4O_{16}$	Epoxidation of alkenes with $H_2O_2$	- Amphiphilic structure of the supported POT acted as a "trapping agent" for both hydrophobic alkene substrates and hydrophilic $H_2O_2$ , promoting catalytic activity.	[300]

19	Ionic copolymer: AVIM	NDMAM-	$H_3PW_{12}O_{40}$	Oxidation of alcohols with $H_2O_2$	- Excellent performance of the supported POT comes from featured structure of polymeric framework giving the catalyst solid nature and stimuli-responsive behavior.	[301]
20	Ionic copolymer: AVIM-DVB and PDIM-DVB		$H_3PW_{12}O_{40}$	Oxidation of benzyl alcohol with $H_2O_2$	- High activity of the catalyst arose from amino functional groups and high BET surface area of polymeric framework.	[302]
21	Poly(ethylene oxide-pyridinium)		$H_3PW_{12}O_{40}$	Oxidation of alcohols with $H_2O_2$	- Using the supported POT, chemoselective oxidation of sterically hindered secondary alcohols in presence of primary alcohols was achieved.	[303]
22	Amphiphilic resins		$H_3PW_{12}O_{40}$	Epoxidation of unsaturated fatty esters with $H_2O_2$	- Catalytic properties of the supported POT varied with hydrophilic/lipophilic balance (carbon chain number, spacer arm between benzene cycle and imidazole group, N-substitution of imidazole ring).	[304]
23	Polymer-immobilised ionic liquid phase		$[PO_4\{WO(O_2)_2\}_4]^{3-}$	Epoxidation of allylic alcohols and alkenes with $H_2O_2$	- A new polymeric support with tuneable surface properties and microstructure has been prepared by ring-opening metathesis polymerisation.	[305]
24	Poly(divinylbenzene)		$[PO_4\{WO(O_2)_2\}_4]^{3-}$	Epoxidation of olefins with $H_2O_2$	- High catalytic activity and epoxide selectivity was attributed to an optimized hydrophilicity/hydrophobicity balance in the mesoporous environment, as well as facile diffusion of the reactants and products.	[306]
25	Poly(methyl methacrylate)		$[\{CH_2=CH(CH_2)_6Si\}_xO_ySiW_wO_z]^{4+}$ (1) $x=2, w=11, y=1, z=39$ (2) $x=2, w=10, y=1, z=36$ (3) $x=4, w=9, y=3, z=34$	Oxidation of organic sulfides with $H_2O_2$	- Catalytic efficiency was affected by fine-tuning of the polymer composition, including tailored design of the POT-based monomers.	[307]
26	A modified porous resin		$(NBu_4)_6[\alpha_2-P_2W_{17}O_{61}(SiC_6H_4CH_2N_3)_2O]$	Oxidation of tetrahydrothiophene	- The POT was functionalized, and the resin was modified prior to immobilization to be able to have strong covalent bonding between the POT clusters and the macroporous resin surface.	[308]
27	Biopolymer: chitosan		$H_3PW_{12}O_{40}$	Degradation of chitosan with $H_2O_2$	- The POT was easy to separate from chitosan at the end of reaction, improving purity of the products.	[309]
28	Magnetic NPs Ferromagnetic nanocrystals (iron oxide)		$(DODA)_3PW_{12}O_{40}$	Oxidation of sulfides to sulfones	- Nanospaces and increased surfactant alkyl chain density around the POT in the nanocones provided enhanced catalytic performance.	[310]

29		Poly(ionic liquid) coated iron oxide	$\text{H}_3\text{PW}_{12}\text{O}_{40}$	Epoxidation of bio-derived olefins with $\text{H}_2\text{O}_2$	- Catalytically active centers were amino-functionalized W species, while the amphiphilic catalyst structure acted as a “trapping agent” for both hydrophobic olefin substrates and $\text{H}_2\text{O}_2$ molecules in aqueous phase.	[311]
30	Alumina	Au/ $\text{Al}_2\text{O}_3$	$\text{K}_8[\text{BW}_{11}\text{O}_{39}\text{H}]\cdot n\text{H}_2\text{O}$	Epoxidation of cyclooctene with molecular oxygen	- Adding Au NPs and combining catalytic activities of the POT and gold, an efficient and recoverable catalyst was developed.	[312]
31	Other supports	layered double hydroxides (LDHs)	$[\text{WZn}_3(\text{ZnW}_9\text{O}_{34})_2]^{12-}$	Epoxidation of allylic alcohols with aqueous $\text{H}_2\text{O}_2$	- The first report of direct immobilization of a self-assembled POT in LDH, which showed excellent activity, high dispersion and good hydrothermal stability.	[313]
32		$\text{Mg}_3\text{Al}-\text{NO}_3$	$[\text{WZn}_3(\text{H}_2\text{O})_2(\text{ZnW}_9\text{O}_{34})_2]^{12-}$	Oximation of aldehydes by $\text{H}_2\text{O}_2$	- Selectivity of oximation of various aldehydes was increased under mild conditions by using the supported POT.	[314]

DODA=dimethyldioctadecylammonium  
 BBTZ = 1,4-bis-(1,2,4-triazol-1-ylmethyl)benzene

For example, Villanneau et al. have reported successful covalent immobilization of the hybrid POT  $[\text{AsW}_9\text{O}_{33}\{\text{P}(\text{O})(\text{CH}_2\text{CH}_2\text{CO}_2\text{H})_2\}_2]^{5-}$  onto  $\text{NH}_2$ -functionalized mesoporous SBA-15, which obviously resulted in better stability of the supported catalyst and less leaching of active sites compared to common electrostatic interactions-based supported POTs. They prepared anchored homogeneous catalysts retaining important mesoporosity, in which the POT would play the role of polydentate inorganic ligands for active centers [315]. Furthermore, such hybridization of polyoxometallates via an organic-inorganic association has been exploited to develop a heterogeneous catalyst with tunable functionality imparted through supramolecular assembly [316]. Employing two hydrophilic (mica) and hydrophobic supports (highly oriented pyrolytic graphite), Raj et al. have investigated the role of surface hydrophilicity/hydrophobicity in determining supramolecular organization of POT ( $[\text{PW}_{12}\text{O}_{40}]^{3-}$ )-support. They have also demonstrated that organo-functionalization of the POT with dimethyldioctadecylammonium bromide is an efficient strategy to control the final product morphology and obtain highly dispersed POT active species on various hydrophilic and hydrophobic supports (Figure 2.20) [317]. Uchida et al. reported complexation of  $[\text{SiW}_{12}\text{O}_{40}]^{4-}$  (ca. 1.0 nm in size) and a large macro cation of  $[\text{Cr}_3\text{O}(\text{OOCH})_6(\text{H}_2\text{O})_3]^+$  (ca. 0.7 nm in size) in the presence of  $\text{K}^+$ , which left nano-sized channels in the lattice of the produced complex,  $\text{K}_3[\text{Cr}_3\text{O}(\text{OOCH})_6(\text{H}_2\text{O})_3]\text{SiW}_{12}\text{O}_{40}\cdot 12\text{H}_2\text{O}$ , resulting in catalytically interesting properties [318]. Table 2.16 lists the reported solid POTs which have exploited a combination of the three strategies to enhance their catalytic efficiencies in various liquid-phase organic reactions.

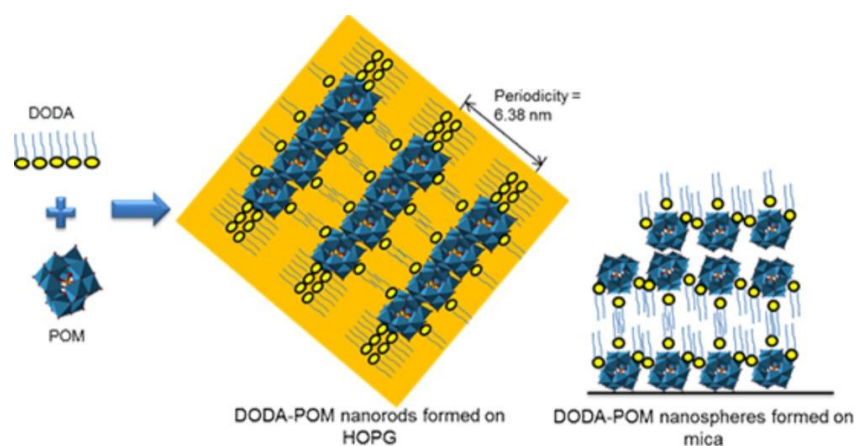


**Figure 2.20.** Controlling morphology and dispersion of supported POT heterogeneous catalysts via organo-modification of the POT [317].

**Table 2.16.** POTs heterogenized via combined strategies.

Entry	POT	Inorganic cation	Organic part	Support	Reaction	Remarks	Ref.
1	Fe <sup>III</sup> AspPW <sub>12</sub>	Fe <sup>3+</sup>	Amino acid: aspartic acid (Asp)	-	Fenton-like degradation of 4-chlorophenol with H <sub>2</sub> O <sub>2</sub>	- Adding Fe to the POT's structure, the catalyst showed superior catalytic performance from acidic to neutral pH values.	[319]
2	Na <sub>7</sub> H <sub>2</sub> LaW <sub>10</sub> O <sub>36</sub> ·32 H <sub>2</sub> O	Na <sup>+</sup>	-	Ionic liquid-modified SiO <sub>2</sub>	Desulfurization of DBT, BT, and 4,6-DMDBT	- The POT was highly dispersed in the support resulting in good activity of the catalyst.	[320]
3	(TBA) <sub>7</sub> H <sub>3</sub> [Co <sub>4</sub> (H <sub>2</sub> O) <sub>2</sub> (PW <sub>9</sub> O <sub>34</sub> ) <sub>2</sub> ]	-	Quaternary ammonium surfactant: TBA	MOF: MIL-101	Oxidation of olefins with H <sub>2</sub> O <sub>2</sub>	- Immobilization of this sandwich-type POT on MOF was reported for the first time, which showed high activity for oxidation of various hydrocarbons.	[321]
4	[Cu <sub>2</sub> (BTC) <sub>4/3</sub> (H <sub>2</sub> O) <sub>2</sub> ] <sub>6</sub> [H <sub>n</sub> XW <sub>12</sub> O <sub>40</sub> ](C <sub>4</sub> H <sub>12</sub> N) <sub>2</sub> (X = Si, Ge, P, As)	-	Quaternary ammonium surfactant: TMA	Cu-BTC-based MOF	Hydrolysis of esters	- The catalysts exhibited (i) good dispersion of POTs at the molecular level, prohibiting conglomeration, (ii) high immobilization of POTs, preventing catalyst leaching, and (iii) highly stable crystalline framework, allowing for catalyst recycling.	[322]
5	H <sub>3</sub> [(Cu <sub>4</sub> Cl) <sub>3</sub> (BTC) <sub>8</sub> ] <sub>2</sub> [PW <sub>12</sub> O <sub>40</sub> ](C <sub>4</sub> H <sub>12</sub> N) <sub>6</sub> ·3H <sub>2</sub> O	-	Quaternary ammonium surfactant: TMA	Cu-BTC-based MOF	Adsorption and decomposition of dimethyl methylphosphonate	- A novel POT/MOF with sodalite topology was obtained by a simple hydrothermal method, which showed excellent activity and stability.	[323]
6	[Cu <sub>3</sub> (C <sub>9</sub> H <sub>3</sub> O <sub>6</sub> ) <sub>2</sub> ] <sub>4</sub> {(CH <sub>3</sub> ) <sub>4</sub> N} <sub>4</sub> CuPW <sub>11</sub> O <sub>39</sub> H]	-	Quaternary ammonium surfactant: TMA	MOF-199 (HKUST-1)	Aerobic oxidations	- The supported POT exploited attractive features of both POT and MOF, and exhibited mutual enhancement of stability by each component, and high efficiency in detoxification of various sulfur compounds.	[324]
7	PYI-Ni <sub>2</sub> H[BW <sub>12</sub> O <sub>40</sub> ]	Ni <sup>2+</sup>	Asymmetric organocatalytic group: 1-pyrrolidin-2-ylimidazole (PYI), or d-	Chiral MOF	Asymmetric dihydroxylation of aryl olefins with H <sub>2</sub> O <sub>2</sub>	- Hydrophilic/hydrophobic properties of channels of the enantiomorphs POT-MOF were modulated to adsorb oxidant and olefins, resulting in excellent stereoselectivity.	[325]
8	[Cu <sub>3</sub> (4,4'-bpy) <sub>3</sub> ][HSiW <sub>12</sub> O <sub>40</sub> ](C <sub>3</sub> H <sub>4</sub> N <sub>2</sub> )[Cu(Phen)(4,4'-bpy)(H <sub>2</sub> O)] <sub>2</sub> [PW <sub>12</sub> O <sub>40</sub> ](4,4'-bpy)	-	Imidazole and bipyridine	MOF	Oxidation of alcohols with H <sub>2</sub> O <sub>2</sub>	- The synthesized POT exhibited higher activity compared to the corresponding Mo-based POMs.	[326]

9	$\text{TBA}_{4.2}\text{H}_{0.8}[\text{PW}_{11}\text{Zn}(\text{H}_2\text{O})\text{O}_{39}]$		Quaternary ammonium surfactant: TBA	MOF: MIL-101 (Cr)	Oxidative desulfurization of fuels	- The POT was homogeneously encapsulated within cages of the support without affecting its crystal structure and morphology.	[327]
10	$\text{K}_6\text{P}_2\text{W}_{18}\text{O}_{62}$ $\text{K}_{14}[\text{NaP}_5\text{W}_{30}\text{O}_{110}]$	$\text{K}^+$	-	Silica: MCM-48, SBA-3, SBA-15 and $\text{NH}_3^+$ functionalized $\text{SiO}_2$	Oxidation of thioethers with $\text{H}_2\text{O}_2$	- Preyssler complex was more active compared to its Dawson analog. Characteristics of the support also affect the catalytic activity.	[328]
11	$\text{TBA}_4\text{HPW}_{11}\text{CoO}_{39}$ $\text{TBA}_5\text{PW}_{11}\text{CoO}_{39}$	-	Quaternary ammonium surfactant: TBA	$\text{NH}_2^-$ and $\text{NH}_3^+$ -modified mesoporous silica	Aerobic oxidation of aldehydes	- Catalytic activities of the supported POTs were comparable to those of homogeneous parent POTs, however they showed leaching of active sites after 3 <sup>rd</sup> cycle.	[329]
12	$\text{Cs}_{2.5}\text{H}_{0.5}\text{PW}_{12}\text{O}_{40}/\text{CTAB}$	$\text{Cs}^+$	Quaternary ammonium surfactant: CTAB	-	Regioselective bromination of aromatic compounds	- The catalyst exhibited high yields in regioselective bromination of phenol and phenol derivatives and some other aromatic compounds with molecular bromine at room temperature.	[330]
13	$\text{MoO}_2(\text{acac})-\text{K}_8[\text{SiW}_{11}\text{O}_{39}]$	$\text{K}^+$	Molybdenylacetylacetonate complex	-	Epoxidation of alkenes with <i>tert</i> -BuOOH	- Catalytic activity of $\text{MoO}_2(\text{acac})_2$ was modified by incorporation of the POT via covalent bonding because of charge-transfer role of the resultant complex.	[331]
14	$\text{Pd}(\text{salen})-\text{K}_8[\text{SiW}_{11}\text{O}_{39}]$	$\text{K}^+$	Palladium (salen)	-	Suzuki cross-coupling reactions	- The resultant hybrid POT showed greatly improved activity and much higher yields of coupling products compared to its parent organic and inorganic components, even with low catalyst loading.	[332]

DBT: dibenzothiophene

BT: benzothiophene

4,6-DMDBT: 4,6-dimethyldibenzothiophene

TBA: tetrabutylammonium

BTC: benzenetricarboxylate

TMA: tetramethylammonium

Bpy: bipyridine

Phen = 1,10-phenanthroline

salen = *N,N'*-bis(salicylidene)ethylenediamine

## 2.5 Conclusion and perspective

As shown here, many efforts have been done in the context of the high demands for development of sustainable and green chemistry in order to find an alternative for hazardous ozonolysis of UFAs, which is currently the industrial method for the production of dicarboxylic acids from oils and fats. Replacing ozone with a more benign oxidant, like hydrogen peroxide, makes it necessary to employ an active catalyst in the reaction. To push this catalyst to its use in multikilogram-scale toward industrial production, the substantial feature of recyclability should, also, be considered. This chapter indicates that several catalytic systems in homogeneous and heterogeneous forms have been developed for oxidative cleavage of UFAs. Transition metals such as osmium, cobalt, molybdenum, chrome, gold, manganese, iron, ruthenium, and tungsten have been used as catalytic active sites, with considerably more emphasis on W.

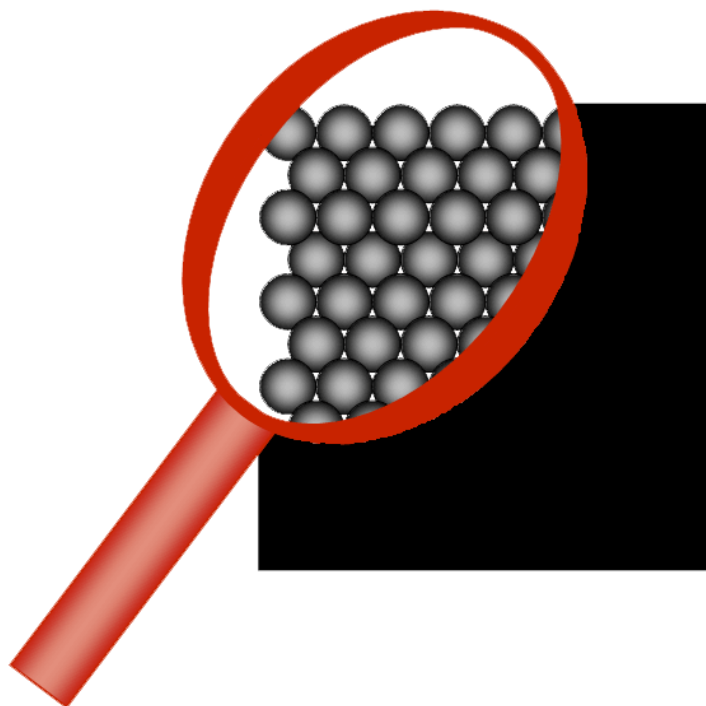
Homogeneous catalysts, on which more researches have been done, showed excellent conversion and selectivity. However, their large-scale application has been always restricted due to the lack of catalyst recovery. Curiously, the use of heterogeneous catalysts with recycling ability has been scarcely reported, which would be ascribed to their lower conversion compared to homogeneous catalysts. This is mainly because of low catalyst/reactant contact from either low active site availability or pore diffusion limitations. The available results for NP-based catalysts, although they are very rare, confirm that they could show improved performances compared to solid catalysts. Insufficiently explore of nanocatalysts in oxidative cleavage of UFAs, called for further works in this field. It even makes more sense given the fact that surface properties of metals oxides NPs provide a great promise in their further modifications, which can increase their catalytic efficiency in the biphasic oxidative cleavage of UFAs. Interestingly, considering the high degree of dispersion of organo-functionalized NPs, one can properly assume that such catalysts are at the frontier of homogenous and heterogeneous catalysts as they possess the best aspects of the both, simultaneously. The good dispersion of a catalyst in a solvent, although it increases the catalytic activity, can be a double-edged sword if it makes the separation of catalyst from product complicated. Owing to the recent advances, however, recovery of NP-based catalysts is possible via facile and highly efficient methods.

Furthermore, the excellent inherent properties of polyoxotungstates (e.g. strong acidity, high thermal stability, and hydrophobicity) hold, nowadays, a promise for application in various organic reactions chiefly including oxidation and acid catalysis reactions. However, POTs are originally soluble in water and polar solvents, resulting in lack and/or difficulty of recovery. The fabrication of hybrid organic-inorganic POT-based catalysts is currently a hot topic being enthusiastically explored, not only for heterogenization purposes, but also for their versatilities in liquid organic reactions arising from the wide variety of organic groups and proper adjustment of the surface state. The obtained advantages of organo-solidified POTs can be succinctly listed as (i) formation of pseudo-homogeneous phase and/or stabilization of Pickering emulsion medium resulting in enhancement of catalyst efficiency, (ii) increasing catalyst hydrophobicity which results in prevention of catalyst particles aggregation and poisoning of acid sites by water, (iii) enabling self-separation of the catalyst at the end of reaction, and even (iv) preparation of size-selective catalysts to selectively allow desired molecules to ingress and egress.

Considering the fast pace of catalysis progress, it is definitely only a matter of time before an environmentally benign process for oxidative cleavage of UFAs in industry is achieved.



## Chapter 3. Characterization techniques and reaction analysis



This chapter:

- (i) Succinctly explains the underlying principles of the characterization techniques, employed in our works, with emphasis on how we exploited these techniques and which information we acquired regarding the physical and chemical properties of the prepared materials.
- (ii) Describes calculation of the reaction efficiencies and quantitative analysis of the fatty acids with GC-MS.

## 3.1 Characterization techniques

### 3.1.1 X-ray Diffractometry

X-ray diffraction (XRD) is among the most powerful techniques for the characterization of solids. It is used to identify crystalline phases by means of lattice structural parameters, and to obtain an indication of crystallite size. X-ray diffraction occurs in the elastic scattering of X-ray photons by atoms in a periodic lattice. The scattered monochromatic X-rays that are in phase give constructive interference. According to Bragg's law, the constructive interference occurs only when the path length difference between two or more beams diffracted in the same direction is an integer multiple of the wavelength (Figure 3.1). The path length difference is dependent on the lattice spacing of the atoms and the sine function of the angle between the incident angle and the scattering angle.

$$n\lambda = 2d\sin\theta \quad (3.1)$$

where  $\lambda$  is the wavelength of the X-rays,  $d$  is the distance between two lattice planes,  $\theta$  is the angle between the incoming X-rays and the normal to the reflecting lattice plane,  $n$  is an integer called the order of the reflection.

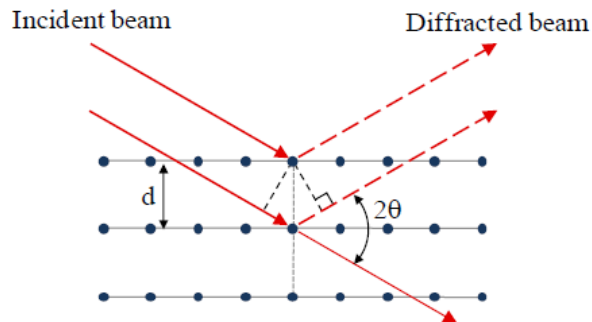


**Figure 3.1.** Schematic illustration of the Bragg's law.

A typical XRD instrument consists of three main parts: X-ray tube, specimen stage, and X-ray detector. The X-ray beam generated by the X-ray tube passes through special slits, which collimate the X-ray beam and prevent beam divergence. After passing through the slits, the X-ray

beam strikes the specimen that is supported by the plane of specimen. The X-rays diffracted by the specimen interfere constructively when they are in phase and produce a convergent beam at receiving slits before entering the detector. By continuously changing the incident angle of the X-ray beam, diffraction intensity is recorded in a range of  $2\theta$ .

In our study, XRD was used to identify the crystalline phases of various structures of tungsten and molybdenum oxides. We have worked with X'Pert HighScore Software to analyze the XRD data. The obtained spectra were compared with the updated database of ICDD<sup>3</sup> library of spectra. In principle, if the angles,  $2\theta$ , under which constructively interfering X-rays leave the crystal, can be measured, the Bragg relation gives the corresponding lattice spacings, which can be used to identify the crystalline phase of the sample.

### **3.1.2 Infrared Spectroscopy**

Infrared spectroscopy (IR) studies the changes in the vibrational and rotation movements of the molecules. It is commonly used to show the presence or absence of functional groups which have specific vibration frequencies. In our research, since XRD technique revealed bulk chemical structure of the obtained samples, FTIR analysis was employed to learn more about the composition of organic part of the hybrid organic-inorganic samples as well as different available tungsten and molybdenum bonds in crystalline structures of the samples.

In principle, at ordinary temperatures, organic molecules are in a constant state of vibrations, each bond having its characteristic stretching and bending frequencies. When infrared light radiations with frequency between  $4000-400\text{ cm}^{-1}$  are passed through a sample of an organic compound, some of these radiations are absorbed by the sample and are converted into energy of molecular vibrations. The other radiations which do not interact with the sample are transmitted through the sample without being absorbed. The infrared spectrum of the sample or compounds is the plot of % transmittance against frequency. The presence of characteristic vibrational bands in an IR spectrum indicates the presence of the corresponding bonds in the sample under investigation.

---

<sup>3</sup> The International Center for Diffraction Data

### 3.1.3 Thermogravimetric analysis

Thermogravimetric analysis (TGA) is a technique in which the mass of a substance is monitored as a function of temperature or time while the temperature of the sample, in a specified atmosphere, is programmed. TGA is a very useful technique for analysis of thermal decomposition, oxidization, dehydration, heat resistance, and kinetics analysis. By combining with other measurement techniques, variety of information on one sample can be achieved. Simultaneous thermogravimetry and differential thermal analysis (TGA/DTA) is a method in which thermogravimetry and differential thermal analysis are combined and measured simultaneously by a single apparatus. In our works, TGA/DTA was efficiently used to not only determine the amount of surfactant molecules adsorbed on the surface of metal oxide catalysts, but also provide information related to certain physical and chemical phenomena that occur during heating.

In DTA, the temperature difference between the sample and a reference material is monitored against time or temperature while the sample's temperature, in a specified atmosphere, is programmed. Figure 3.2, which shows the measurement principles of DTA, elucidates its role in our works. It shows the temperature change of the furnace, the reference and the sample against time (Figure 3.2 a), and the change in temperature difference ( $\Delta T$ ) against time detected with the differential thermocouple.  $\Delta T$  signal is referred to as the DTA signal. Materials that do not change in the measurement temperature range (usually  $\alpha$ -alumina) are used as reference. When the furnace is heating, the reference and the sample begin to be heated with a slight delay depending on their respective heat capacity, and eventually heat up according to the furnace temperature. Therefore,  $\Delta T$  changes until a static state is reached, and after achieving stability, reaches a set amount compliant with the difference in heat capacity between the sample and the reference. The signal at the static state is known as the baseline. Since then, by increasing the furnace temperature some either endothermic or exothermic phenomena might occur, which result in sudden decrease or increase in  $\Delta T$ . For example, if melting occurs (as an endothermic process), the rise in the sample's temperature stops as shown in Figure 3.2 a, and the absolute value of  $\Delta T$  increases. When the melting ends, the temperature curve rapidly reverts to the baseline. At this point, the  $\Delta T$  signal reaches the peak, as shown in Figure 3.2 b. From this, we can detect the sample's transition temperature and the reaction temperature from the  $\Delta T$  signal (DTA signal). In Figure 3.2 b, the

temperature difference due to the sample's endothermic change is shown as a negative direction and the temperature difference due to the sample's exothermic change is shown as a positive direction.

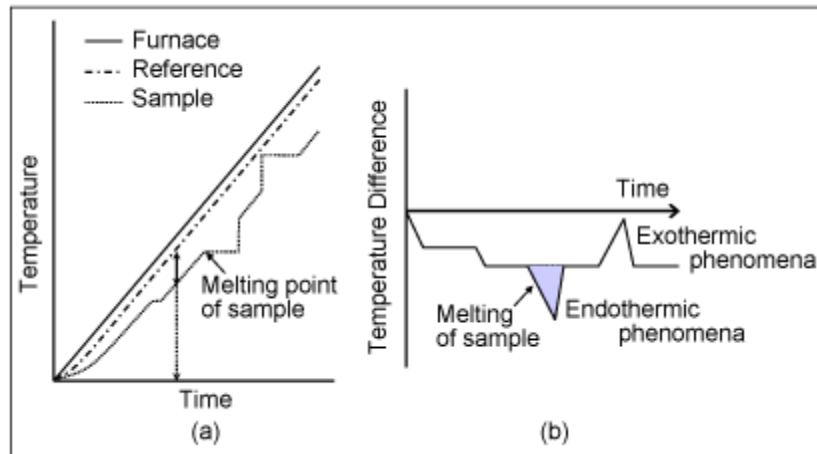
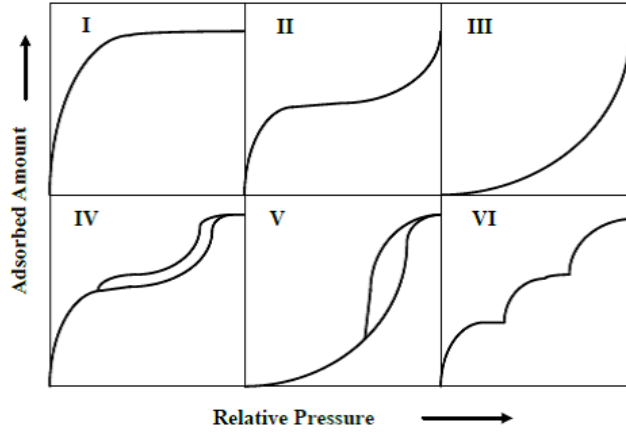


Figure 3.2. Measurement principles of DTA.

### 3.1.4 Nitrogen physisorption

Nitrogen physisorption is a widely used method for the characterization of porous materials with regard to the determination of surface area, pore size, pore size distribution, and porosity. This technique is based on the measurement of adsorption and desorption equilibrium isotherms of nitrogen on a solid surface at different partial pressures of nitrogen. The resulting relationship of volume of nitrogen adsorbed and desorbed vs. relative pressure at constant temperature is known as sorption isotherms. The shape of the isotherms strongly depends on the porous structure of the materials.

In 1985, the International Union of Pure and Applied Chemistry (IUPAC) published a classification of six types of sorption isotherms (Figure 3.3). Type I isotherms are characteristic of microporous materials. Type II and III isotherms are the normal form of adsorption by nonporous or macroporous adsorbents in which the adsorption proceeds via multilayer formation. Type IV and V isotherms are characteristic of multilayer adsorption consisting of capillary condensation onto mesoporous materials. Type VI isotherms represent stepwise multilayer adsorption on a uniform nonporous surface.



**Figure 3.3.** IUPAC classification of the physisorption isotherms.

To date, various theories are introduced to determine the surface area of porous materials. The Brunauer-Emmett-Teller (BET) method is the most widely used one. The BET equation is as follows:

$$\frac{P/P_0}{n(1-P/P_0)} = \frac{1}{n_m c} + \frac{c-1}{n_m c} \times \frac{P}{P_0} \quad (3.2)$$

Where  $n$  is the number of moles adsorbed at the relative pressure  $P/P_0$ ,  $n_m$  is the monolayer capacity,  $c$  is a constant related exponentially to the heat of adsorption in the first adsorbed layer. A linear relationship between  $\frac{P/P_0}{n(1-P/P_0)}$  and  $P/P_0$  is obtained by the BET equation. The intercept  $\frac{1}{n_m c}$  and slope  $\frac{c-1}{n_m c}$  can be used to calculate the values of  $n_m$  and  $c$ . Therefore, the surface area can be computed from the monolayer capacity on the assumption of close packing:

$$A = n_m \alpha_m L \quad (3.3)$$

Where  $\alpha_m$  is the molecular cross-sectional area of the adsorbate,  $n_m$  is the monolayer capacity, and  $L$  is the Avogadro constant. Nitrogen is the most appropriate gas for surface area determination. If it is assumed that the BET monolayer is close-packed, then  $\alpha_m$  will be  $0.162 \text{ nm}^2$  at  $77 \text{ K}$ .

The pore-size distribution is usually determined by the BJH model (named after its discoverers Barrett, Joyner and Halenda) or non-local density functional NLDFT theory. The DFT methods were developed by taking into account the particular characteristics of the hysteresis like pore shape. Non-intersecting pores of different size are assumed to be of the same regular shape (cylinders, slits or spheres). Correspondingly, pore size distributions are calculated for a given pore geometry, using a series of theoretical isotherms (kernels) for pores of a given chemical composition of the respective geometry with different diameters. In principle, NLDFT method may be applied over the complete range of nanopore sizes when suitable kernels are available.

### **3.1.5 Electron microscopy**

Electron microscopy has emerged as an extremely powerful tool to characterize micro and nanoscale materials. This technique can provide information about not only the size and shape of materials, but also their crystallographic structures and elemental compositions. In principle, electron microscopes use a beam of highly energetic electrons to examine objects on a very fine scale. The power and versatility of electron microscopy derives from the variety of ways in which the primary electron beam interacts with the sample, and the fact that the strength of the various interactions is very dependent on the sample's physical structure, topography, crystallography and chemistry. There are generally two types of electron microscope: transmission electron microscope (TEM) and scanning electron microscope (SEM). They exploit different signals generated from electron beam-atom interactions for material characterization. In the present research, electron microscopy was used to reveal the morphology, size, and shape of the samples. Moreover, SEM instrument provided some information on chemical composition of the samples via X-ray energy dispersive spectrometer (EDS).

### **3.1.6 Elemental analysis**

The most reliable elemental analysis method to determine the contents of light elements like H, C, and N in a compound, to my knowledge, is Carbon/Hydrogen/Nitrogen/Sulphur (C/H/N/S) analysis, which is performed via the quantitative '*dynamic flash combustion*' method.

This technique is based on the complete and instantaneous oxidation of the sample. In our works, we have used this analysis to verify the structure of and propose a chemical formula for the prepared polyoxotungstates. The used instrument was EA 1108 Fisons, and the method of analysis is briefly explained here:

1. Approximately 2 mg of sample are weighed in a tin container, which is placed inside an autosampler drum purged with a continuous flow of helium. The samples are introduced at preset intervals into a combustion reactor (quartz tube maintained at 1021 °C).
2. Inside this furnace, the helium stream is temporarily enriched with pure oxygen when the samples are dropped. The sample and its container melt. The tin promotes a violent reaction under these conditions, which leads to a complete oxidation of all the substances (even the thermally resistant ones). Quantitative conversion in combustion products (CO<sub>2</sub>, H<sub>2</sub>O, N<sub>2</sub>, SO<sub>2</sub>) is achieved by passing the mixtures of gases over the different layers of the reactor.
3. The combustion gases are separated by gas chromatography using helium as carrier gas. The detection is done using a thermal conductivity detector (TCD) giving an output signal proportional with the concentration of the components: C, H, N, S.
4. The calibration of the instrument is performed using certified standards and 'quality control' samples are run for validation of the results (see detailed procedure below).

A calibration curve is built using standards. Standards are also analysed as unknown for quality control purpose. The analyses are performed as follows:

- 3-6 analyses of standards (calibration curve)
- 1 analysis of a standard as unknown ('quality control' sample)
- 6-10 analyses (unknown)
- 1 analysis of a standard as unknown ('quality control' sample)
- 6-10 analyses (unknown)
- 3-6 analyses of standards (calibration curve)
- 1 analysis of a standard as unknown ('quality control' sample)



- 6-10 analyses (unknown)
- 1 analysis of a standard as unknown ('quality control' sample)
- 6-10 analyses (unknown)
- 3-6 analyses of standards (calibration curve)
- .....

Certified standards from the company Isomass are used. The standards having % C, N, H, S close to those of the unknown samples are chosen. For the 'quality control' samples the validation criteria versus the expected values for the standards used are presented in Table 3.1.

**Table 3.1.** Concordance criteria of CHNS analysis <sup>1</sup>.

% of each element	Accepted difference
	<b><i>C, H, N</i></b>
5.00 – 9.99	± 0.15
10.0 – 24.9	± 0.25
25.0 – 90.0	± 0.30
	<b><i>S</i></b>
< 25.0 <sup>1</sup>	± 1.00

1. For the samples containing more than 25 % S, the instrument is less reliable.

Duplicate analyses are always performed for each unknown sample. The strict concordance criteria for the two analyses of the same sample are presented in Table 3.1 (differences of ± 0.30 % for C, H, N, and ± 1.00 % for S are usually considered acceptable). The results not being concordant could indicate: presence or impurities, heterogeneity, decomposition, other. The detection limits for the analyses are the following: 0.3 % for C, H, N and 1.0 % for S.

### 3.1.7 Zeta potential analysis

Zeta potential analysis is critical in understanding the electrical charge characteristics of sample particles. The electrical charge properties control the interactions between particles and therefore determine the overall behavior of a sample suspension.

The liquid layer surrounding the particle exists as two parts; an inner region (Stern layer) where the ions are strongly bound and an outer (diffuse) region where they are less firmly associated. Within the diffuse layer, there is a notional boundary inside which the ions and particles

form a stable entity. When a particle moves (*e.g.*, due to gravity), ions within the boundary move with it. Those ions beyond the boundary stay with the bulk dispersant. The potential at this boundary (surface of hydrodynamic shear) is the zeta potential (Figure 3.4).

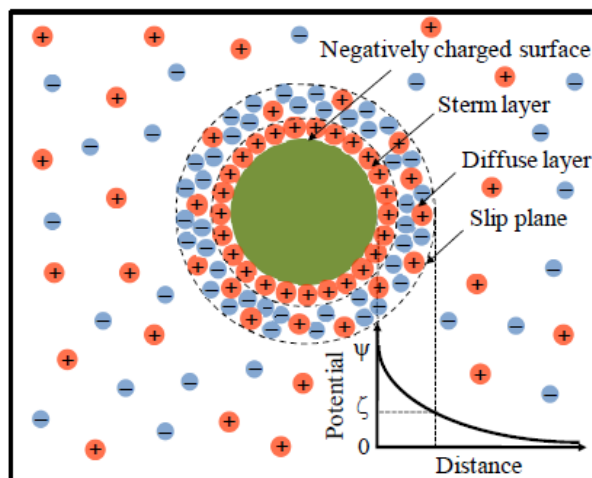


**Figure 3.4.** Zeta potential and ionic distribution of a negatively charged particle.

The zeta potential of a particle cannot be measured directly, but can be calculated from measurements of the velocity of a particle in suspension when an electric field is applied. Particle velocity in the liquid, referred to as electrophoretic velocity, depends on the strength of the electric field, the dielectric constant of the liquid, the viscosity of the liquid, and the size and zeta potential of the particle. The electrophoretic velocity can be measured by using techniques called laser doppler velocimetry and phase analysis light scattering. The frequency shift or phase shift of an incident laser beam scattered by the sample particles moving in an electric field is measured and used to calculate the electrophoretic mobility.

The magnitude of the zeta potential gives an indication of the potential stability of the colloidal system. If all the particles in suspension have a large negative or positive zeta potential, then they will tend to repel each other and there will be no tendency for the particles to come together. However, if the particles have low zeta potential values then there will be no force to prevent the particles coming together and flocculating. In our study, zeta potential analysis was used to characterize the stability of the catalyst colloidal suspension.

## 3.2 Quantitative analysis of the catalytic tests

The most common method for the determination of the fatty acids composition in a lipid mixture is gas-liquid chromatography (GLC). In the terms of fatty acids reactions, since several substrates are usually involved in a reaction, it would be more beneficial to utilize a gas chromatograph equipped with a mass detector. In this way, the Gas chromatography-mass spectrometry (GC-MS) not only quantifies but also identifies the different chemicals in the reaction. Figure 3.5 shows a typical GC-MS system. Therefore, in our works, GC-MS analysis was used for the separation, identification, and quantification of the products after the reaction.

Due to the long chain and, also, presence of carboxyl functional group, fatty acids are highly polar compounds that tend to form hydrogen bonds. This affinity results in adsorption issues of fatty acids on the stationary phase inside of the GC capillary column. Therefore, fatty acids in their free form are difficult and fallible to analyze with GC. Although some polar stationary phases (such as FFAP column from Agilent Company) have been recently developed for direct analysis of free fatty acids, more accurate and reproducible chromatographic data are obtained if the fatty acids are derivatized to their respective methyl esters. Reducing the polarity of fatty acids make them more amenable for analysis. Converting fatty acids to fatty acid methyl esters is the most common method for preparation of fatty acids prior to GC analysis, because methyl esters offer excellent stability, and provide quick and quantitative samples for analysis. Moreover, neutralizing the polar carboxyl group leads to easier distinguish between the very slight differences exhibited by unsaturated fatty acids. Fatty acid methyl esters (FAMES), then, can be separated by boiling point difference, degree of unsaturation, position of unsaturation, and even the *cis* and *trans* configurations of unsaturation.

### 3.2.1 Derivatization process prior to GC-MS analysis

Throughout our catalytic tests, after a typical oxidative cleavage reaction, the products mixture underwent a derivatization reaction, in which the expectedly produced azelaic and pelargonic acids, and possibly unreacted oleic acid were esterified to dimethyl azelate, methyl pelargonate, and methyl oleate, respectively. A general esterification reaction of fatty acids is shown in Equation 3.4. The process involves heating the acid in an alcoholic solvent (commonly

methanol) in the presence of an acidic catalyst. The role of catalyst in this reaction is protonation of oxygen in the carboxyl group (see Scheme 3.1, step 1) to make the acid more reactive to nucleophiles. Methanol molecule then reacts with the protonated acid (step 2) resulting in the loss of water and production of ester (step 3). This reaction is reversible, therefore to obtain a higher yield, removing water is necessary which can be done by using a water scavenger (such as anhydrous sulfuric acid and graphite bisulfate) or performing the reaction at temperatures higher than 100°C.

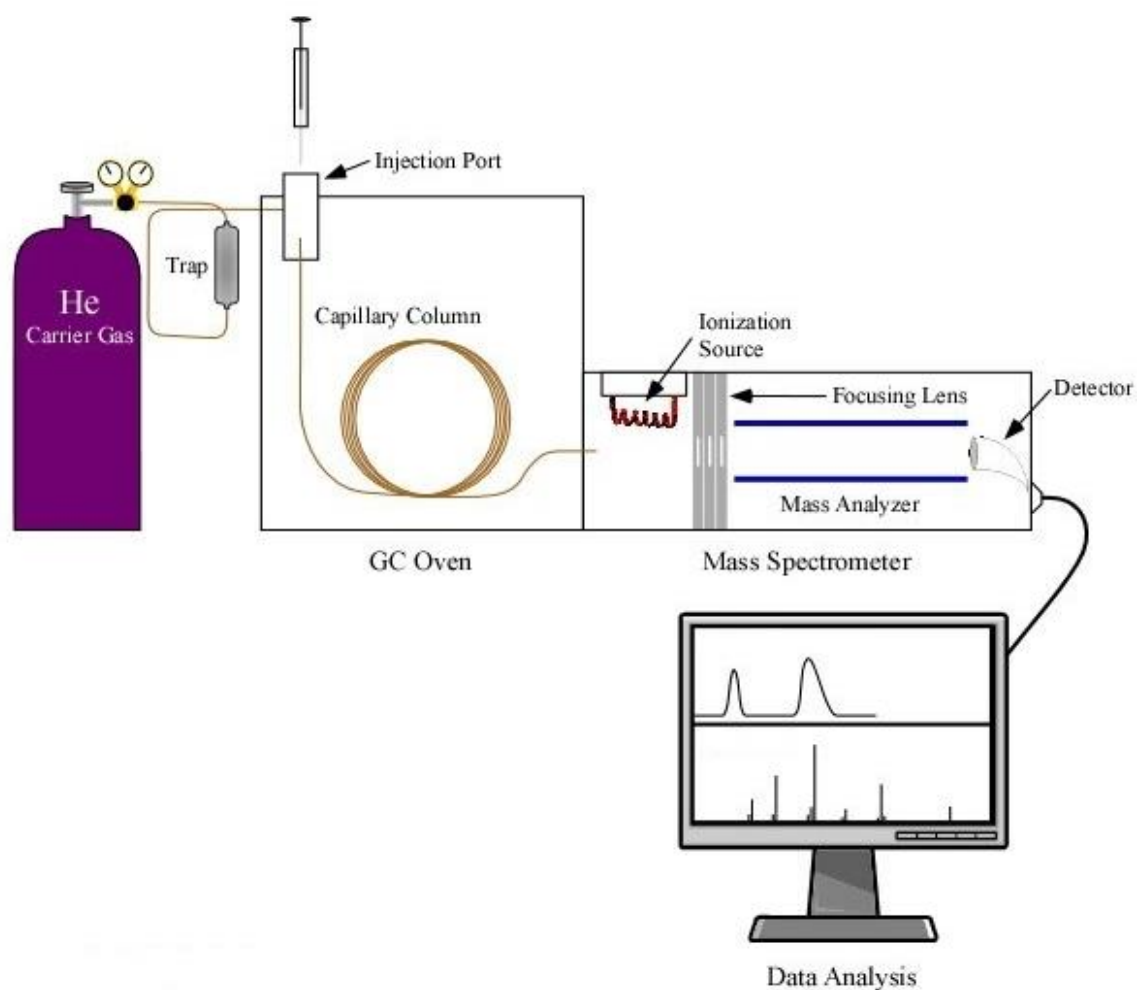
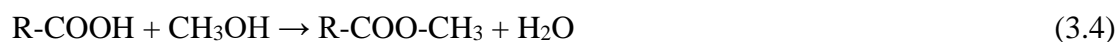
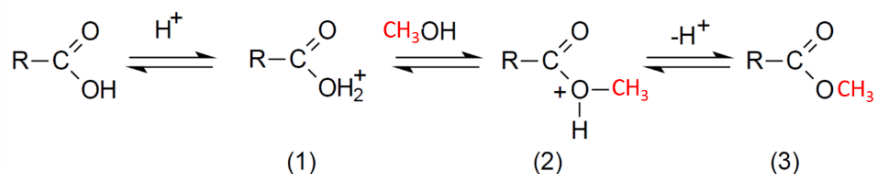


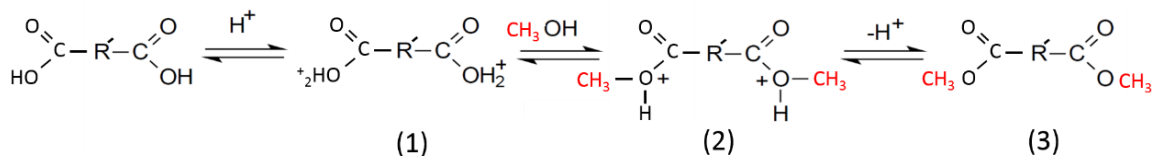
**Figure 3.5.** Different parts of a GC-MS system.



For mono-acids:



For di-acids:



**Scheme 3.1.** Three steps mechanisms of esterification of mono and dicarboxylic acids over acid catalysts.

### 3.2.2 Chromatograms analysis and calculation procedure

First, the GC-MS was calibrated by the analytical standards of dimethyl azelate, methyl pelargonate, and methyl oleate. Obtaining the calibration curves is a very critical step in the quantitative analysis. In addition to the instrument's operating conditions, concentrations of the standard samples must be carefully chosen to obtain a linear calibration curve. A rule of thumb says not more than 500 ppm of analyte should enter to the mass detector to obtain a linear calibration curve. According to this and based on the flow rate of the carrier gas and the split ratio (see section 3.2.3), we calculated the proper concentration of the sample solutions for injection to GC-MS, which resulted in excellent linearity of the calibration curves. Admittedly, the calibration curves must be reproduced regularly. Figure 3.6 shows typical calibration curves obtained for methyl oleate, dimethyl azelate, and methyl pelargonate.

After the catalytic reaction (oxidative cleavage of oleic acid) and the derivatization process, a typical esterified sample, expectedly including dimethyl azelate, methyl pelargonate, and possibly methyl oleate, was injected to GC-MS. A constant and exact amount was injected each time, and the injection was repeated at least four times for each sample to be averaged. The peaks in the obtained chromatograms always had excellent shape and sharpness, owing to the carefully chosen column type and operating conditions of GC (see section 3.2.3), which lead to reliable results. Figure 3.7 shows a typical chromatogram of the reaction products. Based on peak areas in

the chromatograms and the calibration curves, conversion and yields of the oxidative cleavage reaction were calculated, using the following formulas:

$$\text{Conversion} = \frac{\text{Total amount of oleic acid consumed (mole)}}{\text{Initial amount of oleic acid (mole)}} \times 100 \quad (3.5)$$

$$\text{Yield}_{(A)} = \frac{\text{Amount of chemical A produced (mole)}}{\text{Total amount of oleic acid consumed (mole)}} \times 100 \quad (3.6)$$

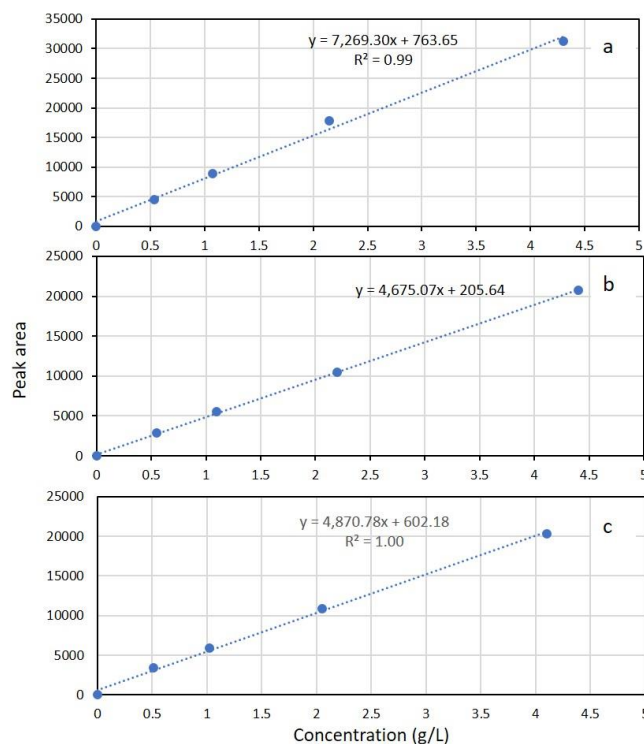


**Figure 3.6.** Typical calibration curves of (a) methyl oleate, (b) dimethyl azelate, and (c) methyl pelargonate.

The properly adjusted temperature programming allowed separation of methyl pelargonate, dimethyl azelate, and methyl oleate with discrete retention times ( $R_t$ ) of 10.4, 15.8, and 26.8 min, respectively (see Figure 3.7). Some other peaks are also observed in the chromatograms, indicating presence of by-products, which were qualitatively analyzed by MS, as follows. Small and often negligible peaks in e.g.  $R_t$ = 6.8, 8.9, 11.2, and 16.7 min belonged to octanal, methyl esters of hexanoic and octanoic acids, and 9,10-dihydroxy octadecanoic acid, respectively, which were

produced by impurities of the reactants and/or insignificant side reactions (e.g. hydroxylation). Two relatively more considerable peaks in  $R_t= 8.6$  and  $13.8$  min belonged to nonanal and 9-oxononanoic acid, respectively, which were produced by partial-oxidation of oleic acid. Since after minute 30 no significant peak was obtained, the chromatograms have been generally monitored up to  $R_t= 30$  min.

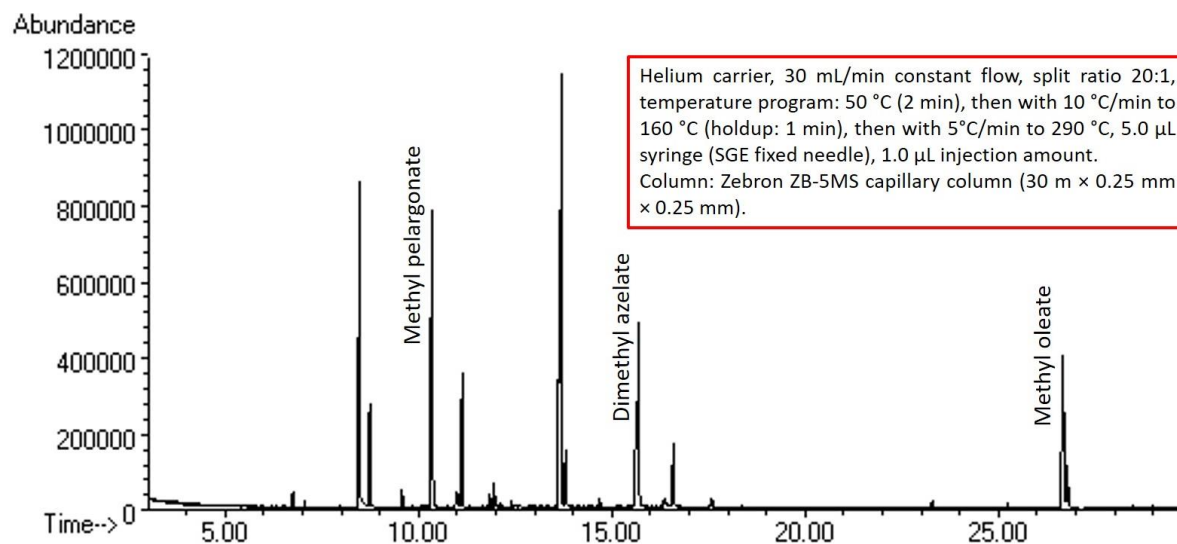


**Figure 3.7.** A typical gas chromatogram of the products (after derivatization) of oxidative cleavage of oleic acid.

It should be noted that such by-products like 9-oxononanoic acid, which are the direct result of involvement of carboxylic group in the reaction, has made oxidative cleavage of unsaturated fatty acids, compared to alkenes and cyclic olefins, more complicated and investigation of their reaction mechanism more difficult. It makes more sense given the fact that 9-oxononanoic acid is not commercially available (in known chemical provider companies), which makes calibration of chromatography systems by the analytical standard of this chemical, and consequently its quantitative analysis by these systems impossible.

### 3.2.3 Apparatus and design

The GC-MS included a Hewlett-Packard HP 5890 series GC system and MSD Hewlett-Packard model 5970. GC system was equipped with Zebron ZB-5MS capillary column (30 m x 0.25 mm x 0.25 mm). Helium was used as a carrier gas with the flow rate of 30 mL/min. A split

ratio of 20:1 was fixed. The front inlet temperature was 280 °C. The oven temperature program consisted of maintaining at 50 °C for 2 min, then a ramp rate of 10 °C/min to 160 °C following by a hold-up time of 1 min, and further increase with the rate of 5°C/min to 290 °C. Direct injection by a 5.0 µL syringe (SGE fixed needle, 23-26 gauge/42mm L/Cone Tip, Phenomenex Co.) was employed with 1.0 µL injection amount for each run. HP Chemstation software was used to analyze data.



# **Chapter 4. Synthesis of mesoporous tungsten oxide/ $\gamma$ -alumina and surfactant-capped tungsten oxide nanoparticles and their catalytic activities in oxidative cleavage of oleic acid**

Amir Enferadi Kerenkan <sup>1</sup>, Aimé Serge Ello <sup>1,2</sup>, Bouselham Echchahed <sup>1</sup> and Trong-On Do <sup>1\*</sup>

1. Department of Chemical Engineering, Université Laval, Québec, G1V 0A6, Canada

2. Laboratoire de Chimie Physique, Université Félix Houphouët-Boigny de Cocody, 22 bp 582 Abidjan, Cote d'Ivoire

*International Journal of Chemical Reactor Engineering*, 2016; 14(4), 899-907

*Special Issue in honor of Dr. Serge Kaliaguine*

## Résumé

Les acides gras insaturés peuvent être convertis en acides mono- et dicarboxyliques, qui sont des matériaux de valeur utile, par réaction de clivage oxydatif en présence d'un système catalyseur / oxydant hautement efficace. Dans ce travail, deux types de catalyseurs hétérogènes avancés ont été développés; (i) oxyde de tungstène mésoporeux / oxyde de  $\gamma$ -alumine à haute surface spécifique et (ii) nanoparticules d'oxyde de tungstène coiffées de tensioactif. Diverses techniques, y compris les isothermes d'adsorption / désorption de  $N_2$ , XRD, SEM, EDS, TGA et test catalytique ont été utilisées pour contrôler les propriétés physico-chimiques et catalytiques de ces matériaux. Les résultats de caractérisation ont révélé que ces types de matériaux (i) présentent une surface spécifique élevée et une distribution granulométrique étroite, et que le tensioactif utilisé pourrait couvrir assez quantitativement la surface de ces types de matériaux(ii).

Les activités catalytiques de ces matériaux dans le clivage oxydatif de l'acide oléique avec  $H_2O_2$  en tant qu'oxydant ont été étudiées. La GC-MS a été utilisée pour déterminer les quantités produites des produits désirés, les acides azélaïques et pélargoniques. Les résultats des essais catalytiques ont montré une conversion de plus de 90% pour ce type de catalyseur (ii) en une réaction de 5 h à  $120^\circ C$  avec des rendements de production acceptables pour les acides azélaïques et pélargoniques. L'activité significativement plus élevée de ce catalyseur par rapport à ce genre (i) provient des propriétés de surface intéressantes des nanoparticules d'oxydes de tungstène qui les rendent capables d'exploiter les bonnes caractéristiques des catalyseurs homogènes et hétérogènes.

## Abstract

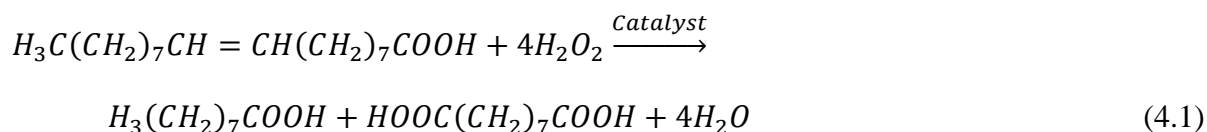
Unsaturated fatty acids can be converted into mono and dicarboxylic acids, which are applicably valuable materials, through oxidative cleavage reaction in the presence of a highly efficient catalyst/oxidant system. In this work, two types of advanced heterogeneous catalysts have been developed; (i) high surface area mesoporous tungsten oxide/ $\gamma$ -alumina mixed metal oxide, and (ii) surfactant-capped tungsten oxide nanoparticles. Various techniques including  $N_2$  adsorption/desorption isotherms, XRD, SEM, EDS, TGA and catalytic test were used to monitor the physicochemical and catalytic properties of these materials. The characterization results revealed that type (i) materials exhibit high surface area and narrow particle size distribution, and the used surfactant could quantitatively enough cap the surface of type (ii) materials. The catalytic activities of these materials in the oxidative cleavage of oleic acid with  $H_2O_2$  as oxidant were investigated. GC-MS was used to determine the produced amounts of the desired products, azelaic and pelargonic acids. The catalytic test results showed more than 90% conversion for type (ii) catalyst in 5 h reaction at  $120\text{ }^\circ\text{C}$  with acceptable production yields for azelaic and pelargonic acids. The significantly higher activity of this catalyst compared to type (i) arises from the interesting surface properties of tungsten oxides nanoparticles, which make them able to exploit the good features of homogeneous and heterogeneous catalysts.

## 4.1 Introduction

Oils and fats of vegetable and animal origin have rapidly attracted a growing interest as renewable materials for feedstock in oleochemical industries [12,6,8,13]. This attention arises from not only environmental reasons, but also economic ones. Unsaturated fatty acids, as the constituents of lipids, could undergo different reactions to produce a variety of products, even more than petrochemistry products [7]. Oxidation of unsaturated fatty acids possesses an industrially great importance, since it results in the production of mono and dicarboxylic acids which are applicably valuable materials. This oxidation reaction, which is called oxidative cleavage due to the cleavage of carbon-carbon double bond(s) during the reaction, can be done in the presence of a highly efficient catalyst/oxidant system. Currently, azelaic acid (C9, dicarboxylic acid) is produced in large-scale via ozonolysis of oleic acid. Pelargonic acid (C9, monocarboxylic acid) is obtained as a co-product but also a valuable chemical [1]. These types of saturated acids that have short and odd hydrocarbon chains are rare in natural resources [2]. On the other hand, they are very attractive initial materials for the development of numerous bio-based products [4,3]. For instance, azelaic acid converts into different esters for the preparation of polymers (Nylon 6:9), plasticizers, adhesives, solvents, biodegradable lubricants, corrosion inhibitors, and anti-acneic agent for cosmetics [2,3]. Pelargonic acid is an intermediate in the production of lubricants, plasticizers, perfumes, herbicides, fungicides, resins [5,3].

Although the ozonolysis of oleic acid has shown high conversion and selectivity [25,2,1,3], hazardous problems associated with the use of ozone have always been a challenge [8]. Using benign oxidants such as hydrogen peroxide in the oxidation reaction (Equation 4.1), however, makes it necessary to employ a highly efficient catalytic system. In our recent review paper, all the catalytic systems reported in literature for this purpose have been thoroughly investigated[91]. Transition metals such as osmium, cobalt, molybdenum, chrome, gold, manganese, iron, ruthenium, and tungsten have been used as catalytic active sites, with more emphasis on Ru and particularly W. In spite of the excellent conversion and selectivity shown by homogeneous catalysts [64,60,59,2,65,63,61,62,58,57,54,56,55,53,3], their large-scale applications have been always restricted due to the lack of catalyst recovery. Curiously, use of heterogeneous catalysts with recycling ability has been scarcely reported [75,48,45], which would arise from their lower

conversion compared to homogeneous catalysts. This is mainly because of low catalyst/reactant contact from either low active site availability or pore diffusion limitations. Mesoporous materials have shown potential applications as either catalysts or supports for liquid-phase reactions of oils and fats [333,37]. Using mesoporous MCM-41 and microporous zeolites as catalyst support in the oxidative cleavage of oleic acid, Dapurkar et al. demonstrated the advantages of mesoporous catalysts compared to microporous ones [75]. Another way to improve the performance of heterogeneous catalysts is employing advanced nanocatalysts. The available results for nanocatalysts, although very rare, confirm that they could increase the activity of solid catalysts in oxidative cleavage of oleic acid [87,1]. Surface properties of metals oxides nanoparticles provide a great promise in their further modifications, which will make them favorable for use as catalysts in the biphasic oxidation reactions of unsaturated fatty acids.



In this work, we report a facile synthesis method for incorporating tungsten oxide into mesostructured  $\gamma$ -alumina with high surface area. In order to investigate the effect of  $WO_3$  on the porosity of the mixed metal oxide, samples with different loadings of tungsten oxide were compared to pure alumina and pure  $WO_3$ . Then, the catalytic activities of  $WO_3/\gamma\text{-Al}_2O_3$  samples in the oxidative cleavage of oleic acid were investigated. Furthermore, capping the surface of tungsten oxide nanoparticles with a surfactant, as a strategy for enhancement of catalytic performance, was developed, and the results were compared to those of the mesostructured catalysts.

## 4.2 Experimental

### 4.2.1 Materials and reagents

Aluminium isopropoxide ( $Al(O\text{-}i\text{-}Pr)_3$ ,  $\geq 98\%$ ), oleic acid (90%), tert-butanol ( $\geq 99\%$ ), and boron trifluoride ( $BF_3$ -methanol, 10% w/w) were purchased from Sigma Aldrich Co. Ammonium tungsten oxide hydrate  $(NH_4)_6W_{12}O_{39}\cdot xH_2O$  and D-(+)-Glucose (anhydrous, 99%) were provided by Alfa Aesar Co. Hydrogen peroxide (aqueous solution, 30 %) was purchased from Fisher Scientific Co.

## 4.2.2 Synthesis

*Mesoporous tungsten oxide/ $\gamma$ -alumina mixed metal oxide.* Tungsten oxide/ $\gamma$ -alumina were synthesized using a facile hydrothermal method followed by calcination. In a typical synthesis, 2.1 g (10.28 mmol) of Al(O-*i*-Pr)<sub>3</sub> and 1.8 g glucose were dissolved into 30 ml water/propanol (50/50 volume ratio). Then, nitric acid (10 wt %) was added dropwise to the solution to adjust the pH at around 5. Subsequently, a certain amount of ammonium tungsten oxide hydrate (0.13, 0.65, and 1.3 g for the samples II, III, and IV, respectively and 1.3 g for sample V) was added to the solution under high stirring. The prepared mixture was, then, transferred to a stainless steel autoclave and thermally treated at 200 °C for 24 h. After naturally cooling down, the obtained powders were separated using centrifuge at 5000 rpm and washed several times with water and ethanol. In the final step, the as-prepared dry products were annealed in a furnace at 600 °C for 3 h in air.

*Surfactant-capped tungsten oxide nanoparticles.* 0.70 g of ammonium tungsten oxide hydrate was dissolved into 15 ml water/ethanol (50/50 volume ratio), followed by adding 0.21 g oleic acid as surfactant, and the prepared solution was then transferred to the stainless steel autoclave for thermal treatment at 200 °C for 24 h. Finally, separation with centrifuge at 5000 rpm and washing several times with water and ethanol were carried out. The prepared samples and synthesis conditions are shown in Table 4.1.

**Table 4.1.** Synthesis conditions and prepared samples.

Sample	Thermal treatment		Calcination temperature (°C)	WO <sub>3</sub> /Al <sub>2</sub> O <sub>3</sub> molar ratio	Surfactant/W molar ratio
	Temperature (°C)	Time (h)			
Mesoporous tungsten oxide/ $\gamma$ -alumina mixed metal oxide					
I	200	24	600	0	-
II	200	24	600	1/10	-
III	200	24	600	5/10	-
IV	200	24	600	10/10	-
V	200	24	600	-	-
Surfactant-capped tungsten oxide nanoparticles					
VI	200	24	-	-	0.26

### 4.2.3 Characterization

N<sub>2</sub> adsorption-desorption isotherms were determined at the temperature of liquid nitrogen with a Quantachrome Autosorb-1 system. The BET surface areas were calculated in the range of 0.05-0.3 P/P<sub>0</sub>. Before the measurements, the samples were outgassed under vacuum for 6 h at 150 °C. The total pore volume (V<sub>pore</sub>) was calculated from the amount of nitrogen adsorbed at P/P<sub>0</sub> = 0.95. Powder X-ray diffraction (XRD) patterns of the samples were obtained on a Bruker SMART APEXII X-ray diffractometer equipped with a Cu K $\alpha$  radiation source ( $\lambda=1.5418$  Å). Scanning electron microscopy (SEM) images were taken on a JEOL 6360 instrument at an accelerating voltage of 3 kV. Thermogravimetric analysis (TGA) was performed with a TGA Q500 V20.13 Build 39 thermogravimetric analyzer from room temperature to 800 °C with a heating rate of 5 °C min<sup>-1</sup> under an air flow of 50 mL min<sup>-1</sup>.

### 4.2.4 Oxidative cleavage reaction of oleic acid

Typically, a 50-mL, round-bottom flask was used to conduct the reactions under a batchwise constant temperature and constant pressure mode. This reactor was equipped with a condenser, a magnetic stirrer and an oil bath. The reaction feed included 2 g oleic acid, 6 mL H<sub>2</sub>O<sub>2</sub> (30% concentration), and 15 mL tert-butanol as solvent. After adding a constant amount of the synthesized catalyst (0.9 g) to the reaction media, the flask was put in the oil bath which was previously heated and maintained at the constant temperature of 120 °C. During the reaction, the reactor content was agitated continuously with the magnetic stirrer. After 5 h reaction, the catalyst particles were separated using centrifuge at 6000 rpm.

*Quantitative analysis of the reaction products:* Gas chromatography-mass spectrometry (GC-MS) was used for the separation and quantification of methyl esters of fatty acids. The GC-MS system included a Hewlett-Packard HP 5890 series GC system and MSD Hewlett-Packard model 5970. The GC system was equipped with Zebron ZB-5MS capillary column (30 m  $\times$  0.25 mm  $\times$  0.25 mm). Helium was used as a carrier gas with the flow rate of 30 mL/min. A split ratio of 15:1 was fixed. The front inlet temperature was 280 °C. The oven temperature program consisted of maintaining at 50 °C for 2 min, then a ramp rate of 10 °C/min to 160 °C following by a hold-up time of 1 min, and further increase with the rate of 5°C/min to 290 °C. Direct injection was

employed with 0.1  $\mu\text{L}$  injection amount for each run. HP Chemstation software was used to analyze data.

Fatty acids are difficult to analyze with GC, because these highly polar compounds tend to form hydrogen bonds with the stationary phase in GC columns, leading to adsorption issues. Reducing their polarity make them more amenable for analysis. Esterification of fatty acids to fatty acid methyl esters is the most common method for preparation of fatty acids prior to GC analysis. Methyl esters offer excellent stability, and provide quick and quantitative samples for analysis. Therefore, All samples were converted to their respective methyl esters before analysis by Metcalfe et al. derivatization procedure [334,335] using boron trifluoride solution in methanol.

In order to present the results more clearly, the terms conversion (mole %) and yields (mole %) are defined as follows:

$$\text{Conversion} = \frac{\text{Total amount of oleic acid consumed}}{\text{Initial amount of oleic acid}} \times 100 \quad (4.2)$$

$$\text{Yield}_{(A)} = \frac{\text{Amount of chemical A produced}}{\text{Total amount of oleic acid consumed}} \times 100 \quad (4.3)$$

## 4.3 Results and discussions

### 4.3.1 Synthesized samples characterization

$\text{N}_2$ -adsorption/desorption isotherms confirmed the formation of mesoporous structures for the samples I-V (Figure 4.1). All of these samples possessed type IV isotherm (based on IUPAC definition) which is characteristic of mesoporous materials. In fact, the presence of glucose in the synthesis media is critical for the formation of the mesoporous structure. It has been shown that in the synthesis of alumina, no uniform pores can be obtained when glucose is not used [336]. The role of glucose would be as a template that interacts with the metals species via hydrogen bonding. The high amount of functional hydroxyl group in the structure of glucose provides an appropriate charge on its surface in the synthesis precursor, which will make adsorption of the metals cations



easier. Such interactions could play an important role in directing the structure to mesophase formation during the gelation [337].

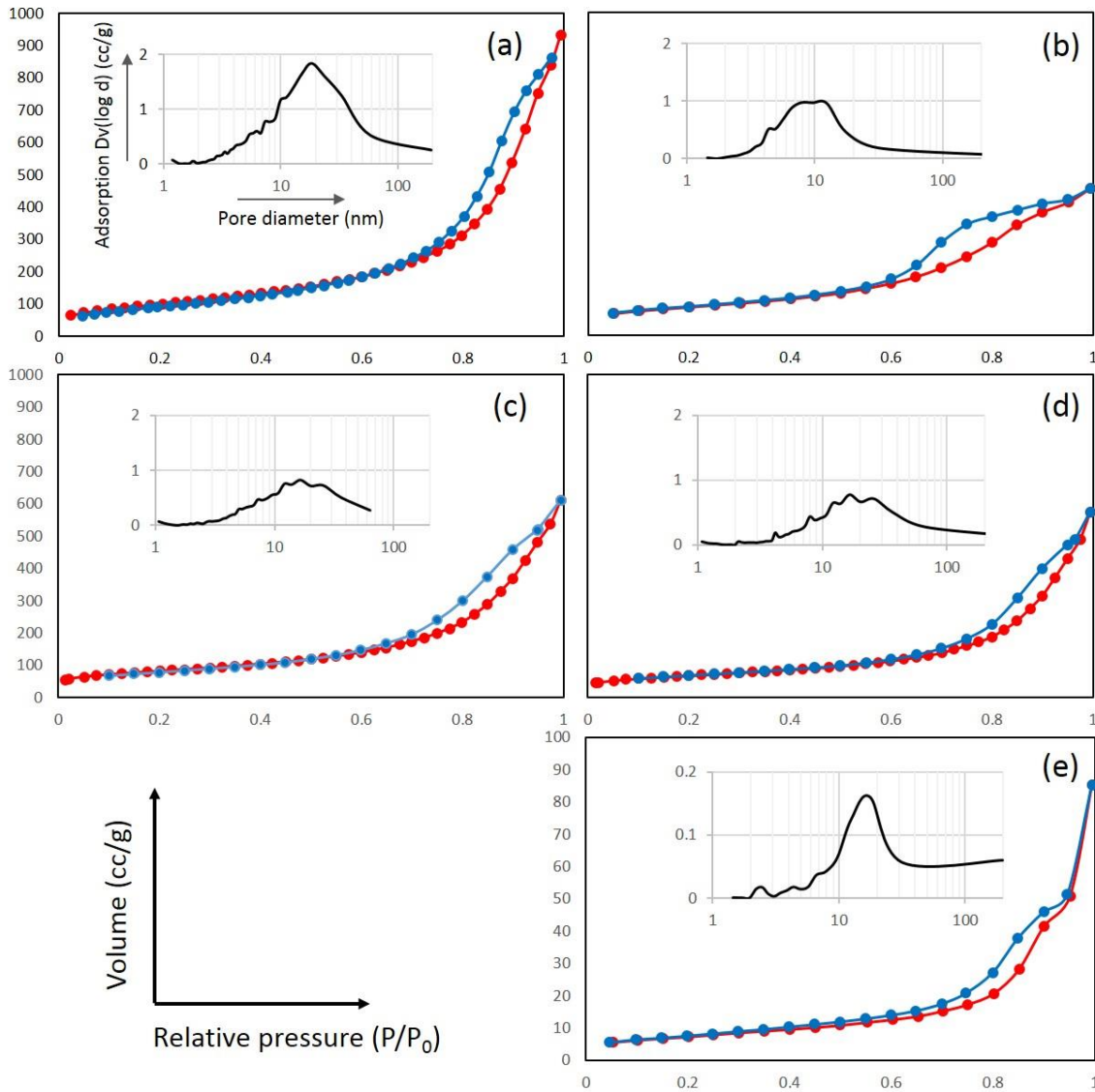


**Figure 4.1.**  $N_2$ -adsorption/desorption isotherms and pore size distributions of (a) sample I, (b) sample II, (c) sample III, (d) sample IV, and (e) sample V.

A high BET surface area ( $361 \text{ m}^2/\text{g}$ ) and a narrow pore size distribution were obtained for pure  $\gamma$ -alumina (sample I, Table 4.2). Increase in tungsten oxide content decreased the surface area; as Table 4.2 shows. Prepared samples with  $\text{WO}_3/\gamma\text{-Al}_2\text{O}_3$  molar ratio of 1/10, 5/10, and 10/10 had

surface area of 308, 251, and 204 m<sup>2</sup>/g, respectively. It should be highlighted that these high surface areas were obtained even after the calcination at 600 °C. This means that the synthesized mesoporous tungsten oxide/ $\gamma$ -alumina mixed metal oxides had very high thermal stability which can arise from thick pore wall. Adding WO<sub>3</sub>, also, reduced the average pore size due to the difference in dimensionality of molecules of tungsten and aluminium oxides. Sample IV, however, did not comply with this trend. It would be because of a disorder in the mesostructure of alumina that happened at high content of WO<sub>3</sub>. Curiously, there was a significant decrease in the surface area of pure tungsten oxide (sample V) compared to previous samples. The main reason is that the hollow structure, which could be obtained by using glucose as template, collapses during the calcination at high temperatures in the absence of alumina because of less thermal stability. This collapse in the hollow structure for sample V is obvious in its SEM image (Figure 4.2 e). Comparing the SEM images of the samples I-IV in Figure 4.2 reveals a slight change in the morphology of the samples, from uniform morphology to two-phase morphology. Also, it is clear in Figure 4.2 f that the presence of oleic acid as surfactant in the synthesis of sample VI strongly affected its morphology.

Powder X-ray diffraction (XRD) patterns of the samples I-V are presented in Figure 4.3. Pure metal oxide samples, samples I and V indicated the crystalline structure of  $\gamma$ -Al<sub>2</sub>O<sub>3</sub> and tungsten oxide, respectively. Incorporating tungsten oxide into the structure of alumina, however, decreased the intensity of the characteristic peaks of  $\gamma$ -alumina. This shows that crystalline structure of mesoporous alumina can be affected by incorporating another metal oxide. On the other hand, by increasing WO<sub>3</sub> content, one of the main peaks of tungsten oxide ( $2\theta \approx 24^\circ$ ) was emerged in sample IV pattern. Energy-dispersive X-ray spectroscopy (EDS) results of the samples I-IV, as shown in Figure 4.4, demonstrate the increase of tungsten oxide content in the mesostructure of  $\gamma$ -alumina.

**Table 4.2.** N<sub>2</sub>-adsorption/desorption isotherms results.

Sample	WO <sub>3</sub> /Al <sub>2</sub> O <sub>3</sub> molar ratio	S <sub>BET</sub> (m <sup>2</sup> /g)	Pore volume (cm <sup>3</sup> /g)	Average pore size (nm)
I	0	361	1.30	14.5
II	1/10	308	0.64	8.3
III	5/10	251	0.68	5.5
IV	10/10	204	0.62	12.2
V	-	26	0.08	11.9

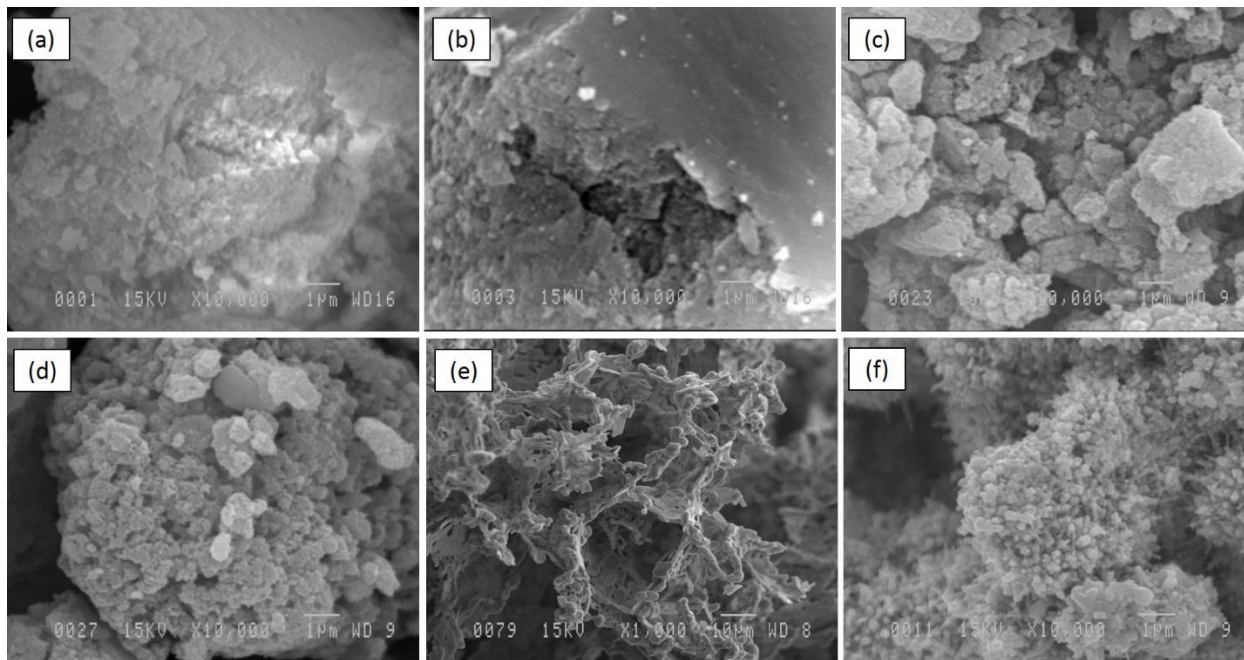


**Figure 4.2.** SEM images of (a) sample I, (b) sample II, (c) sample III, (d) sample IV, (e) sample V, and (f) sample VI.

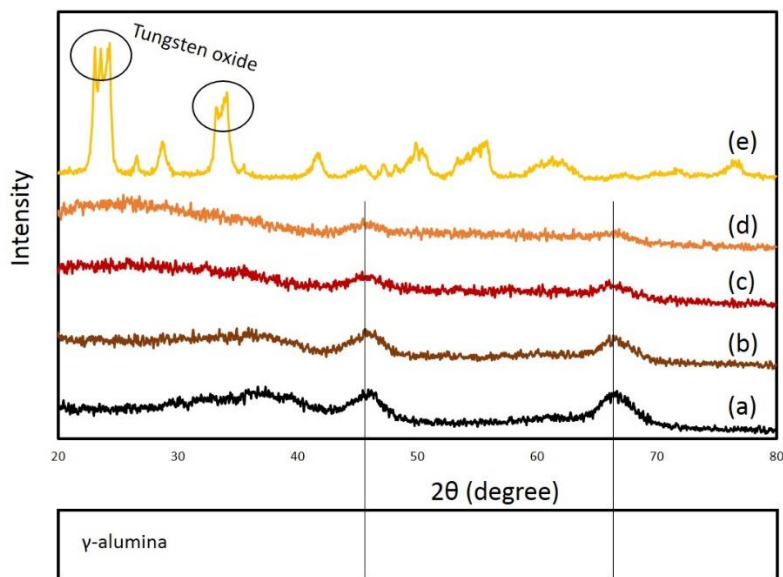


**Figure 4.3.** XRD patterns of (a) sample I, (b) sample II, (c) sample III, (d) sample IV, and (e) sample V.

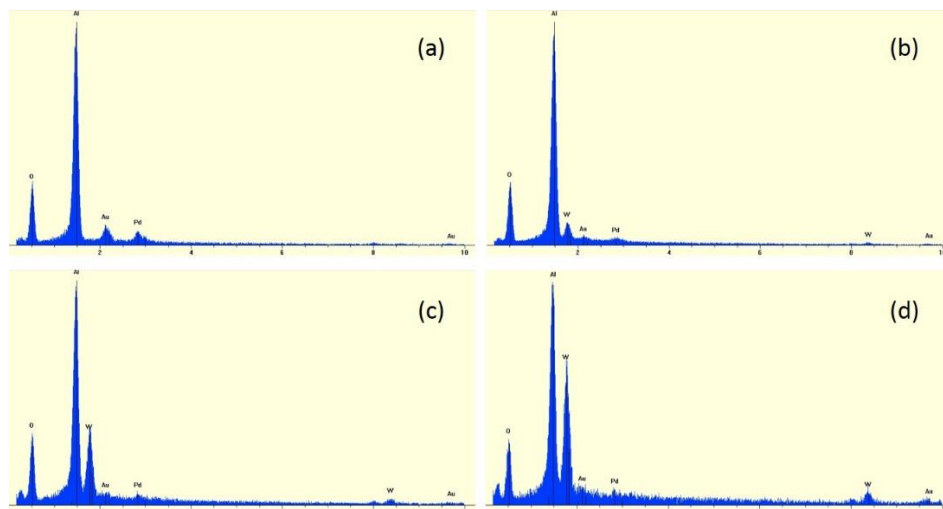


**Figure 4.4.** EDS spectrums of (a) sample I, (b) sample II, (c) sample III, and (d) sample IV.

In order to investigate the presence of surfactant on the surface of tungsten oxide nanoparticles thermogravimetric analysis (TGA) of the sample VI is shown in Figure 4.5. The amount of surfactant oleic acid on the surface of  $\text{WO}_3$  nanoparticles was approximated about 5.25 wt%.

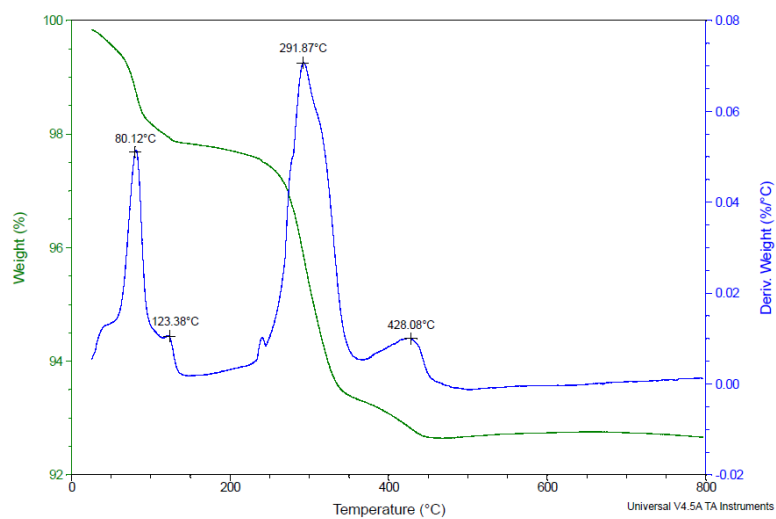


**Figure 4.5.** Thermogravimetric behavior of sample VI.

### 4.3.2 Catalytic study

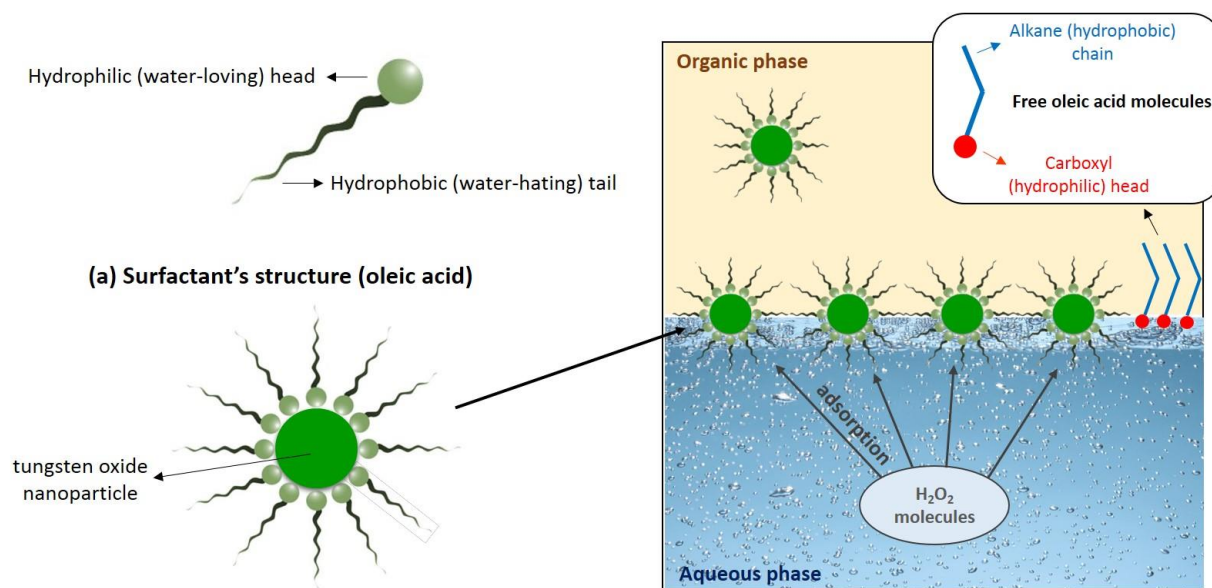
Sample II, III, and IV (mesoporous tungsten oxide/ $\gamma$ -alumina) and sample VI (surfactant-capped tungsten oxide nanoparticles) were employed as catalysts in the oxidative cleavage of oleic acid to investigate the effect of  $\text{WO}_3$  loadings on the catalytic activity, on one hand, and compare the activities of the two types of advanced heterogeneous catalysts, on the other hand. The catalytic tests results are summarized in Table 4.3.

**Table 4.3.** Catalytic test results.

Sample	Conversion (%)	Yield (azelaic acid) (%)	Yield (pelargonic acid) (%)
II	78	20	7
III	72	28	9
IV	60	32	15
VI	95	58	24

After 5 h reaction, sample II could convert 78% of initial oleic acid. The yields of production of the desired products, i.g., azelaic and pelargonic acids, however, were quite low. Increasing  $\text{WO}_3$  loading in samples III and IV although made higher yields, slightly decreased the conversion. Among all the porous structures, mesoporous catalysts seem to be more convenient for oxidative cleavage of oleic acid, because of the higher dimensionality of the interaction between the components and the catalyst surface. Microporous materials, which are widely used as heterogeneous catalysts in the refining and petrochemical industry mainly due to their high surface area, are not useful for the oils and fats reactions because of the relatively large molecular size of oleochemicals; molecules of oleic acid (molecular size about 2 nm [72]) cannot easily enter the pores of microporous catalysts (pore size less than 2 nm [71]), so all the surface area is not accessible. On the other hand, the catalytic activity of macroporous materials is poor as the result of their relatively low surface area. Average pore size of 8.3, 5.5, and 12.2 nm in samples II, III, and IV, respectively, and relatively high surface areas resulted in the acceptable reaction conversion. A downward trend in the reaction conversion from sample II (with higher surface area) to sample IV (with lower surface area) is because of the decrease in contact area between the reactants and catalysts. The obtained higher yields for samples III and IV arise from the presence of more tungsten oxide as active sites in the catalyst structure.

The surfactant-capped nanoparticles catalyst (sample VI) showed excellent activity; 95% conversion for oleic acid and 58% and 24% production yields for azelaic and pelargonic acids, respectively, were obtained. Generally capping the surface of nanoparticles with surfactant could be an efficient strategy to increase their catalytic performance. In particular, in the liquid medium of oxidation of oleic acid reaction, using a proper surfactant could result in better dispersion due to the fact that surfactants can oppose van der Waals forces. In this way, the aggregation of particles will be prevented and, consequently, catalytic activity of the catalyst will not decrease during the reaction [90]. Scheme 4.1 illustrates the performance of surfactant-capped tungsten oxide nanoparticles as catalysts in the oxidative cleavage of oleic acid with hydrogen peroxide in a molecular view[91]. The surfactant capped on the surface of tungsten oxide nanoparticles is oleic acid. Having both hydrophilic head and hydrophobic chain, surfactant molecules reinforce the stability of emulsion in the biphasic reaction which consists of aqueous phase ( $H_2O_2$  solution) and organic phase (oleic acid). Moreover, free molecules of oleic acid, which can be located at the interface due to having hydrophilic and hydrophobic parts, also contribute to the emulsion stability. Since the reaction occurs mostly at the interface, high concentration of the heterogeneous catalyst at the interface is preferred which is highly likely possible with the aid of surfactant. This is the result of two counter effects; while hydrophilic surface of tungsten oxide immerses them into the aqueous phase, hydrophobic chain of surfactant drags the catalyst toward the organic phase.



(b) **Surfactant-capped nanoparticle:** molecules of surfactant oleic acid attach to the surface of tungsten oxide nanoparticles from hydrophilic head.

(c) **Performance in the reaction (under high stirring):** H<sub>2</sub>O<sub>2</sub> molecules are adsorbed on the surface of nanoparticles which are accumulated at the interface.

**Scheme 4.1.** Schematic illustration for surfactant-capped tungsten oxide nanoparticles as efficient nanocatalyst. (a) Surfactant (oleic acid) molecule, (b) hydrophobic surface of surfactant-capped nanoparticles and (c) Performance in the biphasic oxidative cleavage of oleic acid. Presence of surfactant (i) contribute to the stability of emulsion and (ii) prevents aggregation of the catalyst particles [91].

The presence of the surfactant-capped catalysts at the interface makes adsorption of H<sub>2</sub>O<sub>2</sub> molecules from aqueous phase easier. Then, a kind of peroxy-metal complex can be formed at the surface of tungsten oxide particles. On the other hand, the hydrophobic chain of the surfactant attracts the oleic acid molecules, as the main reactant, from organic phase, and then the reaction takes place on the surface of tungsten oxide particles. The peroxy-metal complex is believed to be efficiently responsible for oxidizing of olefins [45]. As soon as one molecule of H<sub>2</sub>O<sub>2</sub> becomes consumed to produce peroxy species, another molecule of hydrogen peroxide will be adsorbed on the surface, and therefore the reaction will be continued. Actually, the role of phase transfer agent in the homogenous systems, to which the high reaction efficiency was ascribed [64,2,65,63,62,3], can be played by the surfactant in this heterogeneous catalytic system. Capping the tungsten oxide nanoparticles with oleic acid, a catalytic system was developed in this work that has the best properties of both homogeneous and heterogeneous systems.

## 4.4 Conclusion

In order to overcome the common disadvantages of heterogeneous catalysts in the oxidation reactions of unsaturated fatty acids, two types of advanced heterogeneous catalysts were developed in this work. To increase the contact area and time between the reactants, high surface area tungsten oxide/ $\gamma$ -alumina mixed metal oxides with different loadings of  $\text{WO}_3$  were successfully synthesized. The mesoporous structure of these catalysts provided a higher dimensionality between the components and the catalyst surface which resulted in an acceptable conversion. Also, to increase the dispersion of the solid catalyst particles in the biphasic oxidative cleavage reaction of oleic acid, surfactant-capped tungsten oxide nanoparticles were synthesized. The catalytic test results demonstrated that capping the surface of tungsten oxide nanoparticles with oleic acid as surfactant could considerably increase the catalytic activity of the solid catalyst. In fact, the unique properties of nanoparticles would propose them as the frontier of homogeneous and heterogeneous catalysts that can exploit the high activity of homogeneous catalyst. However, an obstacle remaining in the application of nanocatalysts is their recovery from the liquid solution after catalytic reactions. To overcome this limitation, the nanomaterials assembled with a super-paramagnetic material such as  $\text{Fe}_3\text{O}_4$  nanoparticles should be studied.

## Acknowledgment

This work was supported by the Natural Science and Engineering Research Council of Canada (NSERC) through the INNOV-UC and Discovery grants. The authors wish to thank the industrial partners (Oleotek and SiliCycle Inc.) for stimulating discussions and comments.



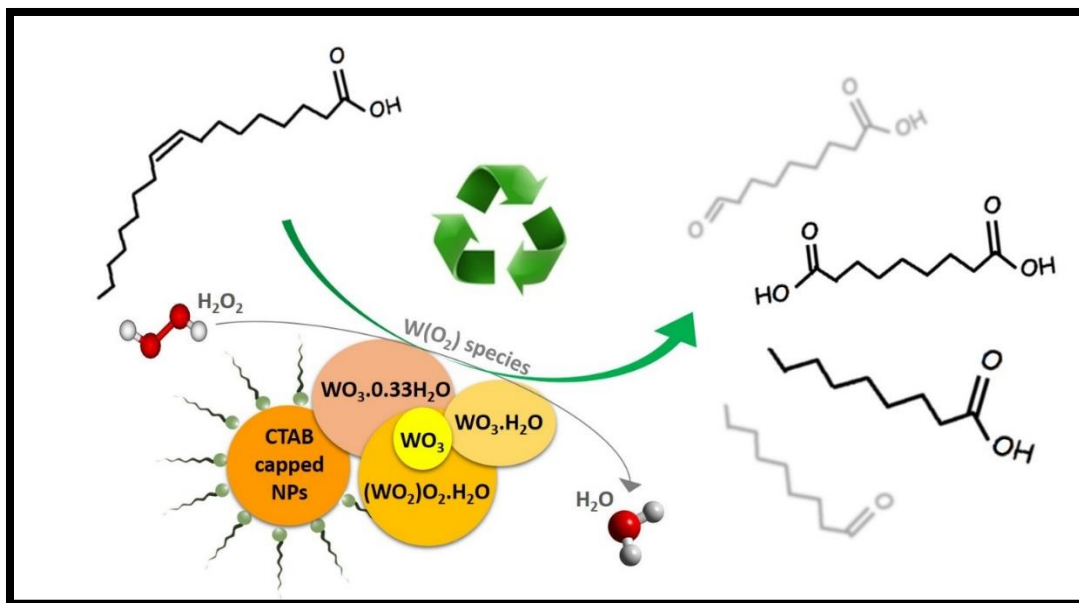
# Chapter 5. Synthesis, organo-functionalization, and catalytic properties of tungsten oxide nanoparticles as heterogeneous catalyst for oxidative cleavage of oleic acid as a model fatty acid into diacids

Amir Enferadi-Kerenkan <sup>1</sup>, Aimé Serge Ello <sup>1,2</sup>, and Trong-On Do <sup>1\*</sup>

1. Department of Chemical Engineering, Université Laval, Québec, G1V 0A6, Canada.

2. Laboratoire de Chimie Physique, Université Félix Houphouët-Boigny de Cocody, 22 bp 582 Abidjan, Cote d'Ivoire.

*Industrial & Engineering Chemistry Research*, 2017, 56 (38), 10639-10647.



## Résumé

Une série de nanoparticules d'oxyde de tungstène (NPs) a été synthétisée par une approche verte et directe exploitant la poudre de tungstène nu comme précurseur. Les NPs synthétisées ont été encore organo-fonctionnalisées par le bromure de cetyltriméthylammonium (CTAB) afin d'ajuster l'état de leur surface et d'améliorer leur compatibilité avec l'oxydation biphasique des huiles végétales avec  $H_2O_2$ . Simplement, différentes structures d'oxyde de tungstène ont été observées, ceux-ci ont été caractérisés par XRD, FTIR, TGA, TEM,  $N_2$  isothermes d'adsorption / désorption, et l'analyse du potentiel zêta. Tous les nanocatalyseurs synthétisés ont pu convertir complètement l'acide oléique, et le rendement le plus élevé de la production du diacide désiré (acide azélaïque), ~ 80%, a été atteint par l'optimisation de la quantité de CTA<sup>+</sup> sur la surface du nanocatalyseur, ce qui montrent une excellente activité par rapport aux divers travaux signalés. Grâce à l'organo-fonctionnalisation, ce catalyseur tolérant à l'eau ne présentait pas de lixiviation significative aussi bien qu'une récupération pratique et une réutilisation régulière sans diminution notable de l'activité, au moins jusqu'à quatre cycles.

## Abstract

A series of tungsten oxide nanoparticles (NPs) has been synthesized via a green and straightforward approach exploiting bare tungsten powder as precursor. The synthesized NPs were further organo-functionalized by cetyltrimethylammonium bromide (CTAB) in order to adjust their surface state and enhance their compatibility with biphasic oxidation of vegetable oils with  $\text{H}_2\text{O}_2$ . Simply, different structures of tungsten oxide were observed, which were characterized by XRD, FTIR, TGA, TEM,  $\text{N}_2$  adsorption/desorption isotherms, and zeta potential analysis. All the synthesized nanocatalysts could fully convert oleic acid, and the highest yield of production of the desired diacid (azelaic acid), ~80 %, was achieved by optimization of the  $\text{CTA}^+$  amount on the nanocatalyst's surface, which show excellent activity compared to the reported heterogeneous works. Thanks to the organo-functionalization, this water-tolerant catalyst exhibited no significant leaching, as well as convenient recovery and steady reuse without a noticeable decrease in activity, at least up to four cycles.

## 5.1 Introduction

Exploiting the synthetic capabilities of nature in oils and fats of vegetable and animal origin has rendered using these renewable raw materials one of the key aspects of sustainable chemistry. Oleic acid (C18:1), the most widely distributed and abundant unsaturated fatty acid (UFA) in natural oils and fats [338,29], can be oxidatively cleaved to produce azelaic (C9 diacid) and pelargonic (C9 monoacid) acids, which are rare in natural resources but very attractive materials, in particular the first one, for preparation of numerous products such as polymers (nylon 6:9), adhesives, biodegradable lubricants, corrosion inhibitors, anti-acneic agent for cosmetics, perfumes, and resins [2,4,1,5,3]. Currently, this reaction is carried out in industry via ozonolysis, which, nowadays, has been converted to a controversial challenge due to the hazardous problems associated with use of ozone. Employing an eco-friendlier oxidant requires an active catalyst to be employed, as well.

Efforts in this context have focused on transition metals like Mo [3], Au [1], Mn, Cr [339], Co [339,54], Fe [56,55], Ru [60,59,87,58,57], and W [64,2,65,340,341,48,61,62,3], as catalytic core, in homogeneous and heterogeneous forms. These have been thoroughly reviewed in our recent review paper [91]. While the use of homogeneous catalysts has been well reported, curiously, heterogeneous ones have been scarcely investigated, probably due to the, often, much lower yields obtained with the latter. Hydrogen peroxide has been always an interesting benign oxidant for oxidation of olefins, especially when its use is associated with employing phase transfer agents via functionalization of catalyst surface to improve compatibility of the aqueous oxidant and organic substrate. Although this could generally increase the efficiency of oxidation of UFAs [64,2,65,341,62,3], the major drawback is that the used catalytic system is not fully recoverable.

Among all the transition metals, tungsten has attracted a great deal of interest in oxidation of UFAs, mostly in W-based complex form and homogeneous catalysis [91,45,39]. Solid W-based catalysts, however, include a variety of chemical structures arising from the distinct inherent properties of tungsten; varying oxidation states from -2 to +6 [120,121] has led to several  $WO_x$  (x mainly between 2 and 3). The most common is tungsten trioxide, which in turn, includes hydrated ( $WO_3 \cdot nH_2O$ ) and anhydrous ( $WO_3$ ) forms. Moreover, peroxotungstic acid is another interesting

structure that has shown great catalytic potential, particularly in oxidation reactions [342-345]. Formation of these different phases are very sensitive to synthesis conditions [346-349], so, choice of a unique synthesis method that can produce all the phases is of importance. Oxidative dissolution of tungsten metal or tungstic acid in  $\text{H}_2\text{O}_2$  was proposed by Kudo et al. to synthesize peroxotungstic acid [350-352], and then was modified to synthesize some other tungsten oxide structures [353-355,349]. Recently, Ozin et al. developed this method to produce nanoparticles and thin films of tungsten oxide, as well as some other metal oxides [356].

In this work, different structures of tungsten oxide like  $[(\text{WO}_2)\text{O}_2\cdot\text{H}_2\text{O}]$ ,  $\text{WO}_3$ ,  $\text{WO}_3\cdot 0.33\text{H}_2\text{O}$ , and  $\text{WO}_3\cdot\text{H}_2\text{O}$  were synthesized via oxidative dissolution of micrometer-scale bare W powder, and then, these materials were examined in the oxidative cleavage of oleic acid. In order to tune hydrophobicity/hydrophilicity properties of the surface and improve compatibility of the solid catalysts with the organic substrate and aqueous oxidant, the nanocatalysts were organo-functionalized with different amounts of cetyltrimethylammonium bromide (CTAB), a well-known cationic surfactant. Employing a simple and green synthesis method, that exploits cheap W powder as a precursor, avoided using time- and energy-consuming operations such as thermal treatment in autoclave and purification, organic solvents, metal salts, and/or coordination compounds, which are commonly required in prior reported synthesis methods.

## 5.2 Experimental

### 5.2.1 Synthetic details and characterization

Tungsten oxide NPs were prepared by simple dispersion of metallic tungsten powder (1.0 g) (APS 1-5  $\mu\text{m}$ , purity 99.9%, Alfa Aesar Co.) in deionized  $\text{H}_2\text{O}$  (10 mL), followed by addition of  $\text{H}_2\text{O}_2$  (10 mL, aqueous solution, 30 %, Fisher Scientific Co.) dropwise. The latter was done at 0  $^\circ\text{C}$  by keeping the reaction vessel in an instant ice bath. The oxidative dissolution process is very exothermic, therefore must be done attentionally under a well-ventilated fume hood. After 4 h, an almost colorless (very slightly light yellow) and clear solution was formed (solution A). This solution was, then, allowed to precipitate through two different ways: (i) it was slowly evaporated at room temperature (RT) for 3 days (sample I), followed by calcination at 600  $^\circ\text{C}$  for 3 h (heating rate: 4  $^\circ\text{C}/\text{min}$ ) under air to obtain sample II, or (ii) it was heated to 120  $^\circ\text{C}$  for 4 h in the absence of CTAB (sample III) and in the presence of CTAB (technical grade, Fisher Scientific Co.) with

molar CTAB/W ratios of 0.1, 0.25, and 0.5 added to the solution just before heating (samples IV, V and VI, respectively). Solid products were separated using a centrifuge at 8000 rpm, washed thoroughly with water and ethanol, and dried at 60 °C overnight (16 h). The used 1 g W gave ~ 1.1-1.6 g products. The synthesized samples were characterized by XRD, FTIR, TGA and DTA, TEM, zeta potential analyzer, and BET surface area measurement. Section 5.5.1 in Supporting Information explains characterization equipment and methodologies.

## 5.2.2 Catalytic test

The reactions were carried out in a 50-mL, round-bottom flask under a batch-wise constant temperature and constant pressure mode. This reactor was equipped with a condenser, a magnetic stirrer, and an oil bath. Typically, the reaction feed included 1 g oleic acid ( $\geq 99\%$ , Sigma-Aldrich Co.), 4 mL H<sub>2</sub>O<sub>2</sub>, 7.5 mL tert-butanol ( $\geq 99.0\%$ , Sigma-Aldrich Co.) as solvent. After adding 0.45 g catalyst, the flask was put in the oil bath which was previously heated and maintained at constant temperature of 120 °C. During reaction, the reactor was continuously agitated with magnetic stirrer (agitation rate ~ 400 rpm). After 5 h reaction, the catalyst was separated using centrifuge at 8000 rpm and recovered via washing with ethanol and water several times and drying at 60 °C overnight to be used in the next catalytic cycle. The products mixture, then, underwent a derivatization reaction, in which the expectedly produced azelaic and pelargonic acids, and possibly unreacted oleic acid were converted to their corresponding methyl esters according to Metcalfe et al. derivatization procedure [334,335], in order to be prepared for GC-MS analysis.

Analysis of the reaction products by GC-MS has been explained in section 5.5.2 of the Supporting Information, covering detailed information about sample preparation prior to injection (section 5.5.2.1), quantitative analysis (section 5.5.2.2), and GC-MS specifications (section 5.5.2.3).

## 5.3 Results and discussions

### 5.3.1 Catalysts synthesis and characterization

Simply taking W powder, adding H<sub>2</sub>O<sub>2</sub>, and then by just altering the temperature of thermal treatment and/or adding a surfactant, different catalytically interesting structures of tungsten oxide

were achieved. Table 5.1 summarizes the synthesis conditions and prepared samples and shows their obtained crystalline phases and chemical structures.

**Table 5.1.** Synthesis conditions and prepared samples.

Sample	CTAB/W molar ratio	Synthesis <sup>1</sup>		Crystalline phase	Chemical structure
		T (°C)	t (h)		
I	-	RT <sup>2</sup>	72	Monoclinic	(WO <sub>2</sub> )O <sub>2</sub> .H <sub>2</sub> O
II <sup>3</sup>	-	600	3	Monoclinic	WO <sub>3</sub>
III	-	120	4	Orthorhombic	WO <sub>3</sub> .0.33H <sub>2</sub> O & WO <sub>3</sub> .H <sub>2</sub> O
IV	0.1	120	4	Orthorhombic	WO <sub>3</sub> .0.33H <sub>2</sub> O >> WO <sub>3</sub> .H <sub>2</sub> O
V	0.25	120	4	Orthorhombic	WO <sub>3</sub> .0.33H <sub>2</sub> O >>> WO <sub>3</sub> .H <sub>2</sub> O
VI	0.5	120	4	Orthorhombic	WO <sub>3</sub> .0.33H <sub>2</sub> O

1. Synthesis conditions: initial amounts of W elemental powder (1 g), H<sub>2</sub>O (10 ml), H<sub>2</sub>O<sub>2</sub> (10 ml), CTAB (0.20, 0.50, and 0.99 g for samples IV, V, and VI, respectively).

2. RT: room temperature

3. Sample II: Sample I followed by calcination at 600 °C for 3 h.

### 5.3.1.1 Crystalline structural features

Fundamentally, oxidative dissolution of W powder in H<sub>2</sub>O<sub>2</sub> gives an almost colorless and strongly acidic solution containing amorphous peroxotungstic acid particles, for which, the empirical formula of WO<sub>3</sub>.xH<sub>2</sub>O<sub>2</sub>.yH<sub>2</sub>O (0.05 ≤ x ≤ 1 and 3 ≤ y ≤ 4) has been suggested in literature [357,355]. This solution, denoted as **A**, then underwent different crystallization approaches to achieve the catalytically desired structures of tungsten oxide. XRD patterns of the synthesized samples are shown in Figure 5.1. While rapid evaporation of solution **A**, expectedly, gave amorphous tungsten oxide, interesting structure of peroxotungstic acid or hydrated tungsten peroxide [(WO<sub>2</sub>)O<sub>2</sub>.H<sub>2</sub>O], which contains active oxidizing agent of tungsten-peroxo, was obtained by slowly evaporation of the solution at RT for 3 days (Sample I). Its well-defined peaks (Figure 5.1 a) could be precisely and purely indexed on monoclinic structure, the most stable phase of tungsten oxides at RT [358], in accordance with PDF no. 50-0233 of ICDD library of spectra. Pecquenard et al. [355], who are the pioneers in structural investigations of hydrated tungsten peroxide, reported that [(WO<sub>2</sub>)O<sub>2</sub>.H<sub>2</sub>O] can be obtained only after heating at 120 °C, while at RT a more hydrated phase [(WO<sub>2</sub>)O<sub>2</sub>.H<sub>2</sub>O].nH<sub>2</sub>O is formed. Our synthesis method, however, made the

formation of  $[(\text{WO}_2)\text{O}_2\cdot\text{H}_2\text{O}]$  at RT in 3 days possible. Anhydrous  $\text{WO}_3$ , another catalytically interesting structure, was obtained by decomposition and annealing of tungsten peroxide (sample I) [359,360] via calcination at  $600\text{ }^\circ\text{C}$  (sample II, Figure 5.1 b). Presence of  $\{200\}$ ,  $\{002\}$ , and  $\{020\}$  reflections confirm that the obtained yellow powder was mainly composed of monoclinic  $\text{WO}_3$  (PDF no. 83-0950).

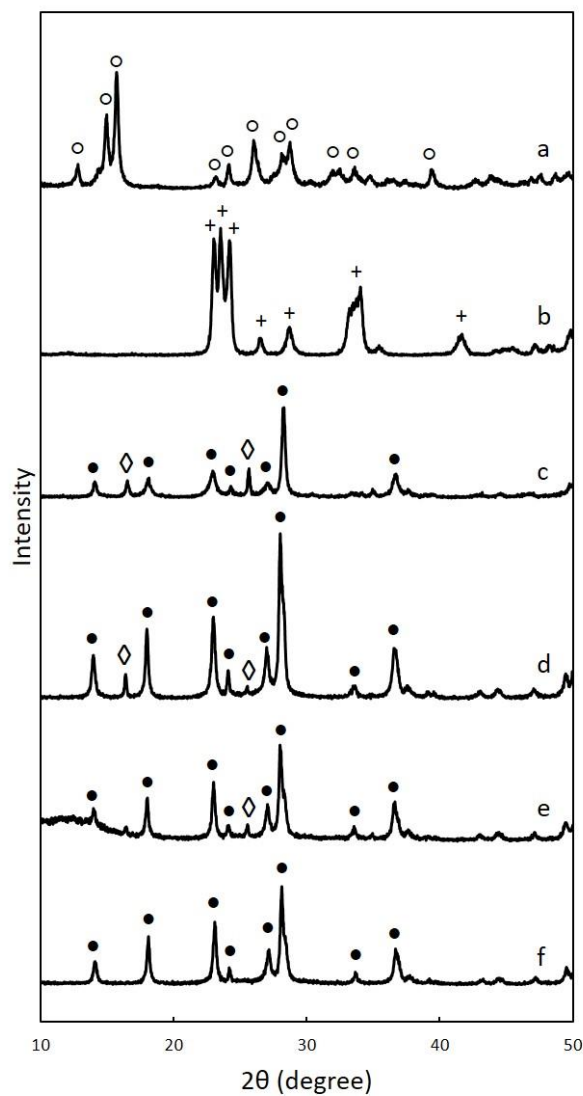


**Figure 5.1.** XRD patterns of (a) sample I, (b) sample II, (c) sample III, (d) sample IV, (e) sample V, and (f) sample VI. (o)  $(\text{WO}_2)\text{O}_2\cdot\text{H}_2\text{O}$  (PDF no. 50-0233), (+)  $\text{WO}_3$  (PDF no. 83-0950), (●)  $\text{WO}_3\cdot 0.33\text{H}_2\text{O}$  (PDF no. 35-0270), and (◊)  $\text{WO}_3\cdot\text{H}_2\text{O}$  (PDF no. 43-0679).



Given the importance of associated water molecules of  $\text{WO}_3$  [122], hydrated tungsten oxides were also synthesized (samples III-VI) via execution of higher thermal treatment (at 120 °C) on solution A, instead of the slow evaporation at RT, which resulted in much shorter crystallization time, as well as, changing the crystalline structure from monoclinic to orthorhombic (in comparison with samples I and II). Heating leads to quick decomposition of the water-soluble amorphous particles of solution A and production of insoluble solids with crystalline structures. XRD pattern of sample III (Figure 5.1 c) shows that it is composed of  $\text{WO}_3 \cdot 0.33\text{H}_2\text{O}$  (PDF no. 35-0270) and  $\text{WO}_3 \cdot \text{H}_2\text{O}$  (tungstite) (PDF no. 43-0679). The high intensity of the peaks at  $2\theta = 28.3$ , 23.1, 36.8, and 18.1 degree demonstrates domination of the less hydrated phase, however, the main reflections of tungstite at  $2\theta = 25.7$  ( $\{111\}$ ) and  $2\theta = 16.5$  ( $\{020\}$ ) are also observed with less intensity. Both phases possess orthorhombic crystalline structure.

Adding CTAB to the synthesis mixture reinforced the dominance of  $\text{WO}_3 \cdot 0.33\text{H}_2\text{O}$ , evidence for which is the gradual diminishing of the intensities of two mentioned peaks of tungstite, in samples IV, V, and VI (Figure 5.1 d, e, and f), insofar as 100% pure  $\text{WO}_3 \cdot 0.33\text{H}_2\text{O}$  (PDF no. 35-0270) was obtained in sample VI (CTAB/W = 0.25) (Figure 5.1 f). This phase of tungsten oxide has been emphasized as very sensitive to the synthesis conditions [349,361]. The reported synthesis methods in the literature are considerably more complicated and time-consuming than the presented method. In fact, a role of structure directing agent (SDA) can be well considered for  $\text{CTA}^+$  cations in this synthesis method that directed the crystals to form pure orthorhombic  $\text{WO}_3 \cdot 0.33\text{H}_2\text{O}$  structure in sample VI.

### 5.3.1.2 Spectral analysis

FTIR analysis was employed to learn more about the composition of the organic part of the samples as well as different available tungsten bonds in crystalline structures of the samples. FTIR spectra of the samples are shown in Figure 5.2 and assignments of the considerable absorption bands are listed in Table 5.3 (Supporting Information).

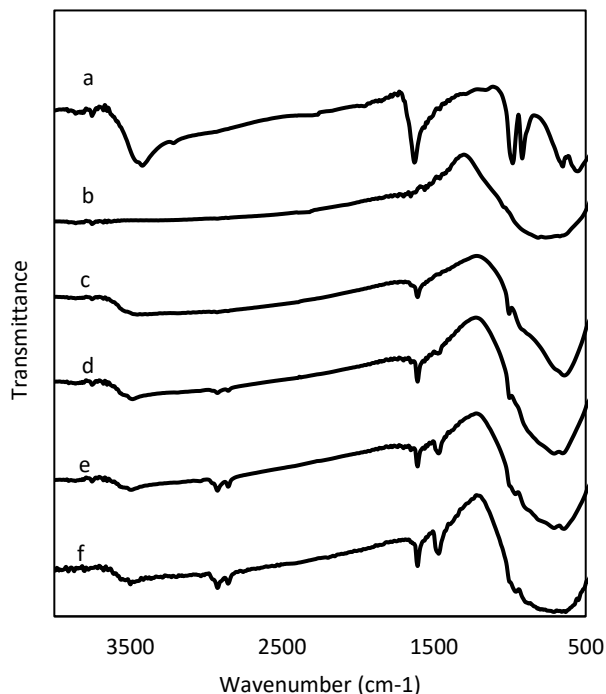


**Figure 5.2.** FTIR spectra of (a) sample I, (b) sample II, (c) sample III, (d) sample IV, (e) sample V, and (f) sample VI.

All the samples exhibit a strong peak located at 641-672  $\text{cm}^{-1}$  which is assigned to stretching vibration of bridging oxygen atom between two tungsten atoms  $\nu(\text{W}-\text{O}-\text{W})$  [362,122,363,364]. Generally, spectra of all the synthesized crystalline powders are very similar in the low-frequency region, except for sample I that shows two more peaks at 548 and 919  $\text{cm}^{-1}$ . These peaks, which are respectively assigned to tungsten-peroxo ( $\text{W}(\text{O})_2$ ) and peroxo ( $\text{O}-\text{O}$ ) groups, are typical vibration bands of peroxotungstic acid [363]. The peak located at 950-1004  $\text{cm}^{-1}$ , which is sharp in sample I and poorly resolved in other hydrated tungsten oxides (samples III-VI), is ascribed to the stretching mode of the terminal  $\text{W}=\text{O}$  double bond [365,122,363,366].

Obviously, the peak(s) between 600 and 900  $\text{cm}^{-1}$  is wider in the presence of  $\text{CTA}^+$  cations (from sample IV to VI). The reason is the emergence of some peaks corresponding to  $\text{RN}(\text{CH}_3)_3^+$  at 910-970  $\text{cm}^{-1}$  [367] and merging with the previous peaks. The spectra of CTAB-assisted synthesized samples (samples IV-VI) exhibit some additional peaks in the higher frequency region,

where the vibration of organic compounds, as well as water molecules, are expected to appear. According to the literature, the peak at  $1467\text{ cm}^{-1}$  can be attributed to  $\text{RN}(\text{CH}_3)_3^+$  and the peaks at  $2850$  and  $2927\text{ cm}^{-1}$  can be assigned to stretching vibrations of methyl ( $-\text{CH}_3$ ) and/or methylene ( $-\text{CH}_2-$ ) groups [367]. These peaks, although weak in sample IV, their intensities increase with increasing CTAB content in the synthetic mixture for samples V and VI. The hydrated crystalline structures (samples I and III-VI) demonstrate a peak at  $1606\text{-}1622\text{ cm}^{-1}$  and a peak at  $3421\text{-}3491\text{ cm}^{-1}$ , which come from, respectively, bending and stretching vibrations of  $\text{H}_2\text{O}$  molecules [362,122,363].

### 5.3.1.3 Thermal analysis

Thermogravimetric analysis (TGA) and differential thermal analysis (DTA) curves of the synthesized samples are illustrated in Figure 5.3. Expectedly, anhydrous  $\text{WO}_3$  (sample II) showed no essential weight loss during the thermal analysis up to  $800\text{ }^\circ\text{C}$ , and therefore, its curve is not included in Figure 5.3.

Initially, thermal analysis of sample III composed of only water and  $\text{WO}_3$  (Figure 5.3 b) indicates that the water molecules were expelled from the tungsten oxide structure at temperatures less than about  $300\text{ }^\circ\text{C}$ . Above this temperature, the sample's weight, belonging to  $\text{WO}_3$  portion, remained constant. Gradual expulsion of water that happened over a relatively wide temperature range ( $25 < T < 300\text{ }^\circ\text{C}$ ) comes from two main groups of the departed water molecules; (i) adsorbed and weakly bonded molecules that are normally released at  $T < 200\text{ }^\circ\text{C}$ , and (ii) HO and HO-O groups and strongly bonded molecules which due to the inherent tendency of tungsten oxide to keep the water of hydration even at high temperatures, release at  $200 < T < 300\text{ }^\circ\text{C}$  as the reaction products of W-OH and W-OOH condensation [353,354]:



Presence of abundant peroxide groups in sample I changed the behavior of departure of water molecules (Figure 5.3 a); its first weight loss at about  $110\text{ }^\circ\text{C}$ , similarly, comes from the departure of weakly bonded water molecules, however, more strongly bonded molecules departed the structure along with the peroxide group at about  $220\text{ }^\circ\text{C}$ , which resulted in more abrupt departure and greater weight loss compared to the other samples.

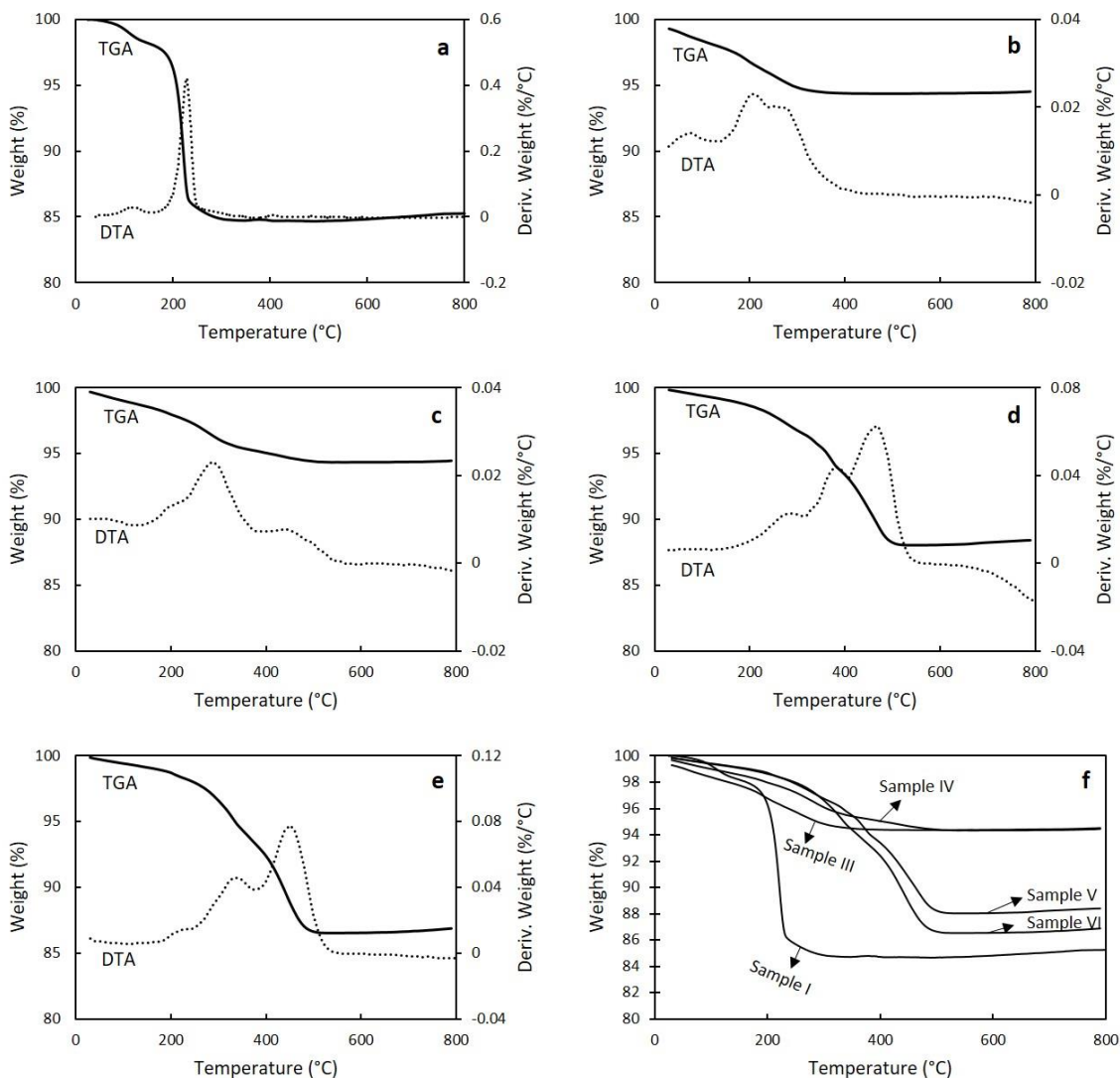


**Figure 5.3.** (a-e): TGA and DTA curves of (a) sample I, (b) sample III, (c) sample IV, (d) sample V, and (e) sample VI. (f): all the TGA curves.

In the high temperature region ( $T > 300$  °C), an additional weight loss is obtained only for the  $\text{CTA}^+$  containing samples (Figure 5.3 c-e). This weight loss, which increases with  $\text{CTA}^+$  content in the synthesis mixture, corresponds to oxidation and consequent removal of  $\text{CTA}^+$  molecules that capped the surfaces of tungsten oxides. Quantitatively, 1.7, 8.7, and 10.0% weight losses (in  $300 < T < 500$  °C) were obtained for samples IV, V, and VI, in which CTAB/W molar ratios of 0.1, 0.25, and 0.5 had been used in the synthetic solution, respectively. Differential thermal analysis indicated

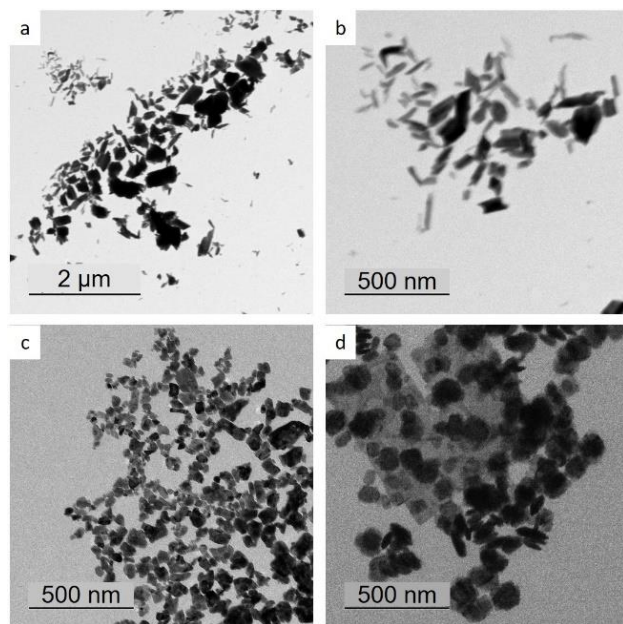
that removal of  $\text{CTA}^+$  took place at two main sub-temperature range: (i)  $300 < T < 350$  °C and (ii)  $440 < T < 470$  °C.

Figure 5.3 f compares TGA curves of all the samples together. As can be seen, at all temperatures lower than 300 °C the curves of  $\text{CTA}^+$ -capped samples (samples IV-VI) stay on top of that of sample III. This confirms lower water contents in the structures of samples IV-VI, concurring with the result of XRD.

#### 5.3.1.4 Other aspects of the synthesized samples

High concentration of charged species and functional groups (and their probable ionization) in the synthesis medium [356], as well as not using autoclave in the employed pseudo-hydrothermal synthesis method could mainly affect the morphologies and surface areas of the resultant solids.

Figures 5.4 and 5.5 display representative TEM images of the samples. NPs of  $(\text{WO}_2)\text{O}_2\cdot\text{H}_2\text{O}$  (sample I, Figure 5.4 a and b) tend to form into irregular-shaped substructure due to the high concentration of peroxy groups on their surface. Firstly, the presence of many hydrogen ions in the precursor solution has been reported that increases the aggregation of tungsten oxide NPs [368]. Moreover, control of morphology to form a stable coordinated structure in the presence of  $\text{H}_2\text{O}_2$  could be difficult due to the chelating feature of peroxy ligands  $[\text{O}_2]^{2-}$  [349]. It makes more sense given the fact that no autoclave was used for hydrothermal treatment. Indeed, this chelating property of  $[\text{O}_2]^{2-}$  ligands has been well-thought-out as the fountainhead of  $\text{H}_2\text{O}_2$  role in the synthesis [349], which led to complete dissolution of  $\text{WO}_3$  in hydrogen peroxide and formation of transparent tungsten peroxide solution, while  $\text{WO}_3$  is not soluble in water.



**Figure 5.4.** TEM images of (a) and (b) sample I (with different magnifications), (c) sample II, and (d) sample III.

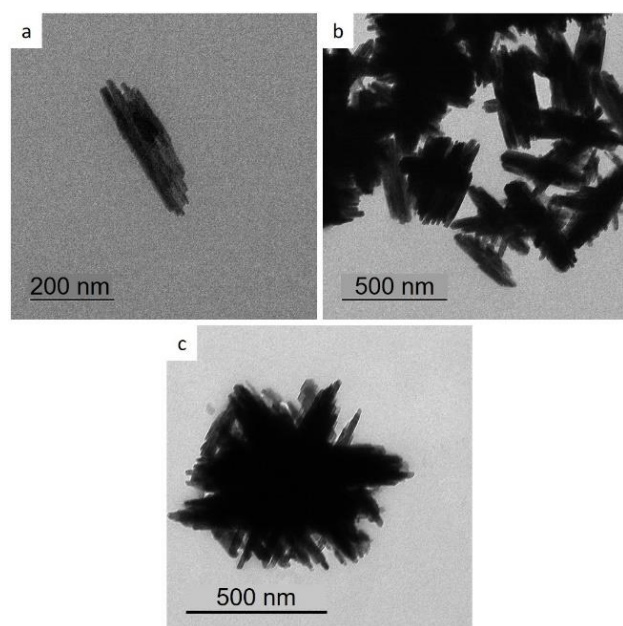


**Figure 5.5.** TEM images of (a) sample IV, (b) sample V, and (c) sample VI.

Calcining at 600 °C and removal of hydrogen peroxide, monoclinic  $\text{WO}_3$  NPs with platelet-like morphology with an average size of  $\approx 40$  nm were obtained (sample II, Figure 5.4 c). Thermal

treatment at higher temperature had little influence on the overall morphology of the product; as shown in Figure 5.4 d, the typical structure of sample III is a mixed morphology of nanoplatelet and nanorod, most likely due to the coexistence of two crystalline phases  $\text{WO}_3 \cdot 0.33\text{H}_2\text{O}$  and  $\text{WO}_3 \cdot \text{H}_2\text{O}$ , and the platelet structure is somehow similar to sample II.

Adding CTAB to the synthesis medium, nanoneedle aggregates were formed (Figure 5.5), a typical morphology for  $\text{WO}_3 \cdot 0.33\text{H}_2\text{O}$  that had been obtained before via more complicated and longer procedures [361,349]. Changing the amount of CTAB, however, did not have a significant effect on the morphology of the products. Only, it seems that at higher concentration of CTAB the particles showed slightly more tendency to aggregate. As consequence, the specific surface area decreased from  $17 \text{ m}^2/\text{g}$  in sample III to about  $4 \text{ m}^2/\text{g}$  in sample VI. Table 5.4 in Supporting Information lists the BET surface areas of the samples. Higher surface area of sample II ( $\sim 29 \text{ m}^2/\text{g}$ ) compared to the other samples highly likely arises from its calcination at a higher temperature, which removed all the surface functional groups, and therefore its NPs strongly avoid aggregation, as can be seen in its TEM image (Figure 5.4 c).

Our efforts to organo-functionalize the tungsten oxides with anionic surfactants (e.g. acetic and valeric acids, instead of CTAB) failed (as TGA and FTIR analyses confirmed), because the anionic functional groups at the head of these surfactants were repelled by negatively charged surface of tungsten oxide. Evidence for this negative charge was obtained by measuring zeta potential of the NPs dispersed in solution A (without CTAB, pH 1.6-1.8, Figure 5.6). The available negatively charged species on the surface mainly consists of peroxy ( $\text{O}_2^{2-}$ ) and hydroxyl group ( $\text{OH}^-$ ) (see Figure 5.2 and well-resolved absorption band of peroxy at  $919 \text{ cm}^{-1}$ . Presence of such band in Figure 5-2 c, although very weak, confirms that even after heating at  $120 \text{ }^\circ\text{C}$ , there is still some  $\text{O}_2^{2-}$  ligands on the surface, while  $\text{W}(\text{O}_2)$  absorption band ( $548 \text{ cm}^{-1}$ ) had been vanished).

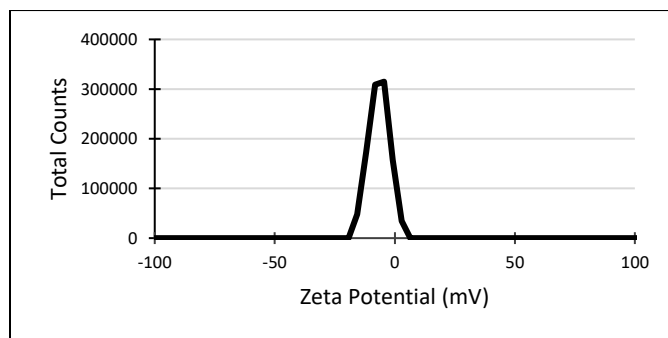


**Figure 5.6.** Surface zeta potential distribution of tungsten oxide NPs dispersed in the synthesis solution without adding CTAB at pH 1.6-1.8.

### 5.3.2 Catalytic test results

Table 5.2 shows conversion of oleic acid and yields of production of azelaic and pelargonic acids ( $Y_{AA}$  and  $Y_{PA}$ , respectively) over different synthesized catalysts with  $H_2O_2$  as oxidant after 5 h reaction at 120 °C (bath temperature). The catalytic test results presented are the average of at least 3 runs over each catalyst. See Supporting Information for more details about the quantitative analysis (section 5.5.2.2).

**Table 5.2.** Catalytic tests results (conversion of oleic acid and yields of production of desired products) and weight fractions of  $WO_3$  in the catalysts as the assumed active sites.

Entry	Catalyst (tungsten oxide)	Chemical structure	$WO_3$ weight fraction in the catalyst (%) <sup>1</sup>	Conversion (%) <sup>2</sup>	$Y_{AA}$ (%) <sup>3</sup>	$Y_{PA}$ (%) <sup>3</sup>
1		-	-	41	2	4
2	Commercial	$WO_3$	-	91	10	18
3	Sample I	$(WO_2)O_2 \cdot H_2O$	84.9	100	71	67
4	Sample II	$WO_3$	100.0	100	41	39
5	Sample III	$WO_3 \cdot 0.33H_2O$ & $WO_3 \cdot H_2O$	94.5	100	51	53
6	Sample IV	$WO_3 \cdot 0.33H_2O \gg WO_3 \cdot H_2O$	94.3	100	39	37
7	Sample V	$WO_3 \cdot 0.33H_2O \gg \gg WO_3 \cdot H_2O$	88.1	100	77	69
8	Sample VI	$WO_3 \cdot 0.33H_2O$	86.5	100	60	64

1. Weight fraction of  $WO_3$ , assumed as active site (regardless of current vast challenges on nature of catalytic centers in metal oxide catalysis), was calculated from quantitative analysis of TGA data.

2. Reaction conditions: time: 5 h, temperature: 120 °C (bath temperature), solvent: tert-butanol, initial amounts of oleic acid: 1 g, t-butanol: 7.5 ml,  $H_2O_2$ : 4 ml, catalyst: 0.45 g, agitation rate ~ 400 rpm.

3. Y: Yield (molar), in this work, is defined as the amount of a product formed per total amount of oleic acid consumed (both in mole,  $Y_{AA}$ : yield of azelaic acid,  $Y_{PA}$ : yield of pelargonic acid).



### 5.3.2.1 Influence of different catalysts on the reaction

The first catalytic test was done without any catalyst (Table 5.2, entry 1); modest 41% conversion and tiny yields percentages ( $\leq 4\%$ ) confirmed that the benign used oxidant is not adequately efficient alone. To compare our catalysts activities with a standard condition, a commercial tungsten oxide ( $\text{WO}_3$ , 99.8%, Alfa Aesar Co.) was employed as a catalyst, also (entry 2), which although, significantly increased the conversion ( $\sim 90\%$ ), the yields were still low (less than 20%). Compared to the commercial  $\text{WO}_3$ , our prepared tungsten oxides showed much better efficiencies (entries 3-8). Complete conversion of initial oleic acid was obtained for all the samples after 5 h reaction time, with high yields particularly for sample I, V, and VI.

The high catalytic efficiency of sample I (entry 3, 71 and 67%  $Y_{AA}$  and  $Y_{PA}$ , respectively) comes from the tungsten-peroxo (as seen by its XRD and FTIR) with a high concentration (as its TGA showed) in its structure  $[(\text{WO}_2)\text{O}_2\cdot\text{H}_2\text{O}]$ . Such peroxo complexes have been mentioned in the literature that shoulder responsibility of advancing UFAs oxidative cleavage reactions [64,65,341,3]. Except sample I, other samples were composed of tungsten trioxide, in anhydrous (sample II) or hydrated (samples III-VI) forms. Sample II in spite of advantages of higher  $\text{WO}_3$  content (Table 5.2) and surface area (Table 5.4), as well as more uniform morphology and smaller particle size (Figure 5.4), yielded lower compared to sample III (entries 4 and 5). The reason could be well ascribed to important role of the linked water molecules of sample III ( $\text{WO}_3\cdot 0.33\text{H}_2\text{O}$  &  $\text{WO}_3\cdot\text{H}_2\text{O}$ ), which can increase in-situ production of instant tungsten-peroxo groups during the reaction. It has been shown that oxidation extent of tungsten trioxide in presence of  $\text{H}_2\text{O}_2$  (to produce tungsten-peroxo) decreases with decreasing water content in its structure [122].

Samples IV-VI, however, did not generally comply with this trend (entries 6-8). As discussed in section 5.3.1.1, adding CTAB favored formation of the less hydrated phase ( $\text{WO}_3\cdot 0.33\text{H}_2\text{O}$ ), and accordingly, it was expected that oxidative capabilities of the samples and, consequently, their catalytic efficiencies decrease by adding CTAB. But, except sample IV, the two other  $\text{CTA}^+$ -capped samples (V and VI) exhibited higher yields compared to sample III. The reason directly comes from the presence of  $\text{CTA}^+$  which tunes surface state of the tungsten oxide, and greatly affects its catalytic activity. Samples IV-VI, despite very slight structural differences in crystallinity (Figure 5.1), morphology (Figure 5.5), and  $\text{WO}_3$  content (Table 5.2), exhibited significantly different yields. The  $\text{CTA}^+$  molecules that capped the hydrophilic surface of

WO<sub>3</sub>.0.33H<sub>2</sub>O could make it partly hydrophobic, and hence, increased surface affinity to adsorb the organic substrate, oleic acid, molecules in the reaction medium. Admittedly, a higher concentration of oleic acid on the surface of the catalyst, where tungsten-peroxo species are accumulated, results in higher reactants collision and consequently increases the reaction efficiency (happened for samples V and VI). However, presence of long-chain CTA<sup>+</sup> on the surface is a double-edged sword; apart from the positive effect of hydrophobization, it would lead to a steric repulsion effect which, considering molecular geometry of CTA<sup>+</sup> and oleic acid, could prevent oleic acid to approach to the surface. The competition between these two positive and negative effects, which depends on the density of CTA<sup>+</sup> on surface, gives rise to the different yields obtained by samples IV, V, and VI; it seems that low density of CTA<sup>+</sup> in sample IV could not provide enough hydrophobicity, and the steric repulsion forces resulted in lower yields (entry 6), while at the higher density (sample VI), the provided hydrophobicity overcame the increase in steric repulsion effects resulting in higher yields (entry 8). The optimized density of CTA<sup>+</sup> on surface, giving 77% Y<sub>AA</sub> (entry 7), was obtained when CTAB/W molar ratio of 0.25 was used in the synthesis (sample V). The obtained reaction efficiencies in this work seem interesting when being compared with the previously reported heterogeneous catalytic oxidative cleavage of oleic acid [339,340,48].

Given the improved compatibility of the solid catalysts with reactants, resulting in deservedly ascribing a phase transfer role to the organo-functionalized tungsten oxides, further works are currently underway in our laboratory to reduce (or even eliminate) the reaction solvent.

### 5.3.2.2 Effects of temperature and time on the reaction

Sample V was subjected to investigate effect of reaction temperature and time. Employing a lower reaction temperature (bath temperature: 85 °C) resulted in slightly lower conversion (92%) and moderately lower Y<sub>AA</sub> and Y<sub>PA</sub> (49 and 47%, respectively). Since complete conversion of oleic acid was obtained at 120 °C, the temperatures higher than this, which would cause decomposition of hydrogen peroxide, were not tried. To study H<sub>2</sub>O<sub>2</sub> loss during the reaction through catalytic or thermal decomposition, some catalytic tests without oleic acid were carried out, and then H<sub>2</sub>O<sub>2</sub> loss was calculated by titrimetry. Results showed a 22% loss in absence of any catalyst and 30-70% in presence of the synthesized catalysts after 5 h reaction at 120 °C.

Employing shorter reaction times resulted in a significantly lower conversion. After 3 *h* reaction at 120 °C, over sample V, 58% of initial oleic acid was converted to azelaic and pelargonic acids with the yields of 62 and 59%, respectively. Longer reaction time (7.5 *h*) caused the yields to slightly reduce, most probably due to degradation of azelaic and pelargonic acids caused by prolonged heating in presence of catalyst [48]. Further works to optimize the reaction temperature and time for all the samples via kinetic studies are ongoing in our lab and will be presented in another article.

### 5.3.2.3 Recyclability of the catalysts

All the synthesized catalysts were recovered after the reactions and reused to examine their recyclability. Up to four cycles, they all showed more than 97% conversion without significant loss in the yields, except sample I which showed a considerable decrease in catalytic efficiency after the first cycle. Figure 5.7 compares the yields of production of azelaic acid in four cycles. Almost the same trend was obtained for  $Y_{PA}$ .

FTIR analysis was performed on the catalysts after each cycle to probe any change in their chemical structures. Except sample I, other catalysts exhibited almost the same FTIR patterns to their original spectra (Supporting Information, Figures 5.16 to 5.21) confirming that they essentially keep their chemical natures during the reaction. This chemical stability is because the catalysts had been already exposed to a thermal treatment at high temperatures (600 °C for sample II and 120 °C for sample III to VI) during the synthesis procedure. Whereas the structure of sample I, which had been synthesized at RT, was dramatically changed after the first cycle. Evidence for this was found in its FTIR analysis, before and after the reaction (Figure 5.16), as well as XRD analysis (Figure 5.22), where disappearance of corresponding peaks of  $[(WO_2)O_2.H_2O]$ , and instead, emerging the characteristic peaks of  $WO_3.0.33H_2O$  (PDF no. 87-1203) imply decomposition of inter-crystalline tungsten-peroxo species during the reaction. This gives rise to the significant loss of catalytic efficiency of sample I after the first reaction cycle.

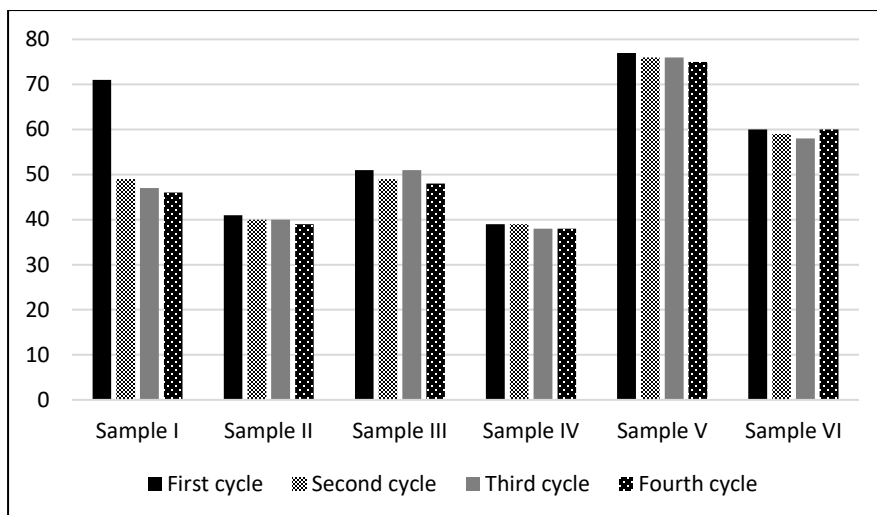


**Figure 5.7.** Recyclability of the synthesized catalysts; yields of production of azelaic acid over the synthesized catalysts in fourth cycles (reaction conditions: time: 5 h, temperature: 120 °C (bath temperature), solvent: tert-butanol, initial amounts of oleic acid: 1 g, t-butanol: 7.5 ml, H<sub>2</sub>O<sub>2</sub>: 4 ml, catalyst: 0.45 g, agitation rate: ~ 400 rpm).

In order to examine leaching of WO<sub>3</sub> species and truly heterogeneity of the reaction, a catalytic test was performed over sample V, which had given the highest yields, and stopped after 2.5 h of reaction. After cooling down and removal of catalyst, the reaction mixture was exposed to the reaction conditions for the remaining reaction time (2.5 h). In the second 2.5 h, conversion slightly increased (from 43% to 51%), as a result of oxidant ability in advancing the reaction alone (see entry 1 of Table 5.2), while changes in the yields were negligible. Moreover, for all the samples, weight loss of catalyst after each reaction cycle was exactly measured (Supporting Information, Table 5.5). Generally, the catalysts weight losses were less than ~ 2 %, with the minimum values, interestingly, obtained for the organo-functionalized catalysts (particularly samples V and VI), most likely because of hydrophobization effects making the CTA<sup>+</sup>-capped catalysts more water-tolerant with less leaching of inherently hydrophilic active sites (WO<sub>3</sub>). These results imply no significant leaching of active sites during the reaction.

## 5.4 Conclusions

A straightforward and green synthetic procedure, simply starting from cheap micrometer-scale W powder and adding H<sub>2</sub>O<sub>2</sub>, resulted in the formation of a clear solution of peroxotungstic species, which were then crystallized into different structures of tungsten oxide via altering temperature and/or adding CTAB. Given the potential of WO<sub>x</sub> as oxidizing catalyst, all the synthesized catalysts were adequately efficient to fully convert oleic acid after 5 h reaction with H<sub>2</sub>O<sub>2</sub> as a benign oxidant. Intriguingly, adding CTAB to the synthesis mixture, not only played a structure-directing role influencing the final product crystalline phase, but also stably capped the surfaces of tungsten oxide NPs resulting in an improved compatibility of the solid catalyst with the organic substrate and aqueous oxidant, and consequently, enhancing production yield of the desired azelaic acid up to just less than 80%. This result seems advantageous when compared to the scarce works reported on heterogeneous catalytic oxidative cleavage of oleic acid. The organofunctionalization by optimized amount of CTA<sup>+</sup> could hydrophobically adjust the inherently hydrophilic surface of tungsten oxide giving more surface affinity to adsorb oleic acid in the reaction. This, together with the solid nature and insolubility of WO<sub>x</sub>, provided the CTA<sup>+</sup>-capped catalyst with additional advantages of no significant leaching of active sites, convenient recovery and steady reuse for up to four cycles without loss of activity. Hopefully, the application of this catalytic process could be extended to other UFAs available in vegetable oils, which would make diacids production more economical, commercially attractive, and environmentally friendly.

### Acknowledgment

This work was supported by the Natural Science and Engineering Research Council of Canada (NSERC) through the INNOV-UC and Discovery grants. The authors wish to thank the industrial partners (Oleotek and SiliCycle Inc.) for stimulating discussions and comments.

## 5.5 Supporting Information

### 5.5.1 Characterization techniques

Powder X-ray diffraction (XRD) patterns of the samples were obtained on a Bruker SMART APEXII X-ray diffractometer equipped with a Cu K $\alpha$  radiation source ( $\lambda = 1.5418 \text{ \AA}$ ). Fourier transform infrared (FTIR) absorption spectra were measured with an FTS 45 infrared spectrophotometer with the KBr pellet technique. Thermo-gravimetric analysis (TGA) and differential thermal analysis (DTA) were performed with a TGA Q500 V20.13 Build 39 thermogravimetric analyzer from room temperature to 800 °C with a heating rate of 5 °C min<sup>-1</sup> under an air flow of 50 mL min<sup>-1</sup>. Transition electron microscopy (TEM) images were taken on a JEOL 6360 instrument at an accelerating voltage of 3 kV. Zeta potential was measured by means of a Zetasizer Nano 6 (Malvern Instruments Ltd) using a 4 mW He–Ne laser at 633 nm wavelength. The BET surface area was calculated by means of a Quantachrome Autosorb-1 system using N<sub>2</sub> adsorption-desorption isotherms at the temperature of liquid nitrogen and the data in the range of 0.05–0.3 P/P<sub>0</sub>.

### 5.5.2 Analysis of the reaction products

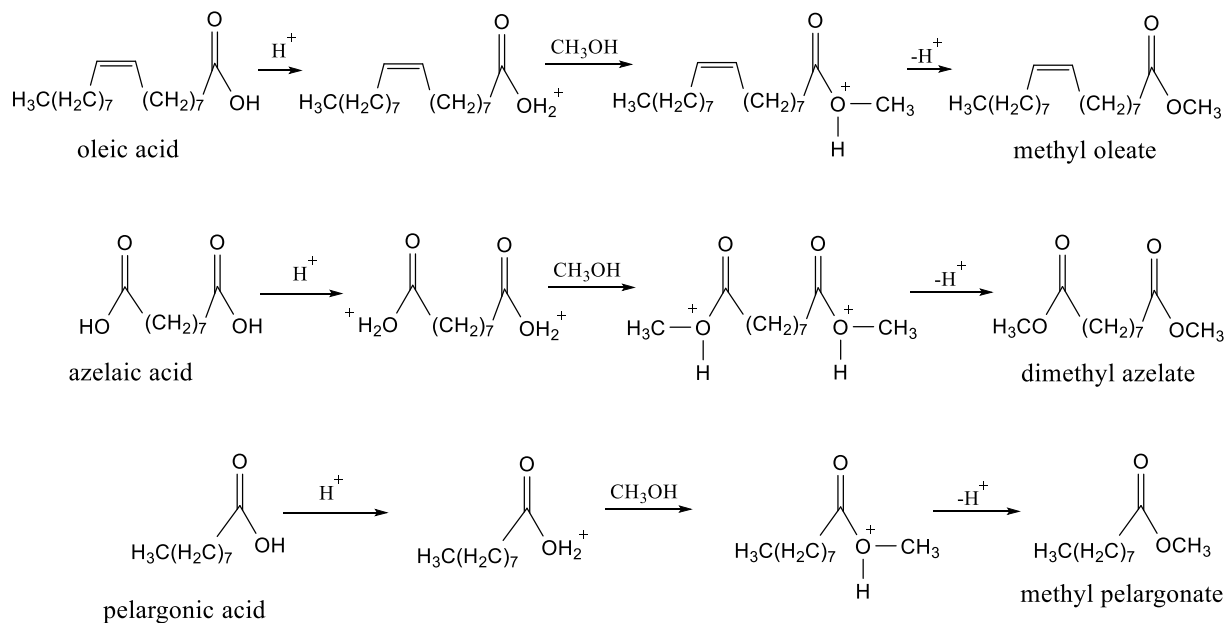
Gas chromatography-mass spectrometry (GC-MS) analysis was used for the separation, identification, and quantification of the products after the reaction.

Fundamentally, fatty acids in their free form are difficult and fallible to analyze with GC, because these highly polar compounds tend to form hydrogen bonds with the stationary phase in GC columns, leading to adsorption issues. Reducing their polarity make them more amenable for analysis. Converting fatty acids to fatty acid methyl esters is the most common method for preparation of fatty acids prior to GC analysis, because methyl esters offer excellent stability, and provide quick and quantitative samples for analysis.

#### 5.5.2.1 Sample preparation for GC-MS analysis

After a typical oxidative cleavage reaction, the products mixture underwent a derivatization reaction, in which the expectedly produced azelaic and pelargonic acids, and possibly unreacted

oleic acid were esterified to dimethyl azelate, methyl pelargonate, and methyl oleate, respectively. The esterification, briefly, involved heating the fatty acids in presence of an acid catalyst, boron trifluoride, in methanol to give fatty acid methyl esters. First,  $\text{BF}_3$  protonates an oxygen atom of the carboxyl group making the acid much more reactive to nucleophiles, and then, methanol molecule combines with the protonated acid, to give the ester products. Scheme 5.1 shows derivatization mechanisms for oleic, azelaic, and pelargonic acids.



**Scheme 5.1.** Esterification of oleic, azelaic, and pelargonic acids with methanol to methyl oleate, dimethyl azelate, and methyl pelargonate, respectively, over an acid catalyst,  $\text{BF}_3$ .

Typically,  $\text{BF}_3$ -methanol (5 ml) (10% w/w, Sigma-Aldrich Co.) was, firstly, added to the fatty acids mixture, in which the total weight of fatty acids is less than 400 mg. Then, the mixture was heated to  $80\text{ }^\circ\text{C}$  for 15 min, followed by cooling down at room temperature for about 20 min. The ester products were extracted by adding 2 ml petroleum ether (Fisher Scientific Co.) and 2 ml water. After carefully removing the organic (upper) layer, the aqueous phase underwent the second extraction. Finally, the obtained organic phase was dehydrated by sodium sulfate (anhydrous,  $\geq 99\%$ , Sigma-Aldrich Co.) and then the solvent was removed by passing a steady stream of dry air. After properly dilution, the obtained esterified mixture was ready for injection to GC-MS.

### 5.5.2.2 Quantitative analysis

A typical derivatized sample, expectedly including dimethyl azelate, methyl pelargonate, and possibly methyl oleate, was injected to the GC-MS which had been previously calibrated by analytical standards of these methyl esters (all were purchased from Sigma-Aldrich Co.). A constant and exact amount of 1.0  $\mu\text{L}$  was injected each time, and the injection was repeated at least four times for each sample to be averaged.

Obtained chromatograms of products for the catalytic tests, which their results have been presented in Table 5.2, entries 1-8, are shown in Figures 5.8-5.15 (Supporting Information). Owing to the carefully chosen column type and operating conditions of GC (see section 5.5.2.3), the obtained peaks had excellent shape and sharpness, which lead to reliable results. Based on peak areas in these chromatograms and the calibration curves of the standard methyl esters (which showed excellent linearity), conversion and yields of the oxidative cleavage reaction, reported in Table 5.2, were calculated (yield, in this work, was defined as number of moles of a product formed per mole of oleic acid consumed). Reproducibility of the results in this Table have been verified by performing at least 3 runs over each catalyst.

The properly adjusted temperature programming allowed separation of methyl pelargonate, dimethyl azelate, and methyl oleate with discrete retention times ( $R_t$ ) of 10.4, 15.8, and 26.8 min, respectively. Some other peaks were also observed in the chromatograms, indicating presence of by-products, which were qualitatively analyzed by MS, as follows. Small and often negligible peaks in e.g.  $R_t = 6.8, 8.9, 11.2,$  and  $16.7$  min belonged to octanal, methyl esters of hexanoic and octanoic acids, and 9,10-dihydroxy octadecanoic acid, respectively, which were produced by impurities of the reactants and/or insignificant side reactions (e.g. hydroxylation). Two relatively more considerable peaks in  $R_t = 8.6$  and  $13.8$  min belonged to nonanal and 9-oxononanoic acid, respectively, which were produced by partial-oxidation of oleic acid. Since after minute 30 no significant peak was obtained, the chromatograms in Figures 5.8-5.15 have been monitored up to  $R_t = 30$  min.

It should be noted that such by-products like 9-oxononanoic acid, which are the direct result of involvement of carboxylic group in the reaction, has made oxidative cleavage of unsaturated



fatty acids, compared to alkenes and cyclic olefins, more complicated and investigation of their reaction mechanism more difficult. It makes more sense given the fact that 9-oxononanoic acid is not commercially available (in known chemical provider companies), which makes calibration of chromatography systems by the analytical standard of this chemical, and consequently its quantitative analysis by these systems impossible.

Further kinetic studies are underway in our laboratory to investigate the competition between partial and over-oxidation of oleic acid and propose a mechanism indicating how both oleic acid and hydrogen peroxide are activated by the synthesized catalysts.

### **5.5.2.3 GC-MS specifications**

The GC-MS included a Hewlett-Packard HP 5890 series GC system and MSD Hewlett-Packard model 5970. GC system was equipped with Zebron ZB-5MS capillary column (30 m × 0.25 mm × 0.25 mm). Helium was used as a carrier gas with the flow rate of 30 mL/min. A split ratio of 20:1 was fixed. The front inlet temperature was 280 °C. The oven temperature program consisted of maintaining at 50 °C for 2 min, then a ramp rate of 10 °C/min to 160 °C following by a hold-up time of 1 min, and further increase with the rate of 5°C/min to 290 °C. Direct injection by a 5.0 µL syringe (SGE fixed needle, 23-26 gauge/42mm L/Cone Tip, Phenomenex Co.) was employed with 1.0 µL injection amount for each run. HP Chemstation software was used to analyze data.

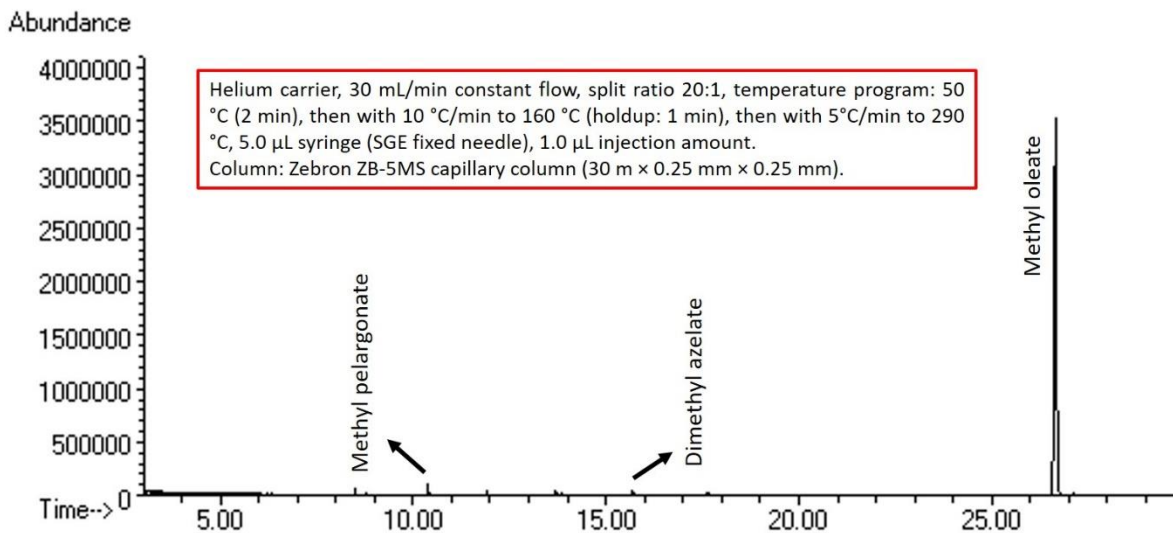


**Figure 5.8.** Gas chromatogram of products of the catalytic test in absence of catalyst (entry 1, Table 5.2).

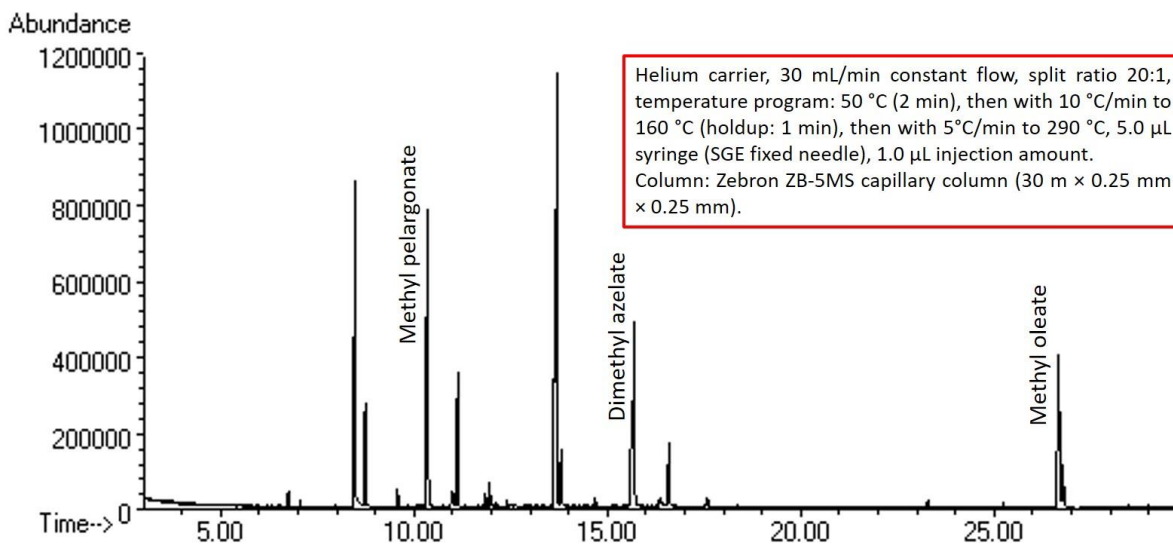


**Figure 5.9.** Gas chromatogram of products of the catalytic test over commercial tungsten oxide (entry 2, Table 5.2).

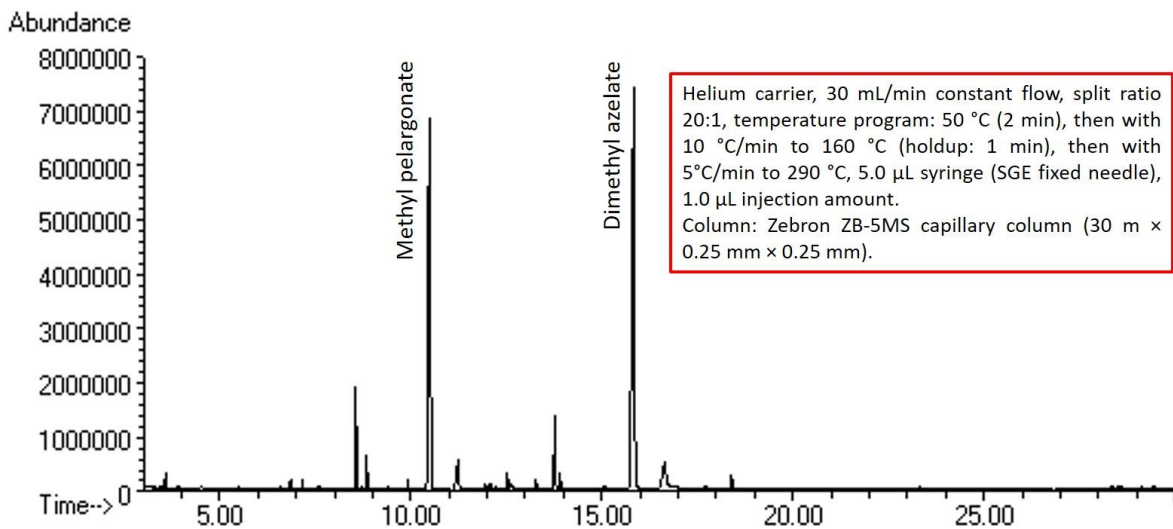


**Figure 5.10.** Gas chromatogram of products of the catalytic test over sample I (entry 3, Table 5.2).

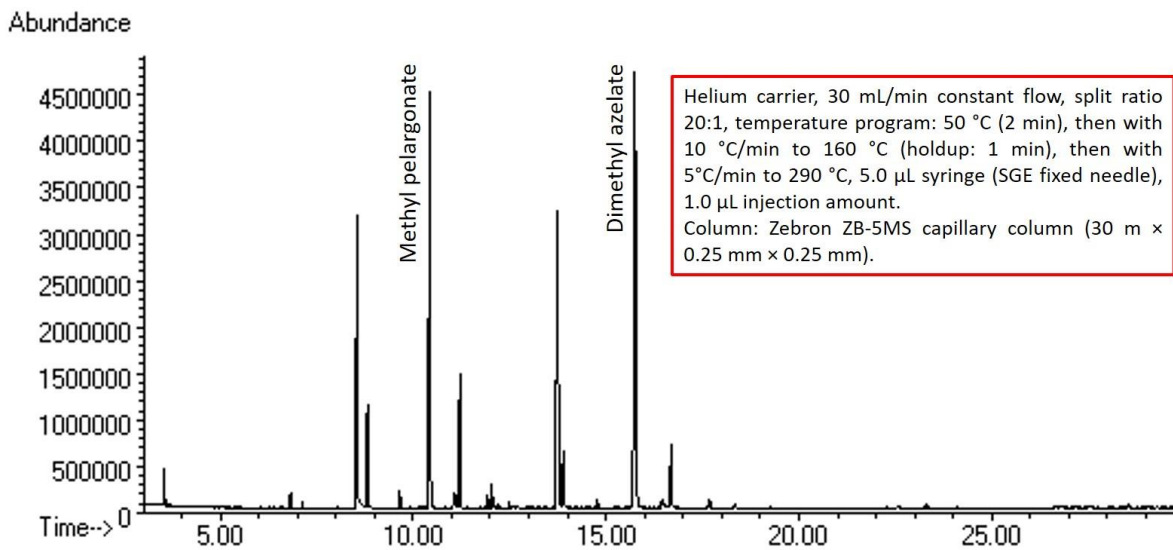


**Figure 5.11.** Gas chromatogram of products of the catalytic test over sample II (entry 4, Table 5.2).

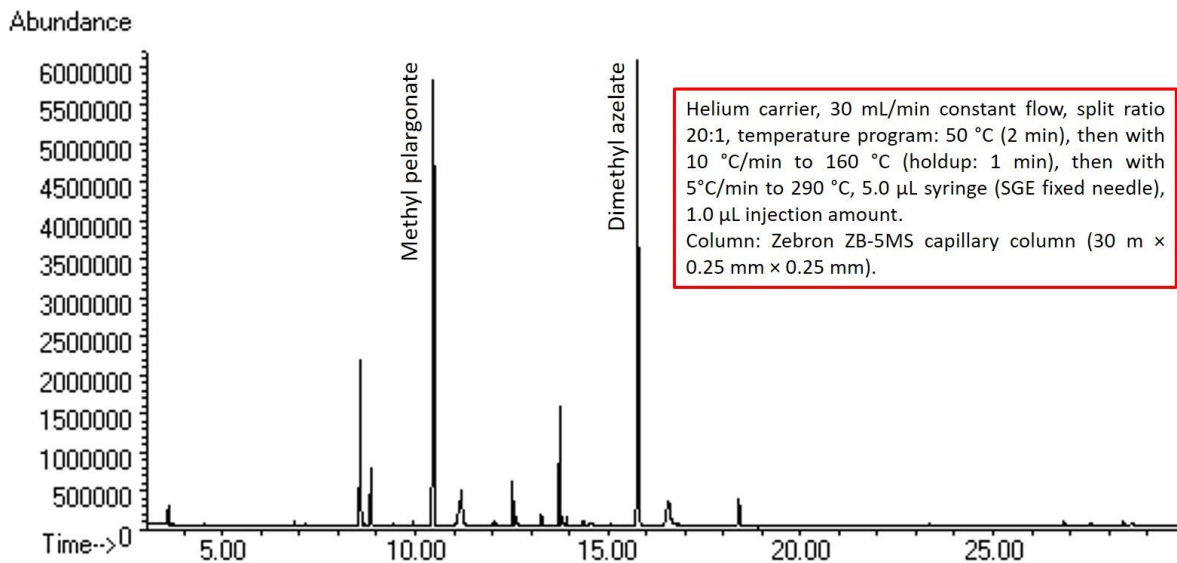


**Figure 5.12.** Gas chromatogram of products of the catalytic test over sample III (entry 5, Table 5.2).

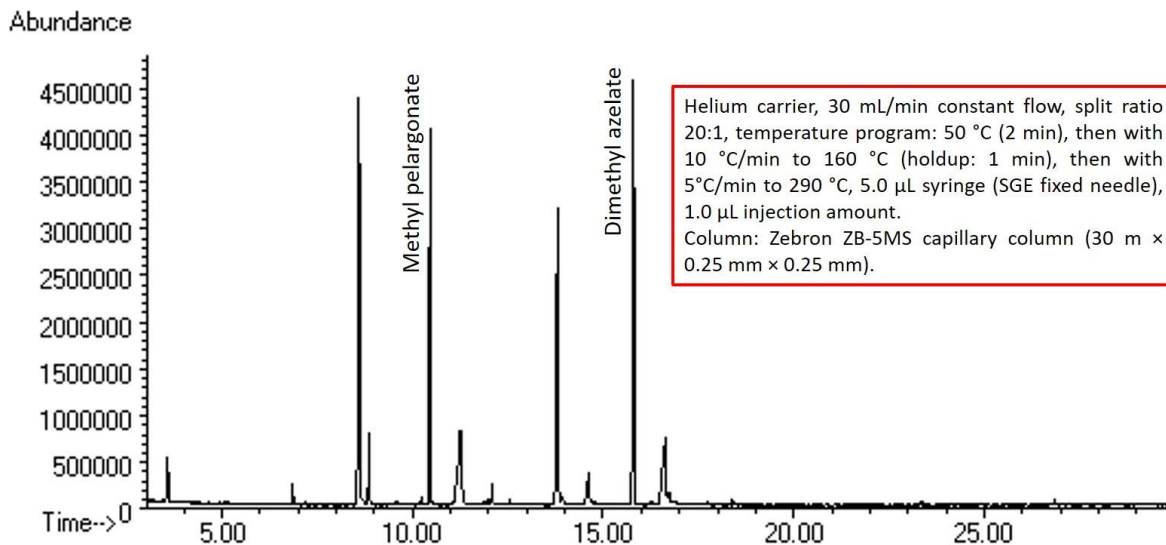


**Figure 5.13.** Gas chromatogram of products of the catalytic test over sample IV (entry 6, Table 5.2).

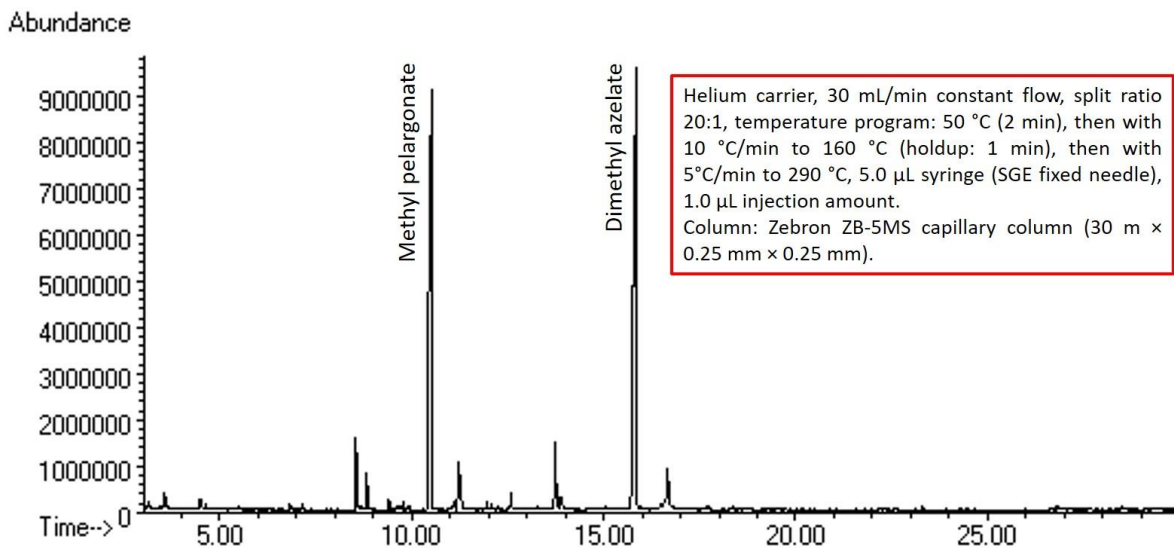


**Figure 5.14.** Gas chromatogram of products of the catalytic test over sample V (entry 7, Table 5.2).

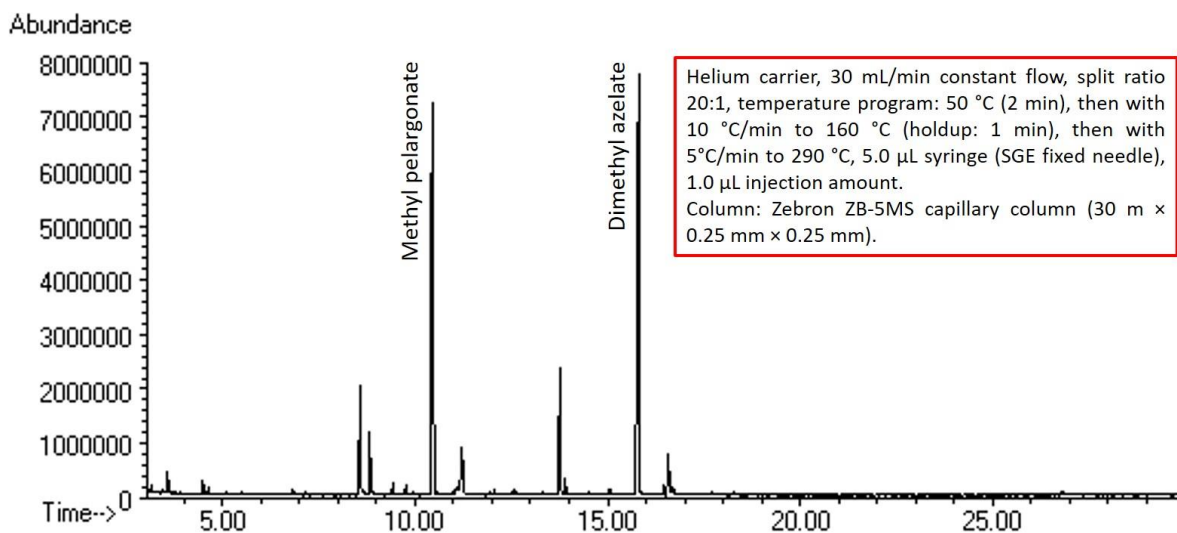


**Figure 5.15.** Gas chromatogram of products of the catalytic test over sample VI (entry 8, Table 5.2).

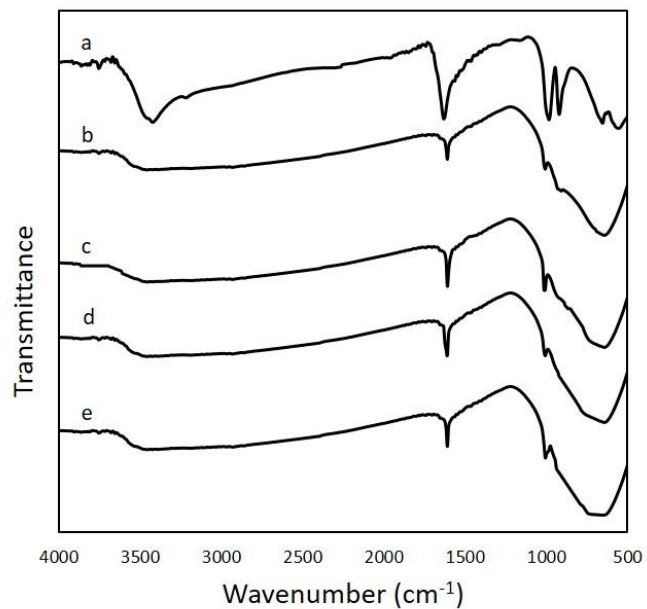


**Figure 5.16.** FTIR spectra of sample I: (a) before reaction, (b) after 1<sup>st</sup> cycle, (c) after 2<sup>nd</sup> cycle, (d) after 3<sup>rd</sup> cycle, and (e) after 4<sup>th</sup> cycle.

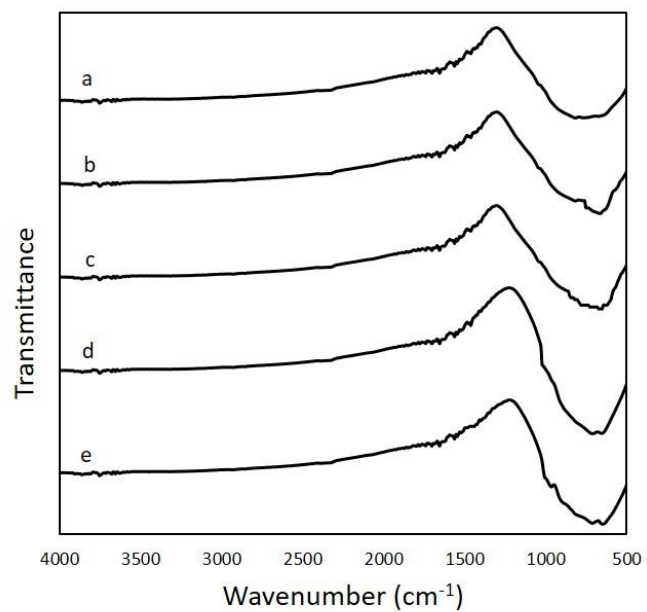


**Figure 5.17.** FTIR spectra of sample II: (a) before reaction, (b) after 1<sup>st</sup> cycle, (c) after 2<sup>nd</sup> cycle, (d) after 3<sup>rd</sup> cycle, and (e) after 4<sup>th</sup> cycle.

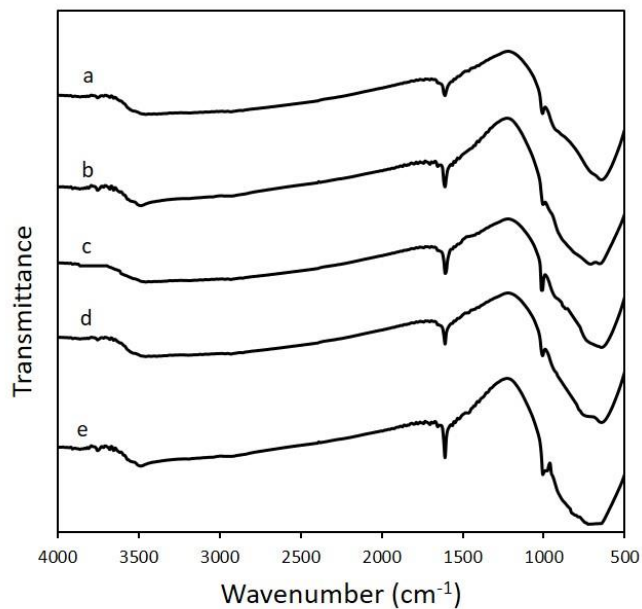


**Figure 5.18.** FTIR spectra of sample III: (a) before reaction, (b) after 1<sup>st</sup> cycle, (c) after 2<sup>nd</sup> cycle, (d) after 3<sup>rd</sup> cycle, and (e) after 4<sup>th</sup> cycle.

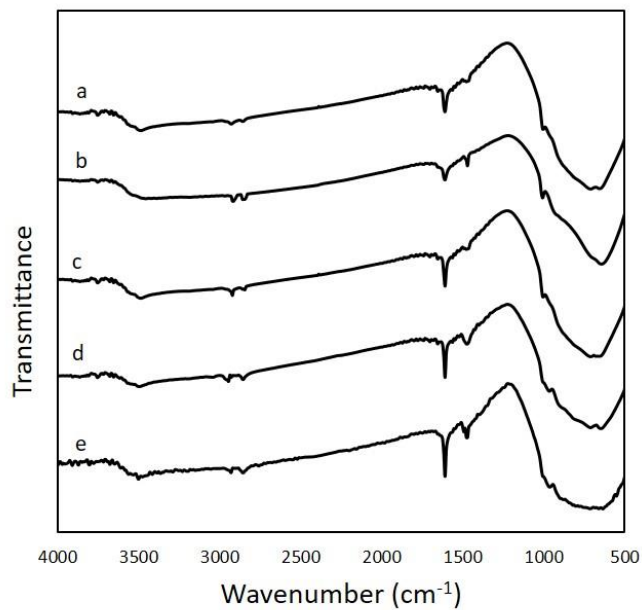


**Figure 5.19.** FTIR spectra of sample IV: (a) before reaction, (b) after 1<sup>st</sup> cycle, (c) after 2<sup>nd</sup> cycle, (d) after 3<sup>rd</sup> cycle, and (e) after 4<sup>th</sup> cycle.

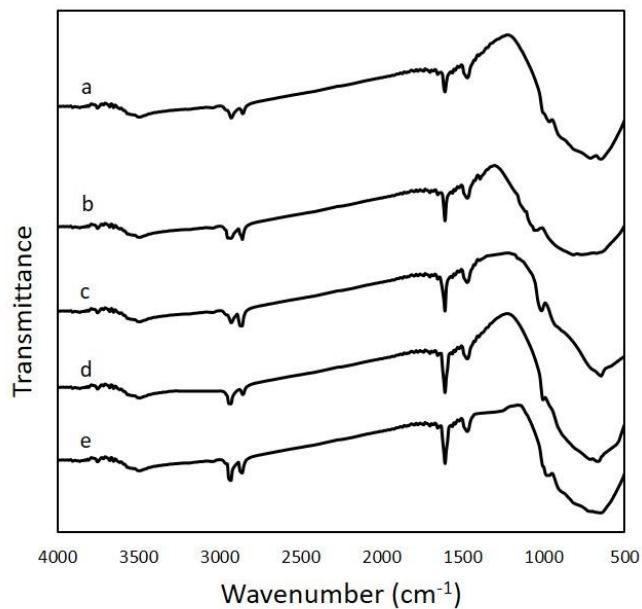


**Figure 5.20.** FTIR spectra of sample V: (a) before reaction, (b) after 1<sup>st</sup> cycle, (c) after 2<sup>nd</sup> cycle, (d) after 3<sup>rd</sup> cycle, and (e) after 4<sup>th</sup> cycle.

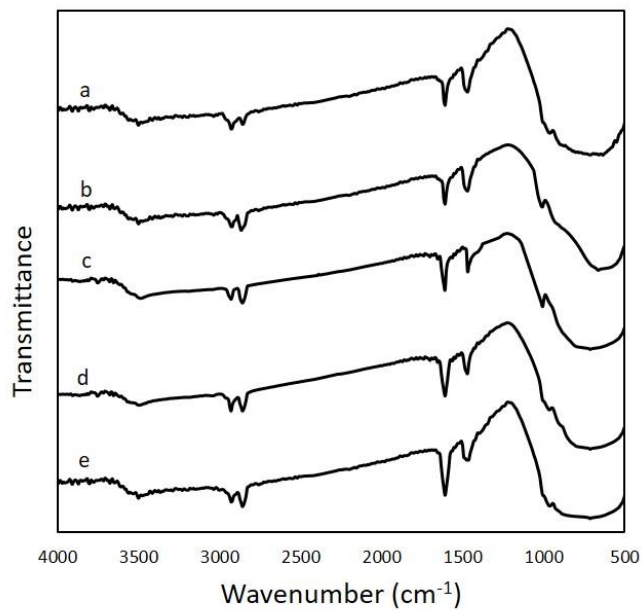


**Figure 5.21.** FTIR spectra of sample VI: (a) before reaction, (b) after 1<sup>st</sup> cycle, (c) after 2<sup>nd</sup> cycle, (d) after 3<sup>rd</sup> cycle, and (e) after 4<sup>th</sup> cycle.



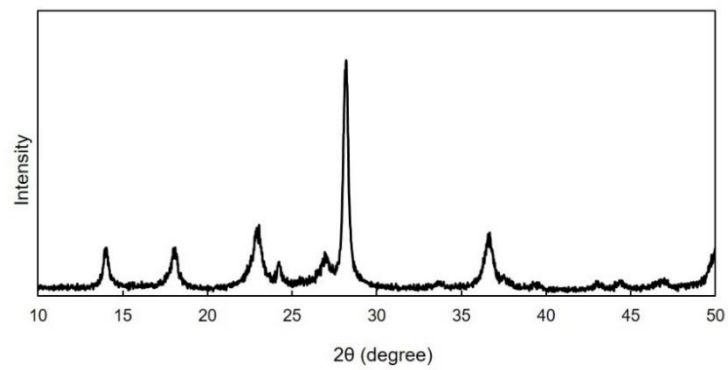


**Figure 5.22.** XRD pattern of sample I after reaction;  $\text{WO}_3 \cdot 0.33\text{H}_2\text{O}$  (PDF no. 87-1203).

**Table 5.3.** Assignments of the FTIR absorption bands of the prepared samples [369].

Sample	Absorption bands (cm <sup>-1</sup> )	Assignment
I	548	W (O <sub>2</sub> )
	649	ν (W-O)
	919	ν (O-O)
	981	ν (W=O)
	1622	δ (H-O-H)
	3421	ν (H-O-H)
II	672	ν (W-O)
III	641	ν (W-O)
	1004	ν (W=O)
	1606	δ (H-O-H)
	3452	ν (H-O-H)
IV	649	ν (W-O)
	973	ν (W=O)
	1467	RN(CH <sub>3</sub> ) <sub>3</sub> <sup>+</sup>
	1606	δ (H-O-H)
	2850, 2927	ν (CH <sub>3</sub> and/or CH <sub>2</sub> )
	3491	ν (H-O-H)
V	641	ν (W-O)
	958	ν (W=O)
	1467	RN(CH <sub>3</sub> ) <sub>3</sub> <sup>+</sup>
	1606	δ (H-O-H)
	2850, 2927	ν (CH <sub>3</sub> and/or CH <sub>2</sub> )
	3491	ν (H-O-H)
VI	656	ν (W-O)
	950	ν (W=O)
	1467	RN(CH <sub>3</sub> ) <sub>3</sub> <sup>+</sup>
	1606	δ (H-O-H)
	2850, 2927	ν (CH <sub>3</sub> and/or CH <sub>2</sub> )
	3491	ν (H-O-H)

**Table 5.4.** BET surface areas of the synthesized samples.

Sample	CTAB/W molar ratio	S <sub>BET</sub> (m <sup>2</sup> /g)
I	-	8.6
II	-	29.1
III	-	17.0
IV	0.1	14.0
V	0.25	7.8
VI	0.5	4.3

**Table 5.5.** Weight losses of the synthesized catalysts during the different cycles of the reaction.

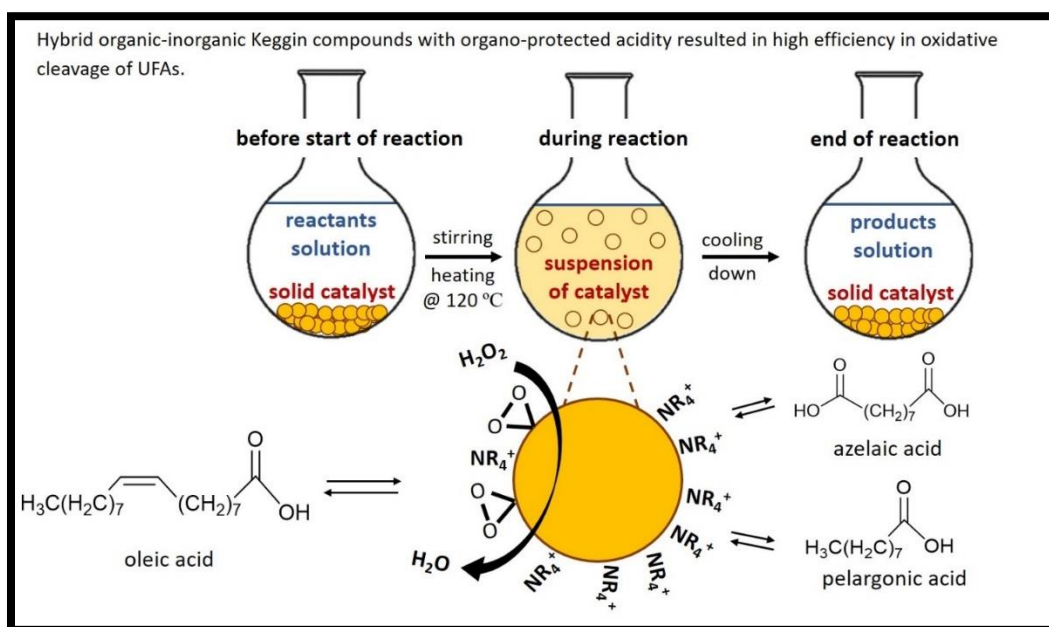
Reaction cycle	Sample I	Sample II	Sample III	Sample IV	Sample V	Sample VI
1 <sup>st</sup>	2.1	1.3	1.8	1.4	1	0.8
2 <sup>nd</sup>	2	1.7	1.6	1.4	1.2	0.9
3 <sup>rd</sup>	1.9	1.2	1.4	1.3	1.3	1
4 <sup>th</sup>	2	1.6	1.7	1.5	1.4	1

# Chapter 6. Novel tetra propyl/butyl ammonium encapsulated Keggin-type polyoxotungstates: synthesis, structural characterization, and catalytic capability in oxidative cleavage of unsaturated fatty acids

Amir Enferadi-Kerenkan, Arnaud Gandon, and Trong-On Do\*

Department of Chemical Engineering, Université Laval, Québec, G1V 0A6, Canada.

*Dalton Transactions, 2017, DOI: 10.1039/C7DT04469K*



## Résumé

Quatre catalyseurs à base d'oxyde de tungstène (TO), (1) TO (sans aucun fragment organique), (2) TO-TMA, (3) TO-TPA, et (4) TO-TBA (TMA: tétraméthylammonium, TPA: tétrapropylammonium, et TBA: cations tétrabutylammonium) ont été directement préparés par une approche hydrothermale douce, basée sur la dissolution oxydative de la poudre de tungstène nue, suivie par l'encapsulation facile des cations tétraalkylammonium ( $\text{NR}_4^+$ ). L'impact significatif des cations  $\text{NR}_4^+$  sur la cristallisation des espèces peroxotungstes amorphes et métastables, formées lors de la synthèse, a été discuté par différentes techniques de caractérisation incluant XRD, FTIR, TGA et DTG, TEM, EDS, N<sub>2</sub> isothermes d'adsorption / désorption, mesure de potentiel zêta, et l'analyse élémentaire. TO-TPA et TO-TBA étaient composés de deux nouveaux polyoxotungstates inorganiques-organiques hybrides, respectivement  $[(\text{CH}_3\text{CH}_2\text{CH}_2)_4\text{N}]_{2.75}[\text{H}_{5.25}\text{W}_{12}\text{O}_{40}] \cdot 7.42\text{H}_2\text{O}$  et  $[(\text{CH}_3\text{CH}_2\text{CH}_2\text{CH}_2)_4\text{N}]_{3.31}[\text{H}_{4.69}\text{W}_{12}\text{O}_{40}] \cdot 1.08\text{H}_2\text{O}$ . La capacité des catalyseurs synthétisés dans l'oxydation avec  $\text{H}_2\text{O}_2$  des acides gras insaturés a été examinée dans la réaction de l'acide oléique, l'acide gras insaturé le plus abondant. C'est le premier rapport sur l'utilisation de groupes de Keggin hétérogènes d'oxyde de tungstène dans le clivage oxydatif des acides gras insaturés. Les catalyseurs présentaient d'excellents rendements, en particulier TO-TPA et TO-TBA en raison de la forte et organo-protégée acidité de leurs structures de Keggin, qui résultait en une conversion complète de l'acide oléique et des rendements supérieurs de production des produits désirés. En dépit de leurs comportements pseudo-homogènes dans la réaction, les catalyseurs encapsulés dans le  $\text{NR}_4^+$  ont démontré une récupération efficace et une réutilisabilité régulière sans décroissance significative de leurs activités jusqu'à au moins 4 cycles.

## Abstract

Four tungsten oxide (TO)-based catalysts, (1) TO (without any organic moiety), (2) TO-TMA, (3) TO-TPA, and (4) TO-TBA (TMA: tetramethylammonium, TPA: tetrapropylammonium, and TBA: tetrabutylammonium cations) were straightforwardly prepared via a mild hydrothermal approach, based on oxidative dissolution of tungsten bare powder, followed by the facile encapsulation of the tetraalkylammonium cations ( $\text{NR}_4^+$ ). The significant impact of the  $\text{NR}_4^+$  cations on crystallization of the amorphous and metastable peroxotungstic species, formed during the synthesis, has been discussed through different characterization techniques including XRD, FTIR, TGA and DTG, TEM, EDS,  $\text{N}_2$  adsorption/desorption isotherms, zeta potential measurement, and elemental analysis. TO-TPA and TO-TBA were composed of two novel hybrid inorganic-organic polyoxotungstates,  $[(\text{CH}_3\text{CH}_2\text{CH}_2)_4\text{N}]_{2.75}[\text{H}_{5.25}\text{W}_{12}\text{O}_{40}] \cdot 7.42\text{H}_2\text{O}$  and  $[(\text{CH}_3\text{CH}_2\text{CH}_2\text{CH}_2)_4\text{N}]_{3.31}[\text{H}_{4.69}\text{W}_{12}\text{O}_{40}] \cdot 1.08\text{H}_2\text{O}$ , respectively. The capability of the synthesized catalysts in oxidation of unsaturated fatty acids (UFAs) has been examined in the reaction of oleic acid, the most abundant UFA, with  $\text{H}_2\text{O}_2$ . This is the first report on employing heterogeneous Keggin clusters of tungsten oxide in oxidative cleavage of UFAs. The catalysts exhibited excellent efficiencies, particularly TO-TPA and TO-TBA owing to the strong and organo-protected acidity of their Keggin structures, which resulted in full conversion of oleic acid and superior yields of production of the desired products. In spite of their pseudo-homogeneous behaviors in the reaction, the  $\text{NR}_4^+$ -encapsulated catalysts demonstrated efficient recovery and steady reusability without any significant decay in their activities up to at least 4 cycles.

## 6.1 Introduction

Tungsten-based heteropoly compounds or their more descriptive synonym, polyoxotungstates (POTs), have attracted a great deal of attention, particularly in the last decade, stemming from potential reinforcement of uniquely interesting catalytic properties of polyoxometalates (e.g. strong acidity, redox capability, and readily tuning of these properties at molecular level) by the distinct inherent properties of tungsten in particular having very strong Brönsted acid sites [370,131]. However, POTs are inherently soluble in water and polar solvents which results in lack of recovery in the water-involving reactions. To tackle this obstacle, heterogenization of homogeneous POTs via different solidification and immobilization strategies are being rapidly developed [371,191]. Heterogenization by means of organo-functionalization has been enthusiastically explored, not only for heterogenization purpose, but also to provide an efficient versatility for the resultant hybrid organic-inorganic catalyst in liquid organic reactions, arising from the wide variety of organic groups and proper adjustment of the catalyst's surface state [177,182,183,175,184,186].

Compared to the other solid acids, heterogeneous POTs have shown excellent water-tolerant properties [131], which gives rise for their widely reported application in water-involving reactions such as hydrolysis, dehydration, esterification, as well as oxidation of olefins with  $H_2O_2$ , where a major problem in the use of solid acids is poisoning of acid sites by water resulting in gradual decay of activity. Curiously the use of POT-based heterogeneous catalysts in oxidation of unsaturated fatty acids (UFAs) has not been reported so far, to our knowledge. Generally, this class of oxidation reactions has been less documented in the literature compared to the oxidation of alkenes and cyclic olefins, most probably due to the complexity of involvement of the carboxylic group in the reaction and its effects on the mechanism and the produced intermediates [91,45,3]. On the other hand, this class is of great industrial importance; exploiting the nature's capabilities, vegetable oils containing UFAs can be converted into valuable products, mono- and diacids, via oxidative cleavage reactions. The enormous abundance of oilseeds, which are nowadays extracted from a variety of plants under all sorts of climates in both northern and southern hemispheres, associated with nontoxicity, biodegradability, and having similar chemical structures to petroleum materials have rendered vegetable oils promising candidates to replace concerning petrochemical feedstock. That is why the recent 30 years have monitored a surprisingly considerable increase in

global extraction of oilseeds and rapid development of oleochemical industries [15]. Currently, oleic acid (C18:1), the most widely distributed and abundant UFA, is used in the industry to produce azelaic (C9 diacid) and pelargonic (C9 monoacid) acids via ozonolysis [91,372]. The hazardous problems associated with the use of ozone, however, have propelled the industry to employ an eco-friendlier oxidant, in accordance with sustainable chemistry, which requires an active catalyst to be employed, as well.

In this work, a new type of hybrid organic-inorganic POTs was prepared and employed as heterogeneous catalyst in oxidative cleavage of oleic acid, for the first time. We have developed a novel, straightforward, and green synthesis method for preparation of the organo-modified Keggin clusters, complying with the principles of “Chimie Douce”, which exploits cheap bare W powder as precursor, by contrast to the prior methods which often used phosphotungstic or tungstic acid. Encapsulation of three different tetraalkylammoniums ( $\text{NR}_4^+$ ) including tetramethylammonium ( $\text{TMA}^+$ ), tetrapropylammonium ( $\text{TPA}^+$ ), and tetrabutylammonium ( $\text{TBA}^+$ ) into the structures of the products has been examined. This one-pot synthesis method avoided using time- and energy-consuming operations such as thermal treatment in autoclave and purification, as well as organic solvents and tungstate complex compounds, which are commonly required in prior reported synthesis methods.

## 6.2 Experimental

### 6.2.1 Materials and synthesis

The employed straightforward synthesis method for preparation of hybrid organic-inorganic catalysts was started by dispersion of bare W powder (2.0 g; APS 1–5  $\mu\text{m}$ , purity 99.9%, Alfa Aesar Co.) in deionized  $\text{H}_2\text{O}$  (20 mL). Then, 25 mL of  $\text{H}_2\text{O}_2$  (aqueous solution, 30%, Fisher Scientific Co.) were added dropwise while the reaction vessel was kept in an instant ice bath (WARNING: the oxidative dissolution process is very exothermic, therefore must be done attentively in ice bath under a well-ventilated fume hood). A slightly light yellow and clear solution, mainly containing soluble amorphous peroxotungstic acid particles ( $\text{WO}_3 \cdot x\text{H}_2\text{O}_2 \cdot y\text{H}_2\text{O}$ ) [357,355], was formed after ~ 3 h. A determined amount of tetraalkylammonium bromides (TMA-



Br (98%), TPA-Br (98%), or TBA-Br ( $\geq 98\%$ ), all from Sigma-Aldrich Co.) to give a fixed molar ratio of  $\text{NR}_4^+$  to tungsten in the synthesis solution (TMA/W, TPA/W, or TBA/W = 0.25) was, then, added to the solution. Consequently, the reaction vessel was connected to a chemical condenser, and thermally treated at 120 °C for 5 h under stirring. After this thermal treatment, the precipitated solid products were separated using a centrifuge at 8000 rpm, washed thoroughly with water and ethanol, and dried at 60 °C overnight (16 h). Four tungsten oxide (TO)-based catalysts, (1) TO (without using any organic moiety), (2) TO-TMA, (3) TO-TPA, and (4) TO-TBA were accordingly prepared.

## 6.2.2 Characterization techniques

Powder X-ray diffraction (XRD) patterns of the samples were obtained on a Bruker SMART APEXII X-ray diffractometer equipped with a Cu  $K\alpha$  radiation source ( $\lambda = 1.5418 \text{ \AA}$ ). Fourier transform infrared (FTIR) absorption spectra were measured with an FTS 45 infrared spectrophotometer with the KBr pellet technique. Thermo-gravimetric analysis (TGA) was performed with a TGA Q500 V20.13 Build 39 thermogravimetric analyzer from room temperature to 800 °C with a heating rate of 5 °C  $\text{min}^{-1}$  under an air flow of 50  $\text{mL min}^{-1}$ . Transition electron microscopy (TEM) images were taken on a JEOL 6360 instrument at an accelerating voltage of 3 kV. Zeta potential was measured by means of a Zetasizer Nano 6 (Malvern Instruments Ltd) using a 4 mW He–Ne laser at 633 nm wavelength. The BET surface area was calculated by means of a Quantachrome Autosorb-1 system using  $\text{N}_2$  adsorption-desorption isotherms at the temperature of liquid nitrogen and the data in the range of 0.05–0.3  $P/P_0$ . Elemental analysis (C/H/N/S) was performed using a EAS1108, Fisons instrument S.p.A., and the detection limit for the analyses was 0.3% for C, H, and N.

## 6.2.3 Catalytic test

The reactions were carried out in a 50 mL, round-bottom flask under a batch-wise constant temperature and constant pressure mode. This reactor was equipped with a condenser, a magnetic stirrer, and an oil bath. Typically, the reaction feed included 1 g of oleic acid ( $\geq 99\%$ , Sigma-Aldrich Co.), 4 mL of  $\text{H}_2\text{O}_2$ , and 7.5 mL of tert-butanol ( $\geq 99.0\%$ , Sigma-Aldrich Co.) as solvent. After adding 0.45 g of catalyst, the flask was put in the oil bath, which was previously heated and maintained at constant temperature of 120 °C. During reaction, the reactor was continuously

agitated with magnetic stirrer (agitation rate  $\approx 400$  rpm). After 5 h reaction, the catalyst was separated using centrifuge at 8000 rpm and recovered via washing with ethanol and water several times and drying at 60 °C overnight to be used in the next catalytic cycle. The products solution then underwent a derivatization process to be prepared for GC-MS injection.

## 6.2.4 Analysis of the reaction products

Gas chromatography-mass spectrometry (GC-MS) was used for separation and quantification of the reaction products. Fatty acids in their free forms are difficult to analyze with GC owing to their adsorption issues on stationary phase in GC columns. Therefore, the reaction products, containing expectedly the produced azelaic and pelargonic acids, and possibly the unreacted oleic acid, were esterified before GC-MS analysis via Metcalfe et al. derivatization procedure [334,335] using boron trifluoride solution in methanol as catalyst. Further details about the derivatization reaction, as well as quantitative analysis and GC-MS specifications are available in Supporting Information of the previous chapter (section 5.5).

## 6.3 Results and discussion

### 6.3.1 Catalysts characterization

The four prepared samples including (1) TO (without using any organic moiety), (2) TO-TMA, (3) TO-TPA, and (4) TO-TBA were characterized using different techniques. The XRD patterns of the prepared samples are shown in Figure 6.1. In the absence of any organic moiety in the synthesis solution, hydrated tungsten trioxide ( $\text{WO}_3 \cdot n\text{H}_2\text{O}$ ) was formed (sample TO). Its XRD pattern (Figure 6.1 a) shows that it is composed of orthorhombic  $\text{WO}_3 \cdot 0.33\text{H}_2\text{O}$  and  $\text{WO}_3 \cdot \text{H}_2\text{O}$  (tungstite) in accordance with PDF no. 35-0270 and 43-0679 of ICDD library of spectra, respectively. Adding  $\text{NR}_4^+$  to the synthesis solution generally caused a surprisingly large increase in crystallinity of the products (since the peaks in Figure 6.1 b–d were highly intense, we had to depict Figure 6.1 a with 2.5 times higher intensities than actual values to make the peaks observable). TO-TMA was a yellow powder composed of orthorhombic tungstite (PDF no. 43-0679) and  $\text{WO}_3 \cdot 0.33\text{H}_2\text{O}$  (PDF no. 87-1203) (Figure 6.1 b). Astonishingly high intensity of the peak at  $2\theta = 16.5$ , which belongs to  $\{020\}$  reflection of tungstite, affect the presence of other peaks.

It reveals a higher growth of crystals in the direction of {020} facet arising from the templating role of TMA<sup>+</sup> cations. In addition to the WO<sub>3</sub>·nH<sub>2</sub>O phases, a less-intense peak at 2θ = 10.1 implies presence of a third crystalline phase. This peak could be well ascribed to the main peak of methylammonium tungsten oxide [MA<sub>x</sub>WO<sub>3+x/2</sub>·nH<sub>2</sub>O] (MA: methylammonium) phase, the crystal structure of which has been calculated and introduced by Zavalij et al. [364].

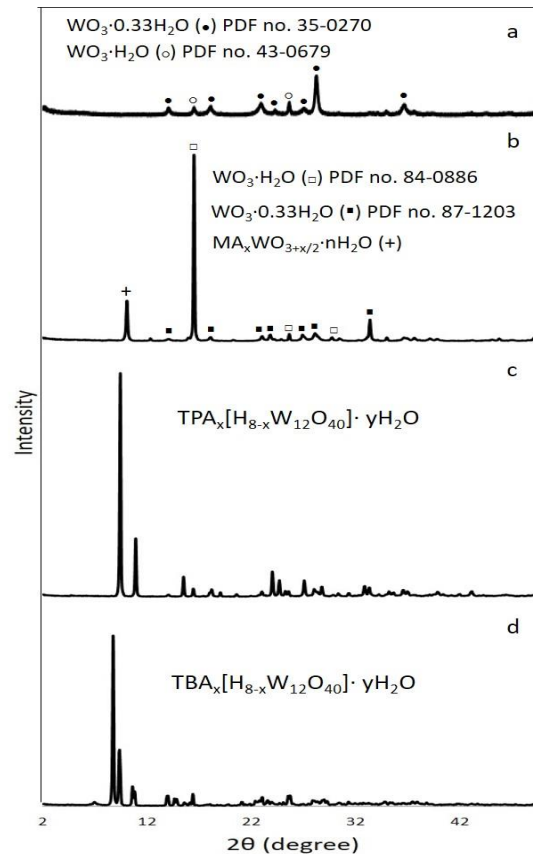


**Figure 6.1.** XRD patterns of (a) TO (intensities are magnified by 2.5), (b) TO-TMA, (c) TO-TPA, and (d) TO-TBA

Additionally, to clarify the effect of TMA<sup>+</sup> cation, XRD patterns of two more samples synthesized with different initial amount of TMA<sup>+</sup> are compared with the pattern of TO-TMA in Figure 6.2 (TO-TMA1/2 and TO-TMA2 samples with half and twice of the TMA<sup>+</sup> amount which was used for TO-TMA, respectively). Tiny amount of TMA<sup>+</sup> in TO-TMA1/2 resulted in pure hydrated tungsten trioxide (WO<sub>3</sub>·0.33H<sub>2</sub>O, PDF no. 87-1203 and WO<sub>3</sub>·H<sub>2</sub>O, PDF no. 18-1418) (Figure 6.2 a). Increasing the amount of TMA<sup>+</sup> in TO-TMA led to higher growth of crystals in the direction of {020} facet of tungstite on one hand (a templating role), and caused the third phase of [MA<sub>x</sub>WO<sub>3+x/2</sub>·nH<sub>2</sub>O] appears, on the other hand (Figure 6.2 b). Further increase in TMA<sup>+</sup> amount

in TO-TMA2 made the intensity of the peak corresponding to methylammonium tungsten oxide (at  $2\theta = 10.1$ ) considerably higher (Figure 6.2 c). Moreover, the sharp peaks of hydrated tungsten oxides available in TO-TMA1/2 and TO-TMA faded away in TO-TMA2, which is in good agreement with the obtained change in color of the samples from yellow powder (TO-TMA) to white powder (TO-TMA2). It can be concluded that the increase in the amount of  $\text{TMA}^+$  cations reduces their templating role (which was the reason of higher crystal growth in  $\{020\}$  facet in TO-TMA), and instead  $\text{TMA}^+$  cations start to crystallize and make a kind of hybrid-like crystalline phase with tungsten oxide,  $\text{MA}_x\text{WO}_{3+x/2}\cdot n\text{H}_2\text{O}$ . Figure 6.2 c also demonstrates the presence of tetragonal tungsten oxide tetra methoxide  $\text{WO}(\text{OCH}_3)_4$  (PDF no. 38-1899), albeit less inconspicuous compared to methylammonium tungsten oxide.

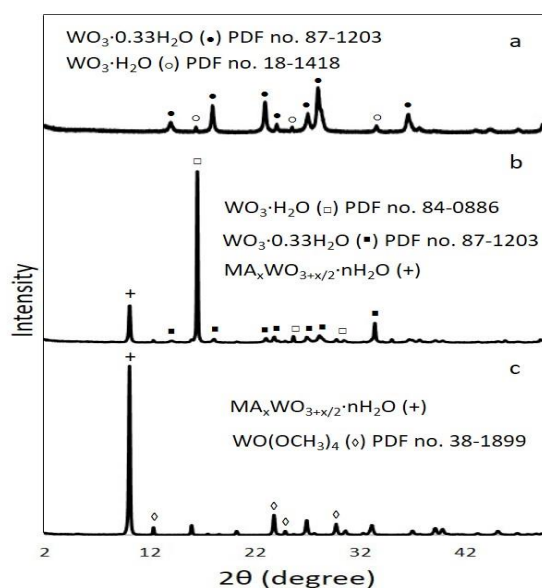
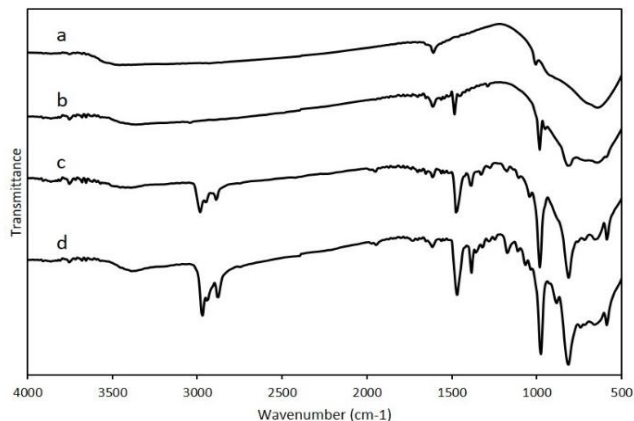


Figure 6.2. XRD patterns of (a) TO-TMA1/2, (b) TO-TMA, and (c) TO-TMA2.

Larger  $\text{NR}_4^+$  ( $\text{TPA}^+$  and  $\text{TBA}^+$ ), led to formation of more complicated hybrid structures. XRD analysis did not give enough information on these structures, since none of the PDF files of all tungsten compounds available in the database of ICDD library of spectra properly matches the intense peaks of TO-TPA and TO-TBA (Figure 6.1 c and d). The reason is the significant effects of  $\text{TPA}^+$  and  $\text{TBA}^+$  cations on crystallite structure of the final product and the fact that this work is the first report on preparation of hybrid  $\text{NR}_4^+$ -POT via oxidative dissolution of tungsten powder.

Fundamentally, oxidative dissolution of W in H<sub>2</sub>O<sub>2</sub> gives an almost colorless solution containing amorphous peroxotungstic acid particles, which need further thermal (or occasionally time) treatment to be crystallized [369]. In the synthesis of metastable transition metals oxides that have relatively open structures like tungsten oxide, the nature of cations present in the solution as surfactant or templating ion significantly affects the crystallization step and final crystalline phase [364], particularly when an organic cation is used which could result in hybrid organic-inorganic structure. The presence of surprisingly intense peaks at low angles ( $2\theta \leq 10$ ) in the XRD patterns of TO-TPA and TO-TBA struck this idea in mind that a well crystallized kind of polyoxotungstate structure has been formed [364]. Further FTIR, TGA, and elemental analysis confirmed this idea.

FTIR analysis was employed to learn more about the different available tungsten bonds in crystalline structures of the samples as well as composition of the organic moiety. Figure 6.3 shows infrared absorption spectra of the samples. A peak at 633–649 cm<sup>-1</sup> is observed for all the samples, which belongs to stretching vibration of bridging oxygen atom between two tungsten atoms  $\nu(\text{W}-\text{O}-\text{W})$  [369,362,122,364]. Another common peak in the low frequency region is located at 973–1019 cm<sup>-1</sup>, which is sharp in TO-TMA, TO-TPA, and TO-TBA and poorly resolved in TO. This peak is well ascribed to the stretching mode of the terminal W=O double bond [369,365,122,363]. The peak at 587 cm<sup>-1</sup> in TO-TPA and TO-TBA is attributed to W(O)<sub>2</sub> in octahedral WO<sub>6</sub> units of the Keggin structure of these samples [363,364]. The presence of more than one strong W–O stretching bands at wavenumber between 750 and 1000 cm<sup>-1</sup>, like what is observed in spectra of TO-TPA and TO-TBA, is characteristic of Keggin-type structure and therefore, suggests the formation of W<sub>12</sub>O<sub>40</sub><sup>8-</sup> ion [373,374,364]. Detailed assignments of absorption bands of the FTIR spectra are listed in Table 6.2 (Supporting Information).



**Figure 6.3.** FTIR spectra of (a) TO, (b) TO-TMA, (c) TO-TPA, and (d) TO-TBA.

The formation of Keggin clusters in TO-TPA and TO-TBA was also confirmed by thermogravimetric analysis. Figure 6.4 shows TGA curves and the total weight losses of the prepared samples. Owing to the molecular weight of the associated organic moiety, the total weight loss amount decreased in the order of TO-TBA (23.06%) > TO-TPA (17.91%) > TO-TMA (8.26%) > TO (5.64%). The first weight loss, which happened gradually for TO (at  $T < 310$  °C) and more sharply for the  $\text{NR}_4^+$ -encapsulated samples (at  $T \sim 200$  °C), corresponds to the departure of (i) absorbed and/or (ii) bonded water. Absorbed and weakly bonded water normally release at  $T < 200$  °C, however, due to the tendency of tungsten trioxide to keep the water of hydration even at high temperatures, chemisorbed and strongly bonded water release at  $200 < T < 350$  °C as the reaction products of  $\text{W-OH}$  condensation [354,369].

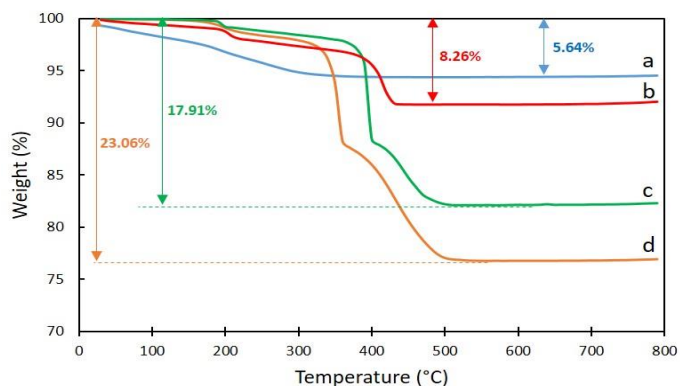


**Figure 6.4.** TGA curves of (a) TO, (b) TO-TMA, (c) TO-TPA, and (d) TO-TBA.

TO-TMA, TO-TPA, and TO-TBA exhibited a second weight loss at  $330 < T < 430$  °C, which arises from the oxidation and consequent removal of the organic moiety, and therefore, increases with the molecular weight of the encapsulated organic cation (4.23, 8.59, and 10.02% for TO-TMA, TO-TPA, and TO-TBA, respectively). In addition to the two aforementioned weight losses, a third weight loss was obtained in the TGA curves of TO-TPA and TO-TBA (Figure 6.4 c and d). Occurrence of this weight loss at higher temperatures, which is another characteristic of Keggin clusters, is due to the decomposition of the Keggin anion ( $[W_{12}O_{40}]^{8-}$ ) into tungsten trioxide. Evidence for this decomposition reaction was found by performing XRD on TO-TBA after TGA (Figure 6.5), which confirms formation of pure orthorhombic  $WO_3$  phase (PDF no. 20-1324). During this decomposition, the Keggin clusters lose all the acidic protons and completely deprotonate [375]. That is why, low thermal stability has always been the main drawback of the POTs.

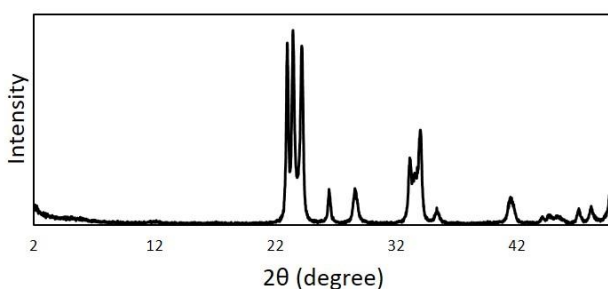


**Figure 6.5.** XRD pattern of TO-TBA after TGA (pure orthorhombic  $WO_3$ , PDF no. 20-1324).

Thermal behavior of the Keggin clusters was more deeply examined by differential thermogravimetry (Figure 6.6). The three weight losses of TO-TBA have been explicitly identified in Figure 6.6 a, along with the temperatures at which the maximum losses happened. The DTA curve (Figure 6.6 b) confirms that the first weight loss, belonging to the evaporation of chemisorbed/physisorbed water molecules, is endothermic. By contrast, the second and third weight losses are exothermic. Great sharpness of the second peak in the DTA curve is due to the considerable amount of energy released from the combustion of carbonaceous compounds of  $TBA^+$ . The exothermicity of the last weight loss stems from the decomposition of the cage like structure of the heteropolyanion compound to yield a more compact crystalline product consisting of a more stable phase (oxides of W(VI)) [376,377,375,124,352]. Differential thermogravimetry

of TO-TPA showed the same trend. According to what was discussed above, thermolysis of the hybrid Keggin clusters of TO-TPA and TO-TBA occurred in three steps, as shown in Scheme 6.1.

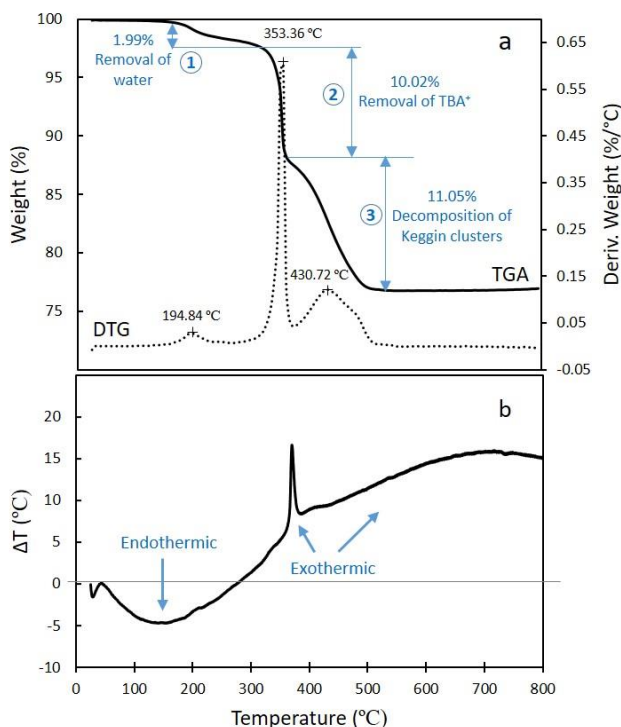
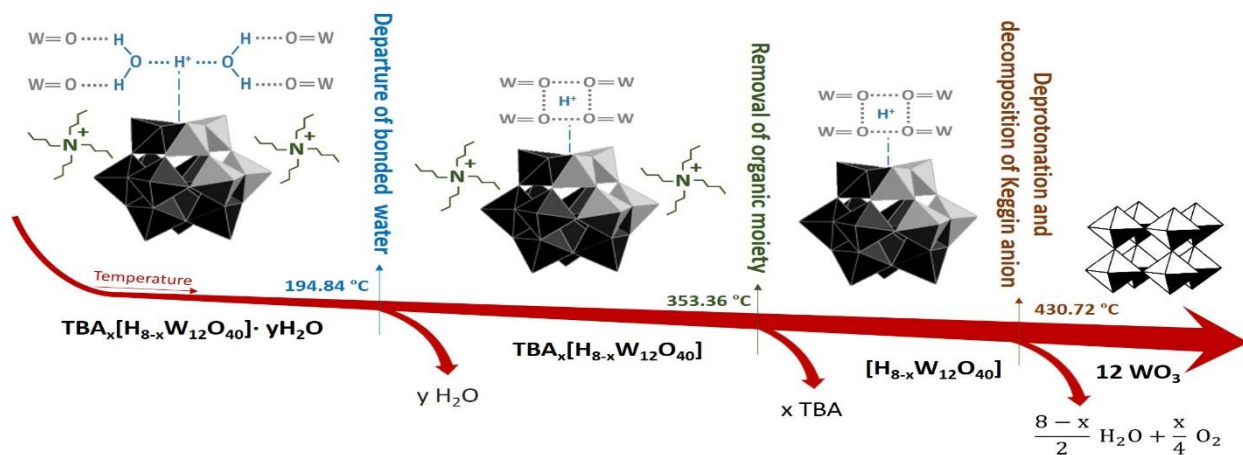


**Figure 6.6.** (a) TGA and DTG ( $dW/dT$ , where  $W$  is weight %) curves and (b) DTA ( $\Delta T = T_s - T_r$  where  $T_s$  is sample's temperature and  $T_r$  is the reference's temperature) curve of TO-TBA versus temperature.



**Scheme 6.1.** Thermolysis of TO-TBA (the bulk proton sites in the Keggin structure are represented as di-aquahydrogen ions,  $H_5O_2^+$ , each of which links four neighboring heteropolyanions by forming hydrogen bonds with the terminal  $W=O$ ).



Furthermore, the second and the third weight losses of TO-TBA have been compared with those of another sample prepared using twice more amount of  $\text{TBA}^+$  (denoted as TO-TBA2, in which the molar ratio of  $\text{TBA}^+/\text{W}$  used in the synthesis was 0.5) in Figure 6.7. The interesting outcome of this comparison is that the third weight loss is independent of  $\text{TBA}^+$  content. Using higher amount of  $\text{TBA}^+$  in TO-TBA2 only increased the second weight loss (pertaining to removal of  $\text{TBA}^+$ ), while the third weight loss (pertaining to decomposition of Keggin structure) remained almost constant. Very slightly higher percentage of the third weight loss in TO-TBA, however, would arise from the slightly lower total molar mass of this sample (owing to the lower  $\text{TBA}^+$  content) compared to TO-TBA2.

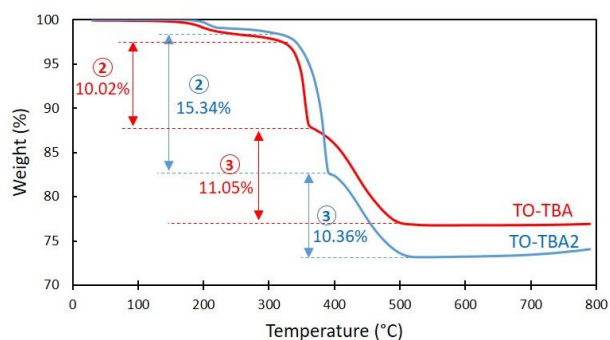


**Figure 6.7.** Comparison of the second and the third weight losses of TO-TBA with those of TO-TBA2.

To understand the detailed morphological characteristics and particles sizes of the resultant products, the TEM technique was employed. Figure 6.8 displays representative transmission electron microscopy images of the samples. As can be seen, TO represents a mixed morphology of nanoplatelet and nanorod, most probably due to the coexistence of two hydrated  $\text{WO}_3$  phases ( $\text{WO}_3 \cdot 0.33\text{H}_2\text{O}$  and  $\text{WO}_3 \cdot \text{H}_2\text{O}$ ) as discussed earlier. The samples prepared with  $\text{NR}_4^+$  exhibited significant changes in morphology and particle size. The mixed crystalline phase of TO-TMA (hydrated tungsten oxides and  $[\text{MA}_x\text{WO}_{3+x/2} \cdot n\text{H}_2\text{O}]$ ) resulted in a mixed morphology; (i) anisotropic rod-like microstructure with diameters between 300–600 nm and microscale lengths, and (ii) aggregated nanorods and nanoneedles are observed in Figure 6.8 b (see more TEM images of this sample, TO, TO-TMA1/2, and TO-TMA2 in the Supporting Information, Figure 6.10). The bigger crystal sizes of TO-TPA and TO-TBA (Figure 6.8 c and d) stem from their Keggin-like structures. Comparison of the cubic shape of crystals of TO-TPA and TO-TBA with lengthwise

shape of crystals of TO-TMA concur with the results of XRD, where comparatively higher growth of crystals in a specific direction was obtained for TO-TMA.

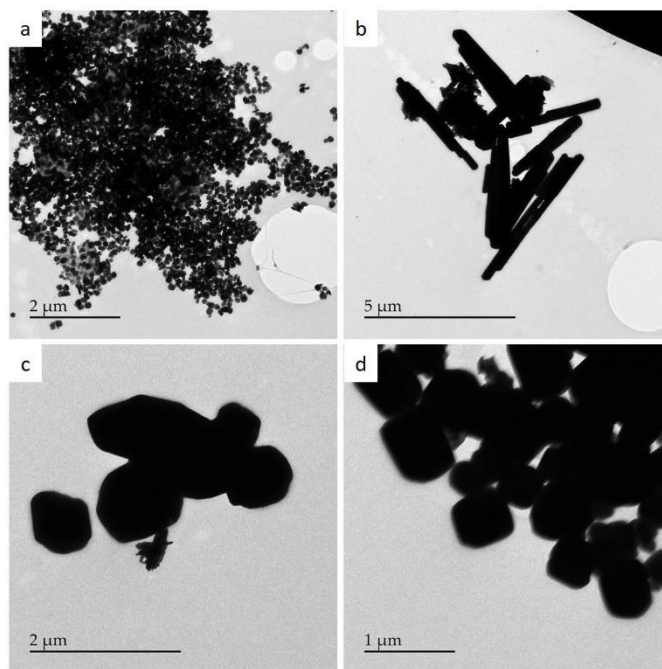


**Figure 6.8.** TEM images of (a) TO, (b) TO-TMA, (c) TO-TPA, and (d) TO-TBA.

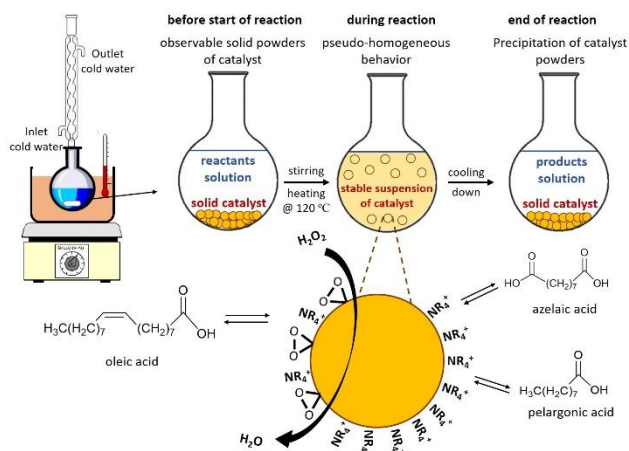
Energy-dispersive X-ray spectroscopy (EDS) of the prepared hybrid inorganic-organic samples (Figure 6.11, Supporting Information) indicate that, except the expected elements (W, C, O, H, and N), there was no other element in the samples structures. Elemental analysis (C/H/N/S analysis) was employed to determine the ratio between Keggin clusters, incorporated organic cations, and associated water. Combining all the above information, the hybrid compounds of TO-TPA and TO-TBA were best and precisely formulated as  $[(\text{CH}_3\text{CH}_2\text{CH}_2)_4\text{N}]_{2.75}[\text{H}_{5.25}\text{W}_{12}\text{O}_{40}] \cdot 7.42\text{H}_2\text{O}$  and  $[(\text{CH}_3\text{CH}_2\text{CH}_2\text{CH}_2)_4\text{N}]_{3.31}[\text{H}_{4.69}\text{W}_{12}\text{O}_{40}] \cdot 1.08\text{H}_2\text{O}$ , respectively. The results of CHNS analysis are shown in Table 6.3 of the Supporting Information.

### 6.3.2 Catalytic tests results

Catalytic efficiency of the prepared catalysts in oxidative cleavage of UFAs were examined in 5 h reaction of oleic acid, the most abundant UFA, with  $\text{H}_2\text{O}_2$  at 120 °C (bath temperature). About 180% excess hydrogen peroxide was used in the reaction to compensate the loss of oxidant

during the reaction via catalytic or thermal decomposition (titrimetry calculation showed 22 to 56% loss of H<sub>2</sub>O<sub>2</sub>, in absence and presence of the catalysts, during a reaction without oleic acid).

During the reaction, the catalysts, except TO, exhibited a pseudo-homogeneous behavior stemming from their organic functionalization and consequent proper adjustment of their surface states. This behavior is schematically represented in Scheme 6.2, along with the reactor setup used. Before starting the reaction, the solid catalyst was clearly observable in the colorless reaction mixture containing oleic acid, H<sub>2</sub>O<sub>2</sub>, and tert-butanol. Upon heating to 120 °C, peroxy moieties on the catalyst were protonated to give surface peroxy groups. Consequently, a light yellow suspension was observed in the reaction mixture, as a result of formation of metal-peroxy complexes,  $-WO(O_2)$ , on surface of the catalyst. Observably, this suspension was stable during the reaction. Evidence for this stability was found by measurement of zeta potential, which intriguingly showed that the absolute potential, and consequently, stability of the suspension [378] increase with the length of organic cation encapsulated in the catalyst's structure (TO-TBA > TO-TPA > TO-TMA, Figures 6.12–6.15). At the end of the reaction, when the majority of H<sub>2</sub>O<sub>2</sub> has been consumed, a low concentration of peroxy groups on the surface and cooling down to room temperature resulted in precipitation of the catalyst particles. This enables self-separation and easy recovery of the catalyst. The increased hydrophobicity of the catalyst caused by encapsulation of NR<sub>4</sub><sup>+</sup> and the bulky molecular geometry of these organic species prevent aggregation of the catalyst particles during the reaction. This gives rise to the excellent activities of the prepared NR<sub>4</sub><sup>+</sup>-encapsulated catalysts despite their relatively non-porous structures (the BET surface areas of the prepared samples are listed in Table 6.4 of the Supporting Information).



**Scheme 6.2.** Schematic view of the reactor setup (left) and the pseudo-homogeneous behavior of TO-TMA, TO-TPA, and TO-TBA catalysts during the reaction.

Table 6.1 reports the conversion of oleic acid and yields of production of the desired products, azelaic and pelargonic acids, over the four prepared catalysts. The catalytic efficiencies presented in this Table are the average of at least 3 runs over each catalyst (details of the quantitative analysis are available in Supporting Information). Compared to TO and TO-TMA, Keggin clusters of TO-TPA and TO-TBA gave higher yields of azelaic and pelargonic acids. The reason most probably stems from the comparatively large number of protons in their structures ( $H_nW_{12}O_{40}$ ), and hence, their strong acidities, for which POTs generally have reputation. It is believed that [39,379-382] tungstenian catalysts direct the oxidative cleavage of olefins with  $H_2O_2$  through epoxidation, then hydrolysis to trans-diols and final re-oxidation to aldehydes, ketones or carboxylic acids. Extension of these steps for oleic acid oxidation is shown in Scheme 6.3 in four steps. It seems that all the catalysts were able to satisfactorily advance the reaction to the third step. Evidence of this is the full conversion of the initial oleic acid over all the catalysts (see Table 6.1) and the emergence of four major peaks in chromatograms of the reactions products, corresponding to (i) azelaic and (ii) pelargonic acids, (iii) nonanal, and (iv) 9-oxononanoic acid (see Scheme 6.3, as well as the chromatograms in Figures 6.16–6.19). Apparently, the differences in the efficiencies of the catalysts arise from their performances in the fourth step, which is hydroxylation of nonanal and 9-oxononanoic acid into pelargonic and azelaic acids, respectively. Admittedly, this acid catalysis reaction could be promoted by the stronger and more stable acidity of the Keggin clusters of TO-TPA and TO-TBA, resulting in higher amounts of azelaic and pelargonic acid produced by

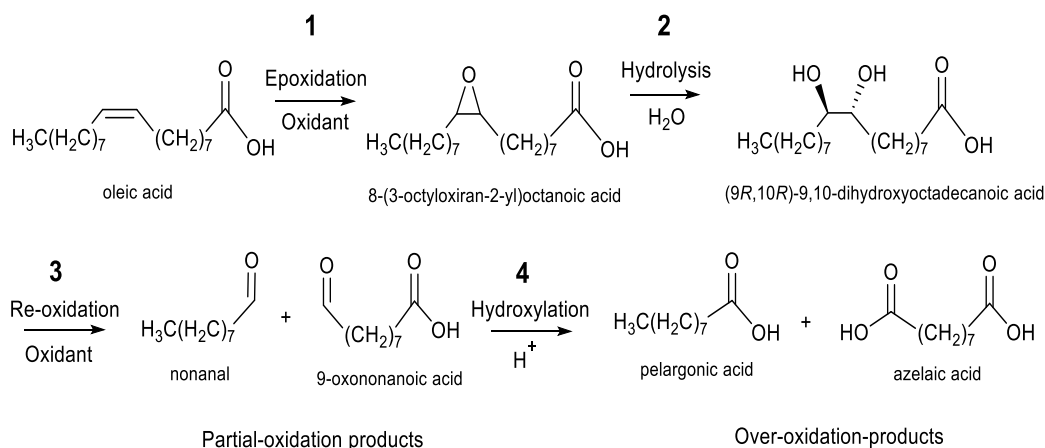
these two catalysts. More detailedly, in the hydroxylation reaction an acid catalyst protonates the carbon of carbonyl group (of the aldehyde or ketone), and makes it highly reactive to accept oxygen from the oxidant, which was used in excess. These solid acids, TO-TPA and TO-TBA, are adequately water-tolerant, as a result of the organo-functionalization, to keep their acid sites during the multi-step oxidative cleavage reaction. Moreover, they do not possess the common disadvantages of the conventional acids (e.g.  $\text{H}_2\text{SO}_4$  and  $\text{AlCl}_3$ ) such as high toxicity, catalyst waste, corrosion, difficulty of separation and recovery.

**Table 6.1.** Catalytic tests results (conversion of oleic acid and yields of production of desired products).

Catalyst	Chemical structure	Conversion (%) <sup>1</sup>	Y <sub>AA</sub> (%) <sup>2</sup>	Y <sub>PA</sub> (%) <sup>2</sup>
No catalyst	-	41	2	4
TO	$\text{WO}_3 \cdot n\text{H}_2\text{O}$	100	49	50
TO-TMA	$\text{WO}_3 \cdot n\text{H}_2\text{O}$ and $[\text{MA}_x\text{WO}_{3+x/2} \cdot n\text{H}_2\text{O}]$	100	62	61
TO-TPA	$[(\text{CH}_3\text{CH}_2\text{CH}_2)_4\text{N}]_{2.75}[\text{H}_{5.25}\text{W}_{12}\text{O}_{40}] \cdot 7.42\text{H}_2\text{O}$	100	72	69
TO-TBA	$[(\text{CH}_3\text{CH}_2\text{CH}_2$	100	79	78

1. Reaction conditions: time: 5 h, temperature: 120 °C (bath temperature), solvent: tert-butanol, initial amounts of oleic acid: 1 g, t-butanol: 7.5 mL,  $\text{H}_2\text{O}_2$ : 4 mL, catalyst: 0.45 g, agitation rate  $\approx$  400 rpm.

2. Y: Yield (molar), in this work, is defined as the amount of a product formed per total amount of oleic acid consumed (both in moles; Y<sub>AA</sub>: yield of azelaic acid, Y<sub>PA</sub>: yield of pelargonic acid).



**Scheme 6.3.** Different steps of oxidative cleavage of oleic acid with  $\text{H}_2\text{O}_2$  over the W-based catalysts.

### 6.3.3 Recyclability of the catalysts

All the prepared catalysts were recovered after the reactions to examine their stability and recyclability up to four cycles. Separation of the catalysts from the reaction mixture was

conveniently performed by simple centrifugation. No significant loss of catalyst was obtained (Table 6.5 lists the exactly measured weight loss of the catalysts after each reaction cycle, which were generally less than 2.3%). Comparatively higher weight loss of TO would arise from the hydrophilic nature of this catalyst resulting in gradual leaching of the catalyst in the water-involving reaction.

The stability of the chemical structures of the catalysts was examined by performing FTIR analysis on the recovered catalysts after each cycle (Figure 6.20). All the samples demonstrated almost the same FTIR spectra to their original ones, which implies that they essentially kept their chemical nature during the reaction. Accordingly, no decay of catalytic activity was obtained, particularly for the  $\text{NR}_4^+$ -encapsulated samples. TO-TMA, TO-TPA, and TO-TBA were able to fully convert the initial oleic acid even after four cycles, however the conversion obtained over TO slightly decreased to 96% at the fourth cycle. Similarly, a modest decrease was obtained in the yields of production of azelaic and pelargonic acids by TO in four cycles, while the yields obtained by the three other catalysts were almost constant. Figure 6.9 shows the yields of production of azelaic acid in the four cycles. The excellently steady reusability of the  $\text{NR}_4^+$ -encapsulated catalysts most probably stems from their enhanced hydrophobicity and proper adjustment of the catalyst's surface state resulting in prevention of poisoning of acid sites by water during the reaction, particularly for the Keggin clusters of TO-TPA and TO-TBA which are inherently a perfect water-tolerant catalyst owing to their special crystalline structure [131].

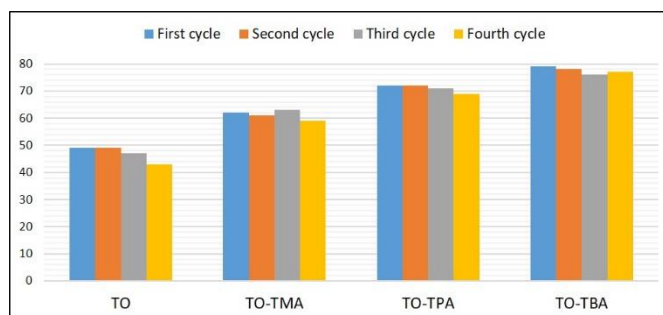


**Figure 6.9.** Yields of production of azelaic acid over the prepared catalysts in four cycles (reaction conditions: time: 5 h, temperature: 120 °C (bath temperature), solvent: tert-butanol, initial amounts of oleic acid: 1 g, t-butanol: 7.5 mL,  $\text{H}_2\text{O}_2$ : 4 mL, catalyst: 0.45 g, agitation rate  $\approx$  400 rpm).

In order to verify that the reaction is truly catalyzed by solid catalyst (and not by dissolved or leached particles, given the obtained pseudo-homogeneous behavior, as discussed) and to examine the leaching of tungsten oxide species in the reaction solution, a catalytic test was performed over TO-TBA and was paused after 2.5 h of reaction, which showed 48% conversion and  $\approx 30\%$  yields of azelaic and pelargonic acids. After cooling down to room temperature, the catalyst was removed, and then, the reaction solution was exposed to the reaction conditions for the remaining reaction time (2.5 h). The conversion increased somewhat (to 59%) in the second 2.5 h, due to the presence of oxidant which could advance the reaction lonely up to the intermediate steps (Scheme 3). The changes in the yields, however, were quite negligible, implying lack of any catalytically active species in the reaction medium. This confirms no significant leaching of catalyst. Further kinetic studies, optimization of the reaction conditions, and the reaction mechanism investigations are currently underway in our lab, and could be the subject of another work.

## 6.4 Conclusion

In summary, the hybrid organic-inorganic catalysts were simply and greenly prepared under mild hydrothermal conditions by adding hydrogen peroxide to bare tungsten powder and facile encapsulation of three  $\text{NR}_4^+$  cations with different chain lengths,  $\text{TMA}^+$ ,  $\text{TPA}^+$ , and  $\text{TBA}^+$ . Driving benefit from metastability of the tungsten oxide, that has relatively open structures, the amorphous peroxotungstic acid particles formed upon dissolution of W powder in  $\text{H}_2\text{O}_2$  were directed to form the Keggin clusters in the presence of  $\text{TPA}^+$  and  $\text{TBA}^+$  cations, while in the absence of any organic moiety simple tungsten trioxide was obtained. The key impacts of the organic cation on the final product was investigated by different characterization techniques. The prepared catalysts were then employed in oxidative cleavage of oleic acid, the most abundant UFA, with  $\text{H}_2\text{O}_2$ . Thanks to the organo-functionalization, the hybrid catalysts exhibited a pseudo-homogeneous behavior resulting in formation of a stable suspension in the reaction. This, along with the strong and organo-protected acidity of the Keggin clusters of TO-TPA and TO-TBA, gives rise to superior catalytic efficiencies despite of the non-porous structures of these catalysts. Furthermore, the prepared solid acids exhibited the advantages of self-separation, ease of recovery, and steady reusability up to four reaction cycles. Given a pioneer application of Keggin-based heterogeneous catalysts in oxidation

of UFAs in this work, the wide variety of organic groups, and the rapid development of oleochemical industries, we hope that this study will encourage future works to enhance the versatility of the hybrid organic-inorganic POTs in several liquid-phase reactions of oils and fats.

### **Acknowledgements**

This work was supported by the Natural Science and Engineering Research Council of Canada (NSERC) through the INNOV-UC and Discovery grants. The authors wish to thank the industrial partners (Oleotek and SiliCycle Inc.) for stimulating discussions and comments.



## 6.5 Supporting Information

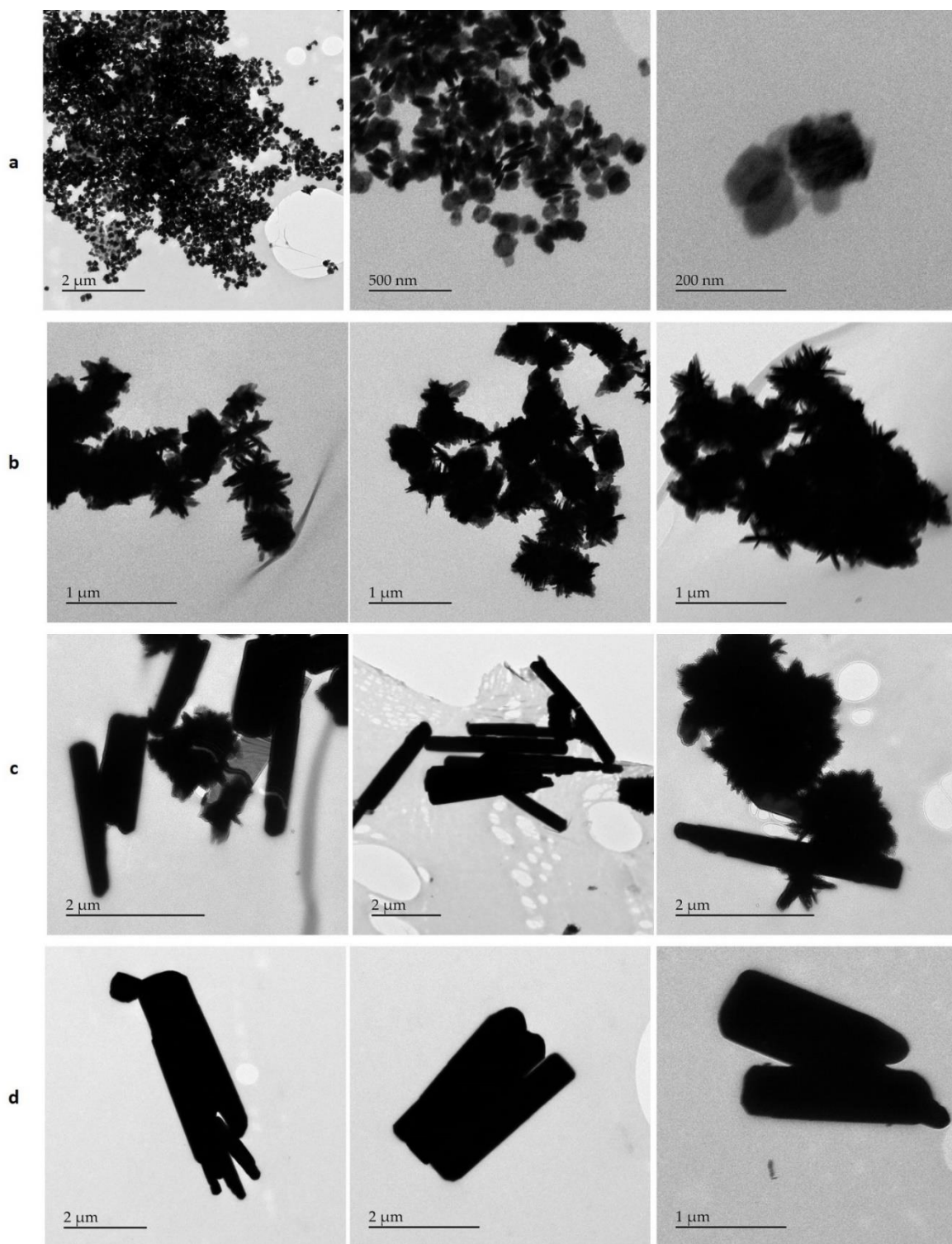


**Figure 6.10.** Additional TEM images of (a) TO, (b) TO-TMA1/2, (c) TO-TMA, and (d) TO-TMA2.

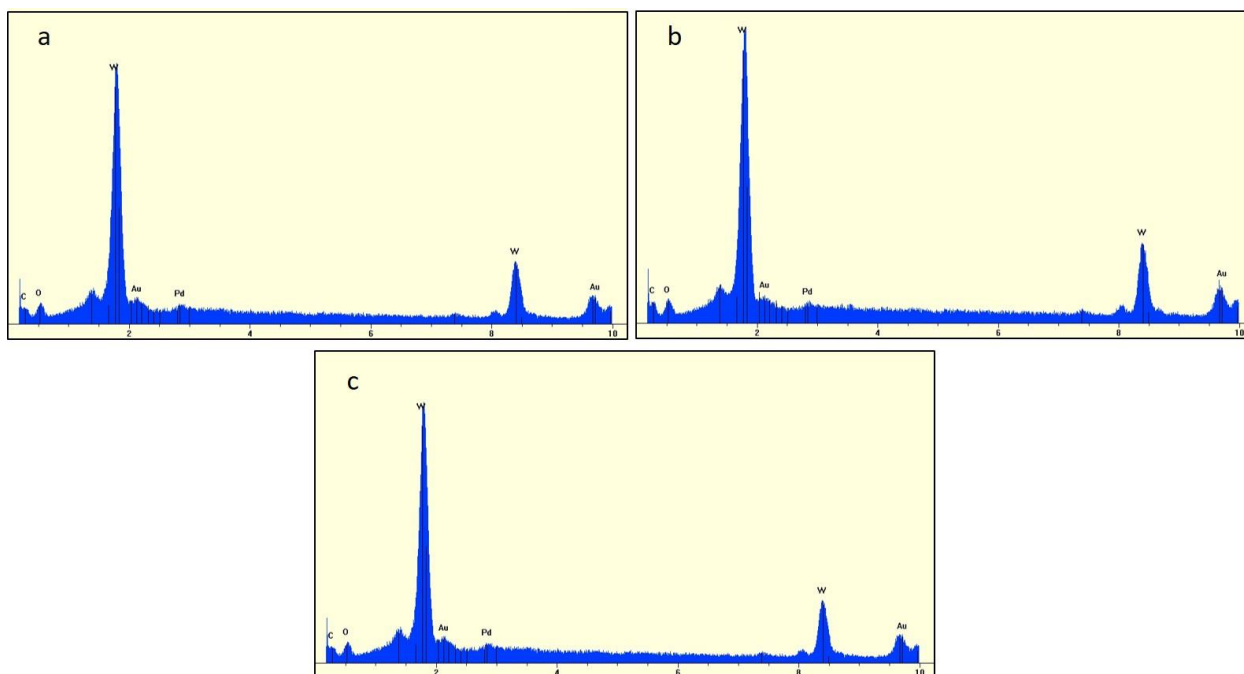


**Figure 6.11.** EDS spectra of (a) TO-TMA, (b) TO-TPA, and (c) TO-TBA (Au and Pd are from the instrument).

	Mean (mV)	Area (%)	St Dev (mV)
<b>Zeta Potential (mV): -6.56</b>	<b>Peak 1: -6.56</b>	100.0	4.29
<b>Zeta Deviation (mV): 4.29</b>	<b>Peak 2: 0.00</b>	0.0	0.00
<b>Conductivity (mS/cm): 0.328</b>	<b>Peak 3: 0.00</b>	0.0	0.00

**Result quality : Good**

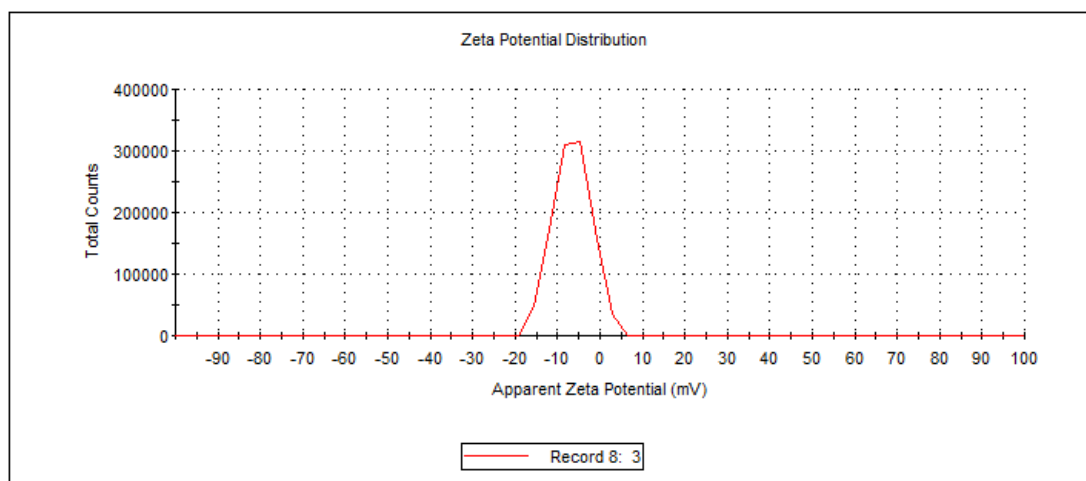


**Figure 6.12.** Surface zeta potential of TO particles (pH 1.7–1.9).

	Mean (mV)	Area (%)	St Dev (mV)
<b>Zeta Potential (mV):</b> -35.9	<b>Peak 1:</b> -35.9	100.0	7.25
<b>Zeta Deviation (mV):</b> 7.25	<b>Peak 2:</b> 0.00	0.0	0.00
<b>Conductivity (mS/cm):</b> 0.0526	<b>Peak 3:</b> 0.00	0.0	0.00

**Result quality :** Good

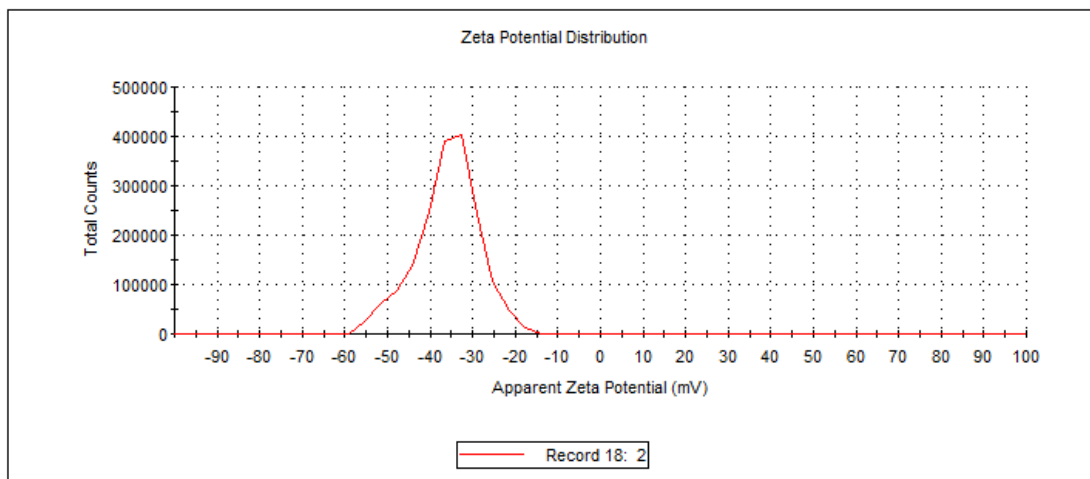


**Figure 6.13.** Surface zeta potential of TO-TMA particles (pH 1.7–1.9).

	Mean (mV)	Area (%)	St Dev (mV)
<b>Zeta Potential (mV):</b> -41.3	<b>Peak 1:</b> -41.3	100.0	8.18
<b>Zeta Deviation (mV):</b> 8.18	<b>Peak 2:</b> 0.00	0.0	0.00
<b>Conductivity (mS/cm):</b> 0.0437	<b>Peak 3:</b> 0.00	0.0	0.00

**Result quality :** Good

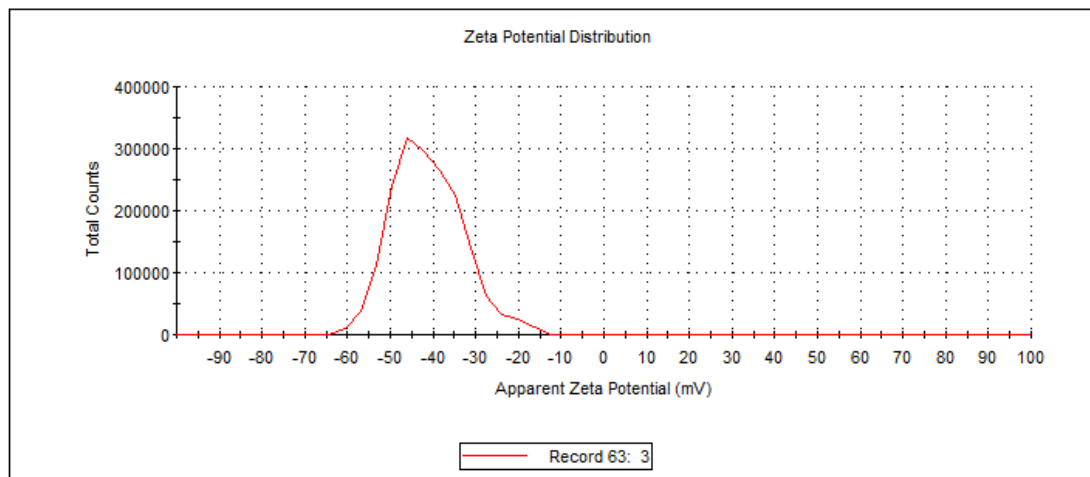


**Figure 6.14.** Surface zeta potential of TO-TPA particles (pH 1.7–1.9).

	Mean (mV)	Area (%)	St Dev (mV)
Zeta Potential (mV): -49.4	Peak 1: -49.4	100.0	8.13
Zeta Deviation (mV): 8.13	Peak 2: 0.00	0.0	0.00
Conductivity (mS/cm): 0.0414	Peak 3: 0.00	0.0	0.00

Result quality : Good

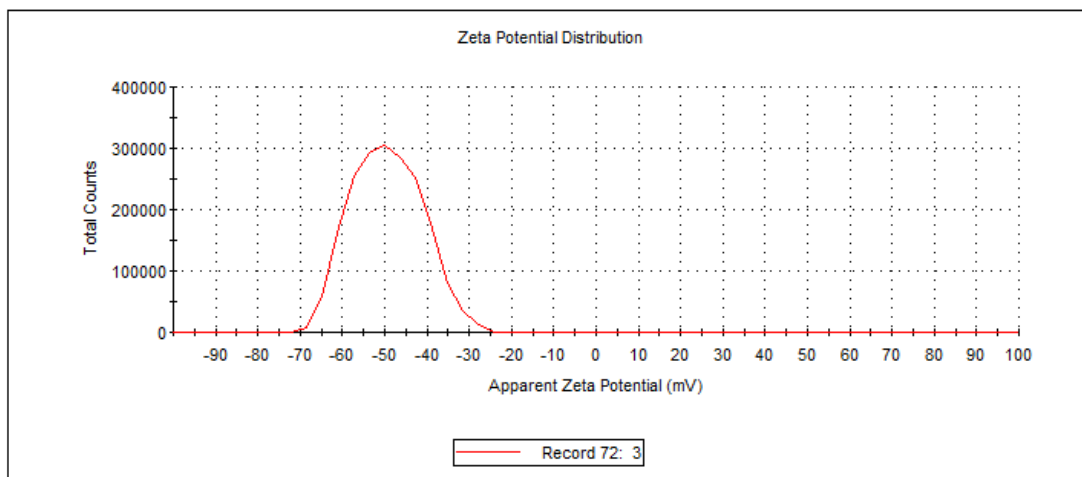


Figure 6.15. Surface zeta potential of TO-TBA particles (pH 1.7–1.9).

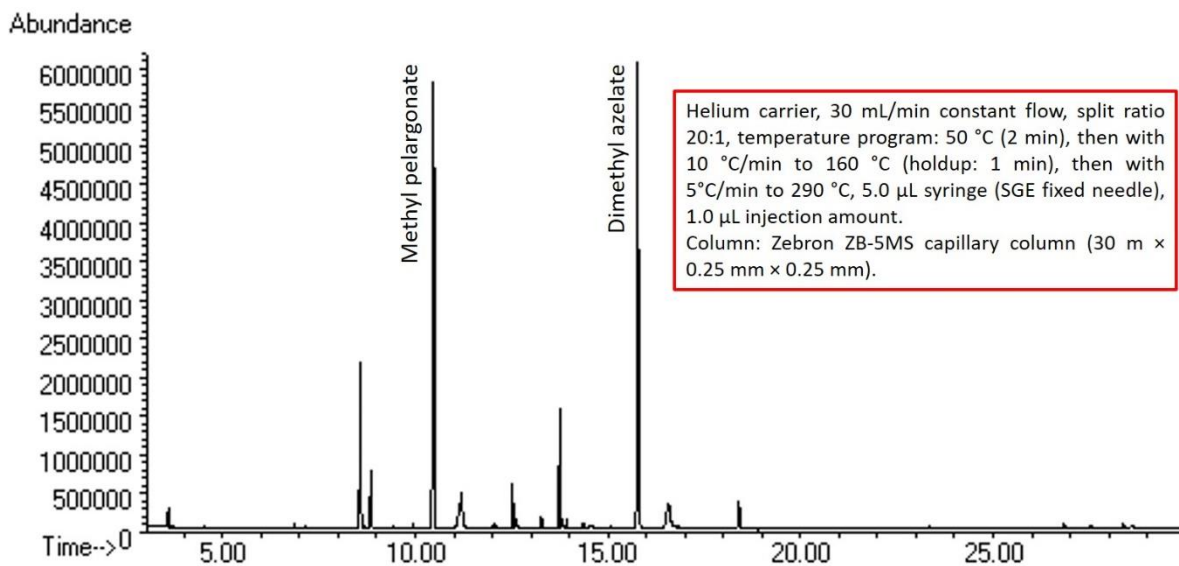
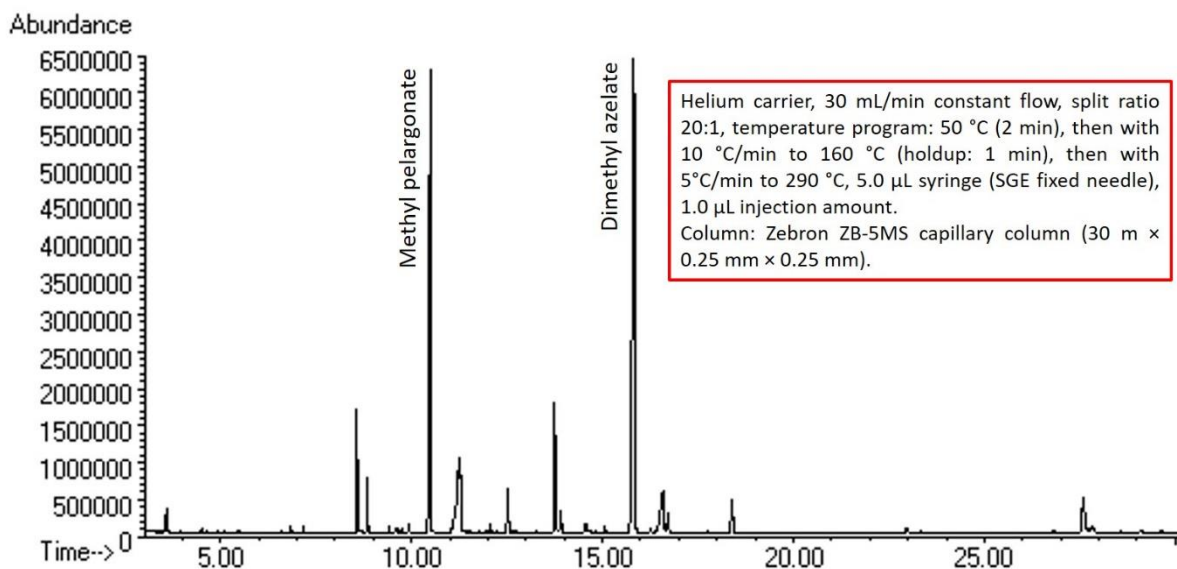
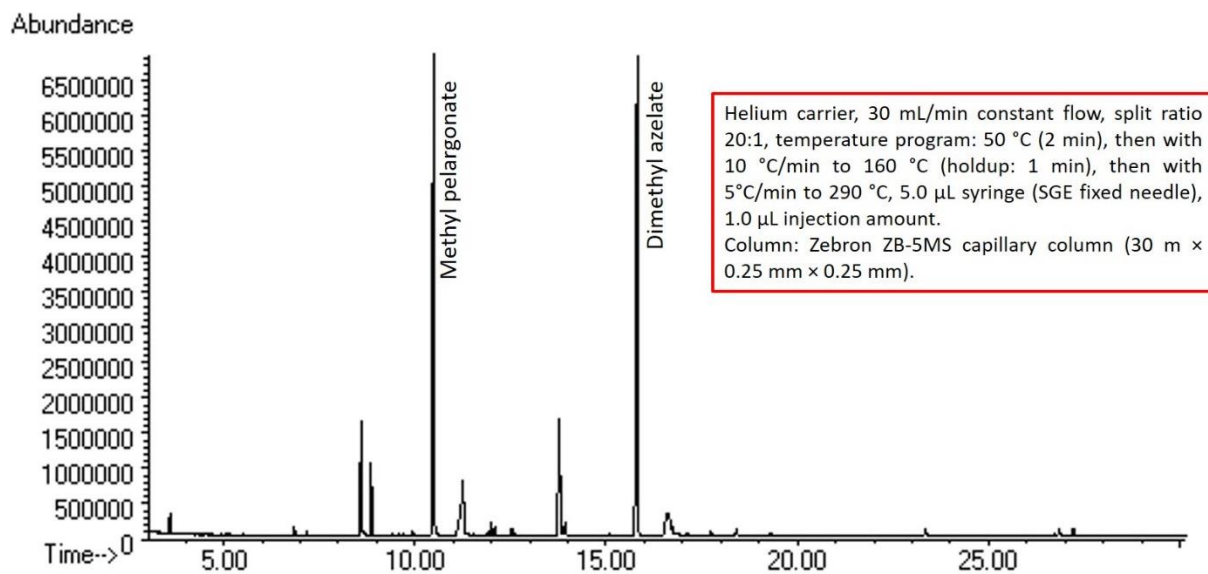


Figure 6.16. Gas chromatogram of products of the catalytic test over TO catalyst.



**Figure 6.17.** Gas chromatogram of products of the catalytic test over TO-TMA catalyst.



**Figure 6.18.** Gas chromatogram of products of the catalytic test over TO-TPA catalyst.

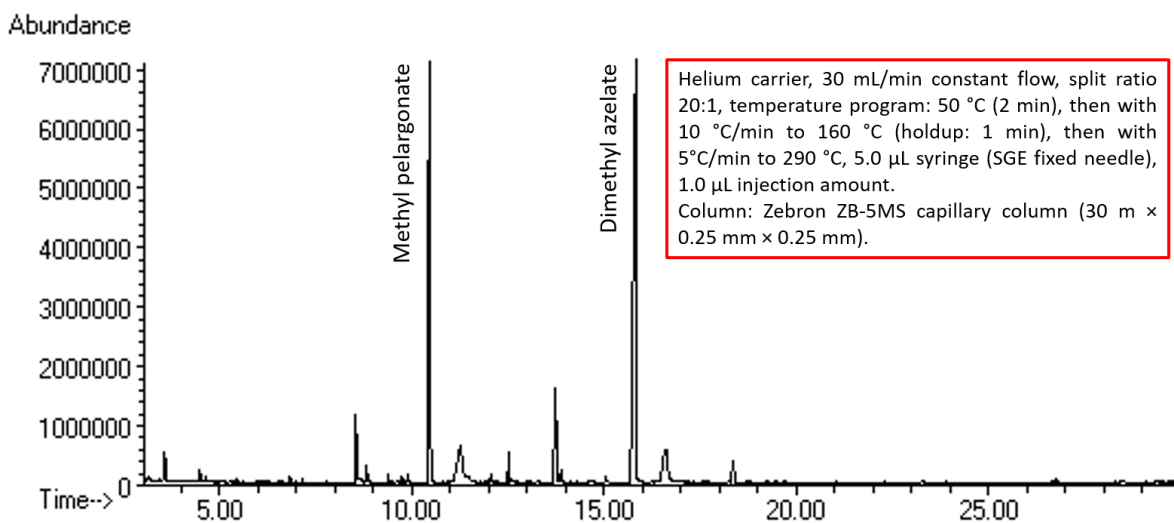


**Figure 6.19.** Gas chromatogram of products of the catalytic test over TO-TBA catalyst.

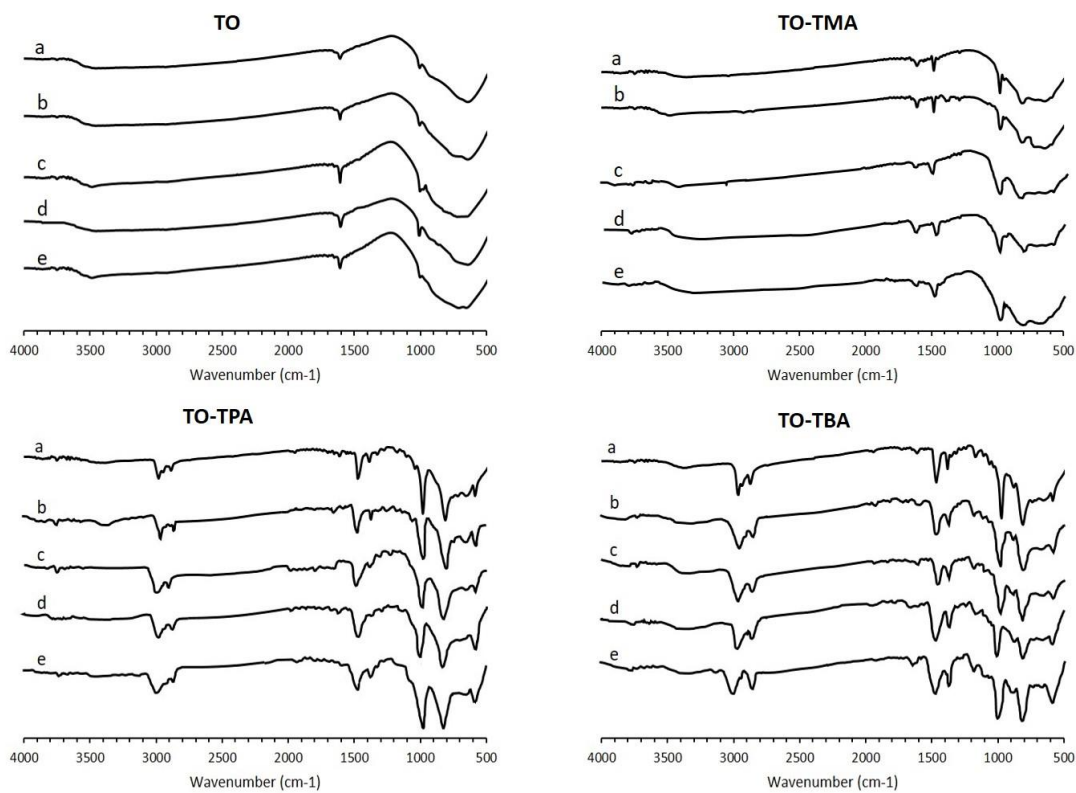


**Figure 6.20.** FTIR spectra of the catalysts: (a) before reaction, (b) after 1<sup>st</sup> cycle, (c) after 2<sup>nd</sup> cycle, (d) after 3<sup>rd</sup> cycle, and (e) after 4<sup>th</sup> cycle.

**Table 6.2.** Assignments of the FTIR absorption bands of the prepared samples [383].

Absorption bands (cm <sup>-1</sup> )	Assignment	Remarks
587	W (O <sub>2</sub> )	Observed in TO-TPA and TO-TBA
633–649	ν (W-O)	Observed in all the samples
811	ν (W-O)	Observed in TO-TMA, TO-TPA, and TO-TBA
880	ν (W-O)	Observed in TO-TBA
973–1019	ν (W=O)	Observed sharply in TO-TMA, TO-TPA, and TO-TBA, and weakly in TO
1382	CH <sub>2</sub>	Observed in TO-TPA and TO-TBA
1475–1482	ν (CH <sub>3</sub> )	Observed in TO-TMA, TO-TPA, and TO-TBA
1606–1614	δ (H-O-H)	Observed in all the samples
2873–2981	ν (CH <sub>2</sub> )	Observed in TO-TPA and TO-TBA
3390-3483	ν (H-O-H)	Observed in all the samples

**Table 6.3.** Elemental analysis (C/H/N/S analysis) results for the prepared hybrid materials <sup>1</sup>.

Sample		% Nitrogen	% Carbon	% Hydrogen	% Sulphur
TO-TMA	1st analysis	0.76	2.75	1.14	0.00
	Duplicate	0.83	2.99	1.14	0.00
	Average	0.80	2.87	1.14	0.00
TO-TPA	1st analysis	1.08	11.49	2.62	0.00
	Duplicate	1.06	11.21	2.47	0.00
	Average	1.07	11.35	2.55	0.00
TO-TBA	1st analysis	1.21	17.46	3.43	0.00
	Duplicate	1.20	17.17	3.43	0.00
	Average	1.21	17.31	3.43	0.00

1. The detection limits for the analyses are the following: 0.3 % for C, H, N and 1.0 % for S. The ratios between Keggin clusters [H<sub>n</sub>W<sub>12</sub>O<sub>40</sub>], incorporated organic cations (TPA<sup>+</sup> or TBA<sup>+</sup>), and associated water molecules in compositions of TO-TPA and TO-TBA were calculated based on C% and H%. Accordingly, the stoichiometric formulas of these hybrid compounds were suggested. Then, the accuracy was validated by determining the amount of N% from the obtained formula. This gives 1.10 and 1.26% for TO-TPA and TO-TBA, respectively, which are in good agreement with those obtained from the elemental analysis (above Table, 1.07 and 1.21%, respectively).

**Table 6.4.** BET surface areas of the prepared samples.

Sample	TO	TO-TMA	TO-TPA	TO-TBA
$S_{\text{BET}}$ (m <sup>2</sup> /g)	16.8	13.3	≤ 10	≤ 10

**Table 6.5.** Weight losses of the synthesized catalysts during the different cycles of the reaction.

Reaction cycle	TO	TO-TMA	TO-TPA	TO-TBA
1 <sup>st</sup>	2.3	2.1	1.9	2
2 <sup>nd</sup>	2.1	1.7	2.1	1.8
3 <sup>rd</sup>	1.9	1.3	1.5	1.2
4 <sup>th</sup>	2.1	1.7	1.6	1.6



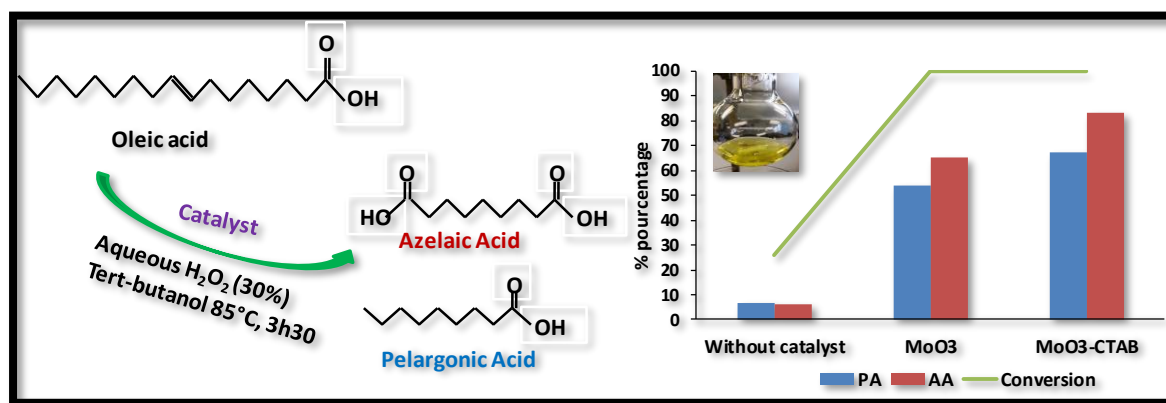
# Chapter 7. Sustainable oxidative cleavage of vegetable oils into diacids by organo-modified molybdenum oxide heterogeneous catalysts

Aimé Serge Ello<sup>1,2</sup>, Amir Enferadi-kerenkan<sup>1</sup>, Albert Trokourey<sup>2</sup>, Trong-on Do<sup>1\*</sup>

1. Department of Chemical Engineering, Laval University, Quebec, G1V 0A6, Canada.
2. Université Félix Houphouët-Boigny de Cocody, Laboratoire de Chimie Physique, 22 bp 582 Abidjan, Côte d'Ivoire.

*Journal of the American Oil Chemists' Society, 2017, 94, 1451-1461*

*Aimé Serge Ello and Amir Enferadi-kerenkan contributed equally to this work.*



## Résumé

L'exploitation d'huiles végétales pour produire des diacides d'une valeur industrielle via un processus respectueux de l'environnement nécessite un catalyseur efficace et recyclable. Dans ce travail, un nouveau système catalytique à base de trioxyde de molybdène organo-modifié a été synthétisé par une méthode hydrothermale verte en une seule étape, en utilisant de la poudre de Mo comme précurseur, du peroxyde d'hydrogène et des tensioactifs amphiphiles. comme agents de coiffage. Les matériaux synthétisés ont d'abord été caractérisés par différentes techniques comprenant XRD, SEM, TGA et FTIR. De manière intéressante, diverses morphologies ont été obtenues en fonction de la nature des agents tensioactifs et des conditions synthétiques. Les catalyseurs synthétisés ont été utilisés dans le clivage oxydatif de l'acide oléique, l'acide gras insaturé le plus abondant, pour produire des acides azélaïques et pélargoniques avec un oxydant bénin, H<sub>2</sub>O<sub>2</sub>. D'excellentes activités catalytiques conduisant à une conversion complète de l'acide oléique initial ont été obtenues, notamment pour l'oxyde de molybdène coiffé de CTAB (rapport molaire CTAB / Mo de 1: 3) qui ont respectivement donné 83 et 68% de production d'acides azélaïque et pélargonique. Ce sont les rendements les plus élevés obtenus jusqu'à présent pour cette réaction par des catalyseurs hétérogènes. De plus, le catalyseur coiffé de CTAB peut être commodément séparé du mélange réactionnel par simple centrifugation et réutilisé sans perte significative d'activité jusqu'à au moins 4 cycles.

## Abstract

Exploiting vegetable oils to produce industrially valuable diacids via an eco-friendly process requires an efficient and recyclable catalyst. In this work, a novel catalytic system based on organo-modified molybdenum trioxide was synthesized by a green hydrothermal method in one simple step, using Mo powder as precursor, hydrogen peroxide, and amphiphilic surfactants cetyltrimethylammonium bromide (CTAB) and tetramethylammonium bromide (TMA) as capping agents. The synthesized materials were, first, characterized by different techniques including XRD, SEM, TGA, and FTIR. Interestingly, various morphologies were obtained depending on the nature of the surfactants and synthetic conditions. The synthesized catalysts were employed in oxidative cleavage of oleic acid, the most abundant unsaturated fatty acid, to produce azelaic and pelargonic acids with a benign oxidant,  $\text{H}_2\text{O}_2$ . Excellent catalytic activities resulting in full conversion of initial oleic acid were obtained, particularly for CTAB-capped molybdenum oxide (CTAB/Mo molar ratio of 1:3) that gave 83 and 68% yields of production of azelaic and pelargonic acids, respectively. These are the highest yields that have been obtained for this reaction on heterogeneous catalysts up to now. Moreover, the CTAB-capped catalyst could be conveniently separated from the reaction mixture by simple centrifugation and reused without significant loss of activity up to at least 4 cycles.

## 7.1 Introduction

A Biomass-derived feedstock is one of the most promising candidates that would substitute the crude oil-based fuels and chemicals. The vast abundance and renewable nature of vegetable oils have attracted growing interest in both academic and industrial researches. Triglycerides are the main component of oleaginous feedstock, i.e. vegetable oils, the unsaturated fatty acids of which can be chemically modified, mainly through their double bonds, to be converted into value-added chemicals. For instance, oleic acid, the most abundant monounsaturated fatty acid [338], can produce a di- and a mono-carboxylic acids, azelaic and pelargonic acids, through oxidative cleavage reaction. These are valuable materials for different industrial applications like production of polymers, plasticizers, adhesives, lubricants, cosmetics, herbicides, fungicides etc. [2,4,1,5,3]. Currently, the oxidative cleavage of oleic acid is performed in industry via ozonolysis. However, using ozone is not in line with the principles of sustainable chemistry due to its inevitable hazardous problems. Attempting to employ a benign oxidant, several catalyst/oxidant systems, in homogeneous and heterogeneous forms, have been reported in the literature for oxidative cleavage of unsaturated fatty acids, which have been thoroughly reviewed in our recent review paper [91].

Homogeneous catalysts have generally shown excellent performances in oxidation of unsaturated fatty acids (e.g. production yield of azelaic acid up to 82% from oleic acid by peroxo complex, oxoperoxo (pyridine-2,6-dicarboxylato) molybdenum (VI) hydrate ( $\text{Mo}(\text{O}_2)[\text{C}_5\text{H}_3\text{N}(\text{CO}_2)_2](\text{H}_2\text{O})$ ) catalysts [3]), but such catalytic systems have been always associated with lack of catalyst recovery. On the other hand, activities of heterogeneous catalysts, with recovery ability, reported so far, are not as high as homogeneous ones [91,45]. Various strategies have been reported in the literature to improve the efficiency of the reaction, like reaction in supercritical fluids with dual oxidants and microwave irradiations and ultrasound-assisted reactions [339,384,58,57]. Works should be encouraged to find a suitable reaction strategy that enjoys both high activity and efficient recovery. Current efforts in this domain can be generally classified into two groups. The first group is involving different transition metal oxide catalysts, which are inherently solid, along with a benign oxidant such as hydrogen peroxide or sodium hypochlorite, and the second group is based on heterogenization of highly active homogeneous catalysts, like polyoxometallates, via immobilization or solidification methods [385,252,186,191]. In these two groups, direct or indirect

selective oxidative cleavage mechanisms have been proposed [386]. Nevertheless, an efficient heterogeneous catalytic system that can afford the excellent reaction yields obtained with the homogeneous catalysts has not been reported so far.

In this work, we have tried to extend the proved potential of molybdenum oxide as an oxidizing solid catalyst [387-389] to oxidative cleavage reaction of unsaturated fatty acids. Curiously, employing MoO<sub>3</sub> heterogeneous catalysts in oxidative cleavage of oleic acid has not been reported so far, to our knowledge. Herein, a series of molybdenum oxides were synthesized via simple oxidative dissolution of Mo powder in H<sub>2</sub>O<sub>2</sub>, with and without organic surfactants. Two well-known quaternary ammonium surfactants, cetyltrimethylammonium bromide (CTAB) and tetramethylammonium bromide (TMA) with different alkyl chain lengths were employed as capping agents. The effects of CTAB and TMA in different concentrations in the synthesis medium on physicochemical properties and morphology of the products, as well as enhancement of catalytic efficiency in the liquid phase oxidative cleavage of oleic acid by organo-modification of the surface of molybdenum oxide have been investigated.

## **7.2 Experimental**

### **7.2.1 Synthetic details**

Surfactant-capped molybdenum oxide particles were synthesized by hydrothermal method using molybdenum powder (99.9%, Alfa Aesar), hydrogen peroxide (30%, Fischer Scientific) and surfactants; CTAB (98%, Fischer Scientific), and TMA (98%, Aldrich). In a typical synthesis, 1 g of metallic molybdenum powder was added to 10 ml of deionized water and the mixture was stirred for 30 minutes at room temperature. Then, the mixture was placed in an ice bath under a well-ventilated fume hood. To this mixture, an aqueous solution of hydrogen peroxide was added dropwise under vigorous stirring until the color of the solution changed to yellow (attention: the reaction is very exothermic and must be done in an ice bath under skilled supervision). The determined amounts of surfactants (CTAB or TMA) to obtain surfactant/ molybdenum molar ratios of 1:2, 1:3, 1:4, were added to the yellow solution. The resultant slurry was refluxed at 100 °C for 4 hours. Finally, the solid product was separated by centrifugation at high speed and dried in air at 70 °C for 10 h.

## 7.2.2 Characterization equipment

The physicochemical properties of the materials were characterized by X-ray diffraction (XRD), Scanning electron microscopy (SEM), Thermo-gravimetric analysis (TGA) and Fourier transform infra-red spectroscopy (FT-IR). Powder X-ray diffraction (XRD) patterns of the samples were obtained on a Bruker SMART APEXII X-ray diffractometer equipped with a Cu K $\alpha$  radiation source ( $\lambda = 1.5418 \text{ \AA}$ ) with steps of  $0.02^\circ$  and step time of 1 second. Scanning electron microscopy (SEM) images were taken on a JEOL 6360 instrument at an accelerating voltage of 3 kV. Materials were spread on a carbon tape prior to analysis. The FT-IR spectra were recorded on an FTS 45 infrared spectrophotometer with the KBr pellet technique. Thermo-gravimetric analyses (TGA) were performed in the temperature range of 30 °C to 800 °C with a TGA Q500 V20.13 Build 39 thermo-gravimetric analyzer at a heating rate of 5 °C min<sup>-1</sup> under an air flow or argon flow of 50 mL min<sup>-1</sup>.

## 7.2.3 Catalytic test

Catalytic reactions were carried out in a glass reactor equipped with an oil bath, magnetic stirrer, and reflux condenser. Typically, the reactor was charged with a suspension of 0.4 g catalyst and 4 ml aqueous H<sub>2</sub>O<sub>2</sub>. Then, 1 g oleic acid ( $\geq 99\%$ , Sigma-Aldrich) was added dropwise under stirring followed by addition of 8 mL tert-butanol as solvent. The reaction mixture was heated to 85 °C and kept at this temperature for a reaction time of 3 h 30 min. After the reaction, the solution was allowed to cool down to room temperature. During the reaction, the system showed homogeneous catalysis properties, while upon cooling down at the end of reaction, the catalyst particles were precipitated, enabling self-separation performance. The precipitated catalyst was separated using a centrifuge at 8000 rpm and recovered via washing with ethanol and water several times and drying at 70 °C for 4 h, in order to be used in the next catalytic cycle. The resultant solution then underwent a derivatization process prior to GC-MS analysis.

## 7.2.4 Quantitative analysis of the product

Gas chromatography-mass spectrometry (GC-MS) was used for separation and quantification of methyl esters of fatty acids. Since fatty acids in their free forms are difficult to

analyze with GC (due to their adsorption issues on stationary phase in GC columns), the reaction products were esterified before GC-MS analysis via Metcalfe et al. derivatization procedure [334,335] using boron trifluoride solution in methanol. Briefly,  $\text{BF}_3$ -methanol (5 ml) (10% w/w, Sigma-Aldrich Co.) was added to the solution of products of the oxidation reaction. Then, the solution was heated to 80 °C for 15 min, followed by cooling down at room temperature for about 20 min. The esterified products were extracted by adding 3 ml petroleum ether and 2 ml water. The extraction was repeated for the aqueous phase (lower layer) twice. After dehydration by sodium sulfate and removal of the solvent by passing a steady stream of dry air, the obtained organic phase was ready for injection to GC-MS.

A typical derivatized sample including methyl esters of the involved fatty acids (expectedly dimethyl azelate, methyl pelargonate, and possibly methyl oleate) was injected to the GC-MS which had been previously calibrated by analytical standards of these methyl esters. The GC-MS system included a Hewlett-Packard HP 5890 series GC system and MSD Hewlett-Packard model 5970. The GC system was equipped with Zebron ZB-5MS capillary column (30 m  $\times$  0.25 mm  $\times$  0.25 mm). Helium was used as a carrier gas with the flow rate of 30 mL/min. A split ratio of 15:1 was fixed. The front inlet temperature was 280 °C. The oven temperature program consisted of maintaining at 50 °C for 2 min, then a ramp rate of 10 °C/min to 160 °C followed by a hold-up time of 1 min, and further increase at the rate of 5°C/min to 290 °C. Direct injection was employed with 1  $\mu\text{L}$  injection amount for each run, and the injection was repeated at least four times for each sample to be averaged. HP Chemstation software was used to analyze data.

## 7.3 Results and discussion

### 7.3.1 Characterization of the catalysts

The crystalline structures of the synthesized samples were analyzed by X-ray diffraction. Figure 7.1 represents the X-ray diffraction patterns of the synthesized molybdenum oxides. The sharp peaks indicate the good crystallinity of the products, which were synthesized even without using autoclave and in a short time. XRD pattern of the sample prepared without using any surfactant, denoted as MO, (Figure 7.1a) confirmed that it was composed of  $\text{MoO}_3\cdot\text{H}_2\text{O}$ , in accordance with PDF no. 26-1449 of ICDD library of spectra. The pattern exhibits 5 well-resolved peaks indexed (010), (100), (120), (020), (030) planes of triclinic molybdenum trioxide hydrate

material, and no peaks corresponding to other phases implies the single triclinic phase of this material.

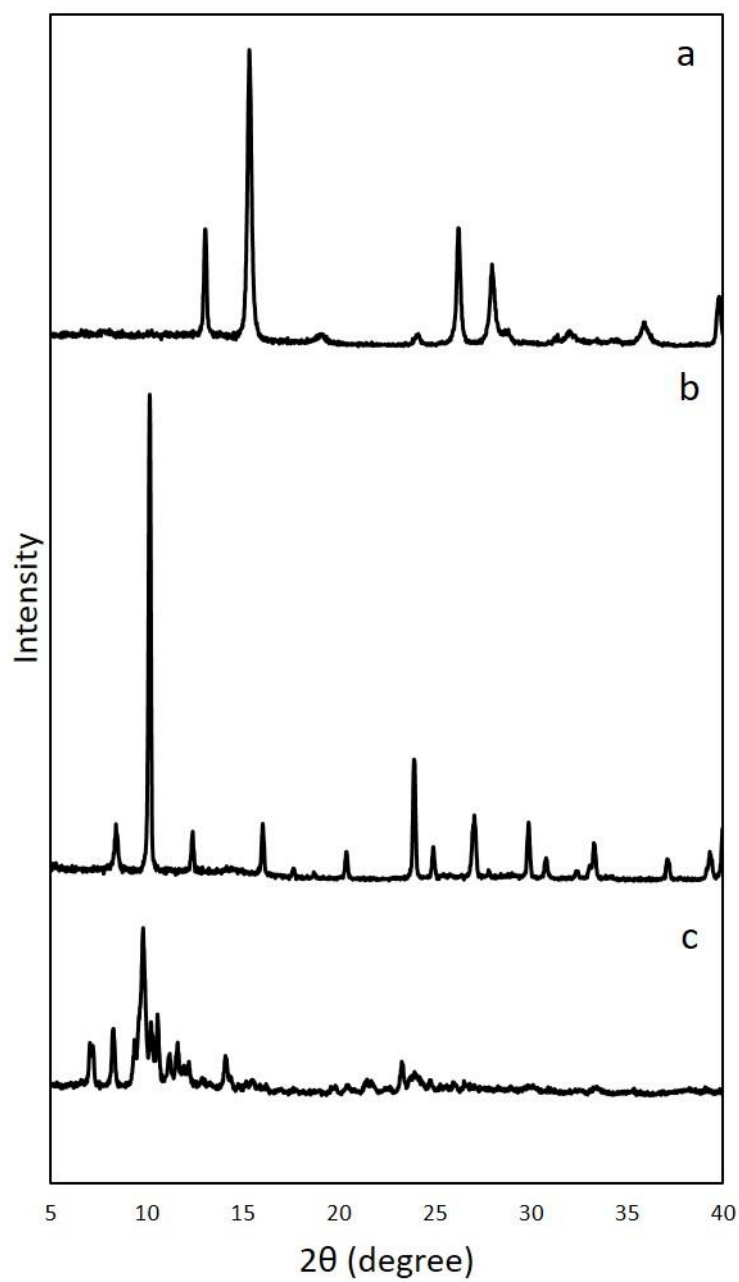


**Figure 7.1.** XRD patterns of the synthesized molybdenum oxides (a) MO (without surfactant) (b) MO-TMA1:2, and (c) MO-CTAB1:2.



The presence of surfactants CTAB and TMA in the synthesis medium dramatically influenced the crystalline phase of molybdenum oxide. Figures 7.1 b and c show XRD patterns of the samples prepared in the presence of these two surfactants with the surfactant/molybdenum molar ratio of 1:2 (denoted as MO-TMA1:2 and MO-CTAB1:2). The XRD pattern of MO-TMA (Figure 7.1b) indicates that the quaternary ammonium cation was incorporated into crystalline structure of the final product. TMA, also, affected the oxidation state of the formed molybdenum oxide. The peaks could be precisely indexed on monoclinic tetramethylammonium tetramolybdate,  $[\text{N}(\text{CH}_3)_4]\text{Mo}_4\text{O}_{12}$  (PDF no. 50-1901), and ammonium octamolybdate tetrahydrate  $(\text{NH}_4)_6\text{Mo}_8\text{O}_{27}\cdot 4\text{H}_2\text{O}$  (PDF no. 50-0607). The surfactant with longer organic chain, CTAB, directed the crystalline phase toward a multiphase structure. As seen in Figure 7.1c, it has much more peaks than the previous samples in  $2\theta$  less than  $15^\circ$ , which could be mainly ascribed to the crystalline phases of  $\text{MoO}_3$  (PDF no. 21-0569), ammonium molybdenum oxide hydrates  $(\text{NH}_4)_6\text{Mo}_7\text{O}_{24}\cdot 4\text{H}_2\text{O}$  (PDF no. 11-0071) and  $(\text{NH}_4)_4(\text{Mo}_8\text{O}_{24.8}(\text{O}_2)_{1.2}(\text{H}_2\text{O})_2)(\text{H}_2\text{O})_4$  (PDF no. 88-1326), and tetramethylammonium tetramolybdate  $[\text{N}(\text{CH}_3)_4]\text{Mo}_4\text{O}_{12}$  (PDF no. 50-1901). This multiphase is probably due to the cationic nature of CTAB during the synthesis reaction, which could be adsorbed by molybdenum oxide nuclei and afterward, it would detach at different times to form multiple phases.

Figure 7.2 shows SEM images of the synthesized materials prepared with and without the surfactants. Apart from 1:2, two other molar ratios of surfactant/molybdenum (1:3 and 1:4) were used in the synthesis to investigate the effects of the surfactant amounts on final morphology. The prepared samples are denoted as MO-CTAB1:4, MO-CTAB1:3, MO-TMA1:4, and MO-TMA1:3. SEM image of MO, synthesized without surfactant, (Figure 7.2a) demonstrates one-dimensional nanorods with a few micrometers length.

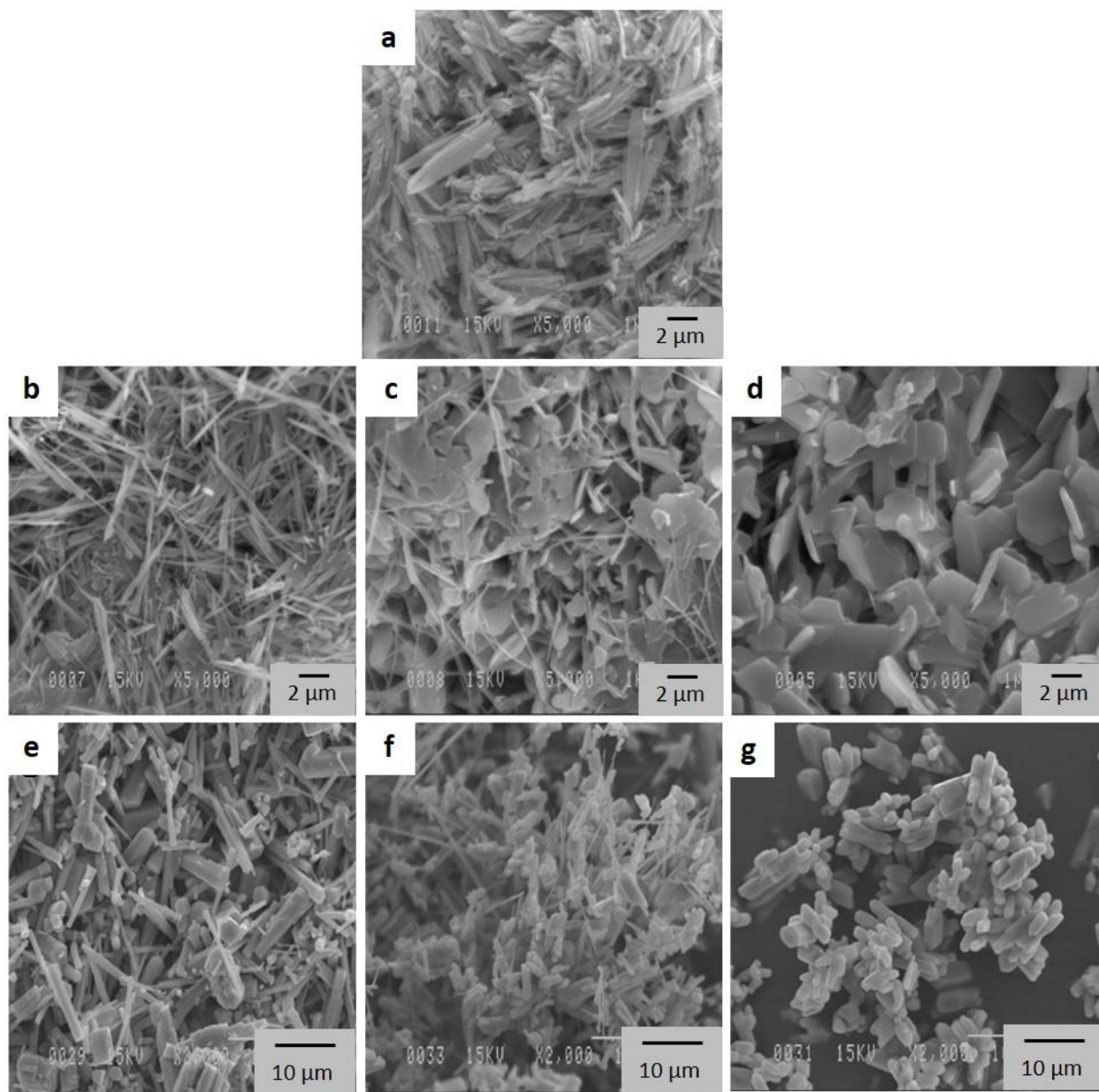


**Figure 7.2.** SEM images of the synthesized molybdenum oxides: (a) MO (b) MO-CTAB1:4, (c) MO-CTAB1:3, (d) MO-CTAB1:2, (e) MO-TMA1:4, (f) MO-TMA1:3, and (g) MO-TMA1:2.

Obviously, different sizes and morphologies were observed depending on the concentration as well as nature of the surfactant used (Figure 7.2 b-g). Lower amount of CTAB in MO-CTAB1:4 (Figure 7.2 b) did not change the morphology significantly; similar nanorods were obtained. Increasing CTAB content in MO-CTAB1:3, however, a heterogeneous mixture of nanorods and

microplatelet-like morphology was obtained (Figure 7.2 c), which became homogeneous microplatelets in MO-CTAB1:2. The effect of high concentration of CTAB is in good agreement with previous works, where stacked micro size of MoO<sub>3</sub> fibers and micro-ellipsoid structure of MoO<sub>3</sub> were predominant [390,391].

Using TMA in the synthesis considerably increased size of the product particles, leading to a heterogeneous mixture of microrods, which turned to agglomerated rods when concentration of TMA increased (Figure 7.2 e-g). By contrast to CTAB, the size of these hybrids particles containing TMA did not change considerably by changing the amount of TMA. From these studies, it can be observed that morphology of the particles has been influenced significantly by the nature of the surfactants.

Generally, the mechanism of MoO<sub>3</sub> formation follows the anisotropic growing of MoO<sub>6</sub> octahedral crystal nuclei as basic building unit of MoO<sub>3</sub> [392,393]. In absence of any surfactant in the synthesis medium, the growth along [010] direction is much more favored, and thus, results in formation of nanofiber, as shown in Figure 7.2 a. Although using a low amount of CTAB in MO-CTAB1:4 did not significantly change the morphology (Figure 7.2 b), further increasing of CTAB in MO-CTAB1:3 and MO-CTAB1:2 led to formation of an emulsion, highly likely because concentration of CTAB reached the critical micelle concentration (CMC). The lipophilic groups of micelles tend to move inward and hydrophobic groups outward. The concentration of CTAB up to 1:3 led to a stable spherical micelle and still generated thin fibers. However, the further increase of CTAB concentration more than CMC increased the deformation of micelle [392]. It has been reported that at higher concentrations of CTAB, the shape of micelles changes from sphere to prolate ellipsoid, and then the preferred orientation growth of MoO<sub>3</sub> is inhibited, resulting in the micro-ellipsoid structure [392]. The concentration of CTAB up to 1:3 led to both spherical and deformed micelles thus the material possesses both fibers and plates morphology in Figure 7.2 c. The highest concentration of CTAB generated homogeneous deformed micelles leading to only large plates in MO-CTAB1:2 (Figure 7.2 b). The use of TMA as a surfactant seems like it could not produce enough micelles and the concentration of TMA appears to have no effect on the size of particles. According to the literature, the Ostwald ripening mechanism [394] leads to the formation of hexagonal rods after growth, and TMA has not shown much effect and this was confirmed by XRD analysis (Figure 7.1 c).

FTIR analysis has been employed to identify the presence of surface functional groups on the catalyst. Figures 7.3 and 7.4 show the FTIR spectra of the samples prepared with CTAB and TMA, respectively. In both figures, FTIR spectra of the corresponding surfactant, as well as, MO sample (prepared without surfactant) have been also included to gain better interpretations.

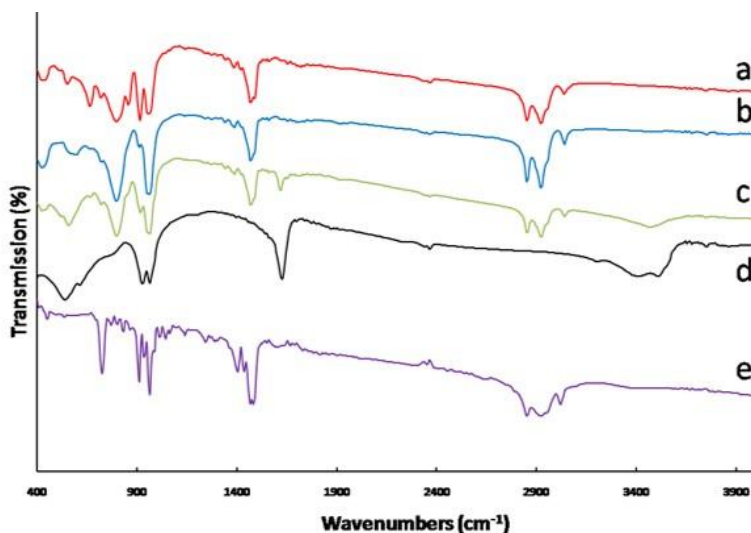


**Figure 7.3.** FTIR Spectra of the molybdenum oxides prepared with CTAB at various concentrations: (a) MO-CTAB1:2, (b) MO-CTAB1:3, (c) MO-CTAB1:4, (d) MO, and (e) CTAB.

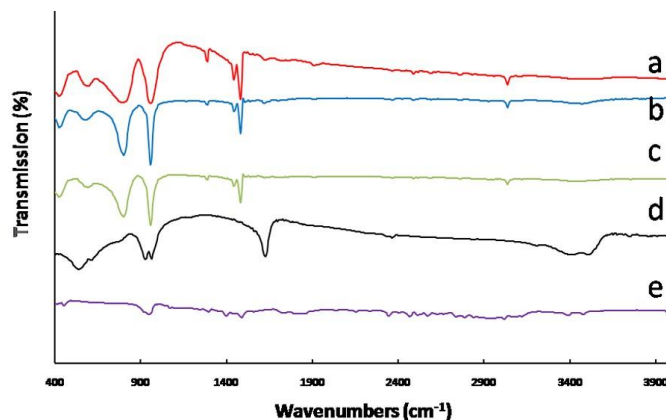


**Figure 7.4.** FT-IR Spectra of the molybdenum oxides prepared with TMA at various concentrations: (a) MO-TMA1:2, (b) MO-TMA1:3, (c) MO-TMA1:4, (d) MO, and (e) TMA.

Figure 7.3 shows two bands at 2920 and 2850 cm<sup>-1</sup> for the CTAB-containing samples (Figure 7.3 a-c), which are attributed to the characteristic peaks of symmetric and asymmetric C–

H stretching vibrations of methylene groups of CTAB. Moreover, the characteristic peak of angular deformation vibrations of methylene group was also observed at  $1475\text{ cm}^{-1}$  in these samples. These results were verified by the spectrum of pure CTAB (Figure 3e).

As seen in Figure 7.4, asymmetric and symmetric deformation modes pertaining to  $(\text{CH}_3)_3\text{N}^+$  of the head group of TMA appear at around  $1490$  and  $1390\text{ cm}^{-1}$ , according to the literature [390]. Pure TMA spectrum (Figure 7.4 e) shows the deformation vibrations of methyl groups at  $1490$  and  $1397\text{ cm}^{-1}$  and all other samples containing TMA confirm these characteristic peaks (Figure 7.4 a-c). Detailed analysis of spectrum of MO sample (Figure 7.3 d or 7.4 d) reveals that the characteristic peak of stretching vibrations of Mo-O appears at  $540\text{ cm}^{-1}$  [394,395,390], which was shifted to  $563$  and  $556\text{ cm}^{-1}$  in the presence of CTAB and to  $580\text{ cm}^{-1}$  in the presence of TMA (Figures 7.3 and 7.4). The stretching mode of Mo=O bands was located at  $965\text{ cm}^{-1}$  and  $934\text{ cm}^{-1}$  [396,397], and no peak was observed around  $995\text{ cm}^{-1}$  which is generally assigned to stretching vibrations of Mo-O-Mo. It is a characteristic of the orthorhombic phase of  $\text{MoO}_3$ .

The peaks observed at  $1630\text{ cm}^{-1}$  and  $3550\text{ cm}^{-1}$  were attributed to stretching and bending vibration of hydrogen bonded -OH groups, qualitatively confirming the presence of OH groups on the surface and water molecules adsorbed in the catalysts, which concur with the results of XRD analysis. Quantitative analysis of water contents of catalysts was performed by thermo-gravimetric analysis (TGA).

Figure 7.5 and 7.6 show TGA curves of the samples synthesized with CTAB and TMA, respectively. TGA curve of MO (without surfactant) (Figure 7.5 d or 7.6 c), shows a primary weight loss ( $\sim 12\%$ ) observed in the range of  $70$  to  $200\text{ }^\circ\text{C}$ , which corresponds to desorption of physically adsorbed water on  $\text{MoO}_3\text{-H}_2\text{O}$ . After  $200\text{ }^\circ\text{C}$  the weight of MO remained constant up to  $700\text{ }^\circ\text{C}$ , confirming the thermal stability of molybdenum oxide without any surfactant attached on its surface. Further heating after  $700\text{ }^\circ\text{C}$  led to a great weight loss not only for MO sample but also for the other samples, which is due to sublimation of molybdenum oxide that has been reported before [398].

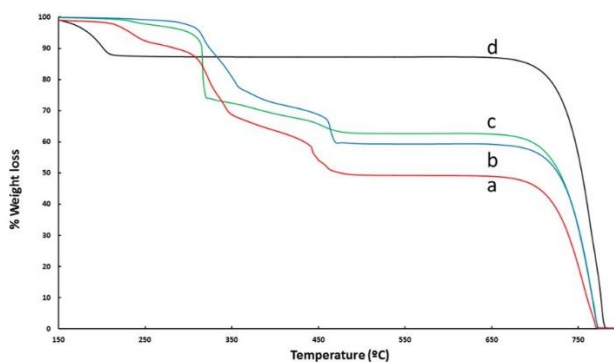


**Figure 7.5.** TGA curves of the molybdenum oxides prepared with different amounts of CTAB: (a) MO-CTAB1:2, (b) MO-CTAB1:3, (c) MO-CTAB1:4, and (d). MO.

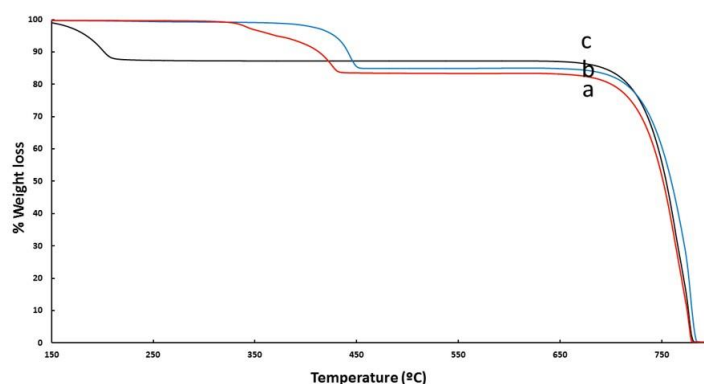


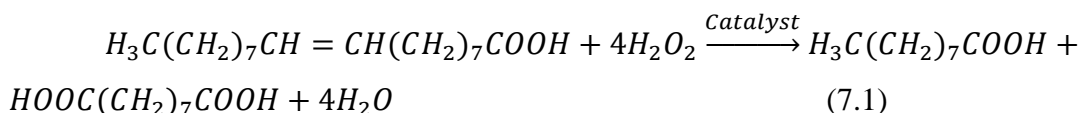
**Figure 7.6.** TGA curves of the molybdenum oxides prepared with different amounts of TMA: (a) MO-TMA1:2, (b) MO-TMA1:3, and (c) MO.

TGA curves of the samples containing CTAB (Figure 7.5 a-c) generally show lower weight losses compared to MO in the low-temperature region of  $< 200$  °C, which was attributed to the hydrogen bonded water molecules present in the crystalline phase; this assumption was confirmed by FTIR. The second weight loss observed at the range of 200-300 °C could be ascribed to decomposition of nitrates and ammonia compounds obtained from the surfactant. In addition, a third weight loss was obtained in high-temperature region ( $300 < T < 500$  °C), for which further differential thermal analysis (DTA) confirmed that it belongs to an exothermic interaction. This weight loss could be ascribed to removal or decomposition of  $\text{CTA}^+$  and elimination of bromide species during oxidation in air. The total amount of weight losses had a positive relationship with CTAB content in the samples; 50, 40, and 37 % weight losses were obtained for MO-CTAB1:2,

1:3, and 1:4, respectively. TGA curves of the samples with TMA (Figure 7.6) and their DTA analysis showed exothermic peaks between 300 and 450 °C corresponding to elimination of  $^+\text{N}(\text{CH}_3)_4$  group and bromide species. The weight losses during oxidation were between 16 and 17% which are much lower compared to those of the CTAB-capped samples. It could be due to the small molar weight of TMA (210.16 g/mol) compared to that of CTAB (364.45 g/mol).

### 7.3.2 Catalytic tests results

Catalytic activities of the surfactant-capped molybdenum oxide catalysts in oxidative scission of oleic acid have been investigated in a glass reactor equipped with condenser, thermocouple, and magnetic stirrer. A reaction was conducted without oleic acid to determine  $\text{H}_2\text{O}_2$  loss via catalytic or thermal decomposition and the loss was determined by titrimetry. For 4 h reaction at 85 °C, the loss of the oxidant was 26 %. Therefore, excess amounts of  $\text{H}_2\text{O}_2$  were used to complete the oxidation reactions (the molar ratio of  $\text{H}_2\text{O}_2$ /oleic acid used in the reaction was 11.1, which shows about 180% excess amount of  $\text{H}_2\text{O}_2$ , based on the stoichiometric reaction, Equation 7.1).



The first step of the reaction involves protonation of peroxo moiety on the catalyst to give surface peroxo groups. A yellow suspension was observed in the reaction solution, due to the formation of metal-peroxo complexes,  $-\text{MoO}(\text{O}_2)$  on surfaces of the surfactant-capped catalysts. Time-lapse observations of the reaction mixture, containing catalyst, oleic acid, hydrogen peroxide and tert-butanol, was recorded during the reactions over the catalysts to track changes that take place slowly over time (Figures S7.1 and S7.2, Supporting Information). Intriguingly, heterogeneity behavior of MO-CTAB1:3 catalyst was changed during the reaction; in the beginning of the reaction, the catalyst was a solid powder observable in the reaction mixture, which, upon heating to 85° C, turned into a homogeneous system. Afterwards, the reaction mixture remained as a clear solution until the end of the reaction. As soon as cooling down to room temperature, the catalyst started to precipitate (Figure S7.1), enabling self-separation and easy recovery of the catalyst. By contrast, all of the TMA containing catalysts kept their solid and heterogeneity natures during the reaction (Figure S7.2). This may be due to the structural differences between these two

surfactants; CTAB has a long hydrophobic chain of cetyl groups, which improves the hydrophobic-hydrophobic interaction between the surface of molybdenum oxide and oleic acid molecules and traps these molecules in the reaction medium resulting in enhancement of contacts between the reactants and active sites on the catalyst. The high dispersion of MO-CTAB1:3 catalyst in the reaction mixture, which arose from the surface organo-modification, created conditions similar to homogeneous catalysis. Moreover, the high concentration of hydrogen peroxide during the reaction results in rapid formation of metal-peroxo complexes and reinforcement of the emulsion, while at the end of the reaction, when a majority of H<sub>2</sub>O<sub>2</sub> has been consumed, the concentration of such complexes on the catalyst's surface drops resulting in precipitation of the catalyst.

Table 7.1 shows the conversion of oleic acid and yields of production of the desired products, azelaic and pelargonic acids, over different synthesized catalysts with H<sub>2</sub>O<sub>2</sub> as oxidant after 3.5 h reaction at 85 °C. The catalytic test results presented are the average of at least 3 runs over each catalyst. The first catalytic test was done without any catalyst (Table 7.1, entry 1), that gives very low conversion (26%) and yields of azelaic and pelargonic acids (6.4 and 6.8%, respectively). Using the catalyst without surfactant, MO, significantly increased the conversion (97%) and yields of azelaic and pelargonic acids (60 and 50%, respectively) (entry 2). The overwhelming majority of the organo-modified catalysts resulted in better efficiencies (entries 3-8). Ideally, oxidative cleavage of oleic acid should give similar yields of azelaic and pelargonic acids (1 mole of oleic acid into 1 mole of each product) based on the stoichiometric equation of the reaction (Equation 7.1). In practice, however, differences were obtained in the yields of these two products, which arise from non-ideality of the catalytic system, different decomposition rates of azelaic and pelargonic acids in the reaction medium, and presence of by-products.

**Table 7.1.** Catalytic tests results (conversion of oleic acid and yields of production of desired products).

Entry	Catalyst	Surfactant: Mo molar ratio	Conversion <sup>1</sup> (%)	Yield <sup>2</sup> of azelaic acid (%)	Yield <sup>2</sup> of pelargonic acid (%)
1	Without catalyst	-	26	6.4	6.8
2	MO	0	97	60	50
3	MO-CTAB1:4	1:4	100	78.2	61
4	MO-CTAB1:3	1:3	100	83	68



5	MO-CTAB1:2	1:2	100	70	55
6	MO-TMA 1:4	1:4	100	68	59
7	MO-TMA 1:3	1:3	100	67.4	60
8	MO-TMA 1:2	1:2	100	58	46

1. Reaction conditions: time: 3.5 h, temperature: 85 °C (bath temperature), solvent: tert-butanol, initial amounts of oleic acid: 1 g, t-butanol: 8 ml, H<sub>2</sub>O<sub>2</sub>: 4 ml, catalyst: 0.4 g.
2. Yield, in this work, is defined as the number of moles of a product formed per mole of oleic acid consumed

Use of the surfactants as capping agent increased both yields of azelaic and pelargonic acids. The maximum yields were achieved with MO-CTAB1:3 catalyst (entry 4), which produced 83 % azelaic and 68% pelargonic acids. Compared to the literature, these obtained yields are superior to what have been obtained by heterogeneous catalysts and are comparable with what homogeneous ones have shown. Table 7.2 lists the results of other works (all the heterogeneous catalysts reported so far, to the best of our knowledge, and some of the best homogeneous catalysts). The excellent catalytic activity of MO-CTAB1:3, as Table 7.2 implies, could be ascribed to the presence of multiple alkyl chains on the catalyst's surface, which improves the interactions of oleic acid with peroxo-molybdenum complexes formed by the reaction of H<sub>2</sub>O<sub>2</sub> with the particles surfaces.

**Table 7.2.** Comparison of catalytic efficiency of MO-CTAB1:3 with recent reported works in the literature.

Catalyst/ oxidant system	Reaction time and temperature	Conversion (%)	Yield <sup>1</sup> (%)	Reference <sup>2</sup>
Peroxo-tungsten complex PTA/H <sub>2</sub> O <sub>2</sub>	5h, 80 °C	-	PA: 82 AA: 79	[2] *
Polyoxomolybdate	5h, 90 °C	-	AA: 82	[3] *
RuCl <sub>3</sub> /NaIO <sub>4</sub>	8h, RT	-	PA: 98 AA 62	[58] *
H <sub>2</sub> WO <sub>4</sub> /H <sub>2</sub> O <sub>2</sub>	8h, 100 °C	-	PA 69 AA 92	[386] *
Tungsten oxide-SiO <sub>2</sub> / H <sub>2</sub> O <sub>2</sub>	1h, 130 °C	79	PA 36 AA 32	[48] #
Tungsten oxide/ H <sub>2</sub> O <sub>2</sub>	1h, 130 °C	56	PA 29 AA 30	[48] #
Chromium supported on MCM-41/O <sub>2</sub>	8 h, 80 °C	> 95	AA: 32.4 PA: 32.2	[339] #
Tungsten oxide/ H <sub>2</sub> O <sub>2</sub>	5 h, 120 °C	95	AA: 58 PA: 24	[399] #
H <sub>2</sub> O <sub>2</sub> /MO-CTAB1:3	3.5 h, °C	100	PA 68% AA 83%	This work #

1. AA: azelaic acid, PA: pelargonic acid.

2. \*: homogeneous catalysis, #: heterogeneous catalysis

### 7.3.3 Recyclability of the catalysts

Stability and consequently reusability of the catalyst, which are important parameters to scale up the process, were also investigated for the catalyst that gave the best efficiency (MO-CTAB1:3). The catalyst was conveniently recovered from the mixture of products after the reaction by simple centrifugation at high rpm. No significant loss of catalyst (or no significant leaching of Mo species to the reaction solution) was found, even after 4 cycles of catalytic reaction. Yield of weight recovery for all the catalysts after the first cycle was more than ~97% and loss of the CTAB-capped catalyst after 4 cycles obtained by ICP analysis was 9.4 wt%. This good recovery could be due to the protective role of the capping surfactant on the catalyst surface. Table 7.3 represents catalytic efficiencies obtained by catalyst MO-CTAB1:3 in the four performed reaction cycles, which shows insignificant activity loss. Yields of desired products slightly decreased during the cycles while the conversion was always the same. Comparing FTIR spectra of MO-CTAB1:3 before and after each cycle (Figure 7.7) does not show any notable difference, which proves stability of the CTAB capped on the catalyst's surface. Even after the fourth cycle, CTAB groups were still attached to the catalyst; all the characteristic peaks of alkyl group and molybdenum oxide remained after the cycles. The slight decrease in the yields may be due to the progressive detachment of CTAB and leaching of molybdenum oxide from the particle surface to the solution (leaching of Mo oxide: ~ 10% after 4 cycles of reaction). Furthermore, to verify that the reaction is truly heterogeneous and to investigate the possibility of leaching of Mo species in the reaction solution after removal of the catalyst, a catalytic test was performed with MoCTAB1:3 catalyst and stopped after 1 h of reaction, which showed 44% conversion and 28 and 21% yields of azelaic and pelargonic acids, respectively. After cooling down to room temperature the catalyst was removed, and the reaction solution was exposed to the reaction conditions for the remaining reaction time (2.5 h, at 85 °C). Although the conversion increased to 61%, the yields were negligibly changed (29 and 23% for azelaic and pelargonic acids, respectively), which could be well ascribed to the lack of catalyst. However, since the oxidant could alone cause the conversion of oleic acid (see Table 7.1 entry 1), the conversion was increased somewhat. From these results, it can be concluded that this new catalytic system displays high activity, good selectivity and environmentally benign

properties (using hydrogen peroxide instead of hazardous ozone) and the efficient reusability of the catalyst makes the process cost effective and eco-friendly.

**Table 7.3.** Catalytic efficiencies obtained by catalyst MO-CTAB1:3 in different reaction cycles.

Catalysts	Reaction cycle	Conversion <sup>1</sup> (%)	Yield <sup>2</sup> of azelaic acid (%)	Yield <sup>2</sup> of pelargonic acid (%)
MO-CTAB1:3	1	100	83	68
MO-CTAB1:3	2	100	80	65
MO-CTAB1:3	3	100	78	63
MO-CTAB1:3	4	99	77	61

1. Reaction conditions: time: 3.5 h, temperature: 85 °C (bath temperature), solvent: tert-butanol, initial amounts of oleic acid: 1 g, t-butanol: 8 ml, H<sub>2</sub>O<sub>2</sub>: 4 ml, catalyst: 0.4 g.
2. Yield, in this work, is defined as the number of moles of a product formed per mole of oleic acid consumed.

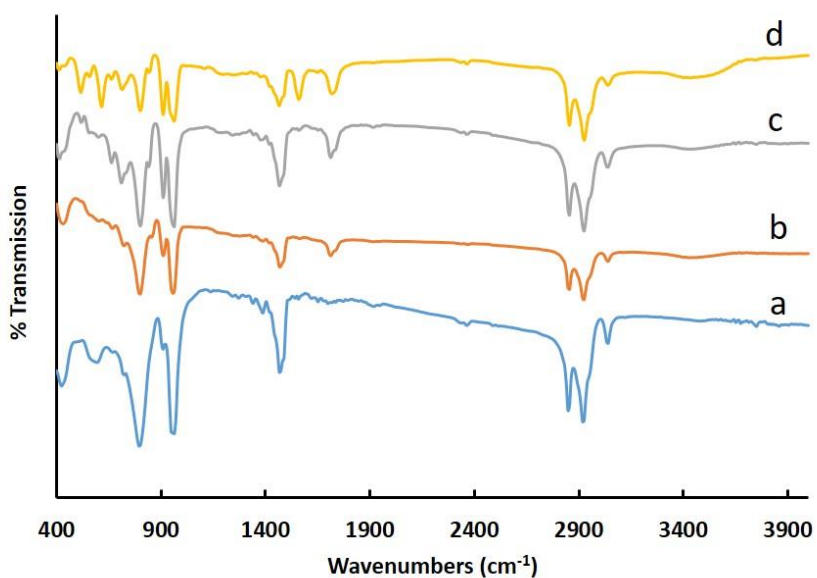


**Figure 7.7.** FT-IR Spectra of MO-CTAB1:3 catalyst after different reaction cycles: (a) after cycle 1, (b) after cycle 2, (c) after cycle 3, and (d) after cycle 4.

## 7.4 Conclusions

In summary, we have reported successful synthesis of surfactant-capped molybdenum oxide catalysts by simple oxidative dissolution method at 100 °C, which were characterized by different techniques including XRD, FTIR, TGA, and SEM analyses. CTAB and TMA were used

as surfactant to organo-modify surfaces of molybdenum oxides. The physicochemical analysis revealed that the morphology of the products strongly depends on the nature and concentration of capping agents. The synthesized surfactant-capped catalysts showed excellent catalytic efficiency in oxidative cleavage of oleic acid to mono and dicarboxylic acids. The highest efficiency was obtained for the CTAB-capped molybdenum oxide (with CTAB/Mo molar ratio of 1/3), resulting in full conversion of oleic acid and 83 and 68 % yields of production of azelaic and pelargonic acids, respectively. This catalyst exhibited convenient recovery, good stability, and steady reusability over recycling experiments without significant activity loss up to four cycles. Employing an environmentally benign oxidant, hydrogen peroxide, this catalytic system would open a new pathway for production of diacids and fuel components from renewable feedstock.

### **Funding**

This study was funded by Programme Canadien de Bourses de la Francophonie” (PCBF) and Nature Sciences and Engineering Research Council of Canada (NSERC) through an INNOV-UC Grant.

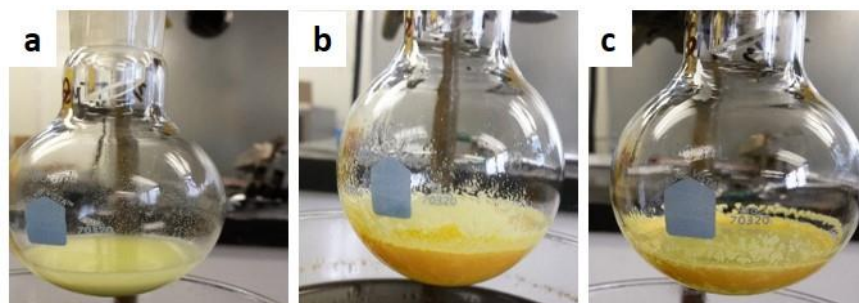
### **Acknowledgments**

This work was supported by the “Programme Canadien de Bourses de la Francophonie” (PCBF) and the Nature Sciences and Engineering Research Council of Canada (NSERC) through an INNOV-UC Grant. ASE thanks the Department of Chemical Engineering at Laval University for welcoming him as a visiting scientist during his stay in Canada. The authors would like to thank the industrial partners (Oleotek and SiliCycle Inc.) for stimulating discussions and comments.

## 7.5 Supporting Information



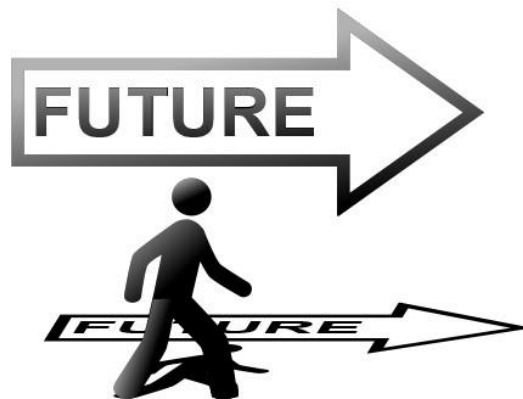
**Figure S7.1.** Time-lapse views of the reaction mixture in the presence of MO-CTAB1:3 catalyst: (a) beginning of the reaction, (b) during the reaction, and (c) end of the reaction.



**Figure S7.2.** Time-lapse views of the reaction mixture in the presence of MO-TMA1:3 catalyst: (a) beginning of the reaction, (b) during the reaction, and (c) end of the reaction.

## Chapter 8. Conclusion and future scope

Con**clu**sion

A magnifying glass with a black handle and a silver rim is positioned over the word "Conclusion". The lens of the magnifying glass is centered over the letters "clu", which are significantly enlarged and appear to be floating slightly above the rest of the word. The word "Conclusion" is written in a bold, black, sans-serif font.

## 8.1 General conclusions

The main goal of this research, as described before in the thesis, was to propose an alternative process for the hazardous ozonolysis of oleic acid. To do so, an efficient catalyst/oxidant system is required to oxidatively cleave the oleic acid (C18:1) into a mono- and a di-C9 acids. Our interest was to develop a catalyst that not only possesses high efficiency, but also exhibits other appealing characteristic to the industry including excellent recyclability and low-cost production. In order to follow a systematic research path for this PhD project, first of all we have reviewed all the reported works regarding use of different catalyst/oxidant systems in the oxidative cleavage of UFAs and their derivatives. This comprehensive theoretical study, which has been presented in Chapter 2, elucidated the plan of our experimental works. It clearly indicated that among all the used transition metals as catalytic core in such reactions (Os, Co, Ru, Cr, Au, Mn, Fe, Mo, and W), tungsten has attracted a great deal of attention. We found that homogeneous tungsten-based catalysts have shown great potentials in oxidation of UFAs, but such catalysts generally have low recovery efficiency. Then, our focus was chiefly placed on tungsten-based heterogeneous catalysts. Also, molybdenum as an inherently close to tungsten metal, the compounds of which have occasionally shown even better catalytic activity, was our secondary interest. Accordingly, different advanced heterogeneous catalysts were prepared and tried, including high surface area mesoporous tungsten oxide supported on  $\gamma$ -alumina, nanoparticles (NPs) of different structures of tungsten trioxide (hydrated and anhydrous), tungsten peroxide, and molybdenum oxide, as well as Keggin clusters of polyoxotungstates (POTs). The catalysts were thoroughly characterized with different techniques such as SEM, TEM, FTIR, XRD, TGA, DTA, EDS,  $N_2$  adsorption/desorption isotherms, zeta potential measurement, and elemental analysis, which have been explained in Chapter 3.

In the first phase of our experimental works, mesoporous tungsten oxide was prepared. As discussed in Chapter 4, we have developed a solvothermal synthesis method for preparation of high surface area mesoporous  $WO_3$  supported on  $\gamma$ -alumina with narrow particle size distribution using glucose as template. Our interest was to reach a higher dimensionality of the interaction between the components and the catalyst surface by increasing the surface area via incorporation of the active sites in the mesostructured support. The obtained catalytic efficiencies although were comparable to what has been obtained in the literature for heterogeneous catalysts, did not show a

great achievement, most likely because of the pore diffusion controls on large and kinky shape of the oleic acid molecules exerted by mesostructures.

Given the potential of  $\text{WO}_x$  in oxidation of olefins on one hand, and the fact that tungsten oxide has several catalytically interesting crystalline structures on the other hand, we then synthesized different structures of tungsten oxide like  $[(\text{WO}_2)\text{O}_2\cdot\text{H}_2\text{O}]$ ,  $\text{WO}_3$ ,  $\text{WO}_3\cdot 0.33\text{H}_2\text{O}$ , and  $\text{WO}_3\cdot\text{H}_2\text{O}$  via a unique and facile method, which has been shown in Chapter 5. Moreover, organo-functionalization of nanocatalysts surfaces, as an efficient strategy for enhancement of catalytic performance in the biphasic reaction of oxidative cleavage of oleic acid, was done by CTAB. In order to prepare and organo-functionalization of the metal oxide NPs, we have developed a green and straightforward approach based on oxidative dissolution of bare micrometer scale metal powder in  $\text{H}_2\text{O}_2$ . Simply taking W powder, adding  $\text{H}_2\text{O}_2$ , and then by just altering the temperature of thermal treatment and/or adding a surfactant, different aforementioned structures of tungsten oxide were achieved. Exploiting cheap W powder as precursor and avoiding use of time- and energy-consuming operations in the synthetic procedure such as thermal treatment in autoclave and purification, as well as avoiding use of organic solvents, metal salts, and/or coordination compounds, which are commonly required in prior reported synthesis methods, are of the advantages of the employed synthesis method. In terms of catalytic test, the obtained conversion (100%) and yield of production of azelaic acid (~80 %) showed a great achievement in the reaction efficiency when being compared to the scarce works reported on heterogeneous catalytic oxidative cleavage of oleic acid. In addition to the simple preparation and superior catalytic activity, the organo-functionalized catalyst exhibited advantages of no active sites leaching, convenient recovery and steady reuse without loss of activity up to at least four cycles, which are important features for an industrial catalyst.

Despite of the proved advantages of polyoxotungstate heterogeneous catalysts in different water-involving organic reactions such as hydrolysis, dehydration, esterification, and oxidation of olefins with  $\text{H}_2\text{O}_2$ , curiously their application in oxidation of UFAs has not been examined so far. In Chapter 6, we reported, for the first time, the use of solid POT catalysts in the oxidative cleavage of oleic acid. We have developed a novel, one-pot, and green synthesis method, complying with the principles of “Chimie Douce”, for preparation of the hybrid organic-inorganic POTs, starting



with bare tungsten powder as precursor, by contrast to the prior methods that often use phosphotungstic or tungstic acid. Two novel hybrid organic-inorganic Keggin compounds were prepared and introduced in this chapter via employing three tetraalkylammonium cations ( $\text{NR}_4^+$ ) with different alkyl chain length (TMA: tetramethylammonium, TPA: tetrapropylammonium, and TBA: tetrabutylammonium) in the synthesis; while in the absence of any organic moiety, simple tungsten trioxide was obtained, the Keggin clusters of  $\text{TPA}_x[\text{H}_{8-x}\text{W}_{12}\text{O}_{40}]\cdot n\text{H}_2\text{O}$  and  $\text{TBA}_x[\text{H}_{8-x}\text{W}_{12}\text{O}_{40}]\cdot n\text{H}_2\text{O}$  were formed in the presence of  $\text{TPA}^+$  and  $\text{TBA}^+$  cations, respectively. In terms of the catalytic reaction, thanks to the pseudo-homogeneous behavior of the hybrid catalysts in the reaction, the strong and organo-protected acidity of the prepared Keggin compounds, and their known water tolerant properties, the catalysts exhibited excellent efficiency (100% conversion and up to 79% yield of production of azelaic acid), despite of their non-porous structures. Moreover, the  $\text{NR}_4^+$ -encapsulated catalysts demonstrated efficient recovery and steady reusability without any significant decay in their activities up to at least 4 cycles.

Finally, in Chapter 7, we presented the results of our works on molybdenum oxide catalysts organo-functionalized by CTAB and TMA. A series of molybdenum oxides were synthesized via the simple oxidative dissolution of molybdenum powder in  $\text{H}_2\text{O}_2$ , with and without the presence of the two organic surfactants. Effects of concentration of the organic surfactants on physicochemical properties and catalytic activities of the products were investigated. With the aid of surface organo-modification, the molybdenum oxide particles exhibited superior catalytic activity (full conversion of oleic acid and just more than 80% yield of production of azelaic acid) compared to the literature.

## 8.2 Future scope

The comprehensive theoretical studies performed throughout this research, which resulted in presenting two review papers, enabled us to acquire innovative knowledge in the field of materials synthesis and characterization, as well as vegetable oils science and technology. This afforded a wide outlook to foster the future works in these fields. Leveraging our experiences, the following suggestions are succinctly rendered, as the most striking ones:

- Kinetic studies of the reaction not only could decorate the evaluation of the catalysts, but also will results in proposing a mechanism for the reaction. Given the multi-step reaction of oxidative cleavage of oleic acid (see Chapter 6 and Scheme 6.3), and lack of proposed mechanisms of the reaction over solid catalysts in literature, such studies seem highly desirable. Optimization of the reaction conditions could also be achieved by kinetic studies. Since the desired products (azelaic and pelargonic acids) have been reported that are relatively metastable during the prolonged heating in the presence of transition metals, compared to the by-products (nonanal and 9-oxononanoic acid), optimization of the reaction time and temperature should be developed. Quantification of these by-products would provide clues to control selectivities to azelaic and pelargonic acids. Furthermore, we used about 150-180% excess  $\text{H}_2\text{O}_2$  in our catalytic tests. Although use of a large excess  $\text{H}_2\text{O}_2$  has been recommended in the literature for oxidation of UFAs, optimization of the oxidant amount as a result of kinetic studies would effectively reduce the cost of process.
- Preparation of magnetically recyclable nanocatalysts given the high efficiency of magnetic separation compared to the conventional filtration and centrifugation is also proposed. Either magnetic catalysts or non-magnetic catalysts immobilized onto magnetic supports, which have been widely reviewed in literature, could be promising. It is evident that separation by means of applying an external magnetic field requires at least one magnetic metal which can be iron, cobalt or nickel. Magnetic core is generally made of oxides (e.g. iron oxide) or reduced species. Incorporation of another catalytically active metal is, nowadays, readily possible using decorated or core shell structures.
- We performed some catalytic tests in the absence of organic solvent. Our works indicated that a kind of phase transfer catalytic role could be ascribed to the organo-functionalized nanocatalysts. Employing such catalysts would enable to use less amount of solvent. Elimination of organic solvent in accordance with green chemistry will be an important breakthrough in such biphasic reactions. Further studies to rise the yields in the absence of organic solvent are highly encouraged.
- Given the pioneer application of heterogeneous Keggin-type catalysts in oxidation of UFAs in this work, and rapid development of hybrid organic-inorganic POT catalysts, future

works would enhance versatility of such hybrid catalysts by employing different organic moieties.

- To precisely probe the possibility of leaching of catalyst's active sites in the reaction medium, performing elemental analysis like ICPMS is recommended
- Extension of the scope of the prepared catalysts to oxidation of other UFAs, rather than oleic acid, is also called for.
- Our last suggestion is pertained to the preparation of fatty acids prior to GC analysis. Although the employed derivatization process is the most common method for esterification of fatty acids, the used catalyst ( $\text{BF}_3$ ) is not only recyclable, but also relatively expensive. This made our analyses costly. Some efforts are currently underway in lab-scale, and have been reported in the literature, on development of heterogeneous and recyclable catalysts made of hybrid POTs for quick esterification of fatty acids. These efforts should be fostered to make the analysis of fatty acids more economic.

## References

1. Kulik A, Janz A, Pohl M-M, Martin A, Köckritz A (2012) Gold-catalyzed synthesis of dicarboxylic and monocarboxylic acids. *European Journal of Lipid Science and Technology* 114 (11):1327-1332. doi:10.1002/ejlt.201200027
2. Godard A, De Caro P, Thiebaud-Roux S, Vedrenne E, Mouloungui Z (2013) New Environmentally Friendly Oxidative Scission of Oleic Acid into Azelaic Acid and Pelargonic Acid. *Journal of the American Oil Chemists' Society* 90 (1):133-140. doi:10.1007/s11746-012-2134-7
3. Turnwald SE, Lorier MA, Wright LJ, Mucalo MR (1998) Oleic Acid Oxidation Using Hydrogen Peroxide in Conjunction with Transition Metal Catalysis. *Journal of Materials Science Letters* 17 (15):1305-1307. doi:10.1023/a:1006532314593
4. Köckritz A, Blumenstein M, Martin A (2010) Catalytic cleavage of methyl oleate or oleic acid. *European Journal of Lipid Science and Technology* 112 (1):58-63. doi:10.1002/ejlt.200900103
5. Noureddini H, Rempé ML (1996) Pelargonic acid in enhanced oil recovery. *Journal of the American Oil Chemists' Society* 73 (7):939-941. doi:10.1007/BF02517999
6. Biermann U, Bornscheuer U, Meier MA, Metzger JO, Schafer HJ (2011) Oils and fats as renewable raw materials in chemistry. *Angewandte Chemie* 50 (17):3854-3871. doi:10.1002/anie.201002767
7. Biermann U, Friedt W, Lang S, Lühs W, Machmüller G, Metzger JO, Rüschen Klaas M, Schäfer HJ, Schneider MP (2000) New syntheses with oils and fats as renewable raw materials for the chemical industry. *Angewandte Chemie International Edition* 39 (13):2206-2224. doi:10.1002/1521-3773(20000703)39:13<2206::AID-ANIE2206>3.0.CO;2-P
8. Corma A, Iborra S, Velty A (2007) Chemical routes for the transformation of biomass into chemicals. *Chemical Reviews* 107 (6):2411-2502. doi:10.1021/cr050989d
9. Hill K (2000) Fats and oils as oleochemical raw materials. *Pure and Applied Chemistry* 72 (7):1255-1264
10. Mecking S (2004) Nature or petrochemistry?—biologically degradable materials. *Angewandte Chemie International Edition* 43 (9):1078-1085. doi:10.1002/anie.200301655
11. Campbell CJ (2013) The Oil Age in Perspective. In: *Campbell's Atlas of Oil and Gas Depletion*. Springer New York, pp 377-388. doi:10.1007/978-1-4614-3576-1\_77
12. Anastas PT, Kirchhoff MM (2002) Origins, current status, and future challenges of green chemistry. *Accounts of chemical research* 35 (9):686-694
13. Patel MK, Theiß A, Worrell E (1999) Surfactant production and use in Germany: resource requirements and CO<sub>2</sub> emissions. *Resources, Conservation and Recycling* 25 (1):61-78. doi:[http://dx.doi.org/10.1016/S0921-3449\(98\)00063-9](http://dx.doi.org/10.1016/S0921-3449(98)00063-9)
14. AOCs lipid library. AOCs. <http://lipidlibrary.aocs.org/Lipids/whatlip/index.htm>.

15. Mittaine J-F, Mielke T (2012) The globalization of international oilseeds trade. *OCL* 19 (5):249-260
16. AOCs lipid library. AOCs. <http://lipidlibrary.aocs.org/market/nonfood.htm>.
17. Baumann H, Bühler M, Fochem H, Hirsinger F, Zobelein H, Falbe J (1988) Natural fats and oils—renewable raw materials for the chemical industry. *Angewandte Chemie International Edition in English* 27 (1):41-62. doi:10.1002/anie.198800411
18. Nelson DL, Nelson DL, Lehninger AL, Cox MM (2008) *Lehninger principles of biochemistry*. W.H. Freeman, New York
19. AOCs lipid library. AOCs. <http://lipidlibrary.aocs.org/chemistry/db-reactions/index.htm>.
20. Nieschlag HJ, Tallent WH, Wolff IA, Palm WE, Witnauer LP (1967) Diester plasticizers from mixed crambe dibasic acids. *I&EC Product Research and Development* 6 (4):201-204. doi:10.1021/i360024a001
21. Kadesch R (1954) Dibasic acids. *J Am Oil Chem Soc* 31 (11):568-573. doi:10.1007/BF02638574
22. Nieschlag HJ, Rothfus JA, Sohns VE, Perkins RB (1977) Nylon-1313 from brassylic acid. *Product R&D* 16 (1):101-107. doi:10.1021/i360061a021
23. Musser MT (2000) Adipic acid. In: *Ullmann's Encyclopedia of Industrial Chemistry*. Wiley-VCH Verlag GmbH & Co. KGaA. doi:10.1002/14356007.a01\_269
24. Huf S, Krügener S, Hirth T, Rupp S, Zibek S (2011) Biotechnological synthesis of long-chain dicarboxylic acids as building blocks for polymers. *European Journal of Lipid Science and Technology* 113 (5):548-561. doi:10.1002/ejlt.201000112
25. Ackman RG, Retson ME, Gallay LR, Vandenheuvel FA (1961) Ozonolysis of unsaturated fatty acids: I. Ozonolysis of oleic acid. *Canadian Journal of Chemistry* 39 (10):1956-1963. doi:10.1139/v61-262
26. Höfer R, Daute P, Grützmacher R, Westfechtel A (1997) Oleochemical polyols — A new raw material source for polyurethane coatings and floorings. *Journal of Coatings Technology* 69 (869):65-72. doi:10.1007/BF02696155
27. Keller H, Dreyer C, Medin J, Mahfoudi A, Ozato K, Wahli W (1993) Fatty acids and retinoids control lipid metabolism through activation of peroxisome proliferator-activated receptor-retinoid X receptor heterodimers. *Proceedings of the National Academy of Sciences* 90 (6):2160-2164. doi:10.1073/pnas.90.6.2160
28. The nomenclature of lipids (1977). *European Journal of Biochemistry* 79 (1):11-21. doi:10.1111/j.1432-1033.1977.tb11778.x
29. Anneken DJ, Both S, Christoph R, Fieg G, Steinberner U, Westfechtel A (2000) Fatty Acids. In: *Ullmann's Encyclopedia of Industrial Chemistry*. Wiley-VCH Verlag GmbH & Co. KGaA. doi:10.1002/14356007.a10\_245.pub2
30. Wikipedia, the free encyclopedia. <http://en.wikipedia.org/wiki/Epoxyde>.
31. Young JA (2002) Chemical laboratory information profile: Oleic acid. *Journal of Chemical Education* 79 (1):24. doi:10.1021/ed079p24

32. Visioli F, Galli C (2000) Olive oil: more than just oleic acid. *The American Journal of Clinical Nutrition* 72 (3):853
33. Villarreal-Lozoya JE, Lombardini L, Cisneros-Zevallos L (2007) Phytochemical constituents and antioxidant capacity of different pecan [*Carya illinoensis* (Wangenh.) K. Koch] cultivars. *Food Chemistry* 102 (4):1241-1249. doi:<http://dx.doi.org/10.1016/j.foodchem.2006.07.024>
34. Untoro J, Schultink W, West CE, Gross R, Hautvast JG (2006) Efficacy of oral iodized peanut oil is greater than that of iodized poppy seed oil among Indonesian schoolchildren. *The American Journal of Clinical Nutrition* 84 (5):1208-1214
35. Thomas A (2000) Fats and fatty oils. In: *Ullmann's Encyclopedia of Industrial Chemistry*. Wiley-VCH Verlag GmbH & Co. KGaA. doi:10.1002/14356007.a10\_173
36. Nutter M, Lockhart E, Harris R (1943) The chemical composition of depot fats in chickens and turkeys. *Oil Soap* 20 (11):231-234. doi:10.1007/BF02630880
37. Mbaraka I, Shanks B (2006) Conversion of oils and fats using advanced mesoporous heterogeneous catalysts. *Journal of the American Oil Chemists' Society* 83 (2):79-91. doi:10.1007/s11746-006-1179-x
38. Tan SG, Chow WS (2010) Biobased epoxidized vegetable oils and its greener epoxy blends: A review. *Polymer-Plastics Technology and Engineering* 49 (15):1581-1590. doi:10.1080/03602559.2010.512338
39. Köckritz A, Martin A (2008) Oxidation of unsaturated fatty acid derivatives and vegetable oils. *European Journal of Lipid Science and Technology* 110 (9):812-824. doi:10.1002/ejlt.200800042
40. Meier MAR, Metzger JO, Schubert US (2007) Plant oil renewable resources as green alternatives in polymer science. *Chemical Society Reviews* 36 (11):1788-1802. doi:10.1039/B703294C
41. Kolot V, Grinberg S (2004) Vernonia oil-based acrylate and methacrylate polymers and interpenetrating polymer networks with epoxy resins. *Journal of Applied Polymer Science* 91 (6):3835-3843. doi:10.1002/app.13583
42. Satyarthi JK, Srinivas D (2011) Selective epoxidation of methyl soyate over alumina-supported group VI metal oxide catalysts. *Applied Catalysis A: General* 401 (1-2):189-198. doi:<http://dx.doi.org/10.1016/j.apcata.2011.05.021>
43. Grinberg S, Linder C, Kolot V, Waner T, Wiesman Z, Shaubi E, Heldman E (2005) Novel cationic amphiphilic derivatives from vernonia oil: synthesis and self-aggregation into bilayer vesicles, nanoparticles, and DNA complexants. *Langmuir : the ACS journal of surfaces and colloids* 21 (17):7638-7645. doi:10.1021/la050091j
44. Criegee R (1975) Mechanism of ozonolysis. *Angewandte Chemie International Edition in English* 14 (11):745-752. doi:10.1002/anie.197507451
45. Spanning P, Bruijninx PCA, Weckhuysen BM, Klein Gebbink RJM (2014) Transition metal-catalyzed oxidative double bond cleavage of simple and bio-derived alkenes and unsaturated fatty acids. *Catalysis Science & Technology* 4 (8):2182-2209. doi:10.1039/C3CY01095C

46. Spannring P (2013) Fe-catalyzed oxidative cleavage of unsaturated fatty acids. Utrecht University,
47. Zaldman B, Kisilev A, Sasson Y, Garti N (1988) Double bond oxidation of unsaturated fatty acids. *Journal of the American Oil Chemists' Society* 65 (4):611-615. doi:10.1007/BF02540689
48. Nouredini H, Kanabur M (1999) Liquid-phase catalytic oxidation of unsaturated fatty acids. *Journal of the American Oil Chemists' Society* 76 (3):305-312. doi:10.1007/s11746-999-0236-7
49. Warwel S, Sojka M, Klaas M (1993) Synthesis of dicarboxylic acids by transition-metal catalyzed oxidative cleavage of terminal-unsaturated fatty acids. In: Herrmann W (ed) *Organic Peroxygen Chemistry*, vol 164. Topics in Current Chemistry. Springer Berlin Heidelberg, pp 79-98. doi:10.1007/3-540-56252-4\_26
50. Dean FM, Knight JC (1962) 930. Spirans. Part IV. The oxidation of 3-alkylidenegrisens to grisen-3-ones by ruthenium tetroxide. *Journal of the Chemical Society (Resumed)* (0):4745-4752. doi:10.1039/JR9620004745
51. Berkowitz LM, Rylander PN (1958) Use of ruthenium tetroxide as a multi-purpose oxidant. *Journal of the American Chemical Society* 80 (24):6682-6684. doi:10.1021/ja01557a053
52. Pappo R, Allen JDS, Lemieux RU, Johnson WS (1956) Notes - osmium tetroxide-catalyzed periodate oxidation of olefinic bonds. *The Journal of Organic Chemistry* 21 (4):478-479. doi:10.1021/jo01110a606
53. Travis BR, Narayan RS, Borhan B (2002) Osmium tetroxide-promoted catalytic oxidative cleavage of olefins: An organometallic ozonolysis. *Journal of the American Chemical Society* 124 (15):3824-3825. doi:10.1021/ja017295g
54. Santacesaria E, Sorrentino A, Rainone F, Di Serio M, Speranza F (2000) Oxidative cleavage of the double bond of monoenic fatty chains in two steps: A new promising route to azelaic acid and other industrial products. *Industrial & Engineering Chemistry Research* 39 (8):2766-2771. doi:10.1021/ie990920u
55. Spannring P, Yazerski V, Bruijninx PCA, Weckhuysen BM, Klein Gebbink RJM (2013) Fe-catalyzed one-pot oxidative cleavage of unsaturated fatty acids into aldehydes with hydrogen peroxide and sodium periodate. *Chemistry – A European Journal* 19 (44):15012-15018. doi:10.1002/chem.201301371
56. Spannring P, Prat I, Costas M, Lutz M, Bruijninx PCA, Weckhuysen BM, Klein Gebbink RJM (2014) Fe(6-Me-PyTACN)-catalyzed, one-pot oxidative cleavage of methyl oleate and oleic acid into carboxylic acids with H<sub>2</sub>O<sub>2</sub> and NaIO<sub>4</sub>. *Catalysis Science & Technology* 4 (3):708-716. doi:10.1039/C3CY00851G
57. Rup S, Zimmermann F, Meux E, Schneider M, Sindt M, Oget N (2009) The ultrasound-assisted oxidative scission of monoenic fatty acids by ruthenium tetroxide catalysis: influence of the mixture of solvents. *Ultrason Sonochem* 16 (2):266-272. doi:10.1016/j.ultsonch.2008.08.003
58. Rup S, Sindt M, Oget N (2010) Catalytic oxidative cleavage of olefins by RuO<sub>4</sub> organic solvent-free under ultrasonic irradiation. *Tetrahedron Letters* 51 (23):3123-3126. doi:<http://dx.doi.org/10.1016/j.tetlet.2010.04.040>

59. Behr A, Tenhumberg N, Wintzer A (2013) Efficient ruthenium-catalysed oxidative cleavage of methyl oleate with hydrogen peroxide as oxidant. *RSC Advances* 3 (1):172-180. doi:10.1039/C2RA22370H
60. Behr A, Tenhumberg N, Wintzer A (2012) An efficient reaction protocol for the ruthenium-catalysed epoxidation of methyl oleate. *European Journal of Lipid Science and Technology* 114 (8):905-910. doi:10.1002/ejlt.201200036
61. Oakley MA, Woodward S, Coupland K, Parker D, Temple-Heald C (1999) Practical dihydroxylation and C–C cleavage of unsaturated fatty acids. *Journal of Molecular Catalysis A: Chemical* 150 (1–2):105-111. doi:[http://dx.doi.org/10.1016/S1381-1169\(99\)00213-7](http://dx.doi.org/10.1016/S1381-1169(99)00213-7)
62. Pai ZP, Tolstikov AG, Berdnikova PV, Kustova GN, Khlebnikova TB, Selivanova NV, Shangina AB, Kostrovskii VG (2005) Catalytic oxidation of olefins and alcohols with hydrogen peroxide in a two-phase system giving mono- and dicarboxylic acids. *Russ Chem Bull* 54 (8):1847-1854. doi:10.1007/s11172-006-0047-z
63. Khlebnikova T, Pai Z, Fedoseeva L, Mattsat Y (2009) Catalytic oxidation of fatty acids. II. Epoxidation and oxidative cleavage of unsaturated fatty acid esters containing additional functional groups. *React Kinet Catal Lett* 98 (1):9-17. doi:10.1007/s11144-009-0054-9
64. Antonelli E, D'Aloisio R, Gambaro M, Fiorani T, Venturello C (1998) Efficient oxidative cleavage of olefins to carboxylic acids with hydrogen peroxide catalyzed by methyltrioctylammonium tetrakis(oxodiperoxotungsto)phosphate(3–) under two-phase conditions. Synthetic aspects and investigation of the reaction course. *The Journal of Organic Chemistry* 63 (21):7190-7206. doi:10.1021/jo980481t
65. Haimov A, Cohen H, Neumann R (2004) Alkylated Polyethyleneimine/Polyoxometalate Synzymes as Catalysts for the Oxidation of Hydrophobic Substrates in Water with Hydrogen Peroxide. *Journal of the American Chemical Society* 126 (38):11762-11763. doi:10.1021/ja046349u
66. Djerassi C, Engle RR (1953) Oxidations with ruthenium tetroxide. *Journal of the American Chemical Society* 75 (15):3838-3840. doi:10.1021/ja01111a507
67. Rüscher M, Klaas G, Bavaj P, Warwel S (1995) Transition-metal catalyzed oxidative cleavage of unsaturated fatty acids. *Lipid / Fett* 97 (10):359-367. doi:10.1002/lipi.19950971002
68. Carlsen PHJ, Katsuki T, Martin VS, Sharpless KB (1981) A greatly improved procedure for ruthenium tetroxide catalyzed oxidations of organic compounds. *The Journal of Organic Chemistry* 46 (19):3936-3938. doi:10.1021/jo00332a045
69. Zimmermann F, Meux E, Mieloszynski J-L, Lecuire J-M, Oget N (2005) Ruthenium catalysed oxidation without CCl<sub>4</sub> of oleic acid, other monoenoic fatty acids and alkenes. *Tetrahedron Letters* 46 (18):3201-3203. doi:<http://dx.doi.org/10.1016/j.tetlet.2005.03.052>
70. Rouquerol J, Avnir D, Fairbridge CW, Everett DH, Haynes JM, Pernicone N, Ramsay JDF, Sing KSW, Unger KK (1994) Recommendations for the characterization of porous solids (Technical Report). *Pure and Applied Chemistry*, vol 66. doi:10.1351/pac199466081739
71. International zeolite association (IZA). <http://www.iza-structure.org/databases/>.



72. Zhang L, He R, Gu H-C (2006) Oleic acid coating on the monodisperse magnetite nanoparticles. *Applied Surface Science* 253 (5):2611-2617. doi:<http://dx.doi.org/10.1016/j.apsusc.2006.05.023>
73. Beck JS, Vartuli JC, Roth WJ, Leonowicz ME, Kresge CT, Schmitt KD, Chu CTW, Olson DH, Sheppard EW (1992) A new family of mesoporous molecular sieves prepared with liquid crystal templates. *Journal of the American Chemical Society* 114 (27):10834-10843. doi:10.1021/ja00053a020
74. Do T-O, Desplandier-Giscard D, Danumah C, Kaliaguine S (2001) Perspectives in catalytic applications of mesostructured materials. *Applied Catalysis A: General* 222 (1-2):299-357. doi:[http://dx.doi.org/10.1016/S0926-860X\(01\)00842-0](http://dx.doi.org/10.1016/S0926-860X(01)00842-0)
75. Dapurkar S, Kawanami H, Yokoyama T, Ikushima Y (2009) Catalytic oxidation of oleic acid in supercritical carbon dioxide media with molecular oxygen. *Topics in Catalysis* 52 (6-7):707-713. doi:10.1007/s11244-009-9212-6
76. Sonnenberg JF, Morris RH (2014) Distinguishing homogeneous from nanoparticle asymmetric iron catalysis. *Catalysis Science & Technology* 4 (10):3426-3438. doi:10.1039/C4CY00468J
77. Astruc D, Lu F, Aranzas JR (2005) Nanoparticles as recyclable catalysts: The frontier between homogeneous and heterogeneous catalysis. *Angewandte Chemie International Edition* 44 (48):7852-7872. doi:10.1002/anie.200500766
78. Chng LL, Erathodiyil N, Ying JY (2013) Nanostructured catalysts for organic transformations. *Accounts of chemical research* 46 (8):1825-1837. doi:10.1021/ar300197s
79. Goesmann H, Feldmann C (2010) Nanoparticulate functional materials. *Angewandte Chemie International Edition* 49 (8):1362-1395. doi:10.1002/anie.200903053
80. Roduner E (2006) Size matters: why nanomaterials are different. *Chemical Society Reviews* 35 (7):583-592. doi:10.1039/B502142C
81. Schätz A, Reiser O, Stark WJ (2010) Nanoparticles as semi-heterogeneous catalyst supports. *Chemistry – A European Journal* 16 (30):8950-8967. doi:10.1002/chem.200903462
82. Somorjai GA, Frei H, Park JY (2009) Advancing the frontiers in nanocatalysis, biointerfaces, and renewable energy conversion by innovations of surface techniques. *Journal of the American Chemical Society* 131 (46):16589-16605. doi:10.1021/ja9061954
83. Bai C, Liu M (2012) Implantation of nanomaterials and nanostructures on surface and their applications. *Nano Today* 7 (4):258-281. doi:<http://dx.doi.org/10.1016/j.nantod.2012.05.002>
84. Mitsudome T, Kaneda K (2013) Advanced core-shell nanoparticle catalysts for efficient organic transformations. *ChemCatChem* 5 (7):1681-1691. doi:10.1002/cctc.201200724
85. Mondloch JE, Bayram E, Finke RG (2012) A review of the kinetics and mechanisms of formation of supported-nanoparticle heterogeneous catalysts. *Journal of Molecular Catalysis A: Chemical* 355 (0):1-38. doi:<http://dx.doi.org/10.1016/j.molcata.2011.11.011>
86. Carrettin S, Concepción P, Corma A, López Nieto JM, Puentes VF (2004) Nanocrystalline ceo<sub>2</sub> increases the activity of au for co oxidation by two orders of magnitude. *Angewandte Chemie International Edition* 43 (19):2538-2540. doi:10.1002/anie.200353570

87. Ho C-M, Yu W-Y, Che C-M (2004) Ruthenium Nanoparticles Supported on Hydroxyapatite as an Efficient and Recyclable Catalyst for cis-Dihydroxylation and Oxidative Cleavage of Alkenes. *Angewandte Chemie International Edition* 43 (25):3303-3307. doi:10.1002/anie.200453703
88. Nguyen T-D, Dinh C-T, Do T-O (2015) Tailoring the assembly, interfaces, and porosity of nanostructures toward enhanced catalytic activity. *Chemical Communications* 51 (4):624-635. doi:10.1039/C4CC05741D
89. Mrabet D, Zahedi-Niaki MH, Do T-O (2008) Synthesis of nanoporous network materials with high surface areas from the cooperative assemblage of alkyl-chain-capped metal/metal oxide nanoparticles. *The Journal of Physical Chemistry C* 112 (18):7124-7129. doi:10.1021/jp7120593
90. Roucoux A, Schulz J, Patin H (2002) Reduced transition metal colloids: a novel family of reusable catalysts? *Chem Rev* 102 (10):3757-3778
91. Enferadi Kerenkan A, Beland F, Do T-O (2016) Chemically catalyzed oxidative cleavage of unsaturated fatty acids and their derivatives into valuable products for industrial applications: a review and perspective. *Catalysis Science & Technology* 6 (4):971-987. doi:10.1039/C5CY01118C
92. Kalidindi SB, Jagirdar BR (2012) Nanocatalysis and prospects of green chemistry. *ChemSusChem* 5 (1):65-75. doi:10.1002/cssc.201100377
93. Kammer FVD, Legros S, Hofmann T, Larsen EH, Loeschner K (2011) Separation and characterization of nanoparticles in complex food and environmental samples by field-flow fractionation. *TrAC - Trends in Analytical Chemistry* 30 (3):425-436. doi:10.1016/j.trac.2010.11.012
94. Lapresta-Fernández A, Salinas-Castillo A, Anderson De La Llana S, Costa-Fernández JM, Domínguez-Meister S, Cecchini R, Capitán-Vallvey LF, Moreno-Bondi MC, Marco MP, Sánchez-López JC, Anderson IS (2014) A general perspective of the characterization and quantification of nanoparticles: Imaging, spectroscopic, and separation techniques. *Critical Reviews in Solid State and Materials Sciences* 39 (6):423-458. doi:10.1080/10408436.2014.899890
95. Sharma RK, Sharma S, Dutta S, Zboril R, Gawande MB (2015) Silica-nanosphere-based organic-inorganic hybrid nanomaterials: Synthesis, functionalization and applications in catalysis. *Green Chemistry* 17 (6):3207-3230. doi:10.1039/c5gc00381d
96. Tsao TM, Chen YM, Wang MK (2011) Origin, separation and identification of environmental nanoparticles: A review. *Journal of Environmental Monitoring* 13 (5):1156-1163. doi:10.1039/c1em10013k
97. Yan N, Xiao C, Kou Y (2010) Transition metal nanoparticle catalysis in green solvents. *Coordination Chemistry Reviews* 254 (9-10):1179-1218. doi:<http://dx.doi.org/10.1016/j.ccr.2010.02.015>
98. Zhu Y, Hosmane NS (2015) Nanocatalysis: Recent advances and applications in boron chemistry. *Coordination Chemistry Reviews* 293-294:357-367. doi:10.1016/j.ccr.2014.10.002

99. Fletcher D (1991) Fine particle high gradient magnetic entrapment. *Magnetics, IEEE Transactions on* 27 (4):3655-3677. doi:10.1109/20.102936
100. Hubbuch J, Matthiesen D, Hobbey T, Thomas OT (2001) High gradient magnetic separation versus expanded bed adsorption: a first principle comparison. *Bioseparation* 10 (1-3):99-112. doi:10.1023/A:1012034923621
101. Moeser GD, Roach KA, Green WH, Alan Hatton T, Laibinis PE (2004) High-gradient magnetic separation of coated magnetic nanoparticles. *AIChE Journal* 50 (11):2835-2848. doi:10.1002/aic.10270
102. Hudson R, Feng Y, Varma RS, Moores A (2014) Bare magnetic nanoparticles: sustainable synthesis and applications in catalytic organic transformations. *Green Chemistry* 16 (10):4493-4505. doi:10.1039/C4GC00418C
103. Rossi LM, Costa NJS, Silva FP, Wojcieszak R (2014) Magnetic nanomaterials in catalysis: advanced catalysts for magnetic separation and beyond. *Green Chemistry* 16 (6):2906-2933. doi:10.1039/C4GC00164H
104. Wang D, Astruc D (2014) Fast-growing field of magnetically recyclable nanocatalysts. *Chemical Reviews* 114 (14):6949-6985. doi:10.1021/cr500134h
105. Matthias Weil W-DS (2013) The Beautiful Colours of Tungsten Oxides. INTERNATIONAL TUNGSTEN INDUSTRY ASSOCIATION,
106. Zheng H, Ou JZ, Strano MS, Kaner RB, Mitchell A, Kalantar-zadeh K (2011) Nanostructured Tungsten Oxide – Properties, Synthesis, and Applications. *Advanced Functional Materials* 21 (12):2175-2196. doi:10.1002/adfm.201002477
107. J. Christian RPSG, T. Wolfe and J. R. L. Trasorras (2011) Tungsten Chemicals and their Applications. INTERNATIONAL TUNGSTEN INDUSTRY ASSOCIATION,
108. Song J, Huang Z-F, Pan L, Zou J-J, Zhang X, Wang L (2015) Oxygen-Deficient Tungsten Oxide as Versatile and Efficient Hydrogenation Catalyst. *ACS Catalysis* 5 (11):6594-6599. doi:10.1021/acscatal.5b01522
109. Wasmi BA, Al-Amiery AA, Kadhum AAH, Mohamad AB (2014) Novel Approach: Tungsten Oxide Nanoparticle as a Catalyst for Malonic Acid Ester Synthesis via Ozonolysis. *Journal of Nanomaterials* 2014:7. doi:10.1155/2014/715457
110. Barton DG, Shtein M, Wilson RD, Soled SL, Iglesia E (1999) Structure and Electronic Properties of Solid Acids Based on Tungsten Oxide Nanostructures. *The Journal of Physical Chemistry B* 103 (4):630-640. doi:10.1021/jp983555d
111. Barton DG, Soled SL, Iglesia E (1998) Solid acid catalysts based on supported tungsten oxides. *Topics in Catalysis* 6 (1):87-99. doi:10.1023/a:1019126708945
112. Barton DG, Soled SL, Meitzner GD, Fuentes GA, Iglesia E (1999) Structural and Catalytic Characterization of Solid Acids Based on Zirconia Modified by Tungsten Oxide. *Journal of Catalysis* 181 (1):57-72. doi:<http://dx.doi.org/10.1006/jcat.1998.2269>
113. Benitez VM, Querini CA, Figoli NS, Comelli RA (1999) Skeletal isomerization of 1-butene on  $WO_x/\gamma-Al_2O_3$ . *Applied Catalysis A: General* 178 (2):205-218. doi:[https://doi.org/10.1016/S0926-860X\(98\)00287-7](https://doi.org/10.1016/S0926-860X(98)00287-7)

114. Bernholc J, Horsley JA, Murrell LL, Sherman LG, Soled S (1987) Broensted acid sites in transition metal oxide catalysts: modeling of structure, acid strengths, and support effects. *The Journal of Physical Chemistry* 91 (6):1526-1530. doi:10.1021/j100290a047
115. Busca G (1999) The surface acidity of solid oxides and its characterization by IR spectroscopic methods. An attempt at systematization. *Physical Chemistry Chemical Physics* 1 (5):723-736. doi:10.1039/A808366E
116. Carniti P, Gervasini A, Auroux A (1994) Energy Distribution of Surface Acid Sites of Metal Oxides. *Journal of Catalysis* 150 (2):274-283. doi:<http://dx.doi.org/10.1006/jcat.1994.1346>
117. Martín C, Malet P, Solana G, Rives V (1998) Structural Analysis of Silica-Supported Tungstates. *The Journal of Physical Chemistry B* 102 (15):2759-2768. doi:10.1021/jp980614e
118. Thomas R, van Oers EM, de Beer VHJ, Medema J, Moulijn JA (1982) Characterization of  $\gamma$ -alumina-supported Molybdenum oxide and tungsten oxide; reducibility of the oxidic state versus hydrodesulfurization activity of the sulfided state. *Journal of Catalysis* 76 (2):241-253. doi:[http://dx.doi.org/10.1016/0021-9517\(82\)90255-X](http://dx.doi.org/10.1016/0021-9517(82)90255-X)
119. Kosmulski M (2014) The pH dependent surface charging and points of zero charge. VI. Update. *Journal of Colloid and Interface Science* 426:209-212. doi:<https://doi.org/10.1016/j.jcis.2014.02.036>
120. Morse PM, Shelby QD, Kim DY, Girolami GS (2008) Ethylene Complexes of the Early Transition Metals: Crystal Structures of [HfEt<sub>4</sub>(C<sub>2</sub>H<sub>4</sub>)<sub>2</sub>-] and the Negative-Oxidation-State Species [TaHEt(C<sub>2</sub>H<sub>4</sub>)<sub>3</sub>-] and [W(C<sub>2</sub>H<sub>4</sub>)<sub>4</sub>-]. *Organometallics* 27 (5):984-993. doi:10.1021/om701189e
121. O'Neill HSC, Berry AJ, Eggins SM (2008) The solubility and oxidation state of tungsten in silicate melts: Implications for the comparative chemistry of W and Mo in planetary differentiation processes. *Chemical Geology* 255 (3-4):346-359. doi:<https://doi.org/10.1016/j.chemgeo.2008.07.005>
122. Lu Y, Yin H, Wu H, Liu H, Jiang T, Wada Y (2006) Structural effect of tungsten oxides on selective oxidation of cyclopentene to glutaraldehyde. *Catalysis Communications* 7 (11):832-838. doi:<http://dx.doi.org/10.1016/j.catcom.2006.03.006>
123. Dai W-L, Ding J, Zhu Q, Gao R, Yang X (2016) Tungsten containing materials as heterogeneous catalysts for green catalytic oxidation process. In: *Catalysis: Volume 28, vol 28*. The Royal Society of Chemistry, pp 1-27. doi:10.1039/9781782626855-00001
124. Moffat JB (2001) *Metal-Oxygen Clusters: The Surface and Catalytic Properties of Heteropoly Oxometalates*. Springer,
125. Patel A, Narkhede N, Singh S, Pathan S (2016) Keggin-type lacunary and transition metal substituted polyoxometalates as heterogeneous catalysts: A recent progress. *Catalysis Reviews* 58 (3):337-370. doi:10.1080/01614940.2016.1171606
126. Kozhevnikov IV (2007) Sustainable heterogeneous acid catalysis by heteropoly acids. *Journal of Molecular Catalysis A: Chemical* 262 (1-2):86-92. doi:<https://doi.org/10.1016/j.molcata.2006.08.072>

127. Mattes R (1984) Heteropoly and Isopoly Oxometalates. Von M. T. Pope. Springer-Verlag, Berlin 1983. XIII, 180 S., geb. DM 124.00. *Angewandte Chemie* 96 (9):730-730. doi:10.1002/ange.19840960939
128. Pope M (1983) *Inorganic Chemistry Concepts Vol. 8: Heteropoly and Isopoly Oxometalates*. In. Springer,
129. Keggin JF (1934) The Structure and Formula of 12-Phosphotungstic Acid. *Proceedings of the Royal Society of London Series A* 144 (851):75
130. Misono M (1987) Heterogeneous Catalysis by Heteropoly Compounds of Molybdenum and Tungsten. *Catalysis Reviews* 29 (2-3):269-321. doi:10.1080/01614948708078072
131. Okuhara T (2002) Water-Tolerant Solid Acid Catalysts. *Chemical Reviews* 102 (10):3641-3666. doi:10.1021/cr0103569
132. Sato R, Suzuki K, Sugawa M, Mizuno N (2013) Heterodinuclear Lanthanoid-Containing Polyoxometalates: Stepwise Synthesis and Single-Molecule Magnet Behavior. *Chemistry – A European Journal* 19 (39):12982-12990. doi:10.1002/chem.201302596
133. Hill CL, Prosser-McCartha CM (1995) Homogeneous catalysis by transition metal oxygen anion clusters. *Coordination Chemistry Reviews* 143:407-455. doi:[http://dx.doi.org/10.1016/0010-8545\(95\)01141-B](http://dx.doi.org/10.1016/0010-8545(95)01141-B)
134. Yu R, Kuang X-F, Wu X-Y, Lu C-Z, Donahue JP (2009) Stabilization and immobilization of polyoxometalates in porous coordination polymers through host–guest interactions. *Coordination Chemistry Reviews* 253 (23–24):2872-2890. doi:<https://doi.org/10.1016/j.ccr.2009.07.003>
135. Zheng S-T, Yang G-Y (2012) Recent advances in paramagnetic-TM-substituted polyoxometalates (TM = Mn, Fe, Co, Ni, Cu). *Chemical Society Reviews* 41 (22):7623-7646. doi:10.1039/C2CS35133A
136. Mizuno N, Yamaguchi K, Kamata K (2011) Molecular Design of Polyoxometalate-Based Compounds for Environmentally-Friendly Functional Group Transformations: From Molecular Catalysts to Heterogeneous Catalysts. *Catalysis Surveys from Asia* 15 (2):68-79. doi:10.1007/s10563-011-9111-2
137. Kholdeeva OA, Maksimchuk NV, Maksimov GM (2010) Polyoxometalate-based heterogeneous catalysts for liquid phase selective oxidations: Comparison of different strategies. *Catalysis Today* 157 (1–4):107-113. doi:<https://doi.org/10.1016/j.cattod.2009.12.016>
138. Mizuno N, Kamata K (2011) Catalytic oxidation of hydrocarbons with hydrogen peroxide by vanadium-based polyoxometalates. *Coordination Chemistry Reviews* 255 (19–20):2358-2370. doi:<https://doi.org/10.1016/j.ccr.2011.01.041>
139. Mizuno N, Yamaguchi K, Kamata K (2005) Epoxidation of olefins with hydrogen peroxide catalyzed by polyoxometalates. *Coordination Chemistry Reviews* 249 (17–18):1944-1956. doi:<https://doi.org/10.1016/j.ccr.2004.11.019>
140. Narkhede N, Singh S, Patel A (2015) Recent progress on supported polyoxometalates for biodiesel synthesis via esterification and transesterification. *Green Chemistry* 17 (1):89-107. doi:10.1039/C4GC01743A

141. Misono M (2001) Unique acid catalysis of heteropoly compounds (heteropolyoxometalates) in the solid state. *Chemical Communications* (13):1141-1152. doi:10.1039/B102573M
142. Makoto Misono NM, Koichi Katamura, Atsushi Kasai, Yasuo Konishi, Kanji Sakata, Toshio Okuhara, Yukio Yoneda (1982) Catalysis by Heteropoly Compounds. III. The Structure and Properties of 12-Heteropolyacids of Molybdenum and Tungsten (H<sub>3</sub>PMo<sub>12-x</sub>W<sub>x</sub>O<sub>40</sub>) and Their Salts Pertinent to Heterogeneous Catalysis. *Bulletin of the Chemical Society of Japan* 55 (2):400-406. doi:10.1246/bcsj.55.400
143. Misono M (1992) Heterogeneous catalysis by heteropoly compounds. An attempt of molecular design of practical solid acid catalysts. *Catalysis Letters* 12 (1):63-71. doi:10.1007/bf00767189
144. Kozhevnikov IV (2009) Heterogeneous acid catalysis by heteropoly acids: Approaches to catalyst deactivation. *Journal of Molecular Catalysis A: Chemical* 305 (1):104-111. doi:<http://dx.doi.org/10.1016/j.molcata.2008.11.029>
145. Moffat JB, McMonagle JB, Taylor D (1988) Microporous heteropoly oxometalate heterogeneous catalysis. *Solid State Ionics* 26 (2):101-108. doi:[http://dx.doi.org/10.1016/0167-2738\(88\)90020-3](http://dx.doi.org/10.1016/0167-2738(88)90020-3)
146. Okuhara T, Nakato T (1998) Catalysis by porous heteropoly compounds. *Catalysis Surveys from Asia* 2 (1):31-44. doi:10.1023/a:1019053719634
147. Okuhara T, Watanabe H, Nishimura T, Inumaru K, Misono M (2000) Microstructure of Cesium Hydrogen Salts of 12-Tungstophosphoric Acid Relevant to Novel Acid Catalysis. *Chemistry of Materials* 12 (8):2230-2238. doi:10.1021/cm9907561
148. Toshio O, Toru N, Makoto M (1995) Microporous Heteropoly Compound as a Shape Selective Catalyst : Cs<sub>2.2</sub>H<sub>0.8</sub>PW<sub>12</sub>O<sub>40</sub>. *Chemistry Letters* 24 (2):155-156. doi:10.1246/cl.1995.155
149. Okuhara T, Nishimura T, Watanabe H, Misono M (1992) Insoluble heteropoly compounds as highly active catalysts for liquid-phase reactions. *Journal of Molecular Catalysis* 74 (1):247-256. doi:[http://dx.doi.org/10.1016/0304-5102\(92\)80242-9](http://dx.doi.org/10.1016/0304-5102(92)80242-9)
150. Liu M, Deng W, Zhang Q, Wang Y, Wang Y (2011) Polyoxometalate-supported ruthenium nanoparticles as bifunctional heterogeneous catalysts for the conversions of cellobiose and cellulose into sorbitol under mild conditions. *Chemical Communications* 47 (34):9717-9719. doi:10.1039/C1CC12506K
151. Liu Y, Murata K, Inaba M (2016) Heterogeneous carbonylation of dimethyl ether to methyl acetate over bifunctional catalysts containing Rh and heteropoly acids. *Reaction Kinetics, Mechanisms and Catalysis* 117 (1):223-238. doi:10.1007/s11144-015-0914-4
152. Matouq M, Tagawa T, Goto S (1993) Liquid-Phase Synthesis of Methyl *t*-Butyl Ether on Heterogeneous Heteropoly Acid Catalyst. *JOURNAL OF CHEMICAL ENGINEERING OF JAPAN* 26 (3):254-258. doi:10.1252/jcej.26.254

153. Pesaresi L, Brown DR, Lee AF, Montero JM, Williams H, Wilson K (2009) Cs-doped H<sub>4</sub>SiW<sub>12</sub>O<sub>40</sub> catalysts for biodiesel applications. *Applied Catalysis A: General* 360 (1):50-58. doi:<https://doi.org/10.1016/j.apcata.2009.03.003>
154. Okamoto K, Uchida S, Ito T, Mizuno N (2007) Self-Organization of All-Inorganic Dodecatungstophosphate Nanocrystallites. *Journal of the American Chemical Society* 129 (23):7378-7384. doi:10.1021/ja070694c
155. Inumaru K (2006) "Sponge Crystal": a novel class of microporous single crystals formed by self-assembly of polyoxometalate (NH<sub>4</sub>)<sub>3</sub>PW<sub>12</sub>O<sub>40</sub> nanocrystallites. *Catalysis Surveys from Asia* 10 (3):151-160. doi:10.1007/s10563-006-9014-9
156. Ito T, Inumaru K, Misono M (1997) Structure of Porous Aggregates of the Ammonium Salt of Dodecatungstophosphoric Acid, (NH<sub>4</sub>)<sub>3</sub>PW<sub>12</sub>O<sub>40</sub>: Unidirectionally Oriented Self-Assembly of Nanocrystallites. *The Journal of Physical Chemistry B* 101 (48):9958-9963. doi:10.1021/jp9714835
157. Zhang S, Zu Y-G, Fu Y-J, Luo M, Zhang D-Y, Efferth T (2010) Rapid microwave-assisted transesterification of yellow horn oil to biodiesel using a heteropolyacid solid catalyst. *Bioresource Technology* 101 (3):931-936. doi:<https://doi.org/10.1016/j.biortech.2009.08.069>
158. Badday AS, Abdullah AZ, Lee K-T (2013) Ultrasound-assisted transesterification of crude *Jatropha* oil using cesium doped heteropolyacid catalyst: Interactions between process variables. *Energy* 60:283-291. doi:<https://doi.org/10.1016/j.energy.2013.08.002>
159. Costa VV, da Silva Rocha KA, Mesquita RA, Kozhevnikova EF, Kozhevnikov IV, Gusevskaya EV (2013) Heteropoly Acid Catalysts for the Synthesis of Fragrance Compounds from Biorenewables: Cycloaddition of Crotonaldehyde to Limonene,  $\alpha$ -Pinene, and  $\beta$ -Pinene. *ChemCatChem* 5 (10):3022-3026. doi:10.1002/cctc.201300208
160. Chen L, Nohair B, Kaliaguine S (2016) Glycerol acetalization with formaldehyde using water-tolerant solid acids. *Applied Catalysis A: General* 509:143-152. doi:<https://doi.org/10.1016/j.apcata.2015.08.014>
161. Thakur A, Sharma A, Sharma A (2016) Efficient synthesis of xanthenedione derivatives using cesium salt of phosphotungstic acid as a heterogeneous and reusable catalyst in water. *Synthetic Communications* 46 (21):1766-1771. doi:10.1080/00397911.2016.1226340
162. Firouzabadi H, Iranpoor N, Amani K (2002) Heteropoly Acids as Heterogeneous Catalysts for Thioacetalization and Transthioacetalization Reactions. *Synthesis* 2002 (01):0059-0062. doi:10.1055/s-2002-19300
163. Borghese S, Louis B, Blanc A, Pale P (2011) Design of silver(i)-heteropolyacids: toward the molecular control of reactivity in organic chemistry. *Catalysis Science & Technology* 1 (6):981-986. doi:10.1039/C1CY00154J
164. Fan C, Guan H, Zhang H, Wang J, Wang S, Wang X (2011) Conversion of fructose and glucose into 5-hydroxymethylfurfural catalyzed by a solid heteropolyacid salt. *Biomass and Bioenergy* 35 (7):2659-2665. doi:<https://doi.org/10.1016/j.biombioe.2011.03.004>
165. Yang L, Xu L-W, Xia C-G (2008) Heteropoly acids: a green and efficient heterogeneous Brønsted acidic catalyst for the intermolecular hydroamination of olefins. *Tetrahedron Letters* 49 (18):2882-2885. doi:<http://dx.doi.org/10.1016/j.tetlet.2008.03.034>

166. Romanelli G, Ruiz D, Vázquez P, Thomas H, Autino JC (2010) Preyssler heteropolyacid H14[NaP5W29MoO110]: A heterogeneous, green and recyclable catalyst used for the protection of functional groups in organic synthesis. *Chemical Engineering Journal* 161 (3):355-362. doi:<https://doi.org/10.1016/j.cej.2009.12.029>
167. Zhao S, Chen Y, Song Y-F (2014) Tri-lacunary polyoxometalates of Na8H[PW9O34] as heterogeneous Lewis base catalysts for Knoevenagel condensation, cyanosilylation and the synthesis of benzoxazole derivatives. *Applied Catalysis A: General* 475:140-146. doi:<https://doi.org/10.1016/j.apcata.2014.01.017>
168. Vu THT, Au HT, Nguyen TMT, Pham MT, Bach TT, Nong HN (2013) Esterification of 2-keto-l-gulonic acid catalyzed by a solid heteropoly acid. *Catalysis Science & Technology* 3 (3):699-705. doi:10.1039/C2CY20497E
169. Matachowski L, Drelinkiewicz A, Lalik E, Ruggiero-Mikołajczyk M, Mucha D, Kryściak-Czerwenka J (2014) Efficient dehydration of ethanol on the self-organized surface layer of H3PW12O40 formed in the acidic potassium tungstophosphates. *Applied Catalysis A: General* 469:290-299. doi:<https://doi.org/10.1016/j.apcata.2013.10.009>
170. Ramesh Kumar C, Rao KTV, Sai Prasad PS, Lingaiah N (2011) Tin exchanged heteropoly tungstate: An efficient catalyst for benzylation of arenes with benzyl alcohol. *Journal of Molecular Catalysis A: Chemical* 337 (1–2):17-24. doi:<https://doi.org/10.1016/j.molcata.2011.01.008>
171. Li J, Wang X, Zhu W, Cao F (2009) Zn1.2H0.6PW12O40 Nanotubes with Double Acid Sites as Heterogeneous Catalysts for the Production of Biodiesel from Waste Cooking Oil. *ChemSusChem* 2 (2):177-183. doi:10.1002/cssc.200800208
172. Wang J, Luo G, Liu C, Lai J (2014) Polyvalent-metal Salts of Phosphotungstate as Efficient Heterogeneous Catalysts for the Esterification of Fatty Acids. *Energy Sources, Part A: Recovery, Utilization, and Environmental Effects* 36 (5):479-488. doi:10.1080/15567036.2010.542441
173. Xue X, Song F, Ma B, Yu Y, Li C, Ding Y (2013) Selective ammoximation of ketones and aldehydes catalyzed by a trivanadium-substituted polyoxometalate with H2O2 and ammonia. *Catalysis Communications* 33:61-65. doi:<https://doi.org/10.1016/j.catcom.2012.12.021>
174. Shi L-X, Zhao W-F, Xu X, Tang J, Wu C-D (2011) From 1D to 3D Single-Crystal-to-Single-Crystal Structural Transformations Based on Linear Polyanion [Mn4(H2O)18WZnMn2(H2O)2(ZnW9O34)2]4-. *Inorganic Chemistry* 50 (24):12387-12389. doi:10.1021/ic2020572
175. Proust A, Matt B, Villanneau R, Guillemot G, Gouzerh P, Izzet G (2012) Functionalization and post-functionalization: a step towards polyoxometalate-based materials. *Chemical Society Reviews* 41 (22):7605-7622. doi:10.1039/C2CS35119F
176. Organically Functionalized Metallic Oxo-Clusters: Structurally Well-Defined Nanobuilding Blocks for the Design of Hybrid Organic-Inorganic Materials (1999). *Comments on Inorganic Chemistry* 20 (4-6):327-371. doi:10.1080/02603599908021449



177. Dolbecq A, Dumas E, Mayer CR, Mialane P (2010) Hybrid Organic–Inorganic Polyoxometalate Compounds: From Structural Diversity to Applications. *Chemical Reviews* 110 (10):6009-6048. doi:10.1021/cr1000578
178. Loy DA, Shea KJ (1995) Bridged Polysilsesquioxanes. Highly Porous Hybrid Organic-Inorganic Materials. *Chemical Reviews* 95 (5):1431-1442. doi:10.1021/cr00037a013
179. Ivanova S (2014) Hybrid Organic-Inorganic Materials Based on Polyoxometalates and Ionic Liquids and Their Application in Catalysis. *ISRN Chemical Engineering* 2014:13. doi:10.1155/2014/963792
180. Liu Y, Shrestha S, Mustain WE (2012) Synthesis of nanosize tungsten oxide and its evaluation as an electrocatalyst support for oxygen reduction in acid media. *ACS Catalysis* 2 (3):456-463. doi:10.1021/cs200657w
181. Mirzaei M, Eshtiagh-Hosseini H, Alipour M, Frontera A (2014) Recent developments in the crystal engineering of diverse coordination modes (0–12) for Keggin-type polyoxometalates in hybrid inorganic–organic architectures. *Coordination Chemistry Reviews* 275:1-18. doi:<https://doi.org/10.1016/j.ccr.2014.03.012>
182. Nisar A, Wang X (2012) Surfactant-encapsulated polyoxometalate building blocks: controlled assembly and their catalytic properties. *Dalton Transactions* 41 (33):9832-9845. doi:10.1039/C2DT30470H
183. Nlate S, Jahier C (2013) Dendritic Polyoxometalate Hybrids: Efficient and Recoverable Catalysts for Oxidation Reactions. *European Journal of Inorganic Chemistry* 2013 (10-11):1606-1619. doi:10.1002/ejic.201201129
184. Ren Y, Wang M, Chen X, Yue B, He H (2015) Heterogeneous Catalysis of Polyoxometalate Based Organic–Inorganic Hybrids. *Materials* 8 (4):1545
185. Santoni M-P, Hanan GS, Hasenknopf B (2014) Covalent multi-component systems of polyoxometalates and metal complexes: Toward multi-functional organic–inorganic hybrids in molecular and material sciences. *Coordination Chemistry Reviews* 281:64-85. doi:<http://dx.doi.org/10.1016/j.ccr.2014.09.003>
186. Song Y-F, Tsunashima R (2012) Recent advances on polyoxometalate-based molecular and composite materials. *Chemical Society Reviews* 41 (22):7384-7402. doi:10.1039/C2CS35143A
187. Coronado E, Giménez-Saiz C, Gómez-García CJ (2005) Recent advances in polyoxometalate-containing molecular conductors. *Coordination Chemistry Reviews* 249 (17–18):1776-1796. doi:<https://doi.org/10.1016/j.ccr.2005.02.017>
188. Sanchez C, Soler-Illia GJdAA, Ribot F, Lalot T, Mayer CR, Cabuil V (2001) Designed Hybrid Organic–Inorganic Nanocomposites from Functional Nanobuilding Blocks. *Chemistry of Materials* 13 (10):3061-3083. doi:10.1021/cm011061e
189. Wu H, Yang H-K, Wang W (2016) Covalently-linked polyoxometalate-polymer hybrids: optimizing synthesis, appealing structures and prospective applications. *New Journal of Chemistry* 40 (2):886-897. doi:10.1039/C5NJ01257K
190. Bourlinos AB, Raman K, Herrera R, Zhang Q, Archer LA, Giannelis EP (2004) A Liquid Derivative of 12-Tungstophosphoric Acid with Unusually High Conductivity. *Journal of the American Chemical Society* 126 (47):15358-15359. doi:10.1021/ja046821b

191. Zhou Y, Chen G, Long Z, Wang J (2014) Recent advances in polyoxometalate-based heterogeneous catalytic materials for liquid-phase organic transformations. *RSC Advances* 4 (79):42092-42113. doi:10.1039/C4RA05175K
192. Liu S, Tang Z (2010) Polyoxometalate-based functional nanostructured films: Current progress and future prospects. *Nano Today* 5 (4):267-281. doi:<https://doi.org/10.1016/j.nantod.2010.05.006>
193. Zhang G, Keita B, Craescu CT, Miron S, de Oliveira P, Nadjo L (2007) Polyoxometalate Binding to Human Serum Albumin: A Thermodynamic and Spectroscopic Approach. *The Journal of Physical Chemistry B* 111 (38):11253-11259. doi:10.1021/jp072947u
194. Zhou Y, Zheng L, Han F, Zhang G, Ma Y, Yao J, Keita B, de Oliveira P, Nadjo L (2011) Inhibition of amyloid- $\beta$  protein fibrillization upon interaction with polyoxometalates nanoclusters. *Colloids and Surfaces A: Physicochemical and Engineering Aspects* 375 (1-3):97-101. doi:<https://doi.org/10.1016/j.colsurfa.2010.11.068>
195. Leclercq L, Mouret A, Proust A, Schmitt V, Bauduin P, Aubry J-M, Nardello-Rataj V (2012) Pickering Emulsion Stabilized by Catalytic Polyoxometalate Nanoparticles: A New Effective Medium for Oxidation Reactions. *Chemistry – A European Journal* 18 (45):14352-14358. doi:10.1002/chem.201201799
196. Mizuno N, Uchida S, Kamata K, Ishimoto R, Nojima S, Yonehara K, Sumida Y (2010) A Flexible Nonporous Heterogeneous Catalyst for Size-Selective Oxidation through a Bottom-Up Approach. *Angewandte Chemie International Edition* 49 (51):9972-9976. doi:10.1002/anie.201005275
197. Zhao Q, Wang H, Zheng H, Sun Z, Shi W, Wang S, Wang X, Jiang Z (2013) Acid-base bifunctional HPA nanocatalysts promoting heterogeneous transesterification and esterification reactions. *Catalysis Science & Technology* 3 (9):2204-2209. doi:10.1039/C3CY20868K
198. Zhao S, Cheng M, Li J, Tian J, Wang X (2011) One pot production of 5-hydroxymethylfurfural with high yield from cellulose by a Bronsted-Lewis-surfactant-combined heteropolyacid catalyst. *Chemical Communications* 47 (7):2176-2178. doi:10.1039/C0CC04444J
199. Cheng M, Shi T, Guan H, Wang S, Wang X, Jiang Z (2011) Clean production of glucose from polysaccharides using a micellar heteropolyacid as a heterogeneous catalyst. *Applied Catalysis B: Environmental* 107 (1-2):104-109. doi:<https://doi.org/10.1016/j.apcatb.2011.07.002>
200. Leng Y, Wang J, Zhu D, Ren X, Ge H, Shen L (2009) Heteropolyanion-Based Ionic Liquids: Reaction-Induced Self-Separation Catalysts for Esterification. *Angewandte Chemie International Edition* 48 (1):168-171. doi:10.1002/anie.200803567
201. Leng Y, Wang J, Zhu D, Wu Y, Zhao P (2009) Sulfonated organic heteropolyacid salts: Recyclable green solid catalysts for esterifications. *Journal of Molecular Catalysis A: Chemical* 313 (1-2):1-6. doi:<https://doi.org/10.1016/j.molcata.2009.08.011>
202. Zhang W, Leng Y, Zhu D, Wu Y, Wang J (2009) Phosphotungstic acid salt of triphenyl(3-sulfopropyl)phosphonium: An efficient and reusable solid catalyst for esterification. *Catalysis Communications* 11 (3):151-154. doi:<https://doi.org/10.1016/j.catcom.2009.09.009>

203. Han X-X, He Y-F, Hung C-T, Liu L-L, Huang S-J, Liu S-B (2013) Efficient and reusable polyoxometalate-based sulfonated ionic liquid catalysts for palmitic acid esterification to biodiesel. *Chemical Engineering Science* 104:64-72. doi:<https://doi.org/10.1016/j.ces.2013.08.059>
204. Zhang W, Leng Y, Zhao P, Wang J, Zhu D, Huang J (2011) Heteropolyacid salts of N-methyl-2-pyrrolidonium as highly efficient and reusable catalysts for Prins reactions of styrenes with formalin. *Green Chemistry* 13 (4):832-834. doi:10.1039/C0GC00729C
205. Zhang X, Mao D, Leng Y, Zhou Y, Wang J (2013) Heterogeneous Beckmann Rearrangements Catalyzed by a Sulfonated Imidazolium Salt of Phosphotungstate. *Catalysis Letters* 143 (2):193-199. doi:10.1007/s10562-012-0939-5
206. Mao D, Long Z, Zhou Y, Li J, Wang X, Wang J (2014) Dual-sulfonated dipyridinium phosphotungstate catalyst for liquid-phase Beckmann rearrangement of cyclohexanone oxime. *RSC Advances* 4 (30):15635-15641. doi:10.1039/C4RA00552J
207. Li K, Chen L, Wang H, Lin W, Yan Z (2011) Heteropolyacid salts as self-separation and recyclable catalysts for transesterification of trimethylolpropane. *Applied Catalysis A: General* 392 (1-2):233-237. doi:<https://doi.org/10.1016/j.apcata.2010.11.011>
208. Zhang Z, Dong K, Zhao Z (2011) Efficient Conversion of Furfuryl Alcohol into Alkyl Levulinates Catalyzed by an Organic-Inorganic Hybrid Solid Acid Catalyst. *ChemSusChem* 4 (1):112-118. doi:10.1002/cssc.201000231
209. Chen J, Zhao G, Chen L (2014) Efficient production of 5-hydroxymethylfurfural and alkyl levulinate from biomass carbohydrate using ionic liquid-based polyoxometalate salts. *RSC Advances* 4 (8):4194-4202. doi:10.1039/C3RA45632C
210. Zhang M, Zhao P, Leng Y, Chen G, Wang J, Huang J (2012) Schiff Base Structured Acid-Base Cooperative Dual Sites in an Ionic Solid Catalyst Lead to Efficient Heterogeneous Knoevenagel Condensations. *Chemistry – A European Journal* 18 (40):12773-12782. doi:10.1002/chem.201201338
211. Li H, Qiao Y, Hua L, Hou Z, Feng B, Pan Z, Hu Y, Wang X, Zhao X, Yu Y (2010) Imidazolium Polyoxometalate: An Ionic Liquid Catalyst for Esterification and Oxidative Esterification. *ChemCatChem* 2 (9):1165-1170. doi:10.1002/cctc.201000021
212. Kato CN, Ogasawara T, Kondo A, Kato D (2017) Heterogeneous esterification of fatty acids with methanol catalyzed by Lewis acidic organozirconium complexes with Keggin-type mono-aluminum-substituted polyoxotungstates. *Catalysis Communications* 96:41-45. doi:<https://doi.org/10.1016/j.catcom.2017.03.025>
213. Kawahara R, Osuga R, Kondo JN, Mizuno N, Uchida S (2017) Synergetic effect in heterogeneous acid catalysis by a porous ionic crystal based on Al(iii)-salphen and polyoxometalate. *Dalton Transactions* 46 (10):3105-3109. doi:10.1039/C6DT04552A
214. Uchida S, Kamata K, Ogasawara Y, Fujita M, Mizuno N (2012) Structural and dynamical aspects of alkylammonium salts of a silicodectungstate as heterogeneous epoxidation catalysts. *Dalton Transactions* 41 (33):9979-9983. doi:10.1039/C2DT30492A
215. Nisar A, Zhuang J, Wang X (2011) Construction of Amphiphilic Polyoxometalate Mesostuctures as a Highly Efficient Desulfurization Catalyst. *Advanced Materials* 23 (9):1130-1135. doi:10.1002/adma.201003520

216. Li H, Yu X, Zheng H, Li Y, Wang X, Huo M (2014) Catalytic wet peroxide oxidation of phenol by [C<sub>16</sub>H<sub>33</sub>(CH<sub>3</sub>)<sub>3</sub>N]<sub>4</sub>H<sub>2</sub>SiV<sub>2</sub>W<sub>10</sub>O<sub>40</sub> catalyst. *RSC Advances* 4 (14):7266-7274. doi:10.1039/C3RA46453A
217. Xu J, Zhao S, Ji Y, Song Y-F (2013) Deep Desulfurization by Amphiphilic Lanthanide-Containing Polyoxometalates in Ionic-Liquid Emulsion Systems under Mild Conditions. *Chemistry – A European Journal* 19 (2):709-715. doi:10.1002/chem.201202595
218. Huang W, Zhu W, Li H, Shi H, Zhu G, Liu H, Chen G (2010) Heteropolyanion-Based Ionic Liquid for Deep Desulfurization of Fuels in Ionic Liquids. *Industrial & Engineering Chemistry Research* 49 (19):8998-9003. doi:10.1021/ie100234d
219. Rafiee E, Eavani S (2013) Organic–inorganic polyoxometalate based salts as thermoregulated phase-separable catalysts for selective oxidation of thioethers and thiophenes and deep desulfurization of model fuels. *Journal of Molecular Catalysis A: Chemical* 380:18-27. doi:<https://doi.org/10.1016/j.molcata.2013.09.009>
220. Qiao Y, Hou Z, Li H, Hu Y, Feng B, Wang X, Hua L, Huang Q (2009) Polyoxometalate-based protic alkylimidazolium salts as reaction-induced phase-separation catalysts for olefin epoxidation. *Green Chemistry* 11 (12):1955-1960. doi:10.1039/B916766H
221. Li H, Hou Z, Qiao Y, Feng B, Hu Y, Wang X, Zhao X (2010) Peroxopolyoxometalate-based room temperature ionic liquid as a self-separation catalyst for epoxidation of olefins. *Catalysis Communications* 11 (5):470-475. doi:<https://doi.org/10.1016/j.catcom.2009.11.025>
222. Chen J, Hua L, Zhu W, Zhang R, Guo L, Chen C, Gan H, Song B, Hou Z (2014) Polyoxometalate anion-functionalized ionic liquid as a thermoregulated catalyst for the epoxidation of olefins. *Catalysis Communications* 47:18-21. doi:<https://doi.org/10.1016/j.catcom.2014.01.003>
223. Leng Y, Wang J, Zhu D, Zhang M, Zhao P, Long Z, Huang J (2011) Polyoxometalate-based amino-functionalized ionic solid catalysts lead to highly efficient heterogeneous epoxidation of alkenes with H<sub>2</sub>O<sub>2</sub>. *Green Chemistry* 13 (7):1636-1639. doi:10.1039/C1GC15302A
224. Leng Y, Zhao P, Zhang M, Wang J (2012) Amino functionalized bipyridine–heteropolyacid ionic hybrid: A recyclable catalyst for solvent-free oxidation of benzyl alcohol with H<sub>2</sub>O<sub>2</sub>. *Journal of Molecular Catalysis A: Chemical* 358:67-72. doi:<https://doi.org/10.1016/j.molcata.2012.02.012>
225. Leng Y, Zhao P, Zhang M, Chen G, Wang J (2012) A dicationic ionic liquid-modified phosphotungstate hybrid catalyst for the heterogeneous oxidation of alcohols with H<sub>2</sub>O<sub>2</sub>. *Science China Chemistry* 55 (9):1796-1801. doi:10.1007/s11426-012-4722-7
226. Zhao P, Zhang M, Wu Y, Wang J (2012) Heterogeneous Selective Oxidation of Sulfides with H<sub>2</sub>O<sub>2</sub> Catalyzed by Ionic Liquid-Based Polyoxometalate Salts. *Industrial & Engineering Chemistry Research* 51 (19):6641-6647. doi:10.1021/ie202232j
227. Chen G, Zhou Y, Zhao P, Long Z, Wang J (2013) Mesoporous Dihydroxy-Functionalized Guanidinium-Based Polyoxometalate with Enhanced Heterogeneous Catalytic Activity in Epoxidation. *ChemPlusChem* 78 (6):561-569. doi:10.1002/cplu.201300105

228. Chen G, Zhou Y, Long Z, Wang X, Li J, Wang J (2014) Mesoporous Polyoxometalate-Based Ionic Hybrid As a Triphasic Catalyst for Oxidation of Benzyl Alcohol with H<sub>2</sub>O<sub>2</sub> on Water. *ACS Applied Materials & Interfaces* 6 (6):4438-4446. doi:10.1021/am5001757
229. Mirhoseini H, Taghdiri M (2016) Extractive oxidation desulfurization of sulfur-containing model fuel using hexamine–phosphotungstate hybrid as effective heterogeneous catalyst. *Fuel* 167:60-67. doi:<http://dx.doi.org/10.1016/j.fuel.2015.11.042>
230. Zhang Z, Zhao W, Ma B, Ding Y (2010) The epoxidation of olefins catalyzed by a new heterogeneous polyoxometalate-based catalyst with hydrogen peroxide. *Catalysis Communications* 12 (4):318-322. doi:<http://dx.doi.org/10.1016/j.catcom.2010.09.026>
231. Zhao S, Jia Y, Song Y-F (2013) Highly efficient and selective oxidation of various substrates under mild conditions using a lanthanum-containing polyoxometalate as catalyst. *Applied Catalysis A: General* 453:188-194. doi:<http://dx.doi.org/10.1016/j.apcata.2012.12.014>
232. Hua L, Qiao Y, Yu Y, Zhu W, Cao T, Shi Y, Li H, Feng B, Hou Z (2011) A Ti-substituted polyoxometalate as a heterogeneous catalyst for olefin epoxidation with aqueous hydrogen peroxide. *New Journal of Chemistry* 35 (9):1836-1841. doi:10.1039/C1NJ20312F
233. Vasylyev MV, Neumann R (2004) New Heterogeneous Polyoxometalate Based Mesoporous Catalysts for Hydrogen Peroxide Mediated Oxidation Reactions. *Journal of the American Chemical Society* 126 (3):884-890. doi:10.1021/ja036702g
234. Ren Y, Du C, Feng S, Wang C, Kong Z, Yue B, He H (2011) Three POM-based coordination polymers: hydrothermal synthesis, characterization, and catalytic activity in epoxidation of styrene. *CrystEngComm* 13 (23):7143-7148. doi:10.1039/C1CE06037F
235. Dutta D, Jana AD, Debnath M, Bhaumik A, Marek J, Ali M (2010) Robust 1D open rack-like architecture in coordination polymers of Anderson POMs [Na<sub>4</sub>(H<sub>2</sub>O)<sub>14</sub>]{Cu(gly)}<sub>2</sub>[TeMo<sub>6</sub>O<sub>24</sub>] and [Cu(en)<sub>2</sub>]<sub>3</sub>{TeW<sub>6</sub>O<sub>24</sub>}: synthesis, characterization and heterogeneous catalytic epoxidation of olefines. *Dalton Transactions* 39 (48):11551-11559. doi:10.1039/C0DT00426J
236. Zou C, Zhang Z, Xu X, Gong Q, Li J, Wu C-D (2012) A Multifunctional Organic–Inorganic Hybrid Structure Based on Mn<sup>III</sup>–Porphyrin and Polyoxometalate as a Highly Effective Dye Scavenger and Heterogenous Catalyst. *Journal of the American Chemical Society* 134 (1):87-90. doi:10.1021/ja209196t
237. Izumi Y, Hasebe R, Urabe K (1983) Catalysis by heterogeneous supported heteropoly acid. *Journal of Catalysis* 84 (2):402-409. doi:[http://dx.doi.org/10.1016/0021-9517\(83\)90011-8](http://dx.doi.org/10.1016/0021-9517(83)90011-8)
238. Alam MS, Dremov V, Müller P, Postnikov AV, Mal SS, Hussain F, Kortz U (2006) STM/STS Observation of Polyoxoanions on HOPG Surfaces: the Wheel-Shaped [Cu<sub>20</sub>Cl(OH)<sub>24</sub>(H<sub>2</sub>O)<sub>12</sub>(P<sub>8</sub>W<sub>48</sub>O<sub>184</sub>)]<sub>25</sub>- and the Ball-Shaped [Sn(CH<sub>3</sub>)<sub>2</sub>(H<sub>2</sub>O)]<sub>24</sub>{Sn(CH<sub>3</sub>)<sub>2</sub>}<sub>12</sub>(A-PW<sub>9</sub>O<sub>34</sub>)<sub>12</sub>]<sub>36</sub>. *Inorganic Chemistry* 45 (7):2866-2872. doi:10.1021/ic051586z
239. Kaba MS, Song IK, Duncan DC, Hill CL, Barteau MA (1998) Molecular Shapes, Orientation, and Packing of Polyoxometalate Arrays Imaged by Scanning Tunneling Microscopy. *Inorganic Chemistry* 37 (3):398-406. doi:10.1021/ic9705655

240. Song IK, Kaba MS, Nomiya K, Finke RG, Barteau MA (2007) Scanning tunneling microscopy (STM) and tunneling spectroscopy (TS) studies of polyoxometalates (POMs) of the Wells–Dawson structural class. *Journal of Molecular Catalysis A: Chemical* 262 (1–2):216-226. doi:<https://doi.org/10.1016/j.molcata.2006.08.028>
241. AlDamen MA, Clemente-Juan JM, Coronado E, Martí-Gastaldo C, Gaita-Ariño A (2008) Mononuclear Lanthanide Single-Molecule Magnets Based on Polyoxometalates. *Journal of the American Chemical Society* 130 (28):8874-8875. doi:10.1021/ja801659m
242. Compain J-D, Mialane P, Dolbecq A, Mbomekallé IM, Marrot J, Sécheresse F, Rivière E, Rogez G, Wernsdorfer W (2009) Iron Polyoxometalate Single-Molecule Magnets. *Angewandte Chemie International Edition* 48 (17):3077-3081. doi:10.1002/anie.200900117
243. Giusti A, Charron G, Mazerat S, Compain J-D, Mialane P, Dolbecq A, Rivière E, Wernsdorfer W, Ngo Biboum R, Keita B, Nadjo L, Filoramo A, Bourgoin J-P, Mallah T (2009) Magnetic Bistability of Individual Single-Molecule Magnets Grafted on Single-Wall Carbon Nanotubes. *Angewandte Chemie International Edition* 48 (27):4949-4952. doi:10.1002/anie.200901806
244. Orlandi M, Argazzi R, Sartorel A, Carraro M, Scorrano G, Bonchio M, Scandola F (2010) Ruthenium polyoxometalate water splitting catalyst: very fast hole scavenging from photogenerated oxidants. *Chemical Communications* 46 (18):3152-3154. doi:10.1039/B926823E
245. Puntoriero F, La Ganga G, Sartorel A, Carraro M, Scorrano G, Bonchio M, Campagna S (2010) Photo-induced water oxidation with tetra-nuclear ruthenium sensitizer and catalyst: A unique 4 [times] 4 ruthenium interplay triggering high efficiency with low-energy visible light. *Chemical Communications* 46 (26):4725-4727. doi:10.1039/C0CC00444H
246. Puntoriero F, Sartorel A, Orlandi M, La Ganga G, Serroni S, Bonchio M, Scandola F, Campagna S (2011) Photoinduced water oxidation using dendrimeric Ru(II) complexes as photosensitizers. *Coordination Chemistry Reviews* 255 (21):2594-2601. doi:<http://dx.doi.org/10.1016/j.ccr.2011.01.026>
247. Ritchie C, Ferguson A, Nojiri H, Miras HN, Song Y-F, Long D-L, Burkholder E, Murrie M, Kögerler P, Brechin EK, Cronin L (2008) Polyoxometalate-Mediated Self-Assembly of Single-Molecule Magnets: {[XW9O34]2[MnIII4MnII2O4(H2O)4]}12-. *Angewandte Chemie International Edition* 47 (30):5609-5612. doi:10.1002/anie.200801281
248. Toma FM, Sartorel A, Iurlo M, Carraro M, Parisse P, Maccato C, Rapino S, Gonzalez BR, Amenitsch H, Da Ros T, Casalis L, Goldoni A, Marcaccio M, Scorrano G, Scoles G, Paolucci F, Prato M, Bonchio M (2010) Efficient water oxidation at carbon nanotube–polyoxometalate electrocatalytic interfaces. *Nat Chem* 2 (10):826-831. doi:<http://www.nature.com/nchem/journal/v2/n10/abs/nchem.761.html#supplementary-information>
249. Tang Z, Liu S, Wang E, Dong S (2000) Self-Assembled Monolayer of Polyoxometalate on Gold Surfaces: Quartz Crystal Microbalance, Electrochemistry, and in-Situ Scanning Tunneling Microscopy Study. *Langmuir : the ACS journal of surfaces and colloids* 16 (11):4946-4952. doi:10.1021/la9907127

250. Zhong D, Sousa FL, Müller A, Chi L, Fuchs H (2011) A Nanosized Molybdenum Oxide Wheel with a Unique Electronic-Necklace Structure: STM Study with Submolecular Resolution. *Angewandte Chemie International Edition* 50 (31):7018-7021. doi:10.1002/anie.201102274
251. Kim J, Gewirth AA (2003) Interactions between the Keggin-Type Lacunary Polyoxometalate,  $\alpha$ -SiW<sub>11</sub>O<sub>39</sub><sup>8-</sup>, and Electrode Surfaces. *Langmuir : the ACS journal of surfaces and colloids* 19 (21):8934-8942. doi:10.1021/la034708d
252. Du D-Y, Qin J-S, Li S-L, Su Z-M, Lan Y-Q (2014) Recent advances in porous polyoxometalate-based metal-organic framework materials. *Chemical Society Reviews* 43 (13):4615-4632. doi:10.1039/C3CS60404G
253. Carraro M, Gross S (2014) Hybrid Materials Based on the Embedding of Organically Modified Transition Metal Oxoclusters or Polyoxometalates into Polymers for Functional Applications: A Review. *Materials* 7 (5):3956
254. Inumaru K, Ishihara T, Kamiya Y, Okuhara T, Yamanaka S (2007) Water-Tolerant, Highly Active Solid Acid Catalysts Composed of the Keggin-Type Polyoxometalate H<sub>3</sub>PW<sub>12</sub>O<sub>40</sub> Immobilized in Hydrophobic Nanospaces of Organomodified Mesoporous Silica. *Angewandte Chemie International Edition* 46 (40):7625-7628. doi:10.1002/anie.200702478
255. Shiju NR, Alberts AH, Khalid S, Brown DR, Rothenberg G (2011) Mesoporous Silica with Site-Isolated Amine and Phosphotungstic Acid Groups: A Solid Catalyst with Tunable Antagonistic Functions for One-Pot Tandem Reactions. *Angewandte Chemie* 123 (41):9789-9793. doi:10.1002/ange.201101449
256. Liu Z, Cao S, Wang S, Zeng W, Zhang T (2014) Silica-supported phosphotungstic acid as a novel heterogeneous catalyst for  $\beta$ -pinene polymerization. *Reaction Kinetics, Mechanisms and Catalysis* 111 (2):577-590. doi:10.1007/s11144-013-0657-z
257. de Meireles ALP, da Silva Rocha KA, Kozhevnikov IV, Gusevskaya EV (2011) Esterification of camphene over heterogeneous heteropoly acid catalysts: Synthesis of isobornyl carboxylates. *Applied Catalysis A: General* 409:82-86. doi:<http://dx.doi.org/10.1016/j.apcata.2011.09.032>
258. Rocha KAdS, Robles-Dutenhefner PA, Kozhevnikov IV, Gusevskaya EV (2009) Phosphotungstic heteropoly acid as efficient heterogeneous catalyst for solvent-free isomerization of  $\alpha$ -pinene and longifolene. *Applied Catalysis A: General* 352 (1):188-192. doi:<http://dx.doi.org/10.1016/j.apcata.2008.10.005>
259. da Silva Rocha KA, Robles-Dutenhefner PA, Sousa EMB, Kozhevnikova EF, Kozhevnikov IV, Gusevskaya EV (2007) Pd-heteropoly acid as a bifunctional heterogeneous catalyst for one-pot conversion of citronellal to menthol. *Applied Catalysis A: General* 317 (2):171-174. doi:<http://dx.doi.org/10.1016/j.apcata.2006.10.019>
260. Zhen B, Li H, Jiao Q, Li Y, Wu Q, Zhang Y (2012) SiW<sub>12</sub>O<sub>40</sub>-Based Ionic Liquid Catalysts: Catalytic Esterification of Oleic Acid for Biodiesel Production. *Industrial & Engineering Chemistry Research* 51 (31):10374-10380. doi:10.1021/ie301453c
261. Su F, Ma L, Guo Y, Li W (2012) Preparation of ethane-bridged organosilica group and kegginn type heteropoly acid co-functionalized ZrO<sub>2</sub> hybrid catalyst for biodiesel synthesis from eruca sativa gars oil. *Catalysis Science & Technology* 2 (11):2367-2374. doi:10.1039/C2CY20364B

262. Su F, Ma L, Song D, Zhang X, Guo Y (2013) Design of a highly ordered mesoporous H<sub>3</sub>PW<sub>12</sub>O<sub>40</sub>/ZrO<sub>2</sub>-Si(Ph)Si hybrid catalyst for methyl levulinate synthesis. *Green Chemistry* 15 (4):885-890. doi:10.1039/C3GC36912A
263. Su F, Wu Q, Song D, Zhang X, Wang M, Guo Y (2013) Pore morphology-controlled preparation of ZrO<sub>2</sub>-based hybrid catalysts functionalized by both organosilica moieties and Keggin-type heteropoly acid for the synthesis of levulinate esters. *Journal of Materials Chemistry A* 1 (42):13209-13221. doi:10.1039/C3TA12412F
264. Xu L, Guo Y, Ma H, Guan J (2013) Heterogeneous acid catalytic esterification by porous polyoxometalate-tantalum pentoxide nanocomposites. *Journal of Wuhan University of Technology-Mater Sci Ed* 28 (3):580-585. doi:10.1007/s11595-013-0734-1
265. Naik MA, Samantaray S, Mishra BG (2011) Phosphotungstic Acid Nanoclusters Grafted onto High Surface Area Hydrous Zirconia as Efficient Heterogeneous Catalyst for Synthesis of Octahydroquinazolinones and  $\beta$ -Acetamido Ketones. *Journal of Cluster Science* 22 (2):295-307. doi:10.1007/s10876-011-0384-4
266. Rajagopal R, Siddiqui SA, Daniel T, Lahoti RJ, Srinivasan KV (2004) Regioselective side-chain as well as nuclear monobromination of aromatic substrates with N-bromosuccinimide using phosphotungstic acid supported on zirconia as a heterogeneous catalyst. *Journal of Molecular Catalysis A: Chemical* 210 (1):165-169. doi:<http://dx.doi.org/10.1016/j.molcata.2003.09.008>
267. Juan-Alcañiz J, Ramos-Fernandez EV, Lafont U, Gascon J, Kapteijn F (2010) Building MOF bottles around phosphotungstic acid ships: One-pot synthesis of bi-functional polyoxometalate-MIL-101 catalysts. *Journal of Catalysis* 269 (1):229-241. doi:<https://doi.org/10.1016/j.jcat.2009.11.011>
268. Zhang Y, Degirmenci V, Li C, Hensen EJM (2011) Phosphotungstic Acid Encapsulated in Metal-Organic Framework as Catalysts for Carbohydrate Dehydration to 5-Hydroxymethylfurfural. *ChemSusChem* 4 (1):59-64. doi:10.1002/cssc.201000284
269. Chen J, Wang S, Huang J, Chen L, Ma L, Huang X (2013) Conversion of Cellulose and Cellobiose into Sorbitol Catalyzed by Ruthenium Supported on a Polyoxometalate/Metal-Organic Framework Hybrid. *ChemSusChem* 6 (8):1545-1555. doi:10.1002/cssc.201200914
270. Bromberg L, Diao Y, Wu H, Speakman SA, Hatton TA (2012) Chromium(III) Terephthalate Metal Organic Framework (MIL-101): HF-Free Synthesis, Structure, Polyoxometalate Composites, and Catalytic Properties. *Chemistry of Materials* 24 (9):1664-1675. doi:10.1021/cm2034382
271. Wee LH, Bonino F, Lamberti C, Bordiga S, Martens JA (2014) Cr-MIL-101 encapsulated Keggin phosphotungstic acid as active nanomaterial for catalysing the alcoholysis of styrene oxide. *Green Chemistry* 16 (3):1351-1357. doi:10.1039/C3GC41988F
272. Leng Y, Jiang P, Wang J (2012) A novel Brønsted acidic heteropolyanion-based polymeric hybrid catalyst for esterification. *Catalysis Communications* 25:41-44. doi:<https://doi.org/10.1016/j.catcom.2012.04.014>



273. Kamble S, More S, Rode C (2016) Highly selective direct azidation of alcohols over a heterogeneous povidone-phosphotungstic solid acid catalyst. *New Journal of Chemistry* 40 (12):10240-10245. doi:10.1039/C6NJ02500E
274. Betiha MA, Hassan HMA, El-Sharkawy EA, Al-Sabagh AM, Menoufy MF, Abdelmoniem HEM (2016) A new approach to polymer-supported phosphotungstic acid: Application for glycerol acetylation using robust sustainable acidic heterogeneous-homogenous catalyst. *Applied Catalysis B: Environmental* 182:15-25. doi:<http://dx.doi.org/10.1016/j.apcatb.2015.09.010>
275. Zheng X, Zhang L, Li J, Luo S, Cheng J-P (2011) Magnetic nanoparticle supported polyoxometalates (POMs) via non-covalent interaction: reusable acid catalysts and catalyst supports for chiral amines. *Chemical Communications* 47 (45):12325-12327. doi:10.1039/C1CC14178C
276. Duan X, Liu Y, Zhao Q, Wang X, Li S (2013) Water-tolerant heteropolyacid on magnetic nanoparticles as efficient catalysts for esterification of free fatty acid. *RSC Advances* 3 (33):13748-13755. doi:10.1039/C3RA40219C
277. Zillillah, Ngu TA, Li Z (2014) Phosphotungstic acid-functionalized magnetic nanoparticles as an efficient and recyclable catalyst for the one-pot production of biodiesel from grease via esterification and transesterification. *Green Chemistry* 16 (3):1202-1210. doi:10.1039/C3GC41379A
278. Shahbazi F, Amani K (2014) Synthesis, characterization and heterogeneous catalytic activity of diamine-modified silica-coated magnetite-polyoxometalate nanoparticles as a novel magnetically-recoverable nanocatalyst. *Catalysis Communications* 55:57-64. doi:<http://dx.doi.org/10.1016/j.catcom.2014.06.006>
279. Ammar M, Jiang S, Ji S (2016) Heteropoly acid encapsulated into zeolite imidazolate framework (ZIF-67) cage as an efficient heterogeneous catalyst for Friedel-Crafts acylation. *Journal of Solid State Chemistry* 233:303-310. doi:<http://dx.doi.org/10.1016/j.jssc.2015.11.014>
280. Liu Z, Cao S, Wang S, Zeng W, Zhang T, Li P, Lei F (2015) Activated-Carbon-Supported Phosphotungstic Acid as Novel Heterogeneous Catalysts for Cationic Polymerization of  $\alpha$ -Pinene. *JOURNAL OF CHEMICAL ENGINEERING OF JAPAN* 48 (1):29-34. doi:10.1252/jcej.13we330
281. Liu R, Xia X, Niu X, Zhang G, Lu Y, Jiang R, He S (2015) 12-Phosphotungstic acid immobilized on activated-bentonite as an efficient heterogeneous catalyst for the hydroxyalkylation of phenol. *Applied Clay Science* 105:71-77. doi:<http://dx.doi.org/10.1016/j.clay.2014.12.024>
282. Fazaeli R, Aliyan H (2007) Clay (KSF and K10)-supported heteropoly acids: Friendly, efficient, reusable and heterogeneous catalysts for high yield synthesis of 1,5-benzodiazepine derivatives both in solution and under solvent-free conditions. *Applied Catalysis A: General* 331:78-83. doi:<http://dx.doi.org/10.1016/j.apcata.2007.07.030>
283. Yamaguchi K, Yoshida C, Uchida S, Mizuno N (2005) Peroxotungstate Immobilized on Ionic Liquid-Modified Silica as a Heterogeneous Epoxidation Catalyst with Hydrogen Peroxide. *Journal of the American Chemical Society* 127 (2):530-531. doi:10.1021/ja043688e
284. Tan R, Liu C, Feng N, Xiao J, Zheng W, Zheng A, Yin D (2012) Phosphotungstic acid loaded on hydrophilic ionic liquid modified SBA-15 for selective oxidation of alcohols with aqueous

H2O2. Microporous and Mesoporous Materials 158:77-87.  
doi:<https://doi.org/10.1016/j.micromeso.2012.03.023>

285. Zhao H, Zeng L, Li Y, Liu C, Hou B, Wu D, Feng N, Zheng A, Xie X, Su S, Yu N (2013) Polyoxometalate-based ionic complexes immobilized in mesoporous silicas prepared via a one-pot procedure: Efficient and reusable catalysts for H<sub>2</sub>O<sub>2</sub>-mediated alcohol oxidations in aqueous media. Microporous and Mesoporous Materials 172:67-76.  
doi:<https://doi.org/10.1016/j.micromeso.2012.12.040>

286. Xiong J, Zhu W, Ding W, Yang L, Chao Y, Li H, Zhu F, Li H (2014) Phosphotungstic Acid Immobilized on Ionic Liquid-Modified SBA-15: Efficient Hydrophobic Heterogeneous Catalyst for Oxidative Desulfurization in Fuel. Industrial & Engineering Chemistry Research 53 (51):19895-19904. doi:10.1021/ie503322a

287. Masteri-Farahani M, Najafi GR, Modarres M, Taghvai-Nakhjiri M (2016) Wells–Dawson heteropoly acid encapsulated into the nanocages of SBA-16 as heterogeneous catalyst for the oxidation of olefins and alcohols. Journal of Porous Materials 23 (1):285-290. doi:10.1007/s10934-015-0080-0

288. Skliri E, Lykakis IN, Armatas GS (2014) Heteropolytungstic acids incorporated in an ordered mesoporous zirconia framework as efficient oxidation catalysts. RSC Advances 4 (16):8402-8409. doi:10.1039/C3RA46421K

289. Maksimchuk NV, Kovalenko KA, Arzumanov SS, Chesalov YA, Melgunov MS, Stepanov AG, Fedin VP, Kholdeeva OA (2010) Hybrid Polyoxotungstate/MIL-101 Materials: Synthesis, Characterization, and Catalysis of H<sub>2</sub>O<sub>2</sub>-Based Alkene Epoxidation. Inorganic Chemistry 49 (6):2920-2930. doi:10.1021/ic902459f

290. Granadeiro CM, Barbosa ADS, Silva P, Paz FAA, Saini VK, Pires J, de Castro B, Balula SS, Cunha-Silva L (2013) Monovacant polyoxometalates incorporated into MIL-101(Cr): novel heterogeneous catalysts for liquid phase oxidation. Applied Catalysis A: General 453:316-326. doi:<https://doi.org/10.1016/j.apcata.2012.12.039>

291. Sun J-W, Yan P-F, An G-H, Sha J-Q, Li G-M, Yang G-Y (2016) Immobilization of Polyoxometalate in the Metal-Organic Framework rht-MOF-1: Towards a Highly Effective Heterogeneous Catalyst and Dye Scavenger. 6:25595. doi:10.1038/srep25595

<http://dharmasastra.live.cf.private.springer.com/articles/srep25595#supplementary-information>

292. Rafiee E, Nobakht N (2015) Keggin type heteropoly acid, encapsulated in metal-organic framework: A heterogeneous and recyclable nanocatalyst for selective oxidation of sulfides and deep desulfurization of model fuels. Journal of Molecular Catalysis A: Chemical 398:17-25. doi:<http://dx.doi.org/10.1016/j.molcata.2014.11.015>

293. Haddadi H, Hafshejani SM, Farsani MR, Babahydari AK (2015) Heterogeneous epoxidation of alkenes with H<sub>2</sub>O<sub>2</sub> catalyzed by a recyclable organic-inorganic polyoxometalate-based framework catalyst. New Journal of Chemistry 39 (12):9879-9885. doi:10.1039/C5NJ01661D

294. Ma Y-Y, Tan H-Q, Wang Y-H, Hao X-L, Feng X-J, Zang H-Y, Li Y-G (2015) Polyoxometalate-based metal-organic coordination networks for heterogeneous catalytic desulfurization. *CrystEngComm* 17 (41):7938-7947. doi:10.1039/C5CE01533B
295. Yu F, Zheng P-Q, Long Y-X, Ren Y-P, Kong X-J, Long L-S, Yuan Y-Z, Huang R-B, Zheng L-S (2010) Polyoxometalate-Based Metal-Organic Frameworks as Heterogeneous Catalysts for Selective Oxidation of Ethylbenzene. *European Journal of Inorganic Chemistry* 2010 (28):4526-4531. doi:10.1002/ejic.201000491
296. Maksimchuk NV, Timofeeva MN, Melgunov MS, Shmakov AN, Chesalov YA, Dybtsev DN, Fedin VP, Kholdeeva OA (2008) Heterogeneous selective oxidation catalysts based on coordination polymer MIL-101 and transition metal-substituted polyoxometalates. *Journal of Catalysis* 257 (2):315-323. doi:<http://dx.doi.org/10.1016/j.jcat.2008.05.014>
297. Granadeiro CM, Silva P, Saini VK, Paz FAA, Pires J, Cunha-Silva L, Balula SS (2013) Novel heterogeneous catalysts based on lanthanopolyoxometalates supported on MIL-101(Cr). *Catalysis Today* 218:35-42. doi:<http://dx.doi.org/10.1016/j.cattod.2013.03.042>
298. Ribeiro S, Granadeiro CM, Silva P, Almeida Paz FA, de Biani FF, Cunha-Silva L, Balula SS (2013) An efficient oxidative desulfurization process using terbium-polyoxometalate@MIL-101(Cr). *Catalysis Science & Technology* 3 (9):2404-2414. doi:10.1039/C3CY00287J
299. Leng Y, Zhang W, Wang J, Jiang P (2012) A novel heteropolyanion-based amino-containing cross-linked ionic copolymer catalyst for epoxidation of alkenes with H<sub>2</sub>O<sub>2</sub>. *Applied Catalysis A: General* 445-446:306-311. doi:<https://doi.org/10.1016/j.apcata.2012.08.040>
300. Leng Y, Wu J, Jiang P, Wang J (2014) Amphiphilic phosphotungstate-paired ionic copolymer as a highly efficient catalyst for triphase epoxidation of alkenes with H<sub>2</sub>O<sub>2</sub>. *Catalysis Science & Technology* 4 (5):1293-1300. doi:10.1039/C3CY00883E
301. Leng Y, Liu J, Jiang P, Wang J (2012) Heteropolyanion-based polymeric hybrids: highly efficient and recyclable catalysts for oxidation of alcohols with H<sub>2</sub>O<sub>2</sub>. *RSC Advances* 2 (31):11653-11656. doi:10.1039/C2RA22348A
302. Leng Y, Wang J, Jiang P (2012) Amino-containing cross-linked ionic copolymer-anchored heteropoly acid for solvent-free oxidation of benzyl alcohol with H<sub>2</sub>O<sub>2</sub>. *Catalysis Communications* 27:101-104. doi:<https://doi.org/10.1016/j.catcom.2012.07.007>
303. Yamada YMA, Jin CK, Uozumi Y (2010) H<sub>2</sub>O<sub>2</sub>-Oxidation of Alcohols Promoted by Polymeric Phosphotungstate Catalysts. *Organic Letters* 12 (20):4540-4543. doi:10.1021/ol101839m
304. Poli E, Clacens J-M, Pouilloux Y (2011) Synthesis of peroxophosphotungstate immobilized onto polymeric support as heterogeneous catalyst for the epoxidation of unsaturated fatty esters. *Catalysis Today* 164 (1):429-435. doi:<https://doi.org/10.1016/j.cattod.2010.11.006>
305. Doherty S, Knight JG, Ellison JR, Weekes D, Harrington RW, Hardacre C, Manyar H (2012) An efficient recyclable peroxometalate-based polymer-immobilised ionic liquid phase (PIILP) catalyst for hydrogen peroxide-mediated oxidation. *Green Chemistry* 14 (4):925-929. doi:10.1039/C2GC16679H

306. Maradur SP, Jo C, Choi D-H, Kim K, Ryoo R (2011) Mesoporous Polymeric Support Retaining High Catalytic Activity of Polyoxotungstate for Liquid-Phase Olefin Epoxidation using H<sub>2</sub>O<sub>2</sub>. *ChemCatChem* 3 (9):1435-1438. doi:10.1002/cctc.201100045
307. Carraro M, Fiorani G, Mognon L, Caneva F, Gardan M, Maccato C, Bonchio M (2012) Hybrid Polyoxotungstates as Functional Comonomers in New Cross-Linked Catalytic Polymers for Sustainable Oxidation with Hydrogen Peroxide. *Chemistry – A European Journal* 18 (41):13195-13202. doi:10.1002/chem.201201849
308. Xiao Y, Chen D, Ma N, Hou Z, Hu M, Wang C, Wang W (2013) Covalent immobilization of a polyoxometalate in a porous polymer matrix: a heterogeneous catalyst towards sustainability. *RSC Advances* 3 (44):21544-21551. doi:10.1039/C3RA43373K
309. Huang QZ, Zhuo LH, Guo YC (2008) Heterogeneous degradation of chitosan with H<sub>2</sub>O<sub>2</sub> catalysed by phosphotungstate. *Carbohydrate Polymers* 72 (3):500-505. doi:<http://dx.doi.org/10.1016/j.carbpol.2007.09.022>
310. Nisar A, Lu Y, Zhuang J, Wang X (2011) Polyoxometalate Nanocone Nanoreactors: Magnetic Manipulation and Enhanced Catalytic Performance. *Angewandte Chemie* 123 (14):3245-3250. doi:10.1002/ange.201006155
311. Leng Y, Zhao J, Jiang P, Wang J (2014) Amphiphilic Polyoxometalate-Paired Polymer Coated Fe<sub>3</sub>O<sub>4</sub>: Magnetically Recyclable Catalyst for Epoxidation of Bio-Derived Olefins with H<sub>2</sub>O<sub>2</sub>. *ACS Applied Materials & Interfaces* 6 (8):5947-5954. doi:10.1021/am500987s
312. Jameel U, Zhu M-q, Chen X-z, Liu Y, Tong Z-f (2016) Green epoxidation of cyclooctene with molecular oxygen over an ecofriendly heterogeneous polyoxometalate-gold catalyst Au/BW11/Al<sub>2</sub>O<sub>3</sub>. *Journal of Zhejiang University-SCIENCE A* 17 (12):1000-1012. doi:10.1631/jzus.A1500332
313. Liu P, Wang H, Feng Z, Ying P, Li C (2008) Direct immobilization of self-assembled polyoxometalate catalyst in layered double hydroxide for heterogeneous epoxidation of olefins. *Journal of Catalysis* 256 (2):345-348. doi:<http://dx.doi.org/10.1016/j.jcat.2008.03.022>
314. Zhao S, Liu L, Song Y-F (2012) Highly selective oximation of aldehydes by reusable heterogeneous sandwich-type polyoxometalate catalyst. *Dalton Transactions* 41 (33):9855-9858. doi:10.1039/C2DT30092C
315. Villanneau R, Marzouk A, Wang Y, Djamaa AB, Laugel G, Proust A, Launay F (2013) Covalent Grafting of Organic–Inorganic Polyoxometalates Hybrids onto Mesoporous SBA-15: A Key Step for New Anchored Homogeneous Catalysts. *Inorganic Chemistry* 52 (6):2958-2965. doi:10.1021/ic302374v
316. Raj G, Swalus C, Guillet A, Devillers M, Nysten B, Gaigneaux EM (2013) Supramolecular Organization in Organic–Inorganic Heterogeneous Hybrid Catalysts Formed from Polyoxometalate and Poly(ampholyte) Polymer. *Langmuir : the ACS journal of surfaces and colloids* 29 (13):4388-4395. doi:10.1021/la400055t
317. Raj G, Swalus C, Arendt E, Eloy P, Devillers M, Gaigneaux EM (2014) Controlling the dispersion of supported polyoxometalate heterogeneous catalysts: impact of hybridization and the

role of hydrophilicity–hydrophobicity balance and supramolecularity. *Beilstein Journal of Nanotechnology* 5:1749-1759. doi:10.3762/bjnano.5.185

318. Uchida S, Sakamoto S, Mizuno N (2002) Novel channeled compound based on Cr(III) trinuclear complex and polyoxometalate aimed for heterogeneous catalysis: synthesis and structure. *Research on Chemical Intermediates* 28 (5):389-396. doi:10.1163/156856702760346806

319. Zhang L, Zeng H, Zeng Y, Zhang Z, Zhao X (2014) Heterogeneous Fenton-like degradation of 4-chlorophenol using a novel FeIII-containing polyoxometalate as the catalyst. *Journal of Molecular Catalysis A: Chemical* 392:202-207. doi:<http://dx.doi.org/10.1016/j.molcata.2014.05.012>

320. Chen Y, Song Y-F (2014) Immobilization of LaW10 onto Ionic-Liquid-Modified Mesoporous Silica: Deep Desulfurization with Zero-Order Reaction Kinetics. *ChemPlusChem* 79 (2):304-309. doi:10.1002/cplu.201300323

321. Balula SS, Granadeiro CM, Barbosa ADS, Santos ICMS, Cunha-Silva L (2013) Multifunctional catalyst based on sandwich-type polyoxotungstate and MIL-101 for liquid phase oxidations. *Catalysis Today* 210:142-148. doi:<http://dx.doi.org/10.1016/j.cattod.2012.12.003>

322. Sun C-Y, Liu S-X, Liang D-D, Shao K-Z, Ren Y-H, Su Z-M (2009) Highly Stable Crystalline Catalysts Based on a Microporous Metal–Organic Framework and Polyoxometalates. *Journal of the American Chemical Society* 131 (5):1883-1888. doi:10.1021/ja807357r

323. Ma F-J, Liu S-X, Sun C-Y, Liang D-D, Ren G-J, Wei F, Chen Y-G, Su Z-M (2011) A Sodalite-Type Porous Metal–Organic Framework with Polyoxometalate Templates: Adsorption and Decomposition of Dimethyl Methylphosphonate. *Journal of the American Chemical Society* 133 (12):4178-4181. doi:10.1021/ja109659k

324. Song J, Luo Z, Britt DK, Furukawa H, Yaghi OM, Hardcastle KI, Hill CL (2011) A Multiunit Catalyst with Synergistic Stability and Reactivity: A Polyoxometalate–Metal Organic Framework for Aerobic Decontamination. *Journal of the American Chemical Society* 133 (42):16839-16846. doi:10.1021/ja203695h

325. Han Q, He C, Zhao M, Qi B, Niu J, Duan C (2013) Engineering Chiral Polyoxometalate Hybrid Metal–Organic Frameworks for Asymmetric Dihydroxylation of Olefins. *Journal of the American Chemical Society* 135 (28):10186-10189. doi:10.1021/ja401758c

326. Babahydari AK, Fareghi-Alamdari R, Hafshejani SM, Rudbari HA, Farsani MR (2016) Heterogeneous oxidation of alcohols with hydrogen peroxide catalyzed by polyoxometalate metal–organic framework. *Journal of the Iranian Chemical Society* 13 (8):1463-1470. doi:10.1007/s13738-016-0861-7

327. Julião D, Gomes AC, Pillinger M, Cunha-Silva L, de Castro B, Gonçalves IS, Balula SS (2015) Desulfurization of model diesel by extraction/oxidation using a zinc-substituted polyoxometalate as catalyst under homogeneous and heterogeneous (MIL-101(Cr) encapsulated) conditions. *Fuel Processing Technology* 131:78-86. doi:<http://dx.doi.org/10.1016/j.fuproc.2014.10.030>

328. Karimi Z, Mahjoub AR (2011) Novel mesoporous polyoxometalate hybrid catalysts for heterogeneous oxidation of thioethers. *Catalysis Communications* 12 (11):984-988. doi:<http://dx.doi.org/10.1016/j.catcom.2011.03.015>

329. Kholdeeva OA, Vanina MP, Timofeeva MN, Maksimovskaya RI, Trubitsina TA, Melgunov MS, Burgina EB, Mrowiec-Bialon J, Jarzebski AB, Hill CL (2004) Co-containing polyoxometalate-based heterogeneous catalysts for the selective aerobic oxidation of aldehydes under ambient conditions. *Journal of Catalysis* 226 (2):363-371. doi:<http://dx.doi.org/10.1016/j.jcat.2004.05.032>
330. Firouzabadi H, Iranpoor N, Amani K (2003) Heteropoly acid cesium salt/cetyltrimethylammonium bromide a catalytic heterogeneous system which highly controls regioselective bromination of aromatic compounds with bromine. *Journal of Molecular Catalysis A: Chemical* 195 (1):289-294. doi:[http://dx.doi.org/10.1016/S1381-1169\(02\)00589-7](http://dx.doi.org/10.1016/S1381-1169(02)00589-7)
331. Moghadam M, Mirkhani V, Tangestaninejad S, Mohammadpoor-Baltork I, Javadi MM (2010) Polyoxometalate–molybdenylacetylacetonate hybrid complex: A reusable and efficient catalyst for oxidation of alkenes with tert-butylhydroperoxide. *Inorganic Chemistry Communications* 13 (2):244-249. doi:<http://dx.doi.org/10.1016/j.inoche.2009.11.022>
332. Tong J, Wang H, Cai X, Zhang Q, Ma H, Lei Z (2014) Suzuki coupling reaction catalyzed heterogeneously by Pd(salen)/polyoxometalate compound: another example for synergistic effect of organic/inorganic hybrid. *Applied Organometallic Chemistry* 28 (2):95-100. doi:10.1002/aoc.3086
333. Do TO, Desplandier-Giscard D, Danumah C, Kaliaguine S (2001) Perspectives in catalytic applications of mesostructured materials. *Applied Catalysis A: General* 222 (1–2):299-357. doi:[http://dx.doi.org/10.1016/S0926-860X\(01\)00842-0](http://dx.doi.org/10.1016/S0926-860X(01)00842-0)
334. Metcalfe LD, Schmitz AA (1961) The Rapid Preparation of Fatty Acid Esters for Gas Chromatographic Analysis. *Analytical Chemistry* 33 (3):363-364. doi:10.1021/ac60171a016
335. Metcalfe LD, Schmitz AA, Pelka JR (1966) Rapid Preparation of Fatty Acid Esters from Lipids for Gas Chromatographic Analysis. *Analytical Chemistry* 38 (3):514-515. doi:10.1021/ac60235a044
336. Xu B, Xiao T, Yan Z, Sun X, Sloan J, González-Cortés SL, Alshahrani F, Green MLH (2006) Synthesis of mesoporous alumina with highly thermal stability using glucose template in aqueous system. *Microporous and Mesoporous Materials* 91 (1–3):293-295. doi:<http://dx.doi.org/10.1016/j.micromeso.2005.12.007>
337. Wei Y, Xu J, Dong H, Dong JH, Qiu K, Jansen-Varnum SA (1999) Preparation and Physisorption Characterization of d-Glucose-Templated Mesoporous Silica Sol–Gel Materials. *Chemistry of Materials* 11 (8):2023-2029. doi:10.1021/cm981004u
338. Rhead MM, Eglinton G, Draffan GH, England PJ (1971) Conversion of Oleic Acid to Saturated Fatty Acids in Severn Estuary Sediments. *Nature* 232 (5309):327-330
339. Dapurkar SE, Kawanami H, Yokoyama T, Ikushima Y (2009) Catalytic Oxidation of Oleic Acid in Supercritical Carbon Dioxide Media with Molecular Oxygen. *Topics in Catalysis* 52 (6):707-713. doi:10.1007/s11244-009-9212-6
340. Kerenkan Amir E, Ello Aimé S, Echchahed B, Do T-O (2016) Synthesis of Mesoporous Tungsten Oxide/ $\gamma$ -Alumina and Surfactant-Capped Tungsten Oxide Nanoparticles and Their

Catalytic Activities in Oxidative Cleavage of Oleic Acid. *International Journal of Chemical Reactor Engineering*, vol 14. doi:10.1515/ijcre-2015-0101

341. Khlebnikova TB, Pai ZP, Fedoseeva LA, Mattsat YV (2009) Catalytic oxidation of fatty acids. II. Epoxidation and oxidative cleavage of unsaturated fatty acid esters containing additional functional groups. *React Kinet Catal Lett* 98 (1):9-17. doi:10.1007/s11144-009-0054-9

342. Arcoria A, Ballistreri FP, Tomaselli GA, Difuria F, Modena G (1984) THE RELEVANCE OF ACID-BASE EQUILIBRIA IN THE CATALYTIC OXIDATIONS BY TUNGSTEN AND MOLYBDENUM PEROXO COMPLEXES. *Journal of Molecular Catalysis* 24 (2):189-196. doi:10.1016/0304-5102(84)85130-5

343. Jacobson SE, Muccigrosso DA, Mares F (1979) OXIDATION OF ALCOHOLS BY MOLYBDENUM AND TUNGSTEN PEROXO COMPLEXES. *Journal of Organic Chemistry* 44 (6):921-924. doi:10.1021/jo01320a006

344. Jin P, Wei DH, Wen YQ, Luo MF, Wang XY, Tang MS (2011) A combined experimental and DFT study of active structures and self-cycle mechanisms of mononuclear tungsten peroxo complexes in oxidation reactions. *Journal of Molecular Structure* 992 (1-3):19-26. doi:10.1016/j.molstruc.2011.02.023

345. Reynolds MS, Babinski KJ, Bouteneff MC, Brown JL, Campbell RE, Cowan MA, Durwin MR, Foss T, O'Brien P, Penn HR (1997) Kinetics of bromide oxidation by peroxo complexes of molybdenum(VI) and tungsten(VI). *Inorganica Chimica Acta* 263 (1-2):225-230. doi:10.1016/S0020-1693(97)05658-2

346. Balázsi C, Pfeifer J (2002) Development of tungsten oxide hydrate phases during precipitation, room temperature ripening and hydrothermal treatment. *Solid State Ionics* 151 (1-4):353-358. doi:[http://dx.doi.org/10.1016/S0167-2738\(02\)00539-8](http://dx.doi.org/10.1016/S0167-2738(02)00539-8)

347. Nogueira HIS, Cavaleiro AMV, Rocha J, Trindade T, de Jesus JDP (2004) Synthesis and characterization of tungsten trioxide powders prepared from tungstic acids. *Materials Research Bulletin* 39 (4-5):683-693. doi:<http://dx.doi.org/10.1016/j.materresbull.2003.11.004>

348. Pfeifer J, Guifang C, Tekula-Buxbaum P, Kiss BA, Farkas-Jahnke M, Vadasdi K (1995) A reinvestigation of the preparation of tungsten oxide hydrate  $\text{WO}_3 \cdot 1/3\text{H}_2\text{O}$ . *Journal of Solid State Chemistry* 119 (1):90-97. doi:[http://dx.doi.org/10.1016/0022-4596\(95\)80013-F](http://dx.doi.org/10.1016/0022-4596(95)80013-F)

349. Zhou L, Zou J, Yu M, Lu P, Wei J, Qian Y, Wang Y, Yu C (2008) Green Synthesis of Hexagonal-Shaped  $\text{WO}_3 \cdot 0.33\text{H}_2\text{O}$  Nanodiscs Composed of Nanosheets. *Crystal Growth & Design* 8 (11):3993-3998. doi:10.1021/cg800609n

350. Kazusuke Y, Hiroshi O, Hirokazu K, Tetsuichi K (1986) Peroxotungstic Acid Coated Films for Electrochromic Display Devices. *Japanese Journal of Applied Physics* 25 (9R):1420

351. Kudo T, Okamoto H, Matsumoto K, Sasaki Y (1986) Peroxopolytungstic acids synthesized by direct reaction of tungsten or tungsten carbide with hydrogen peroxide. *Inorganica Chimica Acta* 111 (2):L27-L28. doi:[http://dx.doi.org/10.1016/S0020-1693\(00\)84626-5](http://dx.doi.org/10.1016/S0020-1693(00)84626-5)

352. Nanba T, Takano S, Yasui I, Kudo T (1991) Structural study of peroxopolytungstic acid prepared from metallic tungsten and hydrogen peroxide. *Journal of Solid State Chemistry* 90 (1):47-53. doi:[http://dx.doi.org/10.1016/0022-4596\(91\)90170-M](http://dx.doi.org/10.1016/0022-4596(91)90170-M)

353. Deepa M, Kar M, Agnihotry SA (2004) Electrodeposited tungsten oxide films: annealing effects on structure and electrochromic performance. *Thin Solid Films* 468 (1–2):32-42. doi:<http://dx.doi.org/10.1016/j.tsf.2004.04.056>
354. Deepa M, Srivastava AK, Agnihotry SA (2006) Influence of annealing on electrochromic performance of template assisted, electrochemically grown, nanostructured assembly of tungsten oxide. *Acta Materialia* 54 (17):4583-4595. doi:<http://dx.doi.org/10.1016/j.actamat.2006.05.044>
355. Pecquenard B, Castro-Garcia S, Livage J, Zavalij PY, Whittingham MS, Thouvenot R (1998) Structure of Hydrated Tungsten Peroxides [WO<sub>2</sub>(O<sub>2</sub>)H<sub>2</sub>O]·nH<sub>2</sub>O. *Chemistry of Materials* 10 (7):1882-1888. doi:10.1021/cm980045n
356. Redel E, Petrov S, Dag Ö, Moir J, Huai C, Mirtchev P, Ozin GA (2012) Green Nanochemistry: Metal Oxide Nanoparticles and Porous Thin Films from Bare Metal Powders. *Small* 8 (1):68-72. doi:10.1002/sml.201101596
357. Okamoto H, Yamanaka K, Kudo T (1986) Protonic conduction and electrochromism of amorphous peroxopolytungstic acid. *Materials Research Bulletin* 21 (5):551-557. doi:[http://dx.doi.org/10.1016/0025-5408\(86\)90109-1](http://dx.doi.org/10.1016/0025-5408(86)90109-1)
358. Salje E, Viswanathan K (1975) Physical properties and phase transitions in WO<sub>3</sub>. *Acta Crystallographica Section A* 31 (3):356-359. doi:10.1107/S0567739475000745
359. Kudo T (1984) A new heteropolyacid with carbon as a heteroatom in a Keggin-like structure. *Nature* 312 (5994):537-538
360. Meulenkamp EA (1997) Mechanism of WO<sub>3</sub> Electrodeposition from Peroxy-Tungstate Solution. *Journal of The Electrochemical Society* 144 (5):1664-1671. doi:10.1149/1.1837657
361. Gerand B, Nowogrocki G, Figlarz M (1981) A new tungsten trioxide hydrate, WO<sub>3</sub> · 13H<sub>2</sub>O: Preparation, characterization, and crystallographic study. *Journal of Solid State Chemistry* 38 (3):312-320. doi:[http://dx.doi.org/10.1016/0022-4596\(81\)90062-1](http://dx.doi.org/10.1016/0022-4596(81)90062-1)
362. Huo L, Zhao H, Mauvy F, Fourcade S, Labrugere C, Pouchard M, Grenier J-C (2004) Synthesis and mixed conductivity of ammonium tungsten bronze with tunneling structures. *Solid State Sciences* 6 (7):679-688. doi:<http://dx.doi.org/10.1016/j.solidstatesciences.2004.03.036>
363. Pecquenard B, Lecacheux H, Livage J, Julien C (1998) Orthorhombic WO<sub>3</sub> Formed via a Ti-Stabilized WO<sub>3</sub>·13H<sub>2</sub>O Phase. *Journal of Solid State Chemistry* 135 (1):159-168. doi:<http://dx.doi.org/10.1006/jssc.1997.7618>
364. Zavalij P, Guo J, Whittingham MS, Jacobson RA, Pecharsky V, Bucher CK, Hwu S-J (1996) Keggin Cluster Formation by Hydrothermal Reaction of Tungsten Trioxide with Methyl Substituted Ammonium: The Crystal Structure of Two Novel Compounds, [NH<sub>2</sub>(CH<sub>3</sub>)<sub>2</sub>]<sub>6</sub>H<sub>2</sub>W<sub>12</sub>O<sub>40</sub> · ~4H<sub>2</sub>O and [N(CH<sub>3</sub>)<sub>4</sub>]<sub>6</sub>H<sub>2</sub>W<sub>12</sub>O<sub>40</sub> · 2H<sub>2</sub>O. *Journal of Solid State Chemistry* 123 (1):83-92. doi:<http://dx.doi.org/10.1006/jssc.1996.0155>
365. Hashimoto M, Koyano G, Mizuno N (2004) In Situ IR Spectrum of 12-Tungstophosphoric Acid Hexahydrate with Planar H<sub>5</sub>O<sub>2</sub><sup>+</sup>. *The Journal of Physical Chemistry B* 108 (33):12368-12374. doi:10.1021/jp0485744



366. Zayat M, Reisfeld R, Minti H, Orel B, Svegl F (1998) Gasochromic Effect in Platinum-Doped Tungsten Trioxide Films Prepared by the Sol-Gel Method. *Journal of Sol-Gel Science and Technology* 11 (2):161-168. doi:10.1023/a:1008645530803
367. Huang L, Chen X, Li Q (2001) Synthesis of microporous molecular sieves by surfactant decomposition. *Journal of Materials Chemistry* 11 (2):610-615. doi:10.1039/B005770N
368. Pang H-F, Xiang X, Li Z-J, Fu Y-Q, Zu X-T (2012) Hydrothermal synthesis and optical properties of hexagonal tungsten oxide nanocrystals assisted by ammonium tartrate. *physica status solidi (a)* 209 (3):537-544. doi:10.1002/pssa.201127456
369. Enferadi-Kerenkan A, Ello AS, Do T-O (2017) Synthesis, Organo-Functionalization, and Catalytic Properties of Tungsten Oxide Nanoparticles As Heterogeneous Catalyst for Oxidative Cleavage of Oleic Acid As a Model Fatty Acid into Diacids. *Industrial & Engineering Chemistry Research*. doi:10.1021/acs.iecr.7b03001
370. Kozhevnikov IV (2007) Sustainable heterogeneous acid catalysis by heteropoly acids. *Journal of Molecular Catalysis A: Chemical* 262 (1):86-92. doi:<https://doi.org/10.1016/j.molcata.2006.08.072>
371. Kholdeeva OA, Maksimchuk NV, Maksimov GM (2010) Polyoxometalate-based heterogeneous catalysts for liquid phase selective oxidations: Comparison of different strategies. *Catalysis Today* 157 (1):107-113. doi:<https://doi.org/10.1016/j.cattod.2009.12.016>
372. Ello AS, Enferadi-kerenkan A, Trokourey A, Do T-O (2017) Sustainable Oxidative Cleavage of Vegetable Oils into Diacids by Organo-Modified Molybdenum Oxide Heterogeneous Catalysts. *Journal of the American Oil Chemists' Society*. doi:10.1007/s11746-017-3047-2
373. Janauer GG, Doble A, Guo J, Zavalij P, Whittingham MS (1996) Novel Tungsten, Molybdenum, and Vanadium Oxides Containing Surfactant Ions. *Chemistry of Materials* 8 (8):2096-2101. doi:10.1021/cm960111q
374. Rocchiccioli-Deltcheff C, Thouvenot R, Franck R (1976) Spectres i.r. et Raman d'hétéropolyanions  $\alpha$  -  $\text{XM}_{12}\text{O}_{40}\text{n-}$  de structure de type Keggin (X = BIII, SiIV, GeIV, PV, AsV et M = WVI et MoVI). *Spectrochimica Acta Part A: Molecular Spectroscopy* 32 (3):587-597. doi:[https://doi.org/10.1016/0584-8539\(76\)80121-3](https://doi.org/10.1016/0584-8539(76)80121-3)
375. Kozhevnikov I (2010) Sustainable Heterogeneous Acid Catalysis by Heteropoly Acids. In: *Handbook of Green Chemistry*. Wiley-VCH Verlag GmbH & Co. KGaA. doi:10.1002/9783527628698.hgc019
376. Hodnett BK, Moffat JB (1984) Application of temperature-programmed desorption to the study of heteropoly compounds: Desorption of water and pyridine. *Journal of Catalysis* 88 (2):253-263. doi:[https://doi.org/10.1016/0021-9517\(84\)90001-0](https://doi.org/10.1016/0021-9517(84)90001-0)
377. Kozhevnikov I (2002) *Catalysts for Fine Chemicals, Vol. 2. Catalysis by Polyoxometalates*, . John Wiley & Sons
378. Khademi M, Wang W, Reitingner W, Barz DPJ (2017) Zeta Potential of Poly(methyl methacrylate) (PMMA) in Contact with Aqueous Electrolyte-Surfactant Solutions. *Langmuir : the ACS journal of surfaces and colloids*. doi:10.1021/acs.langmuir.7b02487
379. Köckritz A, Martin A (2011) Synthesis of azelaic acid from vegetable oil-based feedstocks. *European Journal of Lipid Science and Technology* 113 (1):83-91. doi:10.1002/ejlt.201000117

380. Kozhevnikov IV, Mulder GP, Steverink-de Zoete MC, Oostwal MG (1998) Epoxidation of oleic acid catalyzed by peroxo phosphotungstate in a two-phase system. *Journal of Molecular Catalysis A: Chemical* 134 (1–3):223-228. doi:[http://dx.doi.org/10.1016/S1381-1169\(98\)00039-9](http://dx.doi.org/10.1016/S1381-1169(98)00039-9)
381. Pai ZP, Khlebnikova TB, Mattsat YV, Parmon VN (2009) Catalytic oxidation of fatty acids. I. Epoxidation of unsaturated fatty acids. *Reaction Kinetics and Catalysis Letters* 98 (1):1-8. doi:10.1007/s11144-009-0069-2
382. Poli E, Clacens J-M, Barrault J, Pouilloux Y (2009) Solvent-free selective epoxidation of fatty esters over a tungsten-based catalyst. *Catalysis Today* 140 (1–2):19-22. doi:<http://dx.doi.org/10.1016/j.cattod.2008.07.004>
383. Enferadi-Kerenkan A, Gandon A, Do T-O (2017) Novel tetra propyl/butyl ammonium encapsulated Keggin-type polyoxotungstates: synthesis, structural characterization, and catalytic capability in oxidative cleavage of unsaturated fatty acids. *Dalton Transactions*. doi:10.1039/C7DT04469K
384. Sparks DL, Antonio Estevez L, Hernandez R (2009) Supercritical-fluid-assisted oxidation of oleic acid with ozone and potassium permanganate. *Green Chemistry* 11 (7):986-993. doi:10.1039/B816515G
385. Dai B, Wu P, Zhu W, Chao Y, Sun J, Xiong J, Jiang W, Li H (2016) Heterogenization of homogenous oxidative desulfurization reaction on graphene-like boron nitride with a peroxomolybdate ionic liquid. *RSC Advances* 6 (1):140-147. doi:10.1039/C5RA23272D
386. Benessere V, Cuccioli ME, De Santis A, Di Serio M, Esposito R, Ruffo F, Turco R (2015) Sustainable Process for Production of Azelaic Acid Through Oxidative Cleavage of Oleic Acid. *Journal of the American Oil Chemists' Society* 92 (11):1701-1707. doi:10.1007/s11746-015-2727-z
387. Chandra P, Doke DS, Umbarkar SB, Biradar AV (2014) One-pot synthesis of ultrasmall MoO<sub>3</sub> nanoparticles supported on SiO<sub>2</sub>, TiO<sub>2</sub>, and ZrO<sub>2</sub> nanospheres: an efficient epoxidation catalyst. *Journal of Materials Chemistry A* 2 (44):19060-19066. doi:10.1039/C4TA03754E
388. Li Z, Li Y, Zhan E, Ta N, Shen W (2013) Morphology-controlled synthesis of [small alpha]-MoO<sub>3</sub> nanomaterials for ethanol oxidation. *Journal of Materials Chemistry A* 1 (48):15370-15376. doi:10.1039/C3TA13402D
389. Ma Z, Wu Y, He Y, Wu T (2013) A novel protocol for the oxidative degradation of chitosan with hydrogen peroxide catalyzed by peroxomolybdate in aqueous solution. *RSC Advances* 3 (30):12049-12051. doi:10.1039/C3RA40424B
390. Song R-Q, Xu A-W, Deng B, Fang Y-P (2005) Novel Multilamellar Mesostructured Molybdenum Oxide Nanofibers and Nanobelts: Synthesis and Characterization. *The Journal of Physical Chemistry B* 109 (48):22758-22766. doi:10.1021/jp0533325
391. Wang S, Zhang Y, Ma X, Wang W, Li X, Zhang Z, Qian Y (2005) Hydrothermal route to single crystalline  $\alpha$ -MoO<sub>3</sub> nanobelts and hierarchical structures. *Solid State Communications* 136 (5):283-287. doi:<http://dx.doi.org/10.1016/j.ssc.2005.08.002>

392. Gong J, Zeng W, Zhang H (2015) Hydrothermal synthesis of controlled morphologies of MoO<sub>3</sub> nanobelts and hierarchical structures. *Materials Letters* 154:170-172. doi:<http://dx.doi.org/10.1016/j.matlet.2015.04.092>
393. Li Y, Liu T, Li T, Peng X (2015) Hydrothermal fabrication of controlled morphologies of MoO<sub>3</sub> with CTAB: Structure and growth. *Materials Letters* 140:48-50. doi:<http://dx.doi.org/10.1016/j.matlet.2014.10.153>
394. Chithambararaj A, Chandra Bose A (2014) Role of synthesis variables on controlled nucleation and growth of hexagonal molybdenum oxide nanocrystals: investigation on thermal and optical properties. *CrystEngComm* 16 (27):6175-6186. doi:10.1039/C4CE00418C
395. Chithambararaj A, Sanjini NS, Bose AC, Velmathi S (2013) Flower-like hierarchical h-MoO<sub>3</sub>: new findings of efficient visible light driven nano photocatalyst for methylene blue degradation. *Catalysis Science & Technology* 3 (5):1405-1414. doi:10.1039/C3CY20764A
396. Chithambararaj A, Bose AC (2011) Hydrothermal synthesis of hexagonal and orthorhombic MoO<sub>3</sub> nanoparticles. *Journal of Alloys and Compounds* 509 (31):8105-8110. doi:<http://dx.doi.org/10.1016/j.jallcom.2011.05.067>
397. Masteri-Farahani M, Mahdavi S, Rafizadeh M (2013) Microemulsion-mediated synthesis and characterization of monodispersed nickel molybdate nanocrystals. *Ceramics International* 39 (4):4619-4625. doi:<http://dx.doi.org/10.1016/j.ceramint.2012.11.059>
398. Mao Y, Li W, Sun X, Ma Y, Xia J, Zhao Y, Lu X, Gan J, Liu Z, Chen J, Liu P, Tong Y (2012) Room-temperature ferromagnetism in hierarchically branched MoO<sub>3</sub> nanostructures. *CrystEngComm* 14 (4):1419-1424. doi:10.1039/C1CE05700F
399. Enferadi Kerenkan A, Ello Aimé S, Echchahed B, Do T-O (2016) Synthesis of Mesoporous Tungsten Oxide/ $\gamma$ -Alumina and Surfactant-Capped Tungsten Oxide Nanoparticles and Their Catalytic Activities in Oxidative Cleavage of Oleic Acid. *International Journal of Chemical Reactor Engineering* 14 (4):899-907

# List of publications

## Journal publications

- ❖ *Chemically catalyzed oxidative cleavage of unsaturated fatty acids and their derivatives into valuable products for industrial applications: a review and perspective*

**Amir Enferadi Kerenkan**, Francois Béland, and Trong-On Do

*Catalysis Science & Technology*, 2016, 6, 971-987.

- ❖ *Heterogeneous catalysis by tungsten-based heteropoly compounds*

**Amir Enferadi Kerenkan**, Trong-On Do, and Serge Kaliaguine

*Catalysis Science & Technology*, 2018, Accepted Manuscript, (DOI: 10.1039/C8CY00281A).

- ❖ *Synthesis of mesoporous tungsten oxide/ $\gamma$ -alumina and surfactant-capped tungsten oxide nanoparticles and their catalytic activities in oxidative cleavage of oleic acid*

**Amir Enferadi Kerenkan**, Aimé Serge Ello, Bousselham Echchahed, and Trong-On Do

*International Journal of Chemical Reactor Engineering*, 2016, 14(4), 899-907.

- ❖ *Synthesis, organo-functionalization, and catalytic properties of tungsten oxide nanoparticles as heterogeneous catalyst for oxidative cleavage of oleic acid as a model fatty acid into diacids*

**Amir Enferadi Kerenkan**, Aimé Serge Ello, and Trong-On Do

*Industrial & Engineering Chemistry Research*, 2017, 56 (38), 10639-10647.

- ❖ *Novel tetra propyl/butyl ammonium encapsulated Keggin-type polyoxotungstates: synthesis, structural characterization, and catalytic capability in oxidative cleavage of unsaturated fatty acids*

**Amir Enferadi Kerenkan**, Arnaud Gandon, and Trong-On Do

*Dalton Transactions*, 2017, DOI: 10.1039/C7DT04469K.

- ❖ *Sustainable oxidative cleavage of vegetable oils into diacids by organo-modified molybdenum oxide heterogeneous catalysts*

Aimé Serge Ello, **Amir Enferadi-kerenkan**, Albert Trokourey, and Trong-on Do

*(equal contribution of the first two authors)*

*Journal of the American Oil Chemists' Society, 2017, 94, 1451-1461.*

## Conference presentations

- ❖ *New class of nanocatalysts for oxidative cleavage of vegetable oil feedstock into valuable products*

**Amir Enferadi Kerenkan**, Aimé Serge Ello, and Trong-On Do

*66th Canadian Chemical Engineering Conference, October 16-19, 2016, Quebec, Canada.*

- ❖ *Efficient nanocatalysts for production of azelaic and pelargonic acids from vegetable oils*

**Amir Enferadi Kerenkan**, Aimé Serge Ello, and Trong-On Do

*XIII International Conference on Nanostructured Materials (NANO 2016), August 7-12, 2016, Quebec, Canada.*

- ❖ *Synthesis of advanced tungsten-based heterogeneous catalysts for liquid-phase oxidative cleavage of oleic acid*

**Amir Enferadi Kerenkan** and Trong-On Do

*6<sup>th</sup> CGCC (Centre in Green Chemistry and Catalysis) Annual Meeting, May 12-15, 2015, Quebec, Canada.*